

https://dspace.org/

Dynamic road damage caused by heavy vehicle rolling motion when including Road Crossfall

Steenkamp, Anton Johan

2021
https://hdl.handle.net/10539/31872

Downloaded from a DSpace repository. https://dspace.org/



DYNAMIC ROAD DAMAGE CAUSED BY HEAVY VEHICLE ROLLING MOTION WHEN INCLUDING ROAD CROSSFALL

Anton Johan Steenkamp

Student number: 1990615

School of Mechanical, Industrial and Aeronautical Engineering

University of the Witwatersrand

Johannesburg, South Africa

Supervisor: Prof Frank Kienhöfer

Co-Supervisor: Dr Christopher de Saxe

A research dissertation submitted to the Faculty of Engineering and the Built Environment, of the University of the Witwatersrand, in fulfilment of the requirements for the degree of Master of Science in Engineering.

Declaration

I declare that this dissertation is my own unaided work. It is being submitted to the Degree of Master of Science to the University of the Witwatersrand, Johannesburg. It has not been submitted before for any degree or examination to any other University.

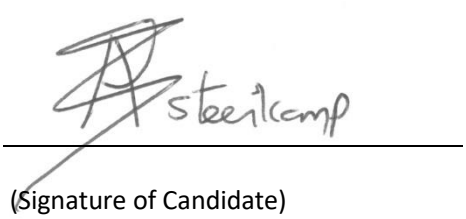

(Signature of Candidate)

On the 16th day of January 2021

Abstract

The rolling motion of heavy vehicles is ignored in almost all road damage studies and is simply assumed to be symmetrical. This dissertation shows that the addition of rolling motion when incorporating road crossfall is essential to accurately capture the true dynamic road damage caused by heavy vehicles. Dual track road profiles were created with road roughness values ranging from 0.5 m/km to 10 m/km. Road crossfall values from 0% to 5% were simulated and corresponded to typical values found in South Africa and across the world. A 9 degree of freedom (DoF) model was developed and implemented in Simulink® that incorporates pitching and rolling motion of a heavy vehicle. Linear suspension was used for this investigation in order to simplify the analysis and generalize the results obtained. The model was validated using a commercially available multibody dynamics software package (TruckSim2019.1®). The road damage criteria studied include the average vertical tyre forces, the dynamic load coefficient, the first power aggregate forces and the fourth power aggregate forces. The most important road damage criterion is the 95th percentile fourth power aggregate force. The patterns produced by the fourth power aggregate forces are similar for the average, 95th percentile and 99th percentile fourth power aggregate forces. The fourth power aggregate forces increase linearly on the left side with an increase in the road crossfall value. Using a typical highway speed and roughness value of 80 km/h and 2 m/km respectively, the percentage difference in the 95th percentile fourth power aggregate forces between the left and right profiles is 43.7% using a crossfall of 2%. It was noted that in the case of a crossfall value of 5% the percentage difference is in excess of 106%. Even with a crossfall of only 1% the percentage difference in the 95th percentile fourth power aggregate forces are 21.9%. The effect of several heavy vehicle parameters on the 95th percentile fourth power aggregate force were studied. In general, it was found that any parameter that improves the roll stability of the heavy vehicle, will decrease the percentage difference in the left and right side 95th percentile fourth power aggregate forces. Most of these vehicle parameters that decreases the percentage difference in the left and right road damage also decreased the overall road damage produced. The exception to this rule is the suspension stiffness and tyre stiffness. An increase in the suspension and tyre stiffness will decrease the percentage difference in the road damage but will increase the overall damage produced. Air suspensions are therefore still more road friendly even if there is a larger percentage difference in the left and right road damage. The damping value was found to have no effect on the percentage difference, but it does decrease the overall road damage produced by the heavy vehicle. It was noted that many of the heavy vehicle parameters had a larger relative influence than the dampers or suspension on the overall vehicle damage as well as the percentage difference in the left and right road damage when crossfall is included. Heavy vehicle rolling motion can therefore not be ignored when road crossfall is present.

Acknowledgements

I firstly want to thank Jesus Christ for the privilege and strength to conduct this research.

I would like to sincerely thank my supervisor Prof. Frank Kienhöfer for his guidance and support during this research work. His insights and expertise have been instrumental in completing this research and obtaining my accreditation as a PBS assessor in South Africa.

I would also like to thank Dr Christopher de Saxe (co-supervisor) for his equally valuable support as my mentor at the CSIR. It is a real privilege to be able to learn from you.

I also want to thank the CSIR for the opportunity to pursue my MSc studies.

A special thanks to my family, whose love and support has been indispensable in ensuring that I stayed motivated during this research.

Table of Contents

Declaration i

Abstract ii

Acknowledgements iii

List of Figures vii

List of Tables xiii

List of Symbols xvii

1. Introduction 1

1.1. Background 1

1.2. Literature review 1

1.2.1. Heavy vehicle modelling 1

1.2.2. Road damage and dynamic heavy vehicle characteristics 4

1.2.3. Road profile modelling 8

1.2.4. Significance of this research 9

1.3. Research question and objectives 10

1.4. Methodology and Resources 11

2. Development and Validation of Vehicle Models 13

2.1. Dual track road profiles and validation 13

2.1.1. Detailed literature road profiles and road damage criteria 13

2.1.2. Coherence function and basic assumptions 20

2.1.3. Creating and validating dual track road profiles 21

2.2. Development of the full-car heavy vehicle dynamic model including rolling motion 25

2.2.1. Validation of model on a flat surface with typical operating conditions 29

2.2.2. Validation of flat surface model at different road roughness values and vehicle speeds 35

2.2.3. Validation of model when including road crossfall, anti-roll bars and eccentric loads 35

3. Results and Discussion 42

3.1. Results for the base model 42
3.1.1. The effect of crossfall on the average vertical tyre forces of the base model 42
3.1.2. The effect of crossfall on the DLC of the base model 43
3.1.3. The effect of crossfall on the first power aggregate forces of the base model 48
3.1.4. The effect of crossfall on the fourth power aggregate forces of the base model 54
3.2. The effect of different vehicle parameters on the fourth power damage when including crossfall 60
3.2.1. The effect of including anti-roll bars 60
3.2.2. The effect of the sprung mass centre of gravity height 62
3.2.3. The effect of the roll centre height 63
3.2.4. The effect of the suspension stiffness 64
3.2.5. The effect of the suspension damping 66
3.2.6. The effect of the track width 67
3.2.7. The effect of the suspension track width 68
3.2.8. The effect of an eccentric vehicle load 70
3.2.9. The effect of sprung mass 71
3.2.10. The effect of tyre stiffness 73
3.3. General discussion on results 74
3.3.1. The influence of road crossfall on road damage 74
3.3.2. The influence of vehicle speed and road roughness on the road damage when including road crossfall. 75
3.3.3. The influence of selected heavy vehicle parameters on the road damage when including road crossfall 76
3.3.4. Recommendations on how to minimize the adverse effects of road crossfall 79
4. Conclusion and Recommendations 81
5. References 85
Appendix A: Additional model information 90
Appendix B: Additional model information 98

Appendix C: Additional model information……100

Appendix D: Additional validation results……111

Appendix E: Additional results……122

List of Figures

Figure 1.1: Full-car, half-car and quarter-car models of vehicles [57] 2
Figure 1.2: Difference in total load between left and ride side of typical B-Double vehicle at various crossfall values as calculated in TruckSim 2019.1® [56]. 3
Figure 1.3:Difference in left wheel path (LWP) and right wheel path (RWP) rutting of a New Zealand road over time [23] 6
Figure 1.4: Tensile strain experienced by a bitumen layer at different roughness values and loading scenarios [22] 7
Figure 1.5: Difference in right and left wheel path loads due to difference in crossfall [22] 7
Figure 1.6: An example of road crossfall [54]. 9
Figure 2.1: DLC of heavy vehicles at various vehicle speeds and loads [10] 14
Figure 2.2: Classification of road profiles according to ISO 8608 for an exponent value of $\boldsymbol{w}$ = 2 [53] 15
Figure 2.3: Typical IRI values and the associated operating speeds of vehicles [36] 16
Figure 2.4: Parallel profiles in an isotropic and homogeneous surface [29] 18
Figure 2.5: Modified ISO-8608 spectral density function in order to represent homogeneous and isotropic road profiles (logarithmic scale) [29] 19
Figure 2.6: Coherence function for an isotropic and homogeneous road for different distances between profiles [29]. 19
Figure 2.7: Comparison of coherence values calculated to commercially available solution (PRP generator) 21
Figure 2.8: Created dual track road profiles with a design IRI of 2m/km. 22
Figure 2.9: The PSD values of the road profiles with a design IRI of 2 m/km 23
Figure 2.10: The Smoothed PSD values of the road profiles with a design IRI of 2 m/km 24
Figure 2.11: Comparison of design and actual coherence values of the dual track road profiles 24
Figure 2.12: Pitching motion of the developed heavy vehicle model 26
Figure 2.13: Rolling motion of the developed heavy vehicle model on flat surface modified from [42] 26
Figure 2.14: Spring and damper in series representing lateral tyre forces from a pneumatic tyre 28
Figure 2.15: Front left vertical tyre force from TruckSim 2019.1® and the model over 200 m test section at 0% crossfall, 2 m/km IRI, 80 km/h and no anti-roll bar 31
Figure 2.16: Front axle lateral tyre force from TruckSim 2019.1® and the model over 200 m test section at 0% crossfall, 2 m/km IRI, 80 km/h and no anti-roll bar 31

Figure 2.17: Rear axle lateral tyre force from TruckSim 2019.1® and the model over 200m test section at 0% crossfall, 2 m/km IRI, 80 km/h and no anti-roll bar.....32
Figure 2.18: Front unsprung mass roll angle from TruckSim 2019.1® and the model over 200 m test section at 0% crossfall, 2 m/km IRI, 80 km/h and no anti-roll bar.....32
Figure 2.19: Sprung mass roll angle from TruckSim 2019.1® and the model over 1 km test section at 0% crossfall, 2 m/km IRI, 80 km/h and no anti-roll bar 33
Figure 2.20: Sprung mass pitch angle from TruckSim 2019.1® and the model over 1 km test section at 0% crossfall, 2 m/km IRI, 80 km/h and no anti-roll bar 33
Figure 2.21: Left side first power aggregate forces from TruckSim 2019.1® and the model over 200 m test section at 0% crossfall, 2 m/km IRI, 80 km/h and no anti-roll bar.....34
Figure 2.22: Left side fourth power aggregate forces from TruckSim 2019.1® and the model over 200 m test section at 0% crossfall, 2 m/km IRI, 80 km/h and no anti-roll bar.....34
Figure 2.23:Left side fourth power aggregate forces from TruckSim 2019.1® and the model over 200 m test section at 0% crossfall, 10 m/km IRI, 80 km/h and no anti-roll bar.....36
Figure 2.24: Left side fourth power aggregate forces from TruckSim 2019.1® and the model over 200 m test section at 0% crossfall, 10 m/km IRI, 40 km/h and no anti-roll bar.....36
Figure 2.25: Left side first power aggregate forces from TruckSim 2019.1® and the initial model over 200 m test section at 2% crossfall, 2 m/km IRI, 80 km/h and no anti-roll bar.....38
Figure 2.26: Right side first power aggregate forces from TruckSim 2019.1® and the initial model over 200 m test section at 2% crossfall, 2 m/km IRI, 80 km/h and no anti-roll bar.....38
Figure 2.27: Front axle lateral force from TruckSim 2019.1® and the initial model over 200 m test section at 2% crossfall, 2 m/km IRI, 80 km/h and no anti-roll bar.....39
Figure 2.28: Forces produced on a vehicle when including crossfall [55] 39
Figure 2.29: Rolling motion of heavy vehicle when including crossfall modified from [47].....40
Figure 2.30: Auxiliary roll moment on the front axle from TruckSim 2019.1® and the final model over 200 m test section at 5% crossfall, 2 m/km IRI, 80 km/h and with an anti-roll bar.....41
Figure 3.1: The average vertical tyre force of the base model at different crossfall values.....43
Figure 3.2: Percentage difference of the left and right tyres in the front and rear of the base model 43
Figure 3.3: DLC of the front left tyre of the base model under all operating conditions 44
Figure 3.4: DLC of all four tyres of the base model at a vehicle speed of 80 km/h and an IRI 2 m/km 45
Figure 3.5: DLC of the front left tyre of the base model as a function of IRI and a crossfall of 0%.46
Figure 3.6: Dynamic load coefficient of the front left tyre of the base model as a function of vehicle speed and a crossfall of 0%. 46

Figure 3.7: The percentage difference in the front left and right tyre DLC values of the base model over all the operating conditions 47
Figure 3.8: The normalized (by the static force) average first power aggregate forces of the left and right side of the base model over all the crossfall values 49
Figure 3.9: The average first power aggregate forces of the left and right side of the base model over all the crossfall values 49
Figure 3.10: The normalized (by the static force) 95th percentile first power aggregate forces of the left side of the base model over all the operating conditions 50
Figure 3.11: The normalized (by the static force) 95th percentile first power aggregate forces of the left and right side of the base model for all the crossfall values 51
Figure 3.12: The normalized (by static values) 95th percentile first power aggregate forces of the left side as a function of road roughness 51
Figure 3.13: The normalized (by the static force) 95th percentile first power aggregate forces of the left side as a function of vehicle speed 52
Figure 3.14: The percentage difference in left and right 95th percentile first power aggregate force as a function of crossfall at a vehicle speed of 80 km/h and road roughness of 2 m/km 52
Figure 3.15: The percentage difference in left and right 95th percentile first power aggregate force as a function of road roughness at a vehicle speed of 80 km/h and crossfall of 2% 53
Figure 3.16: The normalized (by the static force) 99th percentile first power aggregate forces of the left side of the base model as a function of the road roughness 53
Figure 3.17: The normalized (by the static force) 99th percentile first power aggregate forces of the left side of the base model as a function of vehicle speed 54
Figure 3.18: The normalized 95th percentile fourth power aggregate force of the left side of the base model over all of the operating conditions 55
Figure 3.19: The normalized 95th percentile fourth power aggregate force of the right side of the base model over all of the operating conditions 56
Figure 3.20: The normalized (by static values) 95th percentile fourth power aggregate force of the left and right side of the base model for different crossfall values ,a vehicle speed of 80km/h and road roughness of 2m/km 57
Figure 3.21: The normalized (by static values) 95th percentile fourth power aggregate force as a function of road roughness 58
Figure 3.22: The normalized (by static values) 95th percentile fourth power aggregate force as a function of vehicle speed 59
Figure 3.23: Percentage difference in the left and right 95th percentile fourth power aggregate forces for a vehicle speed of 80 km/h and road roughness of 2 m/km 59

Figure 3.24: Percentage difference in the left and right 95th percentile fourth power aggregate forces for a vehicle speed of 80 km/h and road crossfall of 2% 59
Figure 3.25: The percentage difference between the left and right 95th percentile fourth power aggregate forces using different anti-roll bar values at 80 km/h 61
Figure 3.26: The left normalized 95th percentile fourth power aggregate forces using different anti-roll bar values at 80 km/h 61
Figure 3.27: The percentage difference between the left and right 95th percentile fourth power aggregate forces using different sprung mass height values at 80 km/h 62
Figure 3.28: The left normalized 95th percentile fourth power aggregate forces using different sprung mass height values at 80 km/h 63
Figure 3.29: The percentage difference between the left and right 95th percentile fourth power aggregate forces using different roll centre height values at 80 km/h 64
Figure 3.30: The left normalized 95th percentile fourth power aggregate forces using different roll centre height values at 80 km/h 64
Figure 3.31: The percentage difference between the left and right 95th percentile fourth power aggregate forces using different suspension stiffness values at 80 km/h 65
Figure 3.32: The left normalized 95th percentile fourth power aggregate forces using different suspension stiffness values at 80 km/h 65
Figure 3.33: The percentage difference between the left and right 95th percentile fourth power aggregate forces using different suspension damping values at 80 km/h 66
Figure 3.34: The left normalized 95th percentile fourth power aggregate forces using different suspension stiffness values at 80 km/h 67
Figure 3.35: The percentage difference between the left and right 95th percentile fourth power aggregate forces using different track width values at 80 km/h 67
Figure 3.36: The left normalized 95th percentile fourth power aggregate forces using different track width values at 80 km/h 68
Figure 3.37: The percentage difference between the left and right 95th percentile fourth power aggregate forces using different spring track width values at 80 km/h 69
Figure 3.38: The left normalized 95th percentile fourth power aggregate forces using different spring track width values at 80 km/h 69
Figure 3.39: The percentage difference between the left and right 95th percentile fourth power aggregate forces using different eccentric sprung mass values at 80 km/h 70
Figure 3.40: The left normalized 95th percentile fourth power aggregate forces using different eccentric sprung mass values at 80 km/h 71
Figure 3.41: The percentage difference between the left and right 95th percentile fourth power aggregate forces using different sprung mass values at 80 km/h 72

Figure 3.42: The left normalized 95th percentile fourth power aggregate forces using different sprung mass values at 80 km/h....72
Figure 3.43: The percentage difference between the left and right 95th percentile fourth power aggregate forces using different tire stiffness values at 80 km/h....73
Figure 3.44: The left normalized 95th percentile fourth power aggregate forces using different tyre stiffness values at 80 km/h....74
Figure A.1: Dual track road profile with design IRI of 0.5 m/km....90
Figure A.2: Dual track road profile with design IRI of 1.0 m/km....90
Figure A.3: Dual track road profile with design IRI of 2.0 m/km....91
Figure A.4: Dual track road profile with design IRI of 3.0 m/km....91
Figure A.5: Dual track road profile with design IRI of 4.0 m/km....91
Figure A.6: Dual track road profile with design IRI of 5.0 m/km....92
Figure A.7: Dual track road profile with design IRI of 6.0 m/km....92
Figure A.8: Dual track road profile with design IRI of 8.0 m/km....92
Figure A.9: Dual track road profile with design IRI of 10.0 m/km....93
Figure A.10: PSD of Dual track road profile with design IRI of 0.5 m/km....93
Figure A.11: PSD of Dual track road profile with design IRI of 1.0 m/km....94
Figure A.12: PSD of Dual track road profile with design IRI of 2.0 m/km....94
Figure A.13: PSD of Dual track road profile with design IRI of 3.0 m/km....95
Figure A.14: PSD of Dual track road profile with design IRI of 4.0 m/km....95
Figure A.15: PSD of Dual track road profile with design IRI of 5.0 m/km....96
Figure A.16: PSD of Dual track road profile with design IRI of 6.0 m/km....96
Figure A.17: PSD of Dual track road profile with design IRI of 8.0 m/km....97
Figure A.18: PSD of Dual track road profile with design IRI of 10.0 m/km....97
Figure B.1: Driver model parameters specified in TruckSim 2019.1®....99
Figure C.1: Main window of Simunlink® heavy vehicle model....102
Figure C.2: Front unsprung mass sub model....103
Figure C.3: Front left suspension sub model....104
Figure C.4: Unsprung mass positions and velocities sub model....105
Figure C.5: Front axle tyre sub model....106
Figure C.6: Main sprung mass sub model....107
Figure C.7: Sprung mass roll motion sub model....108
Figure C.8: Sprung mass pitch motion sub model....109
Figure C.9: Sprung mass final positions and velocities sub model....110
Figure D.1: Left side first power aggregate forces from TruckSim 2019.1® and the model over 200 m test section at 0% crossfall, 10 m/km IRI, 80 km/h and no anti-roll bar....113

Figure D.2: Left side fourth power aggregate forces from TruckSim 2019.1® and the model over 200 m test section at 0% crossfall, 10 m/km IRI, 80 km/h and no anti-roll bar.....113
Figure D.3: Left side first power aggregate forces from TruckSim 2019.1® and the model over 200 m test section at 0% crossfall, 2 m/km IRI, 40 km/h and no anti-roll bar.....114
Figure D.4: Left side fourth power aggregate forces from TruckSim 2019.1® and the model over 200 m test section at 0% crossfall, 2 m/km IRI, 40 km/h and no anti-roll bar.....114
Figure D.5: Left side first power aggregate forces from TruckSim 2019.1® and the model over 200 m test section at 0% crossfall, 10 m/km IRI, 40 km/h and no anti-roll bar.....115
Figure D.6: Left side fourth power aggregate forces from TruckSim 2019.1® and the model over 200 m test section at 0% crossfall, 10 m/km IRI, 40 km/h and no anti-roll bar.....115
Figure D.7: Left side first power aggregate forces from TruckSim 2019.1® and the model over 200 m test section at 0% crossfall, 2 m/km IRI, 120 km/h and no anti-roll bar.....116
Figure D.8: Left side fourth power aggregate forces from TruckSim 2019.1® and the model over 200 m test section at 0% crossfall, 2 m/km IRI, 120 km/h and no anti-roll bar.....116
Figure D.9:Left side first power aggregate forces from TruckSim 2019.1® and the model over 200 m test section at 0% crossfall, 10 m/km IRI, 120 km/h and no anti-roll bar.....117
Figure D.10: Left side fourth power aggregate forces from TruckSim 2019.1® and the model over 200 m test section at 0% crossfall, 10 m/km IRI, 120 km/h and no anti-roll bar.....117
Figure D.11: Left side first power aggregate forces from TruckSim 2019.1® and the final model over 200 m test section at 2% crossfall, 2 m/km IRI, 80 km/h and no anti-roll bar.....118
Figure D.12: Left side fourth power aggregate forces from TruckSim 2019.1® and the final model over 200 m test section at 2% crossfall, 2 m/km IRI, 80 km/h and no anti-roll bar.....118
Figure D.13: Left side first power aggregate forces from TruckSim 2019.1® and the final model over 200 m test section at 5% crossfall, 2 m/km IRI, 80 km/h and no anti-roll bar.....119
Figure D.14: Left side fourth power aggregate forces from TruckSim 2019.1® and the final model over 200 m test section at 5% crossfall, 2 m/km IRI, 80 km/h and no anti-roll bar.....119
Figure D.15: Left side first power aggregate forces from TruckSim 2019.1® and the final model over 200 m test section at 5% crossfall, 2 m/km IRI, 80 km/h and with an anti-roll bar.....120
Figure D.16: Left side fourth power aggregate forces from TruckSim 2019.1® and the final model over 200 m test section at 5% crossfall, 2 m/km IRI, 80 km/h and with an anti-roll bar.....120
Figure D.17: Left side fourth power aggregate forces from TruckSim 2019.1® and the final model over 200 m test section at 5% crossfall, 2 m/km IRI, 80 km/h and with no anti-roll bar and an eccentric load of 300 mm to the left, ...121

List of Tables

Table 1.1: Summary of data used in an Australian road study [35] 10
Table 1.2: Primary resources required for study 12
Table 2.1: Comparison of design vs actual IRI values achieved in road profiles 22
Table 3.1: Qualitative summary of the impact of various heavy vehicle parameters on the percentage difference in the left and right fourth power aggregate force and the left normalized fourth power aggregate force 77
Table B.1: Lateral tyre stiffness properties used in TruckSim 2019.1® 98
Table B.2: Tyre steer angles as a function of the gearbox output used in TruckSim 2019.1® 98
Table C.1: Vehicle input parameters of the base user defined model 100
Table D.1: Average absolute error of vertical tyre forces for validation simulations compared to TruckSim 2019.1® values at 0% crossfall and no anti-roll bar 111
Table D.2: Average absolute error of first power vertical tyre forces for validation simulations compared to TruckSim 2019.1® values at 0% crossfall and no anti-roll bar 111
Table D.3: Average absolute error of fourth power vertical tyre forces for validation simulations compared to TruckSim 2019.1® values at 0% crossfall and no anti-roll bar 111
Table D.4: Dynamic loading coefficient error for validation simulations compared to TruckSim 2019.1® values at 0% crossfall and no anti-roll bar 111
Table D.5: Average absolute error of vertical tyre forces for validation simulations compared to TruckSim 2019.1® values when including crossfall 112
Table D.6: Average absolute error of first power aggregate vertical tyre forces for validation simulations compared to TruckSim 2019.1® values when including crossfall 112
Table D.7: Average absolute error of the fourth power aggregate vertical tyre forces for validation simulations compared to TruckSim 2019.1® values when including crossfall 112
Table D.8: Average absolute error of the dynamic load coefficient for validation simulations compared to TruckSim 2019.1® values when including crossfall 112
Table E.1: The average vertical tyre force of the front tyres of the base model under all operating conditions 123
Table E.2: The average vertical tyre force of the rear tyres of the base model under all operating conditions 124
Table E.3: The percentage difference in the average vertical tyre forces between the left and right side of the front and rear axles of the base model under all operating conditions 125
Table E.4: The DLC of the front left and right tyres of the base model under all operating conditions 126

Table E.5: The DLC of the rear left and right tyres of the base model under all operating conditions 127
Table E.6: The percentage difference in left and right DLC of the base model under all operating conditions 128
Table E.7: The normalized (by the static values) average first power aggregate forces of the base model under all operating conditions 129
Table E.8: The percentage difference in left and right average first power aggregate forces of the base model under all operating conditions 130
Table E.9: The normalized (by the static values) 95th percentile first power aggregate forces of the base model under all operating conditions 131
Table E.10: The percentage difference in left and right 95th percentile first power aggregate forces of the base model under all operating conditions 132
Table E.11: The normalized (by the static values) 99th percentile first power aggregate forces of the base model under all operating conditions 133
Table E.12: The percentage difference in left and right 99th percentile first power aggregate forces of the base model under all operating conditions 134
Table E.13: The normalized (by the static values) average fourth power aggregate forces of the base model under all operating conditions 135
Table E.14: The percentage difference in left and right average fourth power aggregate forces of the base model under all operating conditions 136
Table E.15: The normalized (by the static values) 95th percentile fourth power aggregate forces of the base model under all operating conditions 137
Table E.16: The percentage difference in left and right 95th percentile fourth power aggregate forces of the base model under all operating conditions 138
Table E.17: The normalized (by the static values) 99th percentile fourth power aggregate forces of the base model under all operating conditions 139
Table E.18: The percentage difference in left and right 99th percentile fourth power aggregate forces of the base model under all operating conditions 140
Table E.19: Ratio of the percentage difference in left and right average fourth power aggregate forces to the percentage difference in the left and right average percentile first power aggregate forces 141
Table E.20: Left normalized (by base model static values) 95th percentile fourth power aggregate forces for different anti-roll bar stiffness values 142
Table E.21: Right normalized (by base model static values) 95th percentile fourth power aggregate forces for different anti-roll bar stiffness values 142

Table E.22: Percentage difference in left and right 95th percentile fourth power aggregate forces for different anti-roll bar stiffness values 142
Table E.23: Left normalized (by base model static values) 95th percentile fourth power aggregate forces for different sprung mass heights 143
Table E.24: Right normalized (by base model static values) 95th percentile fourth power aggregate forces for different sprung mass heights 143
Table E.25: Percentage difference in left and right 95th percentile fourth power aggregate forces for different sprung mass heights 143
Table E.26: Left normalized (by base model static values) 95th percentile fourth power aggregate forces for different roll centre heights 144
Table E.27: Right normalized (by base model static values) 95th percentile fourth power aggregate forces for different roll centre heights 144
Table E.28: Percentage difference in left and right 95th percentile fourth power aggregate forces for different roll centre heights 144
Table E.29: Left normalized (by base model static values) 95th percentile fourth power aggregate forces for different spring stiffness values 145
Table E.30: Right normalized (by base model static values) 95th percentile fourth power aggregate forces for different spring stiffness values 145
Table E.31: Percentage difference in left and right 95th percentile fourth power aggregate forces for different spring stiffness values 145
Table E.32: Left normalized (by base model static values) 95th percentile fourth power aggregate forces for different damping values 146
Table E.33: Right normalized (by base model static values) 95th percentile fourth power aggregate forces for different damping values 146
Table E.34: Percentage difference in left and right 95th percentile fourth power aggregate forces for different damping values 146
Table E.35: Left normalized (by base model static values) 95th percentile fourth power aggregate forces for different track widths 147
Table E.36: Right normalized (by base model static values) 95th percentile fourth power aggregate forces for different track widths 147
Table E.37: Percentage difference in left and right 95th percentile fourth power aggregate forces for different track widths 147
Table E.38: Left normalized (by base model static values) 95th percentile fourth power aggregate forces for different spring track widths 148
Table E.39: Right normalized (by base model static values) 95th percentile fourth power aggregate forces for different spring track widths 148

Table E.40: Percentage difference in left and right 95th percentile fourth power aggregate forces for different spring track widths 148
Table E.41: Left normalized (by base model static values) 95th percentile fourth power aggregate forces for different sprung mass eccentricities 149
Table E.42: Right normalized (by base model static values) 95th percentile fourth power aggregate forces for different sprung mass eccentricities 149
Table E.43: Percentage difference in left and right 95th percentile fourth power aggregate forces for different sprung mass eccentricities 149
Table E.44: Left normalized (by base model static values) 95th percentile fourth power aggregate forces for different sprung mass values 150
Table E.45: Right normalized (by base model static values) 95th percentile fourth power aggregate forces for different sprung mass values 150
Table E.46: Percentage difference in left and right 95th percentile fourth power aggregate forces for different sprung mass values 150
Table E.47: Left normalized (by base model static values) 95th percentile fourth power aggregate forces for different tyre stiffness values 151
Table E.48: Right normalized (by base model static values) 95th percentile fourth power aggregate forces for different tyre stiffness values 151
Table E.49: Percentage difference in left and right 95th percentile fourth power aggregate forces for different tyre stiffness values 151

List of Symbols

Symbol	Description	Units
a	Distance from the front axle to sprung mass the centre of gravity	**m**
a_j	The contact area of tyre j	**m^2**
b	Distance from the rear axle to sprung mass centre of gravity	**m**
C_c	Tyre cornering coefficient	**N/N/rad**
c_f	Damping rate of the front axle suspension (per side)	**kNs/m**
CF	Road crossfall	**%**
c_r	Damping rate of the rear axle suspension (per side)	**kNs/m**
DLC	Dynamic load coefficient	**-**
E_s	Eccentricity of the sprung mass	**m**
f	Front	**-**
F_{dfl}	Front left damper force	**N**
F_{dfr}	Front right damper force	**N**
F_{drl}	Rear left damper force	**N**
F_{drr}	Rear right damper force	**N**
$F_{f\ lat}$	Front lateral tyre force	**N**
fl	Front left	**-**
F_{Lfa}	Front axle lateral force that results in acceleration of the sprung mass (excludes constant forces such as crossfall force on tyres)	**N**

F_{Lra}	Rear axle lateral force that results in acceleration of the sprung mass (excludes constant forces such as crossfall force on tyres)	**N**
fr	Front right	**-**
$F_{r\ lat}$	Rear lateral tyre force	**N**
F_{sfl}	Front left spring force	**N**
F_{sfr}	Front right spring force	**N**
F_{srl}	Rear left spring force	**N**
F_{srr}	Rear right spring force	**N**
F_{vert}	Vertical tyre force	**N**
F_y	Lateral force	**N**
h	Distance from the ground to the sprung mass centre of gravity	**m**
h_{1f}	Distance from the ground to the roll centre height at the front axle	**m**
h_{1r}	Distance from the ground to the roll centre height at the rear axle	**m**
h_{2f}	Distance from the ground to the centre of gravity of the front axle unsprung mass	**m**
h_{2r}	Distance from the ground to the centre of gravity of the rear axle unsprung mass	**m**
I_{sp}	Sprung mass pitch moment of inertia	**kg/m^2**
I_{sr}	Sprung mass roll moment of inertia	**kg/m^2**
I_{uf}	Unsprung mass front roll moment of inertia	**kg/m^2**
I_{ur}	Unsprung mass rear roll moment of inertia	**kg/m^2**

k_f	Spring stiffness of the front axle suspension (per side)	**N/m**
$k_{f\ lat}$	Front lateral tyre stiffness	**N/m**
k_r	Spring stiffness of the rear axle suspension (per side)	**N/m**
$k_{r\ lat}$	Rear lateral tyre stiffness	**N/m**
k_{tf}	Front tyre spring stiffness (per side)	**N/m**
k_{tr}	Rear tyre spring stiffness (per side)	**N/m**
L	Tyre relaxation length	**m**
$L_{f\ relax}$	Front tyre relaxation length	**m**
$L_{r\ relax}$	Rear tyre relaxation length	**m**
m_s	Sprung mass	**kg**
m_{uf}	Unsprung mass front	**kg**
m_{ur}	Unsprung mass rear	**kg**
PSD	Power spectral density	**-**
r	Rear	**-**
rl	Rear left	**-**
rr	Rear right	**-**
R_f	Front anti-roll bar stiffness	**Nm/deg**
RMS	Root mean square	**-**
R_r	Rear anti-roll bar stiffness	**Nm/deg**
S_f	Half front spring track width	**m**
S_r	Half rear spring track width	**m**
T_f	Half front tyre track width	**m**

T_r	Half rear tyre track width	**m**
V	Longitudinal velocity of the vehicle	**m/s**
Wb	Wheelbase from the front to rear axle	**m**
X_s	Sprung mass longitudinal position	**m**
Y_1	Lateral position at point 1 of the first order spring-damper tyre model	**m**
Y_2	Lateral position at point 2 of the first order spring-damper tyre model	**m**
Y_s	Sprung mass lateral position	**m**
$\ddot{Y}_s$	Sprung mass lateral acceleration	**m/s^2**
Z_s	Sprung mass vertical position	**m**
$\ddot{Z}_s$	Sprung mass vertical acceleration	**m/s^2**
Z_{uf}	Unsprung mass front vertical position	**m**
Z_{ur}	Unsprung mass rear vertical position	**m**
α	Tyre slip angle	**deg**
θ_{sx}	Sprung mass roll angle around the roll centre	**deg**
$\ddot{\theta}_{sx}$	Sprung mass roll acceleration around the roll centre	**deg/s^2**
θ_{ufx}	Unsprung mass front roll angle around the unsprung mass centre of gravity	**deg**
$\ddot{\theta}_{ufx}$	Unsprung mass front roll acceleration around the unsprung mass centre of gravity	**deg/s^2**
θ_{urx}	Unsprung mass rear roll angle around the unsprung mass centre of gravity	**deg**
γ	The coherence between the left and right road profiles	**-**

$\boldsymbol{\Phi}$	Road crossfall (%)	**%**
$\boldsymbol{\Phi_{sy}}$	Sprung mass pitch angle around the roll centre	**deg**
$\boldsymbol{\tau_{lat}}$	Time constant for tyre lateral force	**s^{-1}**

1. Introduction

1.1. Background

Transport logistics are a key aspect of an economy and according to the latest Logistics Barometer, constitute 11.8% (or approximately R499 billion) of South Africa's gross domestic product (GDP). In South Africa, approximately 85% of freight is transported by road and similarly 95% of all passenger trips are completed by road [1]. The ever-expanding fleet of heavy vehicles, particularly those that are illegally overloaded, has a detrimental impact on the road and bridge infrastructure. The value of the paved road network in South Africa is estimated to be approximately R2 trillion and represents one of the country's most important assets. As at 2014, South Africa had a road maintenance backlog of R200 billion, which has led to a national network where currently 78% of the roads are older than their intended design life. The situation has deteriorated since then and new estimates of the road maintenance backlog are R416.6 billion in 2018 [2]**.** It is therefore crucial to minimize the road wear caused by heavy vehicles which, if overloaded, can account for more than 60% of all road damage [3]. Minimizing pavement damage requires a detailed understanding of the physics and mechanisms that cause this damage.

A vehicle suspension is critical to the road-friendliness of a vehicle. The Organisation for Economic Cooperation and Development (OECD) study found that well damped suspensions will generally cause between 5% and 10% more road damage when considering a dynamic versus a static analysis [4]. In contrast a poorly damped suspension will cause between 20% and 40% more road damage during dynamic manoeuvres [4].

Most models developed to calculate dynamic tyre forces and pavement damage are limited to quarter-car models. Such models are useful, but information regarding the vehicle roll and pitching are not captured. Provisional work has indicated that variations in road crossfall can have significant impacts on heavy vehicle load transfer as discussed in Section 1.2. This study investigates the influence of road profile and heavy vehicle parameters on the dynamic road damage when including vehicle rolling motion and road crossfall.

1.2. Literature review

This section of the report contains a qualitative literature review on topics of interest for this dissertation. A more detailed qualitative literature review is provided in subsection 2.1.

1.2.1. Heavy vehicle modelling

Heavy vehicle simulations can be divided into user-developed mathematical models with limited degrees of freedom (DOFs), or multibody simulation software packages. Multibody simulation

software packages have the potential to be more accurate as they allow for increased levels of detail and complexity in the models. Multibody simulation software packages still use mathematical models to perform the calculations, but high degrees of freedom are included with user graphical interfaces. User-developed mathematical models are still frequently used as they allow for a more fundamental understanding to be developed [5].

There are three types of user-developed mathematical models commonly used to represent vehicle suspension behaviour [6]. These are the quarter-car, half-car and full-car models. With quarter-car models, the vehicle is constrained to one dimensional movement in the z direction with no pitching or rolling effects considered. With half-car models, the vehicle is constrained to planar motion in the x and z plane and therefore the pitch of the vehicle is included in simulations. In a full-car model the vehicle is allowed full 3 dimensional motion in the x, y and z directions and includes the rotational effects around all three axes namely pitch, yaw and roll [6, 7]. The different types of models are shown in Figure 1.1.

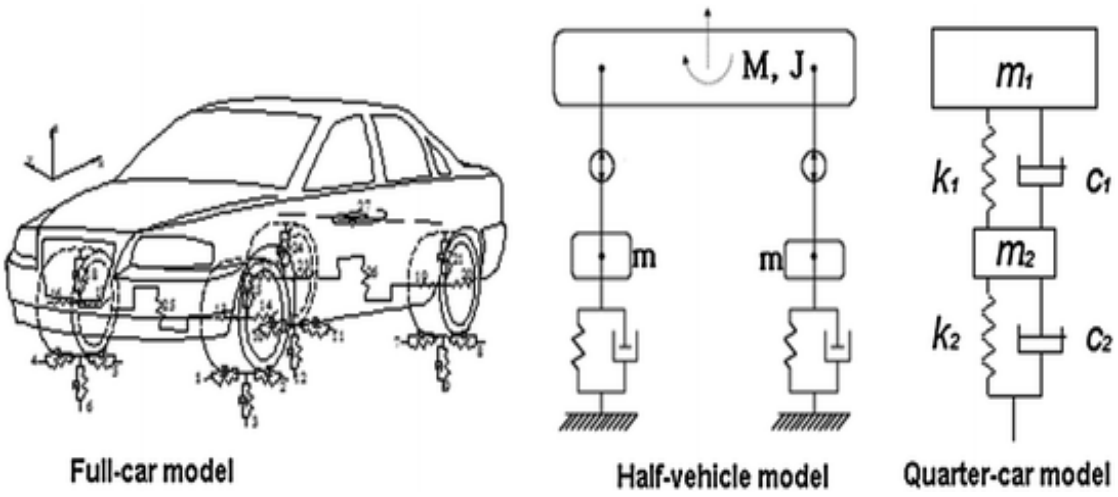

Figure 1.1: Full-car, half-car and quarter-car models of vehicles [57]

Most road damage studies of heavy vehicle suspensions use quarter-car and half-car models. The assumption is therefore made that the left- and right-side loads are identical [8, 9]. Recent research has shown that this assumption of symmetrical loading is however not true when including the crossfall of a road section.

Figure 1.2 shows the difference in the total load on the left and right side of a typical B-double heavy vehicle at various crossfall values. The simulations were conducted using TruckSim®. Due to the exponential nature of road damage as described in section 1.2.2, slight variations in tyre loads can have a magnified impact when considering road damage.

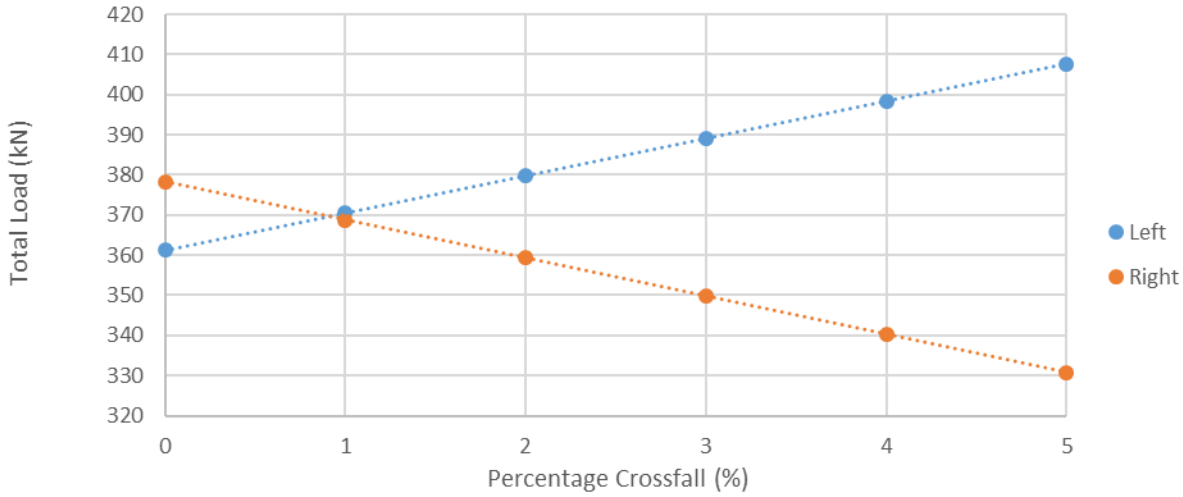

Figure 1.2: Difference in total load between left and ride side of typical B-Double vehicle at various crossfall values as calculated in TruckSim 2019.1® [56].

The quarter-car model has been the most widely adopted for simulating dynamic tyre forces. The quarter-car model is not able to capture complex suspension nonlinearities and the complexities of heavy vehicle body motion, but the frequency content of the quarter-car model is considered to be sufficiently accurate [10]. This has been verified by Hardy and Cebon [11]. In general, researchers try to keep the models as realistic but simple as possible in order to minimize complexities in modelling the combination and to reduce computation time [10].

Even when higher degree of freedom models are developed, they usually ignore rolling motion or conclude that its influence is negligible. As such, dynamic road wear models are usually limited to either quarter-car or half-car models that utilize pitch-plane motion [12]. Cebon specifically states that: “A two-dimensional model (pitch-plane) should be satisfactory for predicting the tyre forces of typical lead-spring articulated vehicles with well damped suspension modes, operating under typical conditions of speed and road roughness” [12]. He however adds that: “It may therefore be necessary to use a three-dimensional model when the unsprung mass roll modes contribute significantly to dynamic tyre forces” [12]. This would be the case if crossfall of a road profile is included.

A possible reason why crossfall has not been included into the research of dynamic tyre loads is due to various studies and guidelines indicating that its effect is negligible [13]. Instead these research projects and guidelines focus primarily on the effect of road roughness, vehicle speeds, loading of the heavy vehicles and suspension characteristics. Also, when crossfall is referred to, emphasis is given on its vital importance in preserving road infrastructure by ensuring adequate drainage [14]. The reasons provide a possible explanation for the void on research related to dynamic road damage when including road crossfall.

No work could be found that implements user defined models to model the dynamic forces of heavy vehicles when including crossfall of a road profile. This study addresses this need and illustrates that a simple pitch-roll heavy vehicle model is sufficiently accurate to capture these phenomena.

The roll stability of a heavy vehicle is primarily determined by the height of the centre of mass, the vehicle track width and the kinematic and compliance properties of the suspensions [15]. The main parameters that influence the rolling motion of a heavy vehicle are [15, 16, 17]:

1. The sprung mass centre of gravity height
2. The sprung mass
3. The roll centre height
4. The suspension stiffness
5. The suspension damping
6. Track width
7. Spring and damper track width
8. Tyre stiffness
9. The eccentricity of the sprung mass
10. Auxiliary roll stiffness (from an anti-roll bar for example)

These are the parameters of interest that are studied in this dissertation.

1.2.2. Road damage and dynamic heavy vehicle characteristics

All road structures can be classified as either flexible, composite or rigid. A flexible pavement is composed of one or more layers of a flexible material (bituminous) which is supported by a granular subgrade. A composite pavement consists of a flexible surface layer but is supported by a stiff base (concrete). A rigid road surface consists of layers of concrete on a granular foundation [8]. These different road types each have their own characteristic failure mechanisms. Fatigue cracking and rutting are the most important failure mechanisms for flexible roads. Fatigue cracking is known for being related to non-uniform contact reaction distributions, whilst rutting has a closer link to vertical tyre forces [12].

Road damage is usually expressed as a load equivalency factor (LEF), that quantifies the damage caused by a particular axle or group of axles relative to a reference axle [18]. The two most well-known methods for quantifying road damage is the fourth power law as developed during the AASHO Road Test and the more recently developed mechanistic empirical approach [4, 18].

The fourth power law was developed from extensive test data gathered during the late 1950s on the damage caused by heavy vehicle axles relative to a reference axle load of 80 kN. It captures all forms of pavement distress and does not distinguish on a specific failure mechanism. Although still

widely used, its applicability for current road pavements and vehicles has been questioned, as the results are based on vehicles and pavements that are no longer in operation [4]. This method however remains valuable and useful if accurate data is available for a specific road section from an accelerated pavement testing program [4].

Classical mechanistic empirical methods develop a material model for the pavement type, and subsequently calculate the engineering parameters of interest such as stresses and strains. These structural parameters are subsequently linked to the structural capacity of the pavement based on observations of the performance of the pavement structure (usually from accelerated heavy vehicle testing). These mechanistic empirical methods are however developed under static or quasi-static conditions and their applicability to dynamic road damage studies is often questioned [18]. The CSIR's mePADS software is an example of such a mechanistic empirical software and is used for various research studies to quantify the impact of road damage [19].

Road damage studies have shown that it is a time dependent phenomenon for any asphalt material. Asphalt is a non-homogenous material and therefore the stress-strain field is not continuous [20]. Developing and using these complex road damage models is difficult and requires substantial expertise in the domains of civil and pavement design engineering. The aim of this study is not to focus on detailed pavement stresses and damage, but rather to focus on the road profile and heavy vehicle parameters that cause road damage. Simpler dynamic tyre force and road damage criteria exist that can be used. The criteria most often used and which are considered in this study are the dynamic load coefficient (DLC) and aggregate tyre forces [8, 12].

The DLC is commonly used to characterize the magnitude of dynamic tyre forces and uses the root mean squared (RMS) of the tyre forces. The DLC values provide an indication of the dynamic performance of the heavy vehicle over the entire road section and do not focus on individual sections on a route [12]. Although the DLC is often used and provides valuable information, it does have notable limitations namely [21]:

- The DLCs measured at different static loads cannot be directly compared as lower masses produce larger DLC values which do not necessarily indicate more damage.
- The DLC does not provide a good measure of the peak loads produced
- DLC also does not provide a measure of spatial repeatability of the loads over a section

The spatial distribution of tyre forces is an important factor in dynamic road damage studies. Such an analysis allows one to identify areas where road damage tends to accumulate relative to other sections on a route. The aggregate tyre forces criteria allow for such spatial distributions to be investigated [8, 12].

The first real study to investigate the effect of crossfall, was a New Zealand study that was conducted after it was noticed that the left wheel path (LWP) always had more rutting than the right wheel path (RWP). This difference in rutting is shown in Figure 1.3 [22].

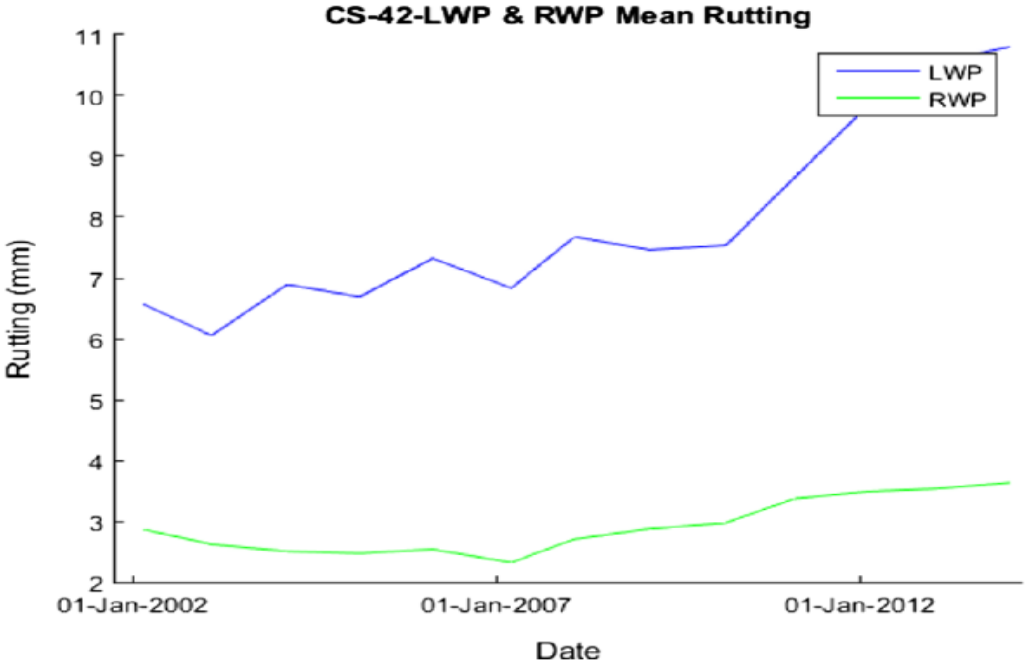

Figure 1.3:Difference in left wheel path (LWP) and right wheel path (RWP) rutting of a New Zealand road over time [23]

The study used the equivalent single axle load (ESAL) or load equivalency factor (LEF) method for quantifying road damage. The ESAL damage is calculated as shown in Equation 1 [22].

$$ESAL = LEF = (\frac{Actual\ axle\ load}{Reference\ load})^n \quad (1)$$

Where n is an appropriate exponent to quantify the damage on a specific pavement. Usually this value is taken as 4 but values in excess of 7 have been proposed [22]. This study found that by including crossfall, the ESAL value can double when using actual wheel loads compared to the equal static wheel loads usually assumed. This study also included the effects of some parameters namely the axle width, height of the centre of mass, the percentage crossfall and the rutting depth. The study concluded that there are no other mechanisms that can account for the difference in rutting between the two wheel tracks except for the road crossfall [22]. The study however did not include any dynamic loading of the combination which provides little information of the performance over different operating conditions as is the aim of this dissertation.

After this study in New Zealand, a more recent article was found that has conducted similar research to this dissertation. The study showed that road crossfall has a definite impact on the difference in left and right wheel path loads and the difference in the average loads are shown in Figure 1.5 [23]. The figure shows that the load differences increase linearly with crossfall/camber.

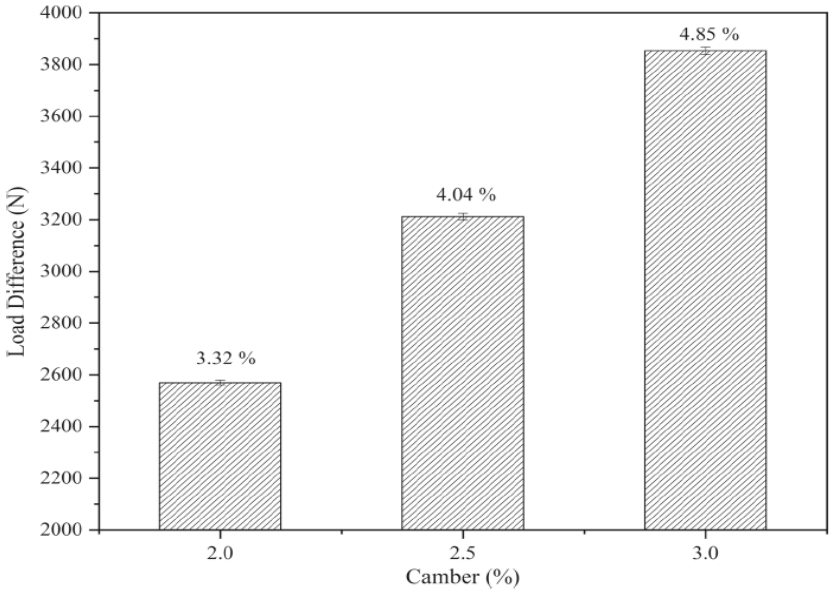

Figure 1.5: Difference in right and left wheel path loads due to difference in crossfall [22]

The study also investigated the impact of different road roughness values and crossfall on the pavement's strains. The results are shown in Figure 1.4. The study shows that ignoring crossfall leads to an underestimation of the tyre loads and road damage [23]. The study however used a multibody simulation software package and not a user defined model as is used in this study. The study did not include the effect of different vehicle parameters on the dynamic road damage caused by the vehicle when including road crossfall. The vehicle selected also had a very low centre of gravity which would underestimate the damage produced when including road crossfall.

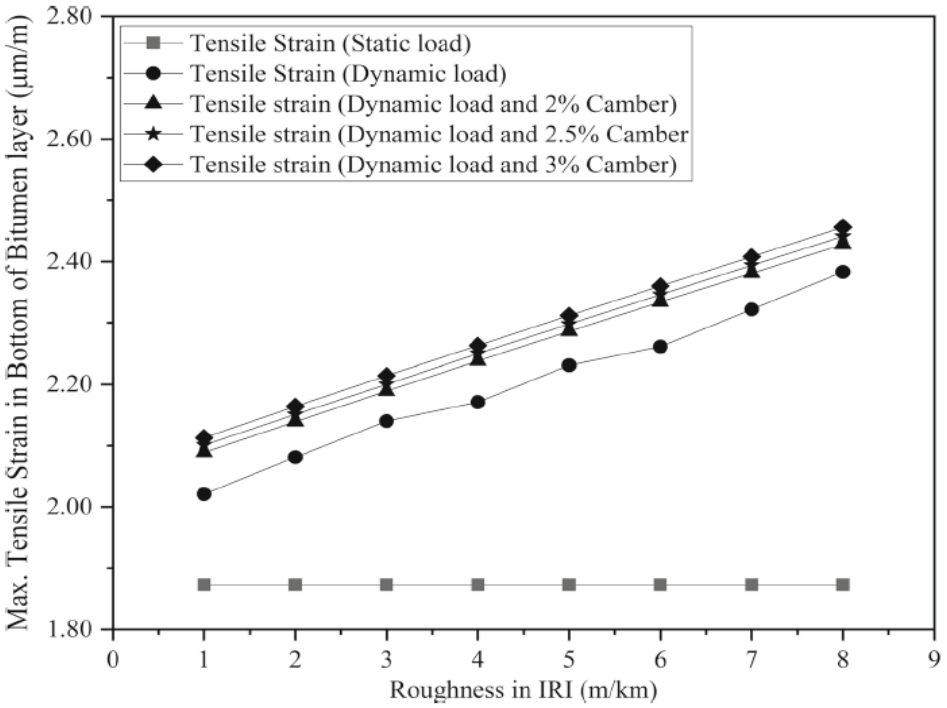

Figure 1.4: Tensile strain experienced by a bitumen layer at different roughness values and loading scenarios [22]

1.2.3. Road profile modelling

The road profile is the primary mechanism that excites the heavy vehicle suspension and produces the subsequent heavy vehicle dynamic forces being studied. In heavy vehicle modelling either measured road profile data can be used, or random road profiles can be created mathematically [24]. In this study, theoretical representative road profiles will be generated.

Road profiles can be represented using power spectral density (PSD) functions. The PSD is used to measure a signal's power content with respect to the frequency. The PSD plots the amplitude squared versus the frequency. The International Organization for Standards (ISO) has developed a classification scheme where all pavements can be grouped into eight different classes based on the PSD values of the road section (Class A to H) [25, 26]. ISO 8608 is frequently used to generate road profiles for use in heavy vehicle studies. The ISO standard uses a two-parameter spectrum to describe the smoothed PSD function of a road profile [25, 26].

The International Roughness Index (IRI) is a single-number value that is the most popular way to describe a road profile [27]. This value is obtained by using a simple 2 DOF linear vehicle model, known as the reference-quarter-car-simulation, and running it across the longitudinal road profile at a constant running speed of 80 km/h. The IRI is equal to the accumulated suspension stroke (m) in a reference passenger car, divided by the travelled distance (km) [27].

The main method used for developing random road profiles is the sinusoidal approximation method [26]. A single-track road profile can be mathematically constructed from the sum of a series of harmonics with different wavelengths, amplitudes and phases. Specifically, it is obtained by overlaying an infinite number of cosine waves ($N \rightarrow \infty$) [26].

The above-mentioned method describes the generation of a single-track road profile. For this study dual track random road profiles will be required for the full-car vehicle models. The second correlated random profile can similarly be generated using a coherence function between the left and right profiles. This coherence function can have different forms, but of those available, the 'isotropic' surface model is the most popular [12]. Many researchers now accept that the classic isotropic surface model is not adequate and better models have been proposed. Due to this large variation in the model values, the isotropic model remains widely used today. It has also been used in this study.

If the hypothesis of homogeneity and isotropy are assumed, then the surface description is simplified. In a homogenous and isotropic road surface every straight profile has the same statistical properties irrespective of the direction and position. Therefore, parallel profiles share statistical properties but are not the same [12].

Crossfall of a road refers to the change in height of the road profile perpendicular to the direction of travel and is illustrated in Figure 1.6. Crossfall values are incorporated into road design to ensure adequate draining of a road surface to prevent water pooling which would severely impact vehicle safety and damage road pavements [28].

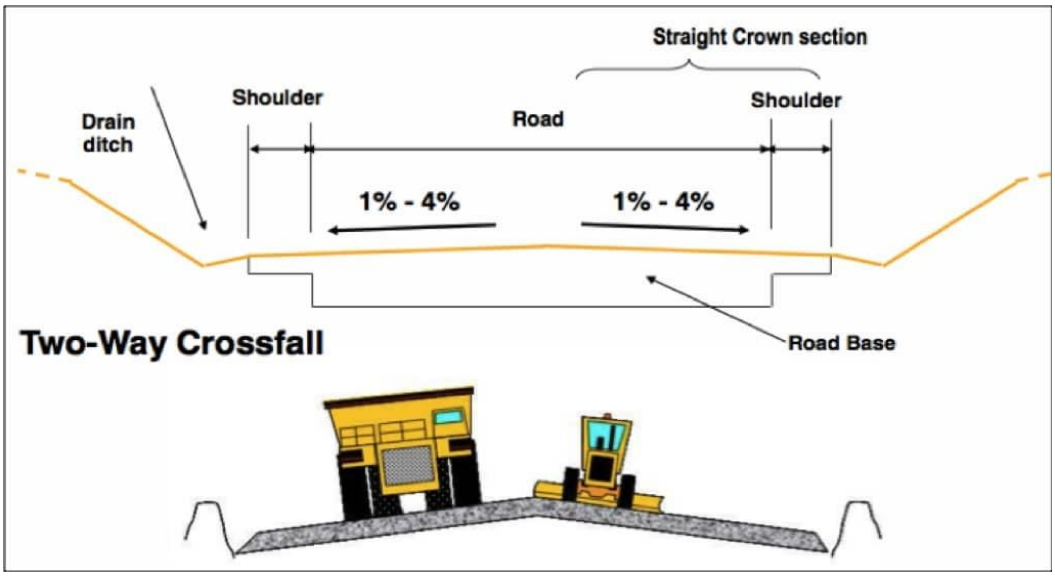

Figure 1.6: An example of road crossfall [54].

Road crossfall values differ across the world depending on local weather and traffic conditions. In South Africa a typical crossfall range of 2-3% is specified. Higher values are typically recommended on urban or gravel roads. Super elevation values can however be much higher and in South Africa for example a maximum value of 10% is specified in some cases, but typically ranges between 2-6% [28]. In South Africa the vehicles travel on the left side of the road and the road typically has a crossfall from right to left (right side is higher than the left), meaning that the left side is the outer edge of the road. This should be taken into consideration when reading this dissertation and adapted for countries where this may differ.

A recent study of actual Australian road surface road roughness values has shown that the left side road roughness was almost always higher than the right side for all the roads sampled. The effect of road crossfall is most likely the reason for a recorded difference in the left and right road roughness values of real road profiles as shown in Table 1.1 [29]. According to this Australian study differences of up to 38% were recorded between the road roughness of the left and right track. This increase in the road roughness on the left side compared to the right side will decrease the life of the road pavement and cause more damage on the vehicles that use the road pavement.

1.2.4. Significance of this research

This research will expand on the limited research done on the effect of road crossfall on dynamic road damage. The current research has either been limited to a static analysis or has not included

Table 1.1: Summary of data used in an Australian road study [35]

Road name	Road type	Length [km]	IRI (left) [m/km]	IRI (right) [m/km]	IRI (mean) [m/km]
Princes Hwy East	Metro. Highway	20.3	1.5	1.4	1.5
Murray Valley Hwy	Country Highway	43.8	1.6	1.4	1.5
Princes Hwy East	Metro. Highway	22.9	1.7	1.7	1.7
Princes Hwy East	Metro. Highway	3.3	1.7	1.6	1.7
Murray Valley Hwy	Country Highway	47.7	1.9	1.7	1.8
Princes Hwy East	Metro. Highway	3.4	2.3	1.8	2.1
South Gippsland Hwy	Country Highway	11.3	2.3	2.0	2.2
South Gippsland Hwy	Country Highway	21.8	2.6	2.1	2.4
South Gippsland Hwy	Country Highway	15.0	3.1	2.6	2.9
Midland Hwy	Country Highway	14.0	3.3	3.2	3.3
South Gippsland Hwy	Country Highway	60.8	3.6	3.3	3.5
Daylesford – Malmsbury Rd	Country Road	25.4	4.0	3.3	3.7
Northern Hwy	Country Highway	5.0	4.1	3.8	4.0
Lismore – Skipton Rd	Country Road	32.6	4.2	3.7	4.0
Bendigo – Maryborough Rd	Country Road	22.3	4.3	3.8	4.1
Wiltshire Lane	Country Road	2.3	4.2	4.1	4.2
Pyrenees Hwy	Country Highway	12.4	4.8	4.2	4.5
Timboon – Port Campbell Road	Country Road	8.0	6.3	4.3	5.3
Euroa – Mansfield Rd	Country Road	8.3	6.1	5.0	5.6

the relative influence of several parameters, especially heavy vehicle parameters. By performing this comprehensive dynamic study, an overview will be created on the relative importance of several vehicle and road parameters when including road crossfall in dynamic road wear studies. This will allow heavy vehicle operators, road designers and road managers to make informed decisions regarding maximizing the life of the road network. The research will also provide researchers with valuable insights on how to adapt their research to include the effect of road crossfall and provide a simple heavy vehicle model.

1.3. Research question and objectives

The literature review identified that current models that only use one dimensional or planar motion of heavy vehicles to study road-tyre forces and road damage underestimate the dynamic forces. This is due to lack of incorporation of the roll motion of the vehicle. A full-car vehicle model is required to study the effects of rolling motion on dynamic heavy vehicle forces and road damage. Only a single general vehicle configuration will be selected namely a 4x2 heavy vehicle (that is one drive and steer axle).

The research question that needs to be answered is: “How does heavy vehicle roll motion influence dynamic tyre forces and road damage and which parameters are most influential?”

The detailed objectives of this dissertation can therefore be summarized as follows:

1. Determine the relative influence of various magnitudes of road crossfall on dynamic road damage. A road crossfall ranging from 0% to 5% will be considered as this corresponds to typical values encountered in South Africa.
2. Identify the relative importance of the major road parameters which influence dynamic road damage due to road crossfall. The vehicle speeds considered range from 40 km/h to 120 km/h while the road roughness varies from 0.5 m/km to 10 m/km as identified from literature.

3. Identify the relative importance of the major vehicle parameters which influence dynamic road damage due to road crossfall. The most important heavy vehicle parameters identified from literature are:
    - Including anti-roll bars (stabilizers)
    - The sprung mass height
    - The roll centre height
    - The suspension stiffness
    - The damping value of the suspension
    - The tyre track width
    - The suspension track width
    - The effect of eccentric loads
    - The effect of the sprung mass value
    - The tyre stiffness values
4. Make recommendations on how to minimize the adverse effects of road crossfall (if any) on road pavements.

1.4. Methodology and Resources

A full-car vehicle model that includes pitch and rolling motion was developed using Simulink® in Matlab®. The dual track road profiles were similarly created using Matlab®. The ISO 8608 method was used to create the first road profile and the assumption of surface homogeneity and isotropy was used to generate the second correlated road profile. The IRI values considered in this study vary from 0.5 m/km to 10 m/km. This represents a range from superhighways to poorly managed paved roads [30]. Road crossfall values between 0% to 5% are included in the road profiles as this corresponds to typical values found in South Africa and across the world. Vehicle speeds between 40 km/h and 120 km/h were simulated. This represents minimum and maximum speeds in South Africa. Heavy vehicles are technically limited to 80 km/h but from telematics data it has been observed that heavy vehicles travel at speeds in excess of 120 km/h. The road profiles were 1 km long.

The validation of the full car model was done using TruckSim 2019.1®. The software is a commercially available multibody simulation tool capable of assessing the performance of complex vehicle models performing complex manoeuvres. The user-defined model has the advantage of requiring significantly cheaper software to develop and has quicker run times compared to the commercially available software package (TruckSim 2019.1®). Although TruckSim 2019.1® is able to take into account a larger amount of vehicle parameters and arguably produce results with higher accuracy, the user-defined model allows one to consider only the critical parameters of interest and

eliminate the other parameters that may potentially cloud and distort the results. This allows for a more fundamental understanding of the impact of the selected parameters to be developed.

A single 4x2 full-car vehicle model was developed that includes the vehicle parameters that most influence the rolling motion of a heavy vehicle. The representative vehicle parameters were obtained from various sources based on other heavy vehicle studies and have been summarized in Appendix C. Linear models were used for suspension components in order to simplify the analysis for the first iteration.

The dynamic tyre forces and road damage criteria selected for this study were the DLC and aggregate tyre forces criterion (first and fourth power aggregate forces). By employing the different criteria, information can be obtained on the road damage for an entire road section or per location.

After the effect of road roughness, vehicle speed and crossfall were studied on the base model, several heavy vehicle parameters that influence vehicle roll over and dynamic road damage were studied. The parameters studied are:

- Including anti-roll bars (stabilizers)
- The sprung mass height
- The roll centre height
- The suspension stiffness
- The damping value of the suspension
- The tyre track width
- The suspension track width
- The effect of eccentric loads
- The effect of the sprung mass value
- The tyre stiffness values

This study is a simulation-based study and the simulation software used has been discussed in this proposal. The software and hardware required for this study are summarized in Table 1.2.

Table 1.2: Primary resources required for study

Resource	Model/Version	Details
Work computer (Obtained from the CSIR)	Dell™ Latitude™ E5590	Processor: Intell Core ™ i7-8650HQ CPU @ 1.90GHz with 16 GB RAM
MATLAB® and SIMULINK® © The MathWorks Inc.	R2020a	Student licence version available via Wits University
TruckSim®	Version 2019 A	Licensed to CSIR BE (Licence #: K121793)

2. Development and Validation of Vehicle Models

The main objective of this study is to develop a full-car heavy vehicle that can include rolling motion to account for the effects of road crossfall. This section of the dissertation discusses the development and validation of the various models required to achieve this objective. Subsection 2.1 provides a more qualitative literature review on the concepts introduced in Subsection 1.2. Subsection 2.2 focusses on the development and validation of the dual track road profiles. Subsection 2.3 focusses on the development and validation of the full-car heavy vehicle model. Additional information and results are presented in Appendix A to Appendix D with Appendix A containing additional information related to the road profiles created and their validation results, Appendix B contains the TruckSim2019.1® input data, Appendix C contains additional information on the user-developed model and Appendix D contains additional validation results.

2.1. Dual track road profiles and validation

2.1.1. Detailed literature road profiles and road damage criteria

A qualitative introduction is given to the road profiles and road damage criteria considered in this dissertation in Subsection 1.2. This section contains a more detailed qualitative description of the relevant literature topics.

The DLC is commonly used to characterize the magnitude of dynamic tyre and is defined as in Equation 22 [12].

$$DLC = \frac{RMS\ dynamic\ tyre\ force}{Static\ tyre\ force} \tag{2}$$

Figure 2.1 shows the effect of heavy vehicle loads and speeds on the DLC of the vehicle when using linear suspension models. A linear increase in the DLC is observed for an increase in the road roughness. The DLC has a linear relationship with the square root of the vehicle speed and decreases with an increase in vehicle loading. [23]. The results also show that lowering the heavy vehicle load, increases the DLC calculated for the vehicle [10]. These studies show that the DLCs of heavy vehicles typically range from 0.05 to 0.3 under typical operating conditions. These studies also all clearly illustrate that softer air suspension is more road friendly and encouraged to reduce dynamic road damage [10].

The spatial distribution of tyre forces is an important factor in dynamic road damage studies. Such an analysis allows one to identify areas where road damage tends to accumulate relative to other sections on a route. The aggregate tyre forces criteria allow for such spatial distributions to be investigated and is defined as shown in Equation 3 [8, 12]

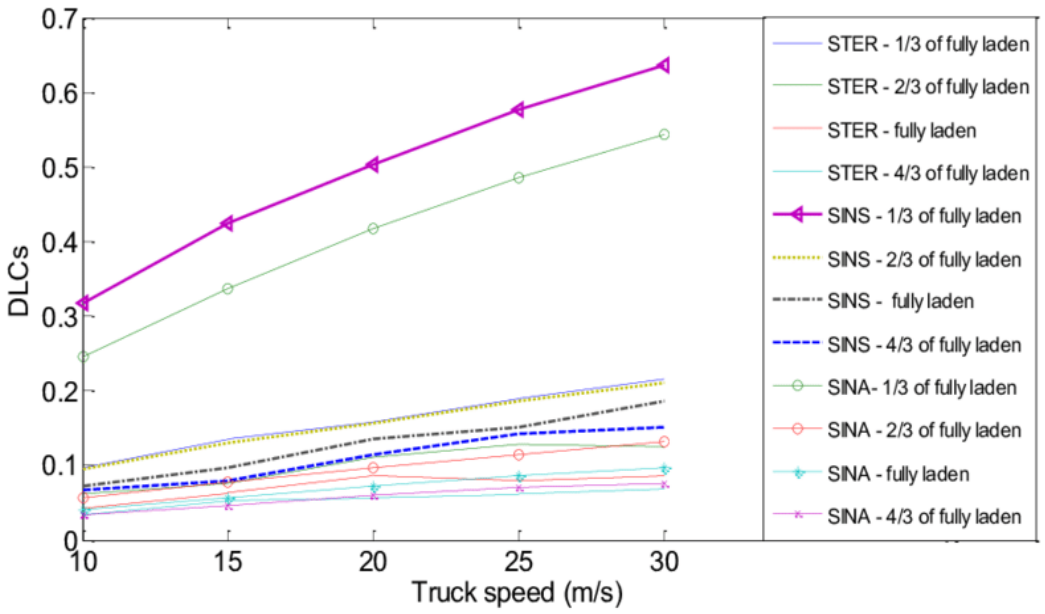

Figure 2.1: DLC of heavy vehicles at various vehicle speeds and loads [10]

$$A_k^n = \sum_{j=1}^{N_a} P_{jk}^n \quad \mathrm{k} = 1,2,3,\dots,\mathrm{Ns} \tag{3}$$

Where A_k^n is the aggregate nth power force, P_{jk} is the force applied by tyre j to location or station k on the road, N_a is the number of axles on the vehicle and N_s is the number of points or stations of interest along the road. The power (n) is chosen based on the type of road damage that is being considered. For flexible pavements a value of $n = 1$ is best suited for permanent road deformation and $n = 4$ is best suited for fatigue damage [8, 12]. It has been found that the ratio of the instantaneous fourth power force to the static fourth power force can exceed 3 which indicates how the peak dynamic loads can be substantially higher at certain locations and cause more damage at specific sections [8, 12].

The ratio of the 95th percentile aggregate force to the static aggregate force is often used as the road damage criteria in numerous road studies. It is also referred to as the dynamic aggregate force coefficient (DAFC) and can be estimated from Equation 4 [8, 12].

$$DAFC = \frac{1.65 \cdot \sigma_A^4}{m_{A^4}} + 1 \tag{4}$$

Where σ_{A^4} is the standard deviation of the fourth power aggregate forces and m_{A^4} is the static fourth power force [8, 12].

Equation 3 can be used to compare the road-damaging potential of different vehicles, provided that all of the tyres are assumed to have the same contact area. The calculation method can be enhanced by dividing each individual wheel force by an appropriate nominal tyre contact area. The damage

prediction is then based on the nominal contact stress. The resulting "damage" is then given as shown in Equation 5 [12].

$$D_k^n = \sum_{j=1}^{N_a} \left(\frac{P_{jk}}{a_j}\right)^n \quad \mathrm{k} = 1,2,3,\dots,N_s \tag{5}$$

Where a_j is the nominal contact area of tyre j [12].

Equation 5 does not account for the dynamic variation of the contact area with varying dynamic tyre loads. This is however usually considered to be a second order effect. Equation 5 can be further refined by including an appropriate material constant and can then be used to consider the fatigue damage caused by the vehicle [12].

The International Organization for Standards (ISO) has developed a classification scheme where all pavements can be grouped into eight different classes based on the PSD values of the road section (Class A to H) [25, 26]. ISO 8608 is frequently used to generate road profiles for use in heavy vehicle studies. The ISO standard uses a two parameter spectrum to describe the smoothed PSD function of a road profile, $Z(x)$, as shown in Equation 6 [25, 26]:

$$G(n) = G(n_o)\left(\frac{n}{n_0}\right)^{-w} \tag{6}$$

Where $G(n)$ is the one-sided PSD (m^3), n is the spatial frequency or wave number (m^{-1}), n_0 is the reference spatial frequency (usually 0.1 m^{-1}), $G(n_o)$ (often referred to as the roughness index) is the PSD value at the reference spatial frequency n_0, and w is referred to as the waviness. The value of w is usually taken as 2 [25, 26] in all ISO calculations and will also be used in this study. The PSDs according to the ISO 8608 classification are shown in Figure 2.2.

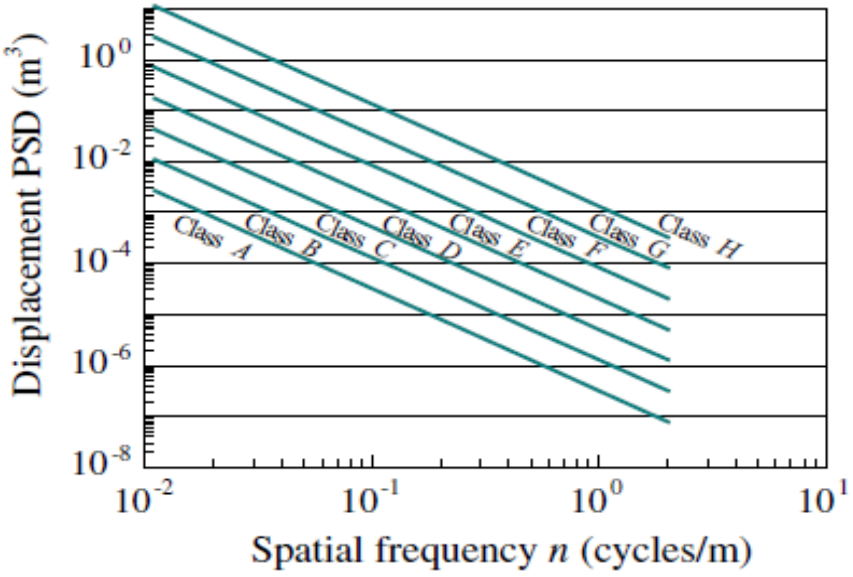

Figure 2.2: Classification of road profiles according to ISO 8608 for an exponent value of w = 2 [53]

The International Roughness Index (IRI) is a single-number value that is the most popular way to describe a road profile [27]. Figure 2.3 shows typical IRI values for different types of roads.

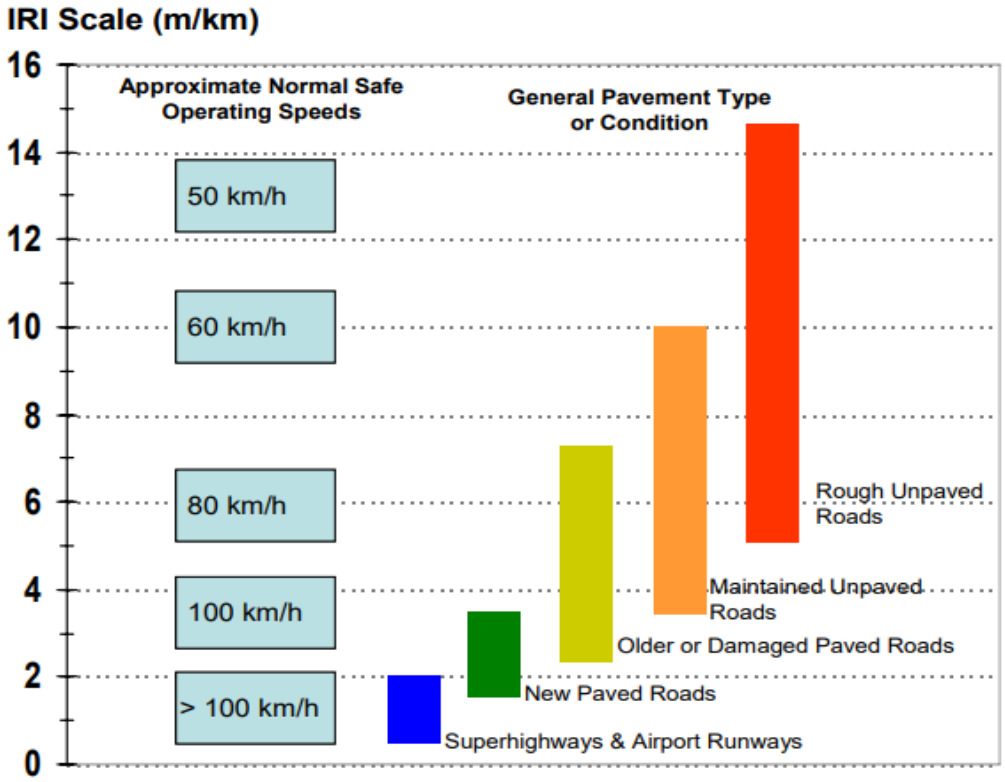

Figure 2.3: Typical IRI values and the associated operating speeds of vehicles [36]

A simple approximate relationship exists between the IRI and roughness index ($G(n_o)$) for a waviness value of $w = 2$, as shown in Equation 7 [26, 27].

$$IRI = a\sqrt{\frac{G(n_o)}{16}} \tag{7}$$

Where *a* is a coefficient equal to 2.21 as obtained from extensive simulation studies [27].

The main method used for developing random road profiles is the sinusoidal approximation method [26]. Specifically it is obtained by overlaying an infinite number of cosine waves ($N \to \infty$) as described in Equation 8 [26].

$$Z(x) = \sum_{i=1}^{N} A_i \cos(2\pi n_i \cdot x + \phi_i) \tag{8}$$

Where $Z(x)$ is the height of a point in the road profile at point x, n_i is the spatial frequency, ϕ_i are phase angles that are treated as a random variable with a uniform distribution in the interval [0,2π]. A_i is defined as shown in Equation 9 [26].

$$A_i = \sqrt{2G(n_i)\Delta n} \tag{9}$$

Where $G(n_i)$ is the calculated PSD value from Equation 6, and $\Delta n = \frac{n_{max}-n_{min}}{N}$. n_{min} is usually taken as 0.01 m^{-1} and n_{max} as 10 m^{-1} which corresponds to wavelengths of 100 m and 0.1 m respectively. N is typically taken as 2 000 or more [26].

The above-mentioned method describes the generation of a single-track road profile. For this study dual track random road profiles will be required for the full-car vehicle models. The second correlated random profile can similarly be generated using a coherence function between the left and right profiles. This coherence function can have different forms, but of those available, the 'isotropic' surface model is the most popular [12]. Many researchers now accept that the classic isotropic surface model is not adequate and better models have been proposed such as the one illustrated in Equation 10.

$$\gamma_{lr}^2(n,\rho) = \left[1 + \left(\frac{n\rho^a}{n_p}\right)^w\right]^{-2p} \tag{10}$$

Where γ is the coherence values between the left and right profiles, n is the spatial frequency, ρ the track width, w the undulation exponent and a, n_p and p are arbitrary constants. Fitting of the model proposed in Equation 10 has yielded a large scatter of the values for the values of a, n_p and p [31]. Due to this large variation in the model values, the isotropic model remains widely used today. It has also been used in this study.

If the hypothesis of homogeneity and isotropy are assumed, then the surface description is simplified. In a homogenous and isotropic road surface every straight profile has the same statistical properties irrespective of the direction and position. Therefore, parallel profiles share statistical properties but are not the same.

To better understand this consider Figure 2.4, with any surface $r(x,y)$ where r is the distance from the two parallel profiles $r_l(x)$ and $r_r(x)$ to the orthogonal $O_{xy}\ plane$ that are spaced a distance of $2b$ apart (the track width). The autocorrelation functions of these two profiles fulfil the condition of being equal as specified in Equation 11 [32].

$$R_L(\delta) = R_R(\delta) = R(\delta) \tag{11}$$

Where R_L and R_L are the autocorrelation function of the left and right profile at a longitudinal distance of δ [32].

The cross-correlation functions will also be equal due to homogeneous and isotropic conditions as shown in Equation 12.

$$R_{LR}(\delta) = R_{RL}(\delta) = R_x(\delta) \tag{12}$$

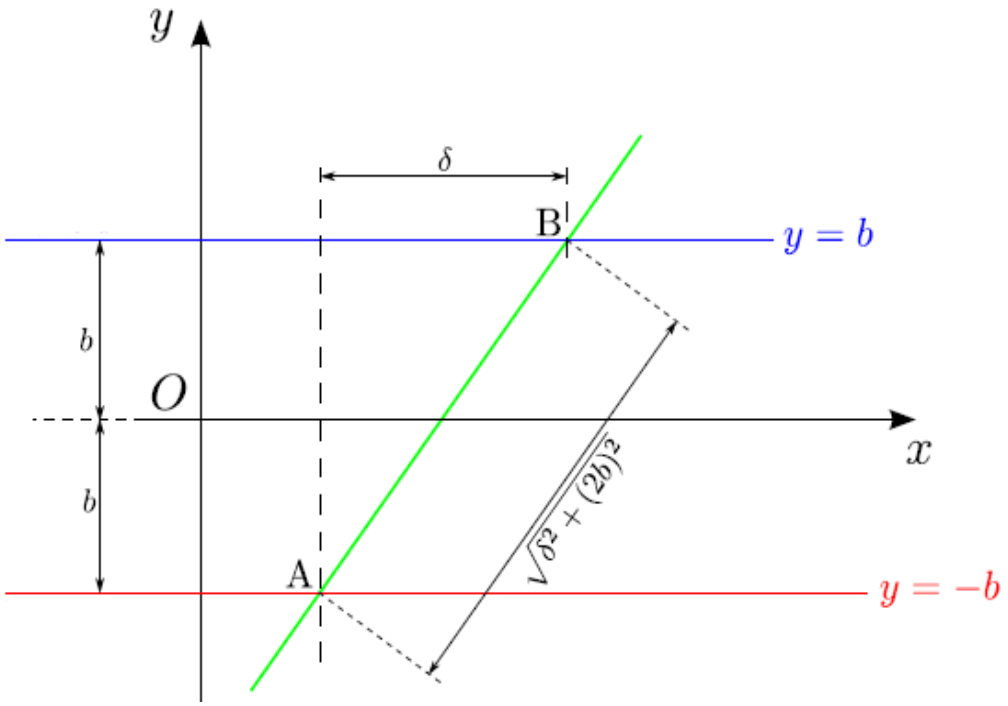

Figure 2.4: Parallel profiles in an isotropic and homogeneous surface [29]

Due to the homogeneous and isotropic conditions, the cross correlation function will be the same at points A and B that are separated by a distance of $\sqrt{\delta^2 + (2b)^2}$ as shown Figure 2.4 and Equation 13.

$$R_x(\delta) = R\left(\sqrt{\delta^2 + (2b)^2}\right) \tag{13}$$

The cross-PSD ($G_x(n)$) for a pair of profiles is unique and can be obtained from the direct spectral density which is identical for both profiles [33, 34]. The PSD as defined in Equation 6 does not satisfy the isotropy admissibility conditions as it is an unbounded integral. The PSD from Equation 6 is altered and set equal to a constant below a limiting wavenumber n_a=n_{min}. The PSD is therefore defined as shown in Equation 14 and Figure 2.5.

$$G(n) = \begin{matrix} G(n_o)\left(\frac{n_a}{n_o}\right)^{-2} \; if \; n \leq n_a \\ G(n_o)\left(\frac{n}{n_o}\right)^{-2} \; if \; n > n_a \end{matrix} \tag{14}$$

The cross correlation R_x between the parallel tracks is unique and given by Equation 15 [34].

$$R_x(\delta) = \frac{2G(n_o)}{n_o^{-2}}\left(n_a^{-1}\frac{\sin\left(2\pi n_a\sqrt{\delta^2 + (2b)^2}\right)}{2\pi n_a\sqrt{\delta^2 + (2b)^2}} + \int_{n_a}^{\infty}\frac{\cos\left(2\pi n\sqrt{\delta^2 + (2b)^2}\right.}{n^2}dn\right) \tag{15}$$

Where δ is the longitudinal distance between two points on a single track and b is half the transverse distance between the road profiles [34].

Once R_x has been computed, G_x is calculated by means of a Fourier Transform or using an analytical method developed by Kamash [34]. Stochastic processes of this kind are typically defined through

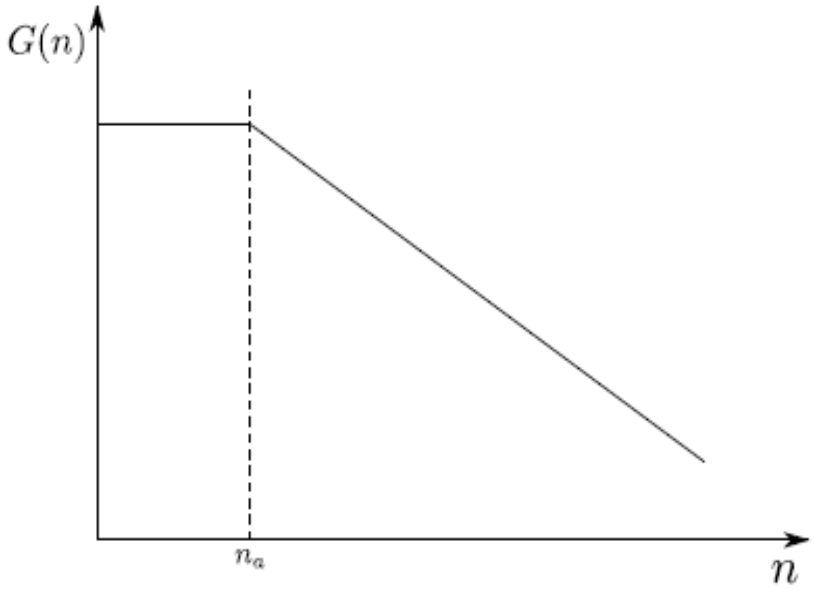

Figure 2.5: Modified ISO-8608 spectral density function in order to represent homogeneous and isotropic road profiles (logarithmic scale) [29]

the coherency function $g(n)$ instead of the cross-PSD. For a homogeneous and isotropic surface, the two parallel direct spectral densities are equal ($G_1(n) = G_2(n) = G(n)$) and the same is true for the two cross-spectral densities ($G_{21}(n) = G_{12}(n) = G_x(n)$). The coherency function is defined as shown in Equation 16 [35]. The isotropic coherence function for different track widths are shown in Figure 2.6.

$$g(n) = \frac{|G_x(n)|}{G(n)} \tag{16}$$

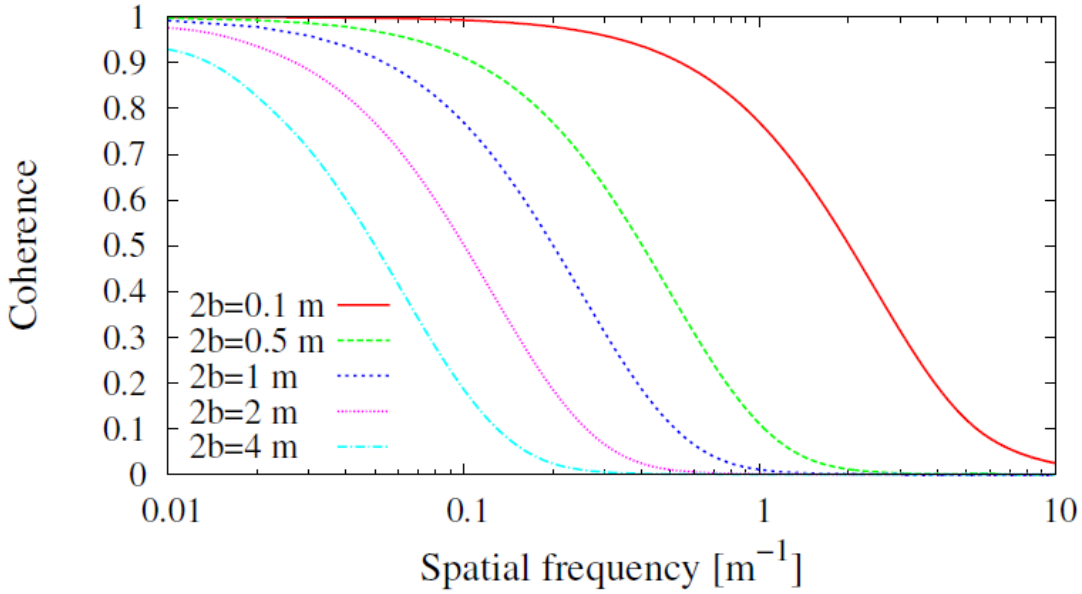

Figure 2.6: Coherence function for an isotropic and homogeneous road for different distances between profiles [29].

The second road profile can now be calculated using Equation 17 [36].

$$Z_2(x) = \sum_{i=1}^{N} \sqrt{2G_x(n_i)\Delta n}\cos(2\pi n_i \cdot x + \phi_i) + \sqrt{2(G(n_i) - G_x(n_i))\Delta n}\cos(2\pi n_i \cdot x + \theta_i)) \quad (17)$$

Where θ_i is a new set of random phase angles in the interval [0,2π].

2.1.2. Coherence function and basic assumptions

The road profile is the primary input into the frequency response of the heavy vehicle and needs to be accurately modelled. This is especially true when considering dual track road profiles.

Different methods exist for creating artificial road profiles, but the most common method overlays an infinite number of cosine waves ($N \to \infty$) as described in Equation 8 [26]. The second road profile is obtained by assuming a specific coherence function between the two profiles. For this study, the isotropic and homogenous coherence model was assumed. The second road profile can now be calculated using Equation 17.

The coherence and cross-PSD values are calculated using the Kamash analytical method [34]. The typical spatial frequency range recommended for creating artificial road profiles is 0.01 m^{-1} and 10 m^{-1} which corresponds to wavelengths of 100 m and 0.1 m respectively [34, 37]. The resolution was set to 0.001 m^{-1} as is recommended in literature [36]. This generates a total of 9991 points to be used in creating artificial road profiles which is more than sufficient as many other authors use 2000 points when creating road profiles [26].

It is not necessary to calculate the coherence and cross-PSD values over this entire spatial frequency range as high frequency values have a negligible effect when creating the second correlated road profile [12, 35]. In other similar studies the maximum spatial frequency used to calculate the cross-PSD value has ranged from 0.04 m^{-1} to 0.4 m^{-1} [12, 35]. For this study the cut off spatial frequency was set at 0.5 m^{-1} with the coherence value being approximately 0.005 (i.e. the cross-PSD value of the road profile is only 0.5% of the road profile PSD value). All other coherence values were set equal to zero which means the cross-PSD values are also then taken as zero. A track width of 2 m was used as this is a typical value used on heavy vehicles [12].

The resultant coherence values obtained are compared to a commercially available package (PRP generator) in Figure 2.7 [32]. The results agree very well and confirm the accuracy of the results obtained.

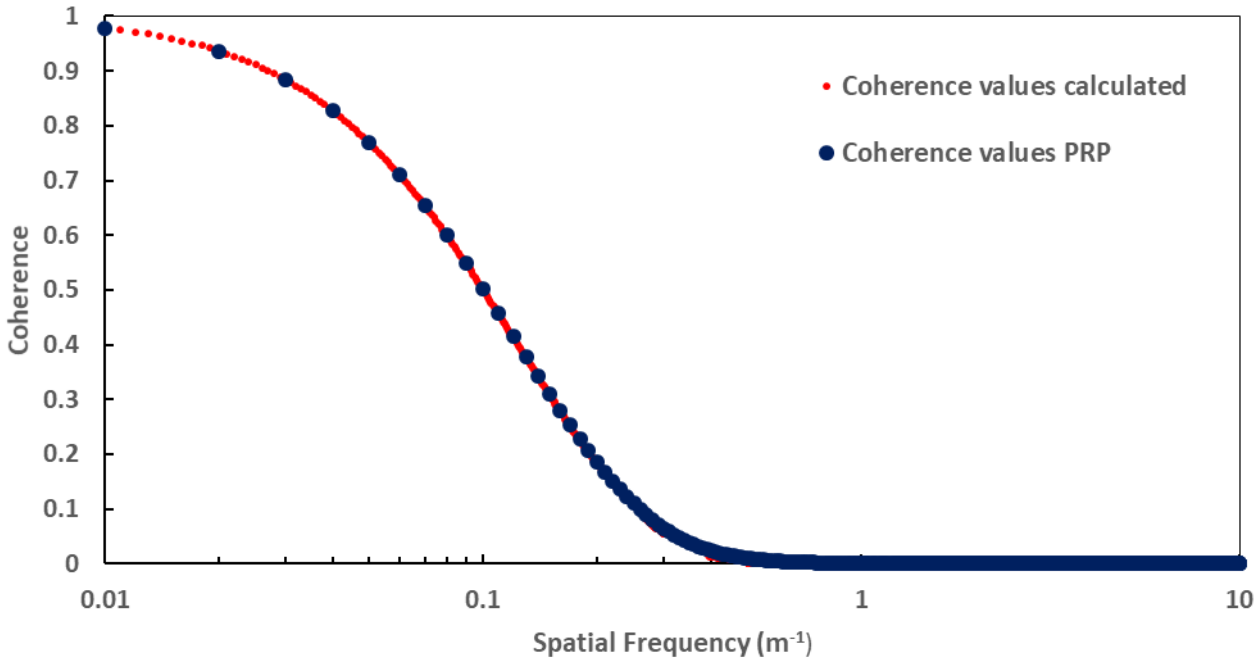

Figure 2.7: Comparison of coherence values calculated to commercially available solution (PRP generator)

In order to accurately capture any dynamic tyre force patterns, the road profile resolution was set to 10 mm. This provides a reasonable accuracy whilst also reducing the computation time required. Higher resolutions will add limited value to the overall result.

2.1.3. Creating and validating dual track road profiles

The profiles used in this study are presented in Appendix A. The results for a road profile with an IRI of 2m/km is discussed in this section. Using Equation 7, any IRI value can be converted to the appropriate reference PSD values ($G(n_o)$). Using Equation 8 and Equation 17, the dual track road profiles can now be created. In Figure 2.8 the road profile for an IRI of 2 m/km is shown. It should be noted that this road profile and the other profiles in Appendix A represent the road profiles without crossfall. In South Africa the vehicles travel on the left side of the road and the road typically has a crossfall from right to left (right side is higher than the left), meaning that the left side is the outer edge of the road. This should be taken into consideration when reading this dissertation and adapted for countries where this may differ.

In order to allow the vehicle models to equalize during initialization an introduction length of 50 m was added. The road profile increases from zero up to the first artificial road profile point created for the left and right track profiles. An alternative approach would be to ignore the initial data points for a selected number of time constants.

The IRI values of the created road profiles can be validated by using the golden quarter-car simulation method [38]. The results of the actual IRI values compared to the design IRI values are summarized for all the road profiles in Table 2.1. The results show that all the road profiles have

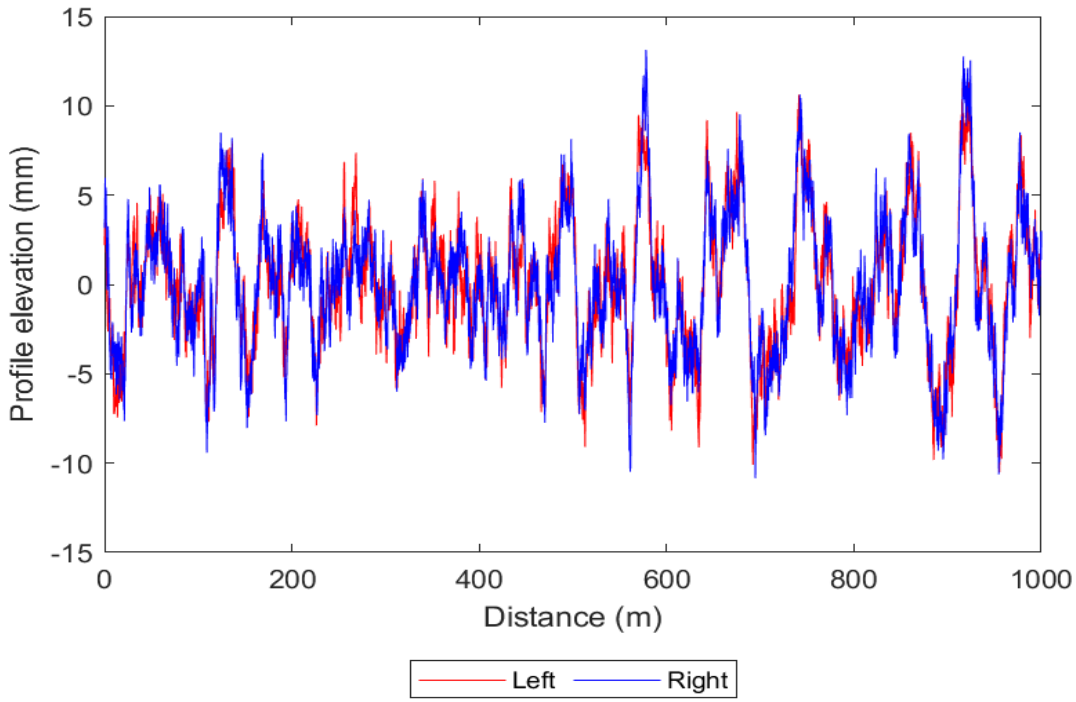

Figure 2.8: Created dual track road profiles with a design IRI of 2m/km.

an actual IRI value close to the design value and that all the left side profiles have an error of 1.7% and the right side an error of 0.6%. This is acceptable and conservative as the crossfall will increase the loads experienced on the left side of the vehicle. Therefore, a lower IRI on the left profile will ensure that the comparison of the left and right profile aggregate forces is conservative and will not exaggerate the results. Recent research in Australia [29] has shown that the left profile always has a higher IRI value compared to the right profile and the two profile values and this can be taken into account in future research as more data is available. This study provides a conservative estimate of the difference in the left and right road damage.

Table 2.1: Comparison of design vs actual IRI values achieved in road profiles

Design IRI (m/km)	Left profile actual IRI (m/km)	% Difference between design and actual IRI (%)	Right profile actual IRI (m/km)	% Difference between design and actual IRI (%)
0.5	0.491	-1.7	0.497	-0.6
1	0.983	-1.7	0.994	-0.6
2	1.965	-1.7	1.989	-0.6
3	2.948	-1.7	2.983	-0.6
4	3.930	-1.7	3.978	-0.6
5	4.913	-1.7	4.972	-0.6
6	5.895	-1.7	5.966	-0.6
8	7.860	-1.7	7.955	-0.6
10	9.825	-1.7	9.944	-0.6

Classifying a road profile by the IRI value alone is insufficient and the PSD distribution of the profile also needs to be validated. The PSD and cross-PSD distributions of the road profiles were calculated

using the Welch approximation method as defined in Matlab® [39, 40]. The PSD and cross-PSD results for a road profile with an IRI of 2 m/km is shown in Figure 2.9.

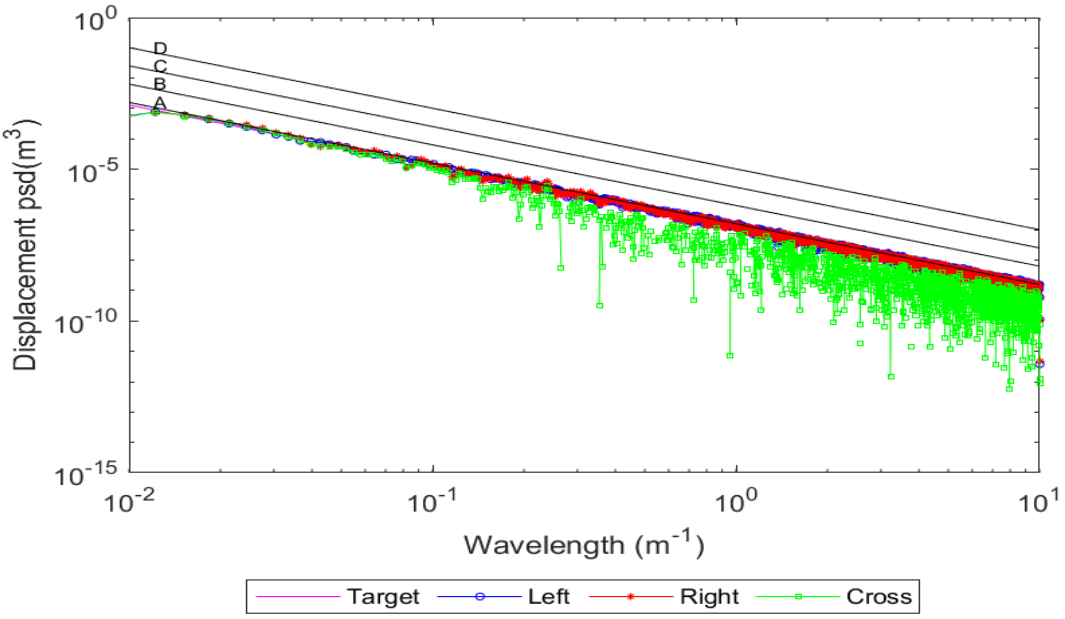

Figure 2.9: The PSD values of the road profiles with a design IRI of 2 m/km

The results shown in Figure 2.9 indicate that the created road profile PSD values for both road profiles very closely follow the target or design PSD values. The cross-PSD value results also appear accurate as the cross-PSD values are equal to the PSD values at lower wavelengths and become smaller than the PSD values at higher wavelengths as expected [41].

The results shown in Figure 2.9 are not yet smoothed according to the ISO 8608 standard [37]. For the test section of 1 km, the unsmoothed results are sufficiently accurate for validation purposes. The smoothed PSD values were however calculated as this is prescribed in the ISO 8608 standard. The smoothed PSD for the road profile with an IRI of 2 m/km is shown in Figure 2.10. The smoothed PSD graphs of the other road profiles are summarized in Appendix A.

The final validation performed on the road profiles was calculating the coherence between the left and right road profiles. The coherence values as a function of the spatial frequency can be calculated as shown in Equation 18.

$$\gamma^2(n) = \frac{|G_{LR}(n)|^2}{G_L(n) \cdot G_R(n)} \tag{18}$$

Where γ is the coherence value between the left and right profiles, n is the spatial frequency $G_{LR}(n)$ is the cross-PSD value of the left and right road profiles, and $G_L(n)$ and $G_R(n)$ are the left and right road profile PSD values. It should be noted that the coherence graph for all dual track road profiles are identical. The coherence values obtained are compared to the design values in Figure 2.11. The results show that the road profiles coherence matches the design coherence values closely.

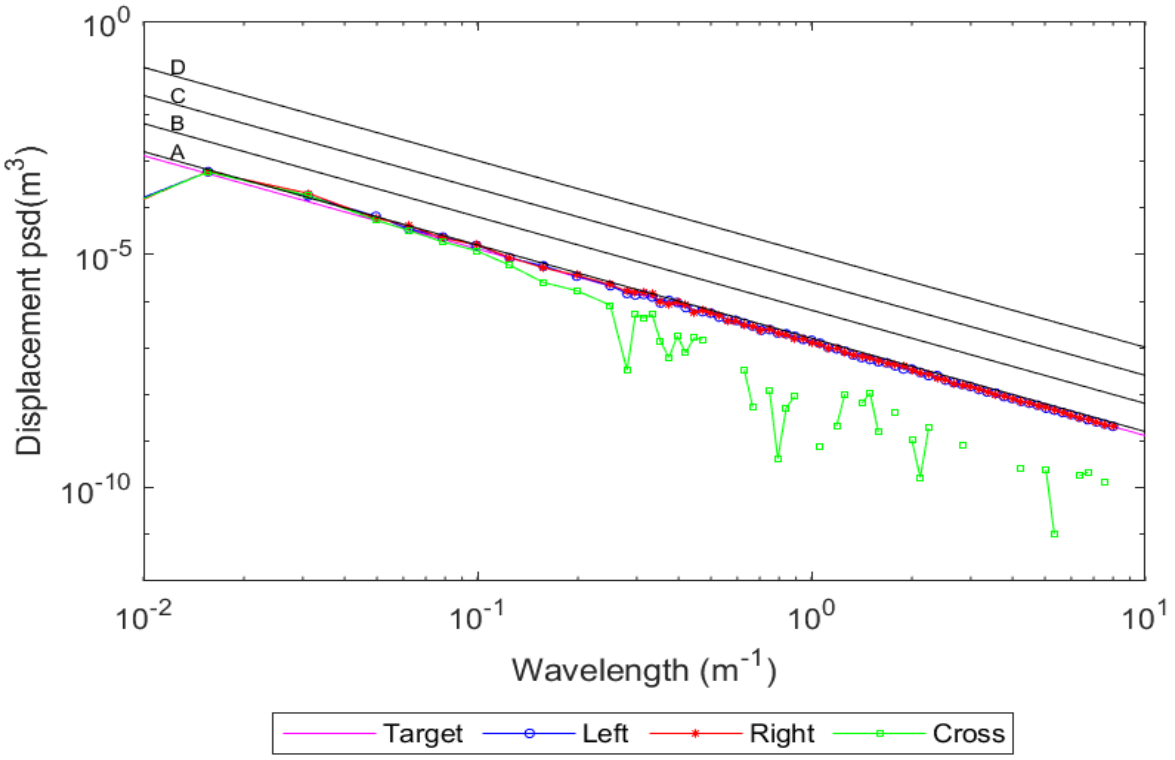

Figure 2.10: The Smoothed PSD values of the road profiles with a design IRI of 2 m/km

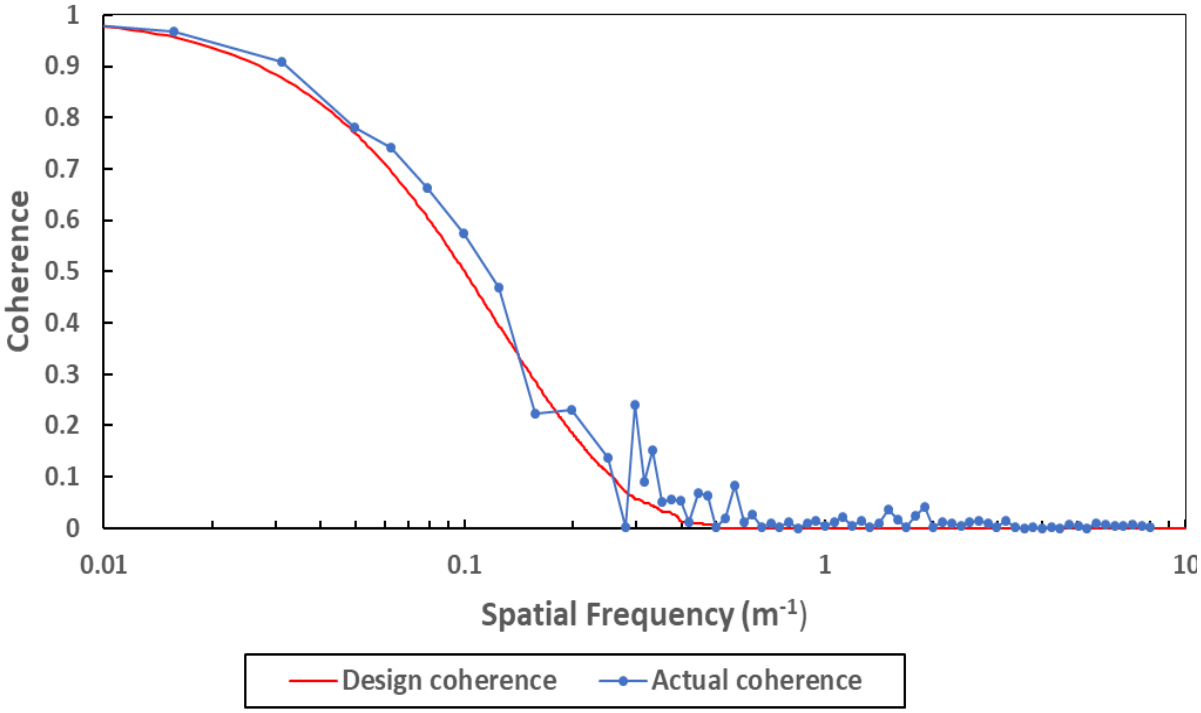

Figure 2.11: Comparison of design and actual coherence values of the dual track road profiles

The results in this subsection indicate that the dual track profiles have been successfully created and validated for further use in this dissertation.

2.2. Development of the full-car heavy vehicle dynamic model including rolling motion

No work could be found that implements user defined models to model the dynamic forces of heavy vehicles when including crossfall of a road profile.

The first aim was to develop and validate a user defined model for a flat surface and is done in subsection 2.3.1. The model was then further validated at different vehicle speeds and road roughness values in subsection 2.3.2. Lastly the model was validated when including road crossfall and other rolling motion in subsection 2.3.3.

The user defined heavy vehicle model proposed is a 9 DoF model that incorporates pitch and rolling motion. The degrees of freedom are:

1. Vertical motion of the sprung mass
2. Lateral motion of the sprung mass
3. Rolling motion of the sprung mass
4. Pitching motion of the sprung mass
5. Vertical motion of unsprung mass
6. Rolling motion of the unsprung mass
7. Eccentricity of the sprung mass
8. Front axle lateral tyre forces
9. Rear axle lateral tyre forces

Yaw motion has been excluded as the vehicle moves in a straight line and the addition of yaw motion adds very little accuracy under typical operating conditions as is shown when validating the heavy vehicle model. The heavy vehicle model developed is based on models developed by Cole and Cebon [42]. The pitch-roll vehicle model is presented in Figure 2.12 and Figure 2.13 for a flat surface.

The pitching motion of the sprung mass on a flat surface is described by Equation 19.

$$\begin{aligned}(I_{sp} + m_s \cdot (h - h_1)^2) \cdot \ddot{\Phi}_{sy} = (F_{srl} + F_{drl} + F_{srr} + F_{drr}) \cdot b \\ -(F_{sfl} + F_{dfl} + F_{sfr} + F_{dfr}) \cdot a\end{aligned} \tag{19}$$

Where I_{sp} is the sprung mass pitching moment of inertia, m_s is the sprung mass, h is the height of the sprung mass from the floor, h_1 is the roll centre height from the floor, $\ddot{\Phi}_{sy}$ is the sprung mass pitch angular acceleration, a is the distance from the front axle to the sprung mass centre of

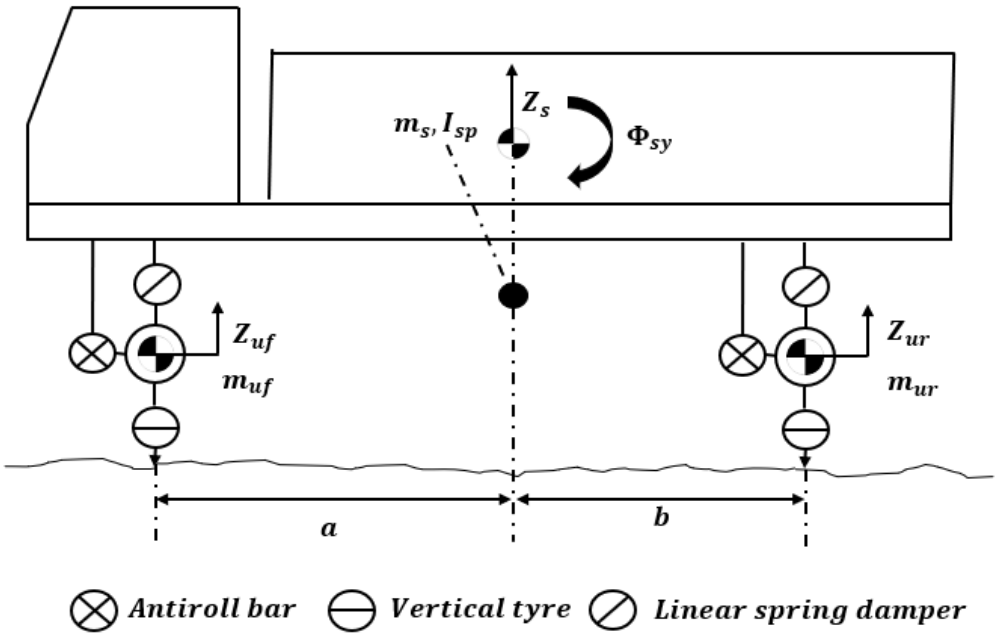

Figure 2.12: Pitching motion of the developed heavy vehicle model

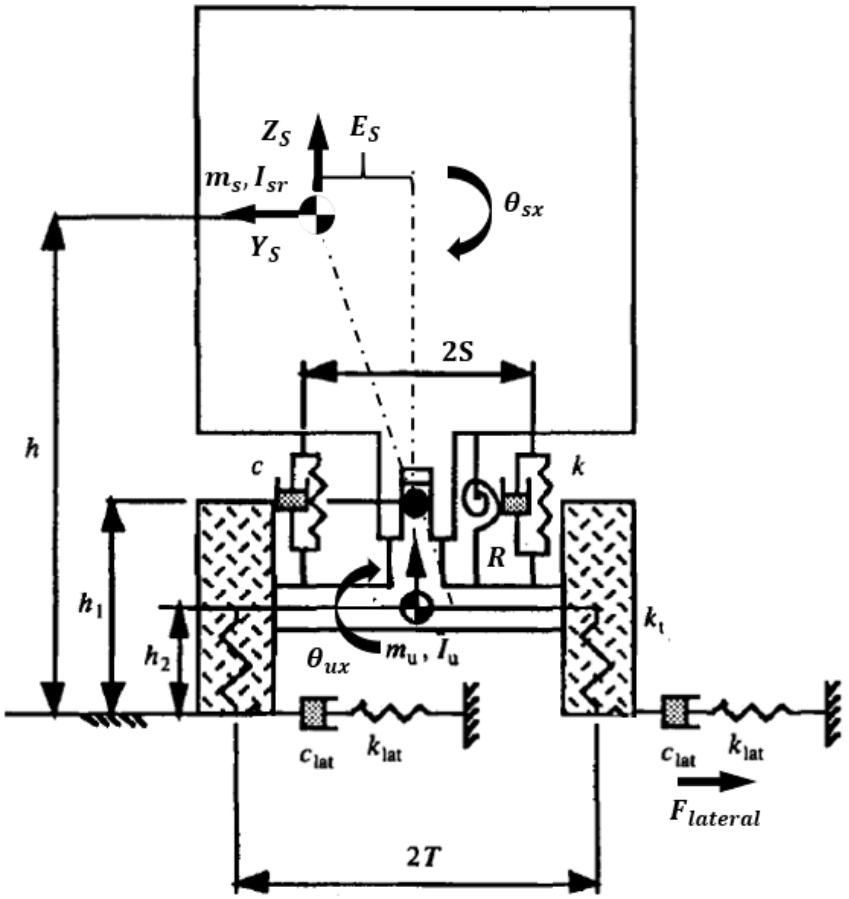

Figure 2.13: Rolling motion of the developed heavy vehicle model on flat surface modified from [42]

gravity, b is the distance from the rear axle to the sprung mass centre of gravity. The first letter of the force subscript refers to whether it is a spring or damper force (F_s refers to a spring force and

F_d refers to a damper force), while the last two letters refer to the position with the second letter referring to either front or rear and the last letter referring to left or right. As an example, F_{drl} refers to the damper force of the rear left tyre position.

The rolling motion of the sprung mass on a flat surface is described by Equation 20

$$(I_{sr} + m_s(h-h_1)^2) \cdot \ddot{\theta}_{sx} = m_s\,(h-h_1) \cdot \left(\ddot{Y}_s + g \cdot (\theta_{sx} + E_s)\right) + (F_{sfl} + F_{dfl} - F_{sfr} - F_{dfr}\,) \cdot S_f \qquad (20)$$
$$+ (F_{drl} + F_{drl} - F_{srr} - F_{drr}\,) \cdot S_r - R_f \cdot (\theta_{sx} - \theta_{ufx}) - R_r \cdot (\theta_{sx} - \theta_{urx})$$

Where I_{sr} is the sprung mass rolling motion moment of inertia, $\ddot{\theta}_{sx}$ is the sprung mass rolling angular acceleration, $\ddot{Y}$ is the sprung mass lateral acceleration, g is the gravitational acceleration, θ_{sx} is the sprung mass roll angle, E_s is the lateral eccentricity of the sprung mass. S_f is half of the front spring track, S_r is half of the rear spring track, R_f is the front anti-roll bar stiffness, R_r is the rear anti-roll bar stiffness, θ_{sx} is the sprung mass roll angle, θ_{ufx} is the front unsprung mass roll angle, θ_{urx} is the rear unsprung mass roll angle. Other symbols have been previously introduced and are available in the list of symbols.

The vertical motion of the sprung mass on a flat surface is described by Equation 21.

$$m_s \cdot \ddot{Z}_s = F_{sfl} + F_{dfl} + F_{sfr} + F_{dfr} + F_{srl} + F_{drl} + F_{srr} + F_{drr} \qquad (21)$$

Where $\ddot{Z}_s$ is the vertical acceleration of the sprung mass and the other symbols have been introduced previously and are available in the list of symbols.

The lateral motion of the sprung mass on a flat surface is described by Equation 22.

$$m_s \cdot \ddot{Y}_s = F_{Lfa} + F_{Lra} \qquad (22)$$

Where $\ddot{Y}_s$ is the lateral acceleration of the sprung mass, F_{Lfa} is the lateral force on the front axle and F_{Lra} is the lateral force on the rear axle. It should be noted this is only the dynamic forces and does not include a constant lateral force produced by the road crossfall.

The vertical motion of the front and rear unsprung masses on a flat surface is described by Equation 23 and Equation 24.

$$m_{uf} \cdot \ddot{Z}_{uf} = F_{sfl} + F_{dfl} + F_{sfr} + F_{dfr} + F_{tfl} + F_{tfr} \qquad (23)$$

$$m_{ur} \cdot \ddot{Z}_{ur} = F_{srl} + F_{drl} + F_{srr} + F_{drr} + F_{trl} + F_{trr} \qquad (24)$$

Where m_{uf} and m_{ur} are the front and rear unsprung masses, $\ddot{Z}_{uf}$ and $\ddot{Z}_{ur}$ are the front and rear unsprung vertical accelerations

The rolling motion of the front and rear unsprung mass on a flat surface is described by Equation 25 and Equation 26.

$$(I_{uf} + m_{uf} \cdot (h_1 - h_2)^2) \cdot \ddot{\theta}_{ufx} = m_{uf}\,(h_1 - h_2) \cdot \left(g \cdot \theta_{ufx}\right)$$
$$+\left(F_{sfl} + F_{dfl} - F_{sfr} - F_{dfr}\right) \cdot S_f + R_f \cdot \left(\theta_{sx} - \theta_{ufx}\right) + \left(F_{tfl} - F_{tfr}\right) \cdot T_f \quad (25)$$

$$(I_{ur} + m_{ur} \cdot (h_1 - h_2)^2) \cdot \ddot{\theta}_{urx} = m_{ur}\,(h_1 - h_2) \cdot (g \cdot \theta_{urx})$$
$$+(F_{srl} + F_{drl} - F_{srr} - F_{drr}) \cdot S_r + R_r \cdot (\theta_{sx} - \theta_{urx}) + (F_{trl} - F_{trr}) \cdot T_r \quad (26)$$

Where I_{uf} and I_{ur} are the front and rear roll moment of inertia of the unsprung mass, h_2 is the height from the floor to the front and rear unsprung masses, m_{uf} is the front unsprung mass, and T_f and T_r are half of the front and rear track widths.

The lateral force generating properties of a tyre can be described by using a first order Equation with time constant τ_{lat} [43]. The tyre lateral properties can therefore be represented using a spring and damper in series as shown in Figure 2.14.

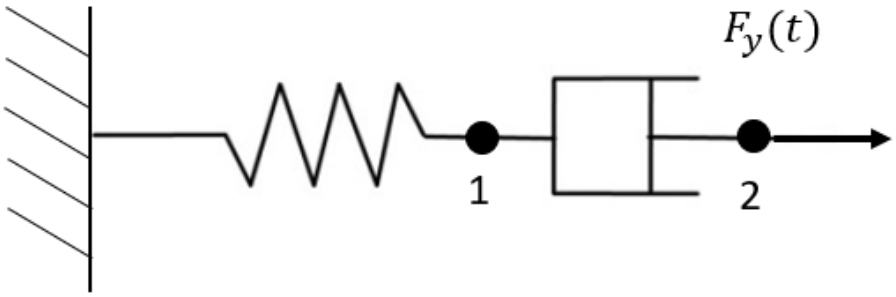

Figure 2.14: Spring and damper in series representing lateral tyre forces from a pneumatic tyre

The force on the spring is described by Equation 27.

$$F_{spring} = k_{lat} \cdot Y_1 \quad (27)$$

Where F_{spring} is the lateral force developed at point 1, k_{lat} is the spring stiffness of the spring at point 1, Y_1 is the lateral position of point 1 relative to the starting point.

The force on the damper is described by Equation 28.

$$F_y(t) = c_{lat} \cdot \left(\dot{Y}_2 - \dot{Y}_1\right) = F_{spring} \quad (28)$$

Where $F_y(t)$ is lateral dynamic tyre force developed at point 2, c_{lat} is the damping rate of the damper between point 1 and 2 and $\dot{Y}_i$ is the lateral velocity of point i. The velocity $\dot{Y}_2$ is obtained through the pendulum motion of the axle as it rotates about the roll centre as shown in Figure 2.13. The tyre forces are obtained by combining these three Equations and solving at each time step.

The damper coefficient is obtained from Equation 29 [42].

$$c_{lat} = \frac{C_c \cdot F_{tyre\ vertical}}{V} \tag{29}$$

Where c_{lat} is the lateral tyre damping value, C_c is the lateral tyre cornering coefficient, $F_{tyre\ vertical}$ is the vertical tyre force and V is the longitudinal velocity of the vehicle.

The stiffness of the spring (k_{lat}) is obtained using Equation 30 [42].

$$k_{lat} = \frac{C_c \cdot F_{tyre\ vertical}}{\tau_{lat} \cdot V} \tag{30}$$

The term $\tau_{lat} \cdot V$ is referred to as the relaxation length L of the tyre [42]. There are large variations in the reported relaxation length of tyres. Cebon and Cole quote this value to be equal to the tyre contact patch length which is approximately 0.3 m [42]. Other sources quote this value as between 25% and 50% of the tyre circumference [44]. A reasonable estimate of the relaxation length is twice the tyre radius [45] and is often recommended in TruckSim® [46]. This value of twice the tyre radius equates to 32% of the tyre circumference which falls in the range of 25% to 50% of the tyre circumference. For this study, the relaxation length is assumed to be 1 m which is twice the tyre loaded radius.

The vehicle parameters used on the developed base model are summarized in Table C.1. The parameters were primarily obtained from similar models developed by Cebon and Cole [12, 42], but also from other sources where appropriate [16, 47, 17, 48, 49] . The parameter that was most difficult to select a representative value for, was the front and rear suspension damping. Values as low as 1 kNs/m have been used on heavy vehicles and sometimes in excess of 40 kNs/m. The values selected seem to be reasonable and have been used in other similar studies [49].

2.2.1. Validation of model on a flat surface with typical operating conditions

To ensure that the developed model functions as expected when introducing crossfall into the road profile, it is first necessary to validate the model on a flat surface under typical operating conditions. In this section the model results are validated against TruckSim2019.1® at a vehicle speed of 80 km/h and an IRI value of 2m/km. This section contains a detailed analysis and comparison of the main parameters of interest. Subsequent subsections will only provide a brief description of the results and only focus on the vertical aggregate first and fourth power forces. Additional information and details on validation results can be obtained in Appendix D.

Information on how the model was developed in TruckSim2019.1® and the values used, can be found in Appendix B. It is however important to note that TruckSim2019.1® does have a driver model to ensure that the vehicle follows the defined path whilst the developed model assumes the vehicle follows a straight path with no yaw motion being included.

Figure 2.15 shows the front left vertical tyre forces as obtained from both TruckSim 2019.1® and the developed user model over the first 200 m of the test section. The results indicate that there is good agreement between the two models with the two graphs coinciding over most of the test section. Table D.1 shows that the average absolute error of the front left tyre over the entire test section is 0.65% and of a similar magnitude for all the tyres at this typical highway operating condition.

To investigate possible sources of deviation, the main vehicle parameters were also investigated. Figure 2.16 illustrates the front axle lateral forces. The user-developed model and TruckSim 2019.1® forces are of the same magnitude and in general have the same patterns across the entire section. The absolute values at each point however do show large variability with some points showing exact agreement and others showing poor agreement. This is due to Truckim® having higher degrees of freedom that include yaw motion and a driver model that introduce additional lateral forces. The effect of the forces is however negligible on the overall result but could be improved by incorporating higher degrees of freedom into the user model. Figure 2.17 shows the lateral axle force of the rear axle and it is evident that the accuracy is higher in the rear axle, most likely due to the lack of steering in the rear axle group.

Considering the motion of the various heavy vehicle components, Figure 2.18 shows clearly that the front unsprung mass roll motions agree well between the user-developed model and TruckSim 2019.1®. The same is true for the rear axle but these results have not been included in the dissertation.

Figure 2.19 and Figure 2.20 shows the roll and pitching motion of the sprung mass. There is once again good agreement between the two models with all the major phenomena being captured in the user-developed model.

Figure 2.21 shows the results for the first power aggregate forces for the left side tyres while Figure 2.22 contains the results for the fourth power aggregate forces. These figures show that the two models produce almost identical results over the test section, especially with regard to the first power aggregate forces. Small errors are exacerbated when taking the fourth power which is manifested in some larger shifts in the fourth power aggregate force results. The errors are however still negligible and the average absolute errors are recorded as 0.49% and 2.0% respectively for the first and fourth power aggregate forces on the left side as summarized in Table D.2 and Table D.3. The average absolute errors for the DLC results are shown in Table D.4.

The results indicate that the user-developed model provides accurate results for a heavy vehicle operating at a typical speed and road roughness value. The next section investigates if this level of performance is maintained under different operating speeds and road roughness values.

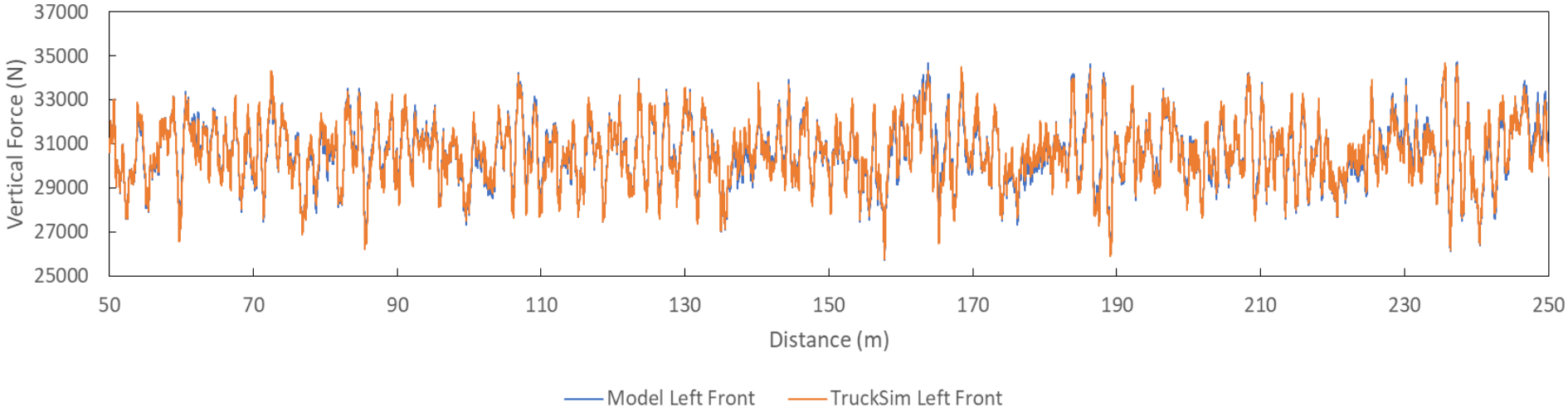

Figure 2.15: Front left vertical tyre force from TruckSim 2019.1® and the model over 200 m test section at 0% crossfall, 2 m/km IRI, 80 km/h and no anti-roll bar

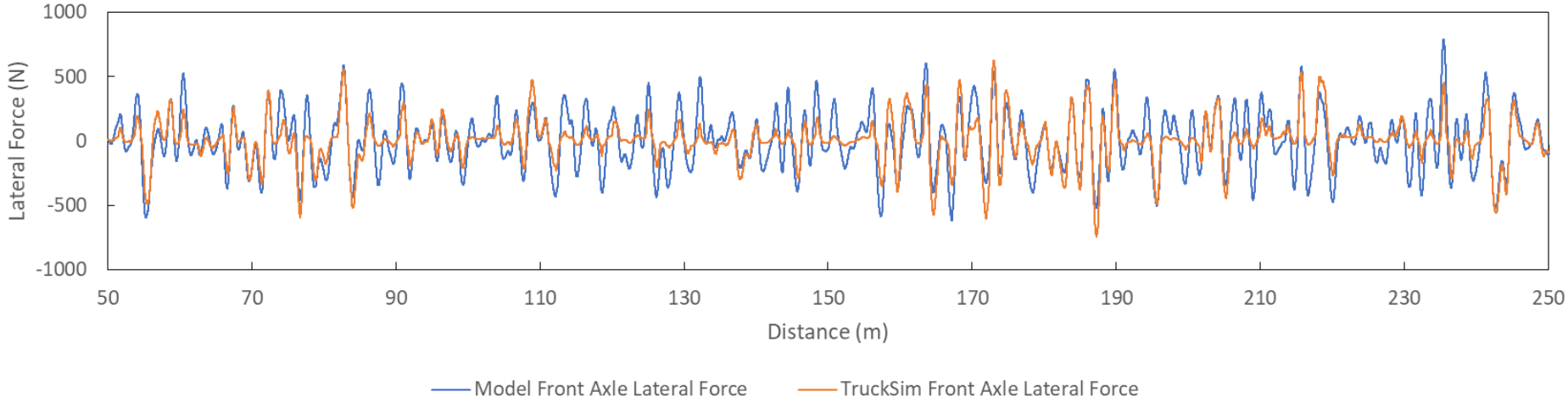

Figure 2.16: Front axle lateral tyre force from TruckSim 2019.1® and the model over 200 m test section at 0% crossfall, 2 m/km IRI, 80 km/h and no anti-roll bar

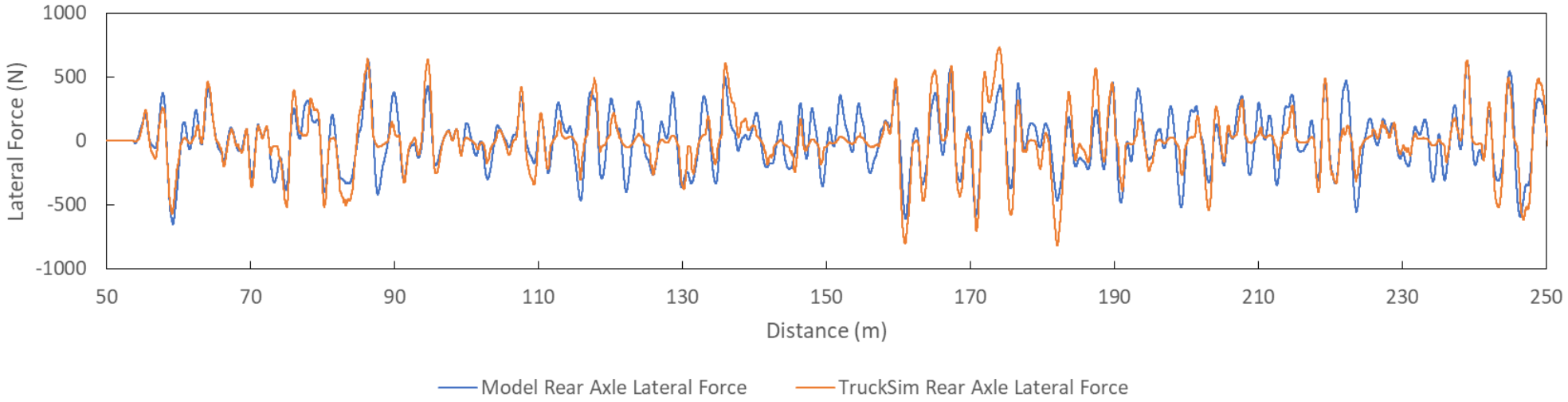

Figure 2.17: Rear axle lateral tyre force from TruckSim 2019.1® and the model over 200m test section at 0% crossfall, 2 m/km IRI, 80 km/h and no anti-roll bar

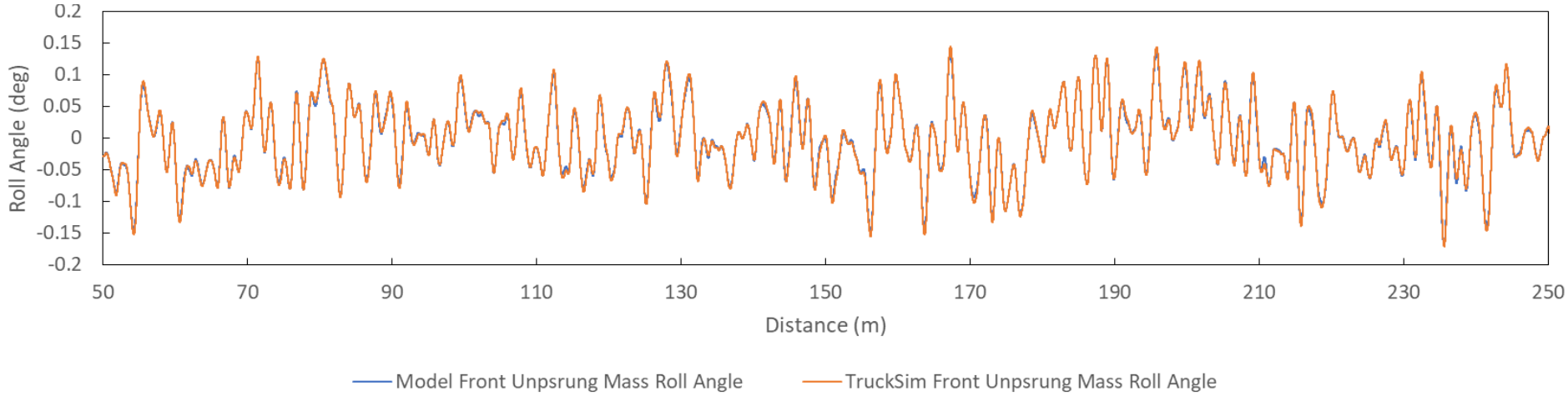

Figure 2.18: Front unsprung mass roll angle from TruckSim 2019.1® and the model over 200 m test section at 0% crossfall, 2 m/km IRI, 80 km/h and no anti-roll bar

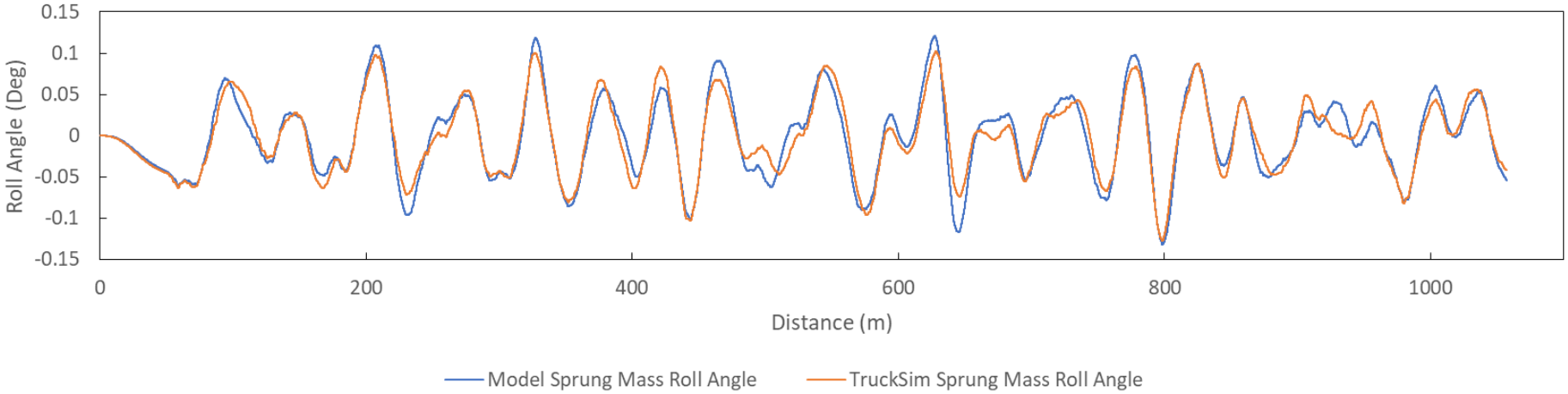

Figure 2.19: Sprung mass roll angle from TruckSim 2019.1® and the model over 1 km test section at 0% crossfall, 2 m/km IRI, 80 km/h and no anti-roll bar

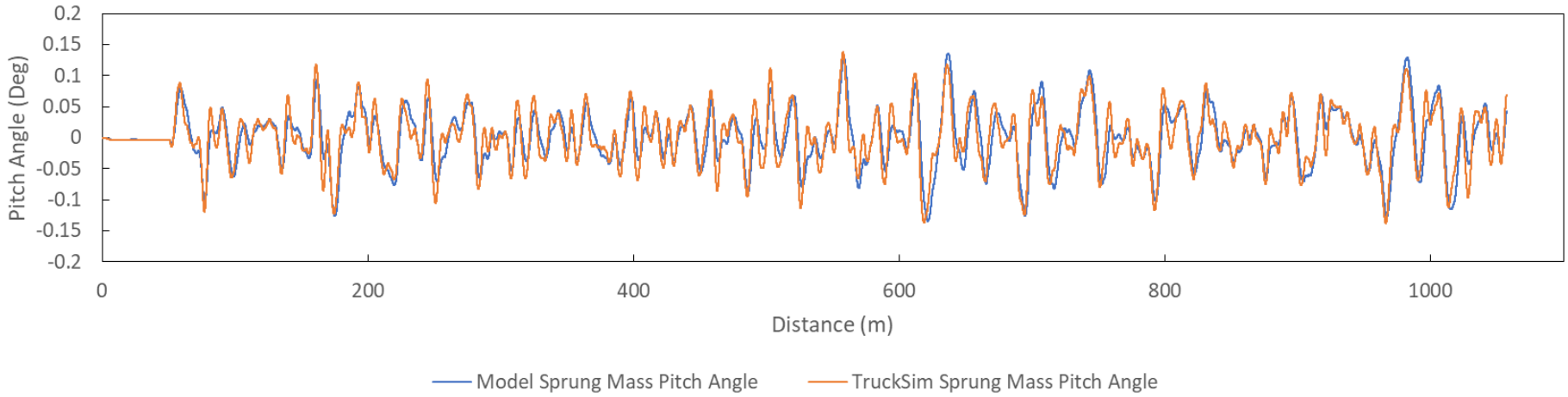

Figure 2.20: Sprung mass pitch angle from TruckSim 2019.1® and the model over 1 km test section at 0% crossfall, 2 m/km IRI, 80 km/h and no anti-roll bar

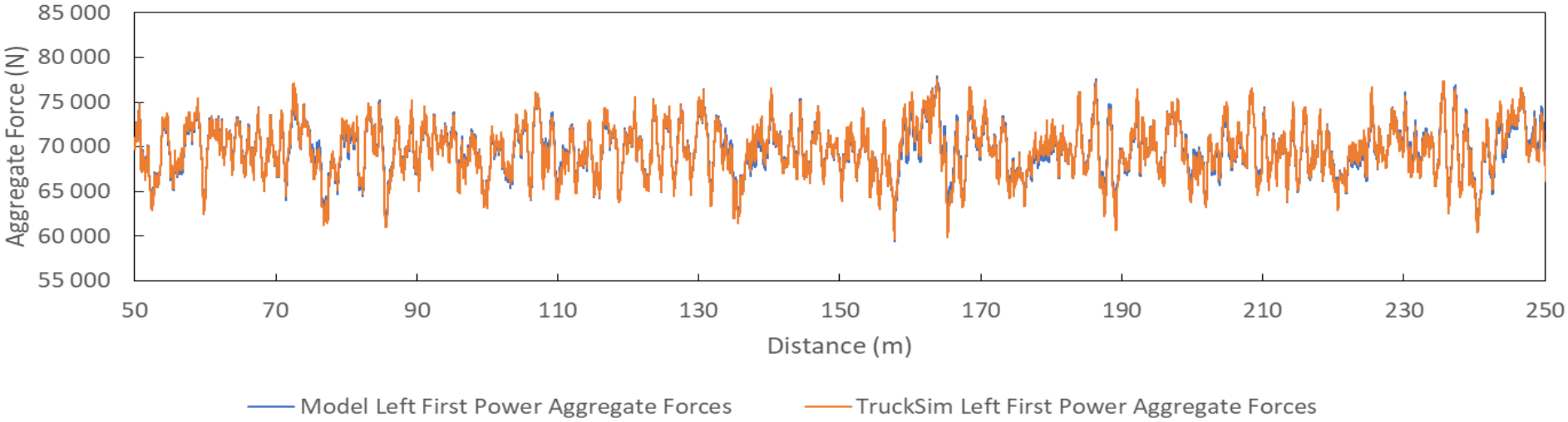

Figure 2.21: Left side first power aggregate forces from TruckSim 2019.1® and the model over 200 m test section at 0% crossfall, 2 m/km IRI, 80 km/h and no anti-roll bar

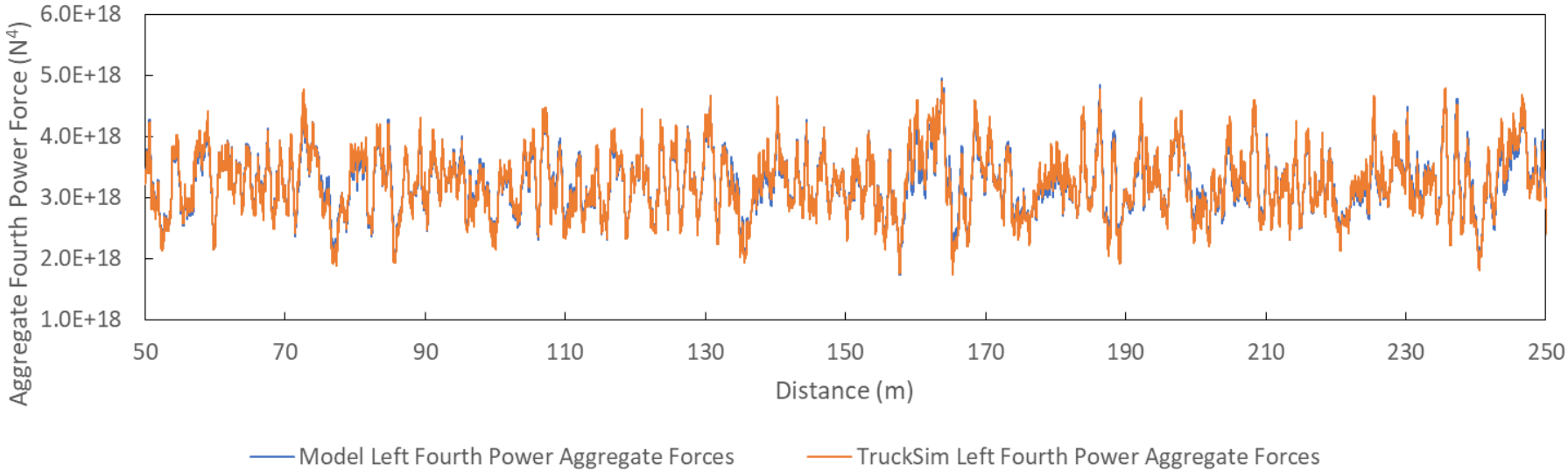

Figure 2.22: Left side fourth power aggregate forces from TruckSim 2019.1® and the model over 200 m test section at 0% crossfall, 2 m/km IRI, 80 km/h and no anti-roll bar

2.2.2. Validation of flat surface model at different road roughness values and vehicle speeds

The previous subsection indicated that the user defined model is accurate under a typical operating speed and road roughness on a flat surface. This subsection illustrates that the model remains accurate under other operating conditions on a flat surface.

The fourth power aggregate force remains the most important criteria in this study. The validation results under the most extreme operating conditions of 40 km/h and 120 km/h for a road roughness value of 10m/km are shown in Figure 2.23 and Figure 2.24 for convenience. Figure D.1 to Figure D.10 illustrates the first and fourth power aggregate forces obtained from TruckSim 2019.1® and the user defined model under different vehicle operating speeds and road roughness values on a flat surface. The results show that the model remains accurate over the entire range of road roughness values and vehicle speeds selected for this study.

The average absolute errors of the tyre forces are summarized in Table D.5 The average absolute errors tend to increase as the road roughness values increases and decreases as the vehicle speed increases. The increase due to the higher IRI values is expected due to the increased bouncing motion of the vehicle that results in low vertical forces being produced at some points. At locations where the tyre forces are quite small, small variations in the tyre force will produce a larger percentage error that will increase the average absolute error of the results. The difference in left and right and front to back errors are however almost identical. The same trends are obtained for the first and fourth power aggregate forces as summarized in Table D.6 and Table D.7. Table D.8 shows that the front dynamic load coefficient errors tend to increase slightly with an increase in road roughness and a decrease in vehicle speed. The rear dynamic load coefficient errors decrease considerably at lower vehicle speeds and only decreases slightly with an increase in vehicle speed. The errors are less than 8% on the rear axles and less than 3% on the front axles. These errors are reasonable as the DLC is a very sensitive value and small changes in vehicle parameters will have a notable effect on the DLC.

The next subsection will validate the user defined model when incorporating crossfall under different operating conditions including an anti-roll bar.

2.2.3. Validation of model when including road crossfall, anti-roll bars and eccentric loads

The final validation is to ensure that the user defined model remains accurate when incorporating road crossfall, anti-roll bars and eccentric loads under different operating conditions.

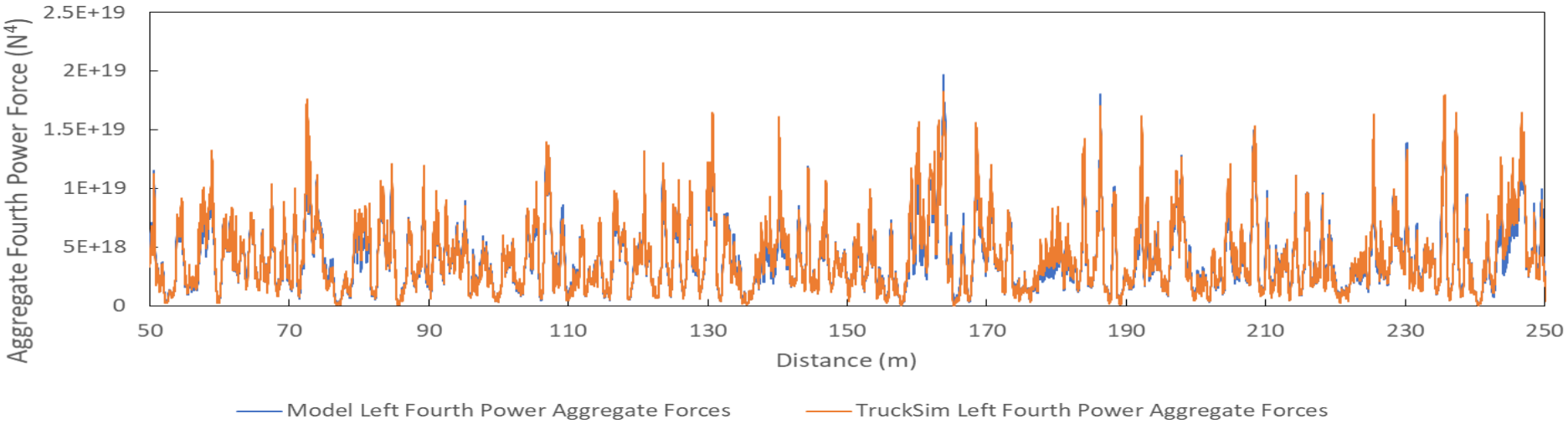

Figure 2.23:Left side fourth power aggregate forces from TruckSim 2019.1® and the model over 200 m test section at 0% crossfall, 10 m/km IRI, 80 km/h and no anti-roll bar

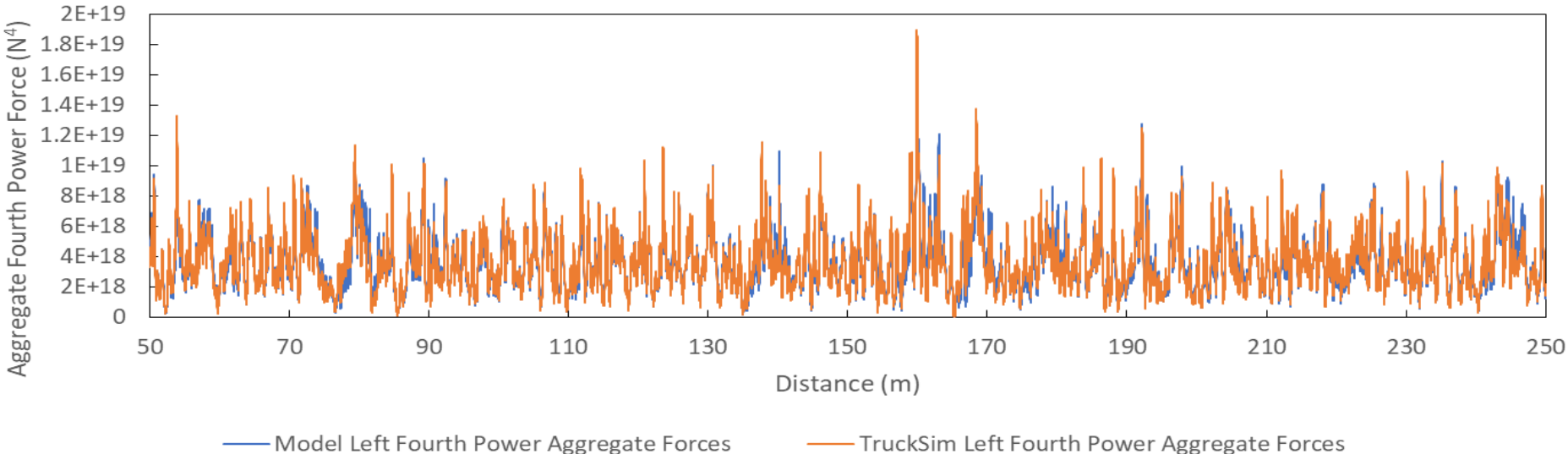

Figure 2.24: Left side fourth power aggregate forces from TruckSim 2019.1® and the model over 200 m test section at 0% crossfall, 10 m/km IRI, 40 km/h and no anti-roll bar

The first attempt was to use the model as is and simply introduce road crossfall. Figure 2.25 and Figure 2.26 show the results for the left and right tyre forces from TruckSim 2019.1® and the user defined model. The results show that the left side tyre forces in the user defined model underestimates the vertical tyre force while the right side is overestimated. This is the result of a lower than expected roll angle of the axle.

Figure 2.27 however shows that the lateral tyre forces are still of the same magnitude and follow similar patterns as in the previous subsections. There is however a notable deviation at the start of the test section which appears to be the result of the driver model in TruckSim 2019.1®. This jerky reaction in the driver model however dissipates quickly, and the models then follow similar trends as before.

The variations in the vertical tyre forces between left and right are a result of the user defined model not taking into account the lateral friction force produced between the tyres and the road surface as illustrated in Figure 2.28. This friction force produced by the crossfall therefore needs to be superimposed on to the model in order to obtain the correct axle rotation and vertical tyre forces.

This update in the user defined model is shown in Figure 2.29. The front and rear lateral friction force produced by the road crossfall is calculated as shown in Equation 31 and Equation 32 respectively. This result is obtained through a simple moment balance.

$$F_{latcf} = m \cdot g \cdot \frac{b}{Wb} \cdot \sin(\Psi) \tag{31}$$

$$F_{latcr} = m \cdot g \cdot \frac{a}{Wb} \cdot \sin(\Psi) \tag{32}$$

The Equations of motion also need to be updated for the unsprung masses as shown in Equation 33 and Equation 34.

$$\begin{aligned}(I_{uf} + m_{uf} \cdot (h_1 - h_2)^2) \cdot \ddot{\theta}_{ufx} = m_{uf}\,(h_1 - h_2) \cdot \left(g \cdot \theta_{ufx}\right) \\ +\left(F_{sfl} + F_{dfl} - F_{sfr} - F_{dfr}\right) \cdot S_f + R_f \cdot \left(\theta_{sx} - \theta_{ufx}\right) + \left(F_{tfl} - F_{tfr}\right) \cdot T_f + F_{latcf}\end{aligned} \tag{33}$$

$$\begin{aligned}(I_{ur} + m_{ur} \cdot (h_1 - h_2)^2) \cdot \ddot{\theta}_{urx} = m_{ur}\,(h_1 - h_2) \cdot (g \cdot \theta_{urx}) \\ +(F_{srl} + F_{drl} - F_{srr} - F_{drr}) \cdot S_r + R_r \cdot (\theta_{sx} - \theta_{urx}) + +(F_{trl} - F_{trr}) \cdot T_r + F_{latcr}\end{aligned} \tag{34}$$

The updated results for the base user model under different operating conditions are shown in Figure D.11 to Figure D.14 and have similar trends to other figures shown in this subsection and have therefore not been added in the main text. The results from the user defined model and the TruckSim 2019.1® are now once again in good agreement as in the previous subsections on a flat surface. There is still a noticeable difference in the forces at the start of the test section due to the instability caused by the driver model in TruckSim 2019.1®.

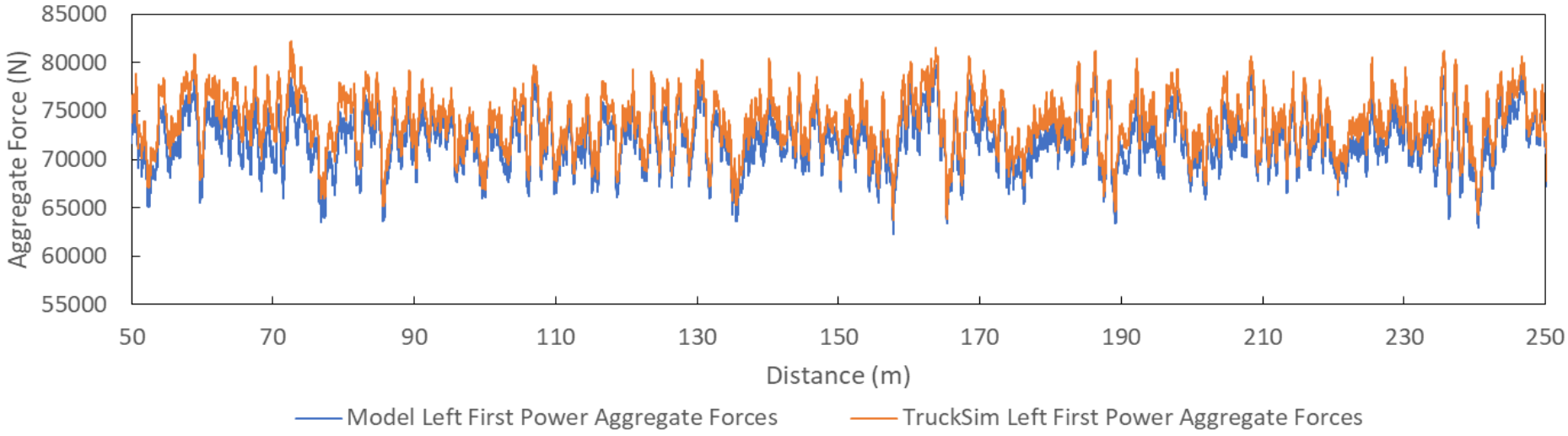

Figure 2.25: Left side first power aggregate forces from TruckSim 2019.1® and the initial model over 200 m test section at 2% crossfall, 2 m/km IRI, 80 km/h and no anti-roll bar

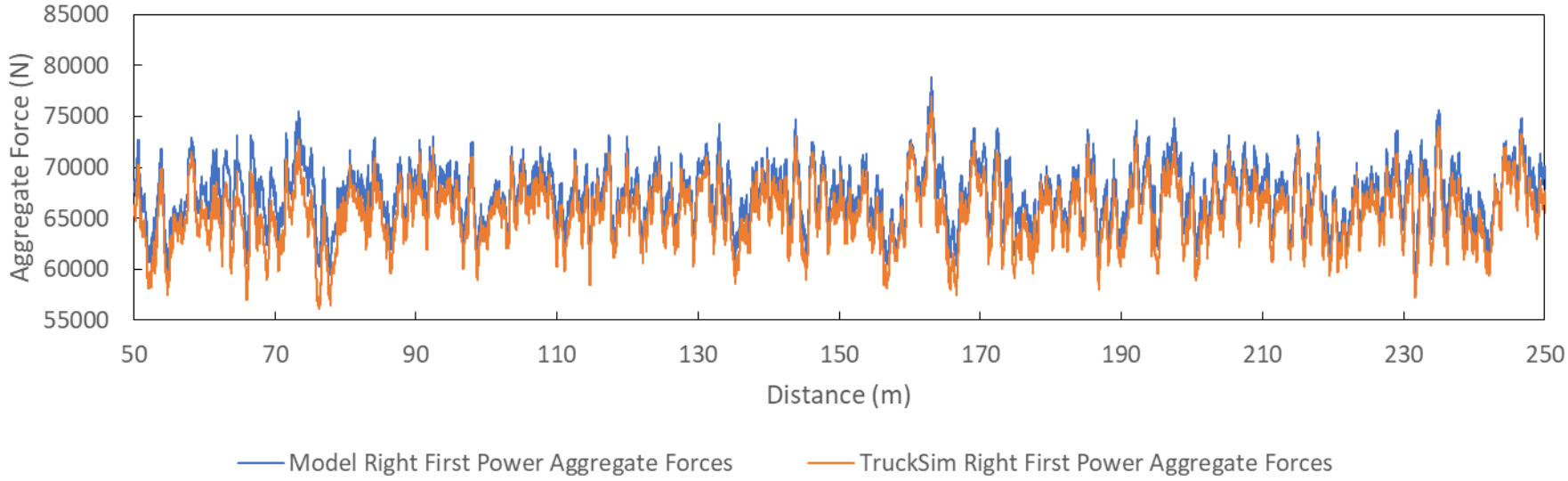

Figure 2.26: Right side first power aggregate forces from TruckSim 2019.1® and the initial model over 200 m test section at 2% crossfall, 2 m/km IRI, 80 km/h and no anti-roll bar

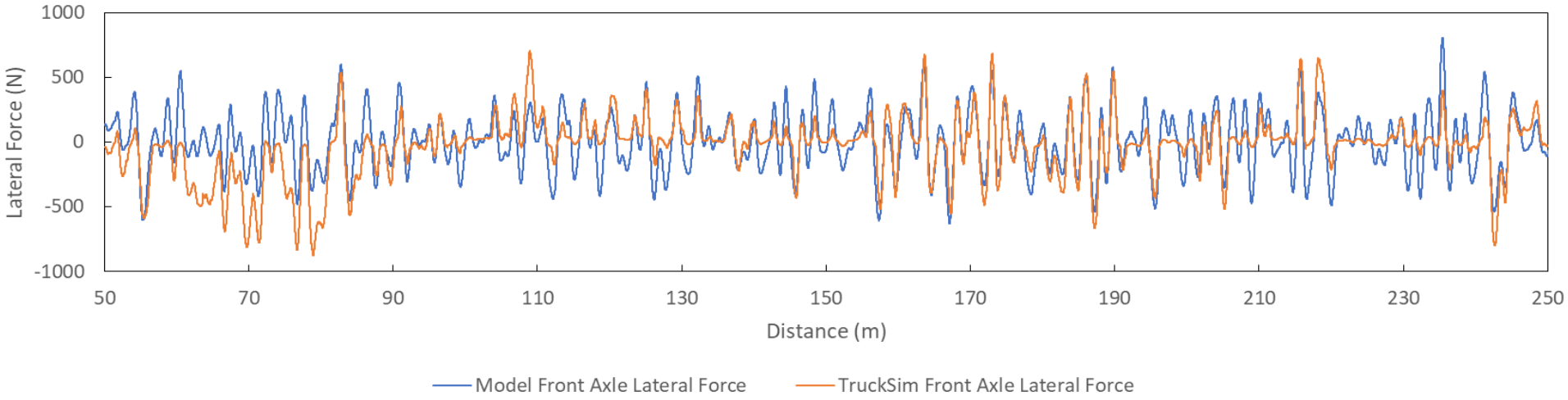

Figure 2.27: Front axle lateral force from TruckSim 2019.1® and the initial model over 200 m test section at 2% crossfall, 2 m/km IRI, 80 km/h and no anti-roll bar

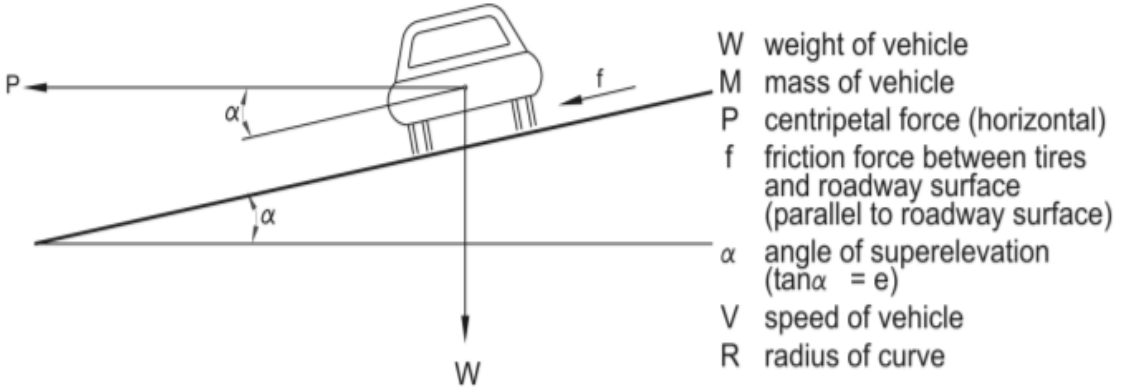

Figure 2.28: Forces produced on a vehicle when including crossfall [55]

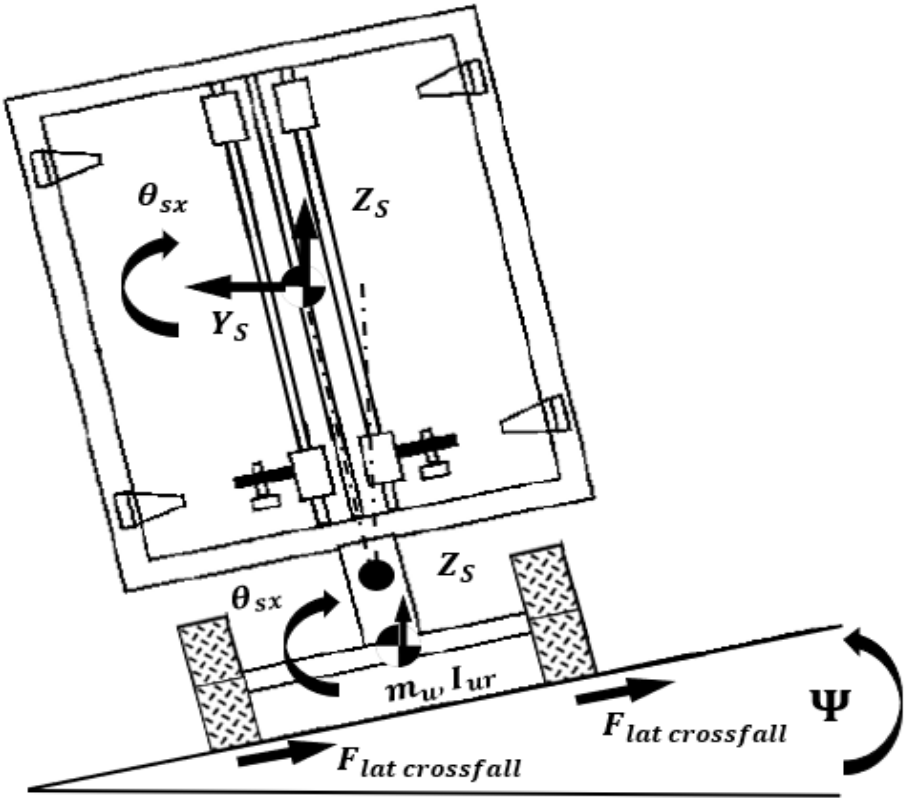

Figure 2.29: Rolling motion of heavy vehicle when including crossfall modified from [47]

The results when incorporating anti-roll bars on the front and rear axles are shown in Figure D.15 and Figure D.16 and have similar trends to other figures shown in this subsection and have therefore not been added in the main text. The results of the model and TruckSim 2019.1® agree well and show that the anti-roll bar is accurately modelled. Figure 2.30 confirms this and shows the auxiliary moment produced by the front anti-roll bar by the model as well as TruckSim 2019.1®.

Lastly the model was validated when including an eccentric sprung mass. The fourth power aggregate force results for the model and TruckSim 2019.1® are shown in Figure D.17 and has similar trends to other figures shown in this subsection and have therefore not been added in the main text. It should be noted that this eccentricity value of 300 mm is rather large, but that the model results still agree well with TruckSim 2019.1® and that this value was taken from literature as a representative value [17].

The errors of the results from the user defined model vs the results from TruckSim 2019.1® under all of the validation conditions are summarized in Appendix D. The errors are reasonable, especially under typical highway operating speeds and road roughness values. The results therefore confirm that the user defined model is sufficiently accurate for the purposes of this study.

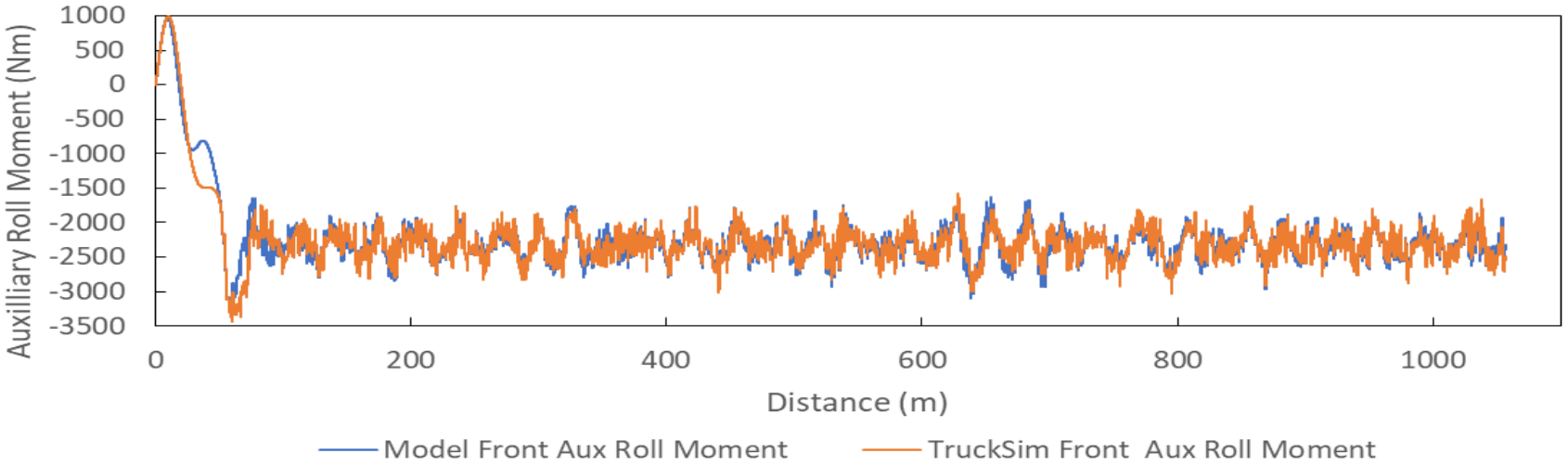

Figure 2.30: Auxiliary roll moment on the front axle from TruckSim 2019.1® and the final model over 200 m test section at 5% crossfall, 2 m/km IRI, 80 km/h and with an anti-roll bar

3. Results and Discussion

Various aspects are investigated in this dissertation and therefore several subsections have been created in order to present the results in a meaningful manner. Subsection 3.1 investigates the effect of vehicle speed, road roughness and crossfall on the dynamic road damage caused by the base model using the different damage criteria identified. The most important criterion is the 95th percentile fourth power aggregate force as this is often referred to as the road damage of a heavy vehicle in literature [42].

Subsection 3.2 focusses on the effects of different vehicle parameters on the 95th percentile fourth power aggregate force. Subsections are dedicated for the 10 heavy vehicle parameters listed in the objective.

Subsection 3.3 contains a general discussion on the results obtained in subsection 3.1 and subsection 3.2.

It should be noted that the percentage difference between the left and right road damage of any of the criteria is calculated using Equation 35. This means that a positive percentage difference shows that the left side damage is higher than the right damage criteria studied.

$$Percentage\ difference = \frac{left\ damage - right\ damage}{Average(left\ damage, right\ damage)} \tag{35}$$

Additional results are presented in Appendix E.

3.1. Results for the base model

3.1.1. The effect of crossfall on the average vertical tyre forces of the base model

As expected, the average vertical tyre forces are independent of vehicle speed and road roughness. Figure 3.1 summarizes the vertical tyre forces for all four tyres at different crossfall values.

Figure 3.1 shows that the front and rear average vertical tyre forces change linearly as a function of the road crossfall for all tyres. The left side tyre values increase linearly with an increase in crossfall and the right side decreases linearly with an increase in crossfall. This means that one can calculate the average vertical force at any crossfall values if this rate of change is known from any two crossfall values. Figure 3.1 also shows that the rate of change for the front and rear tyres are not the same. This is highlighted in Figure 3.2 which shows that the rear tyres have a larger percentage difference in the left and right tyre forces as compared to the front tyres. This shows that axles with a higher relative load will typically have a higher rate of change.

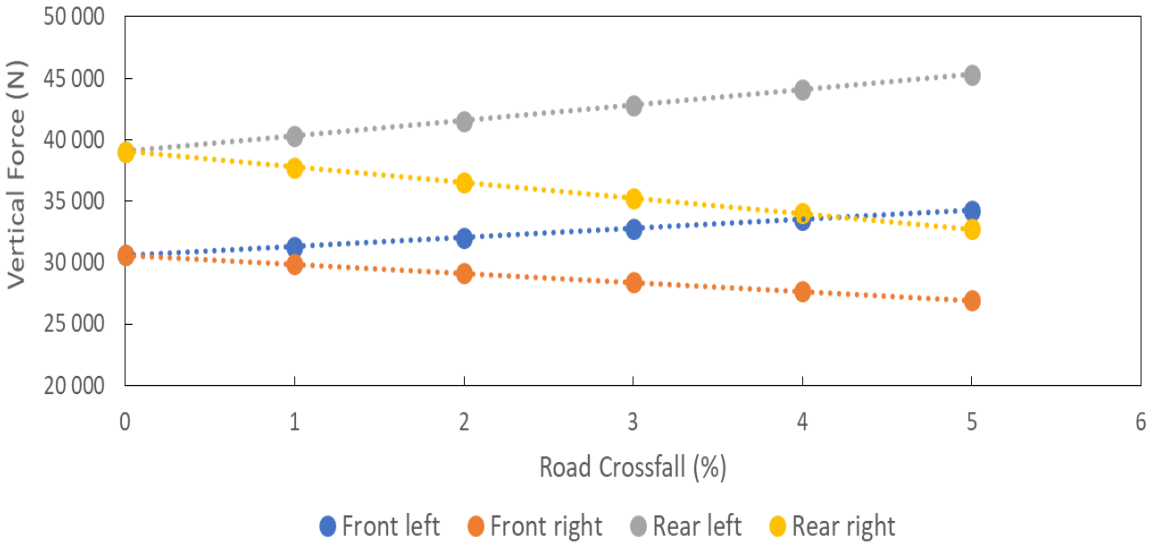

Figure 3.1: The average vertical tyre force of the base model at different crossfall values

The results in Figure 3.2 show that for a typical crossfall value in South Africa of 2%-3%, the front average vertical tyre forces have a difference of 9.6% and 14.4% respectively while the rear tyres show a difference of 12.9% to 19.3% respectively. The difference in the average vertical forces on either side of the vehicle will have a definite impact on road and vehicle damage. The average tyre forces and percentage difference between the left and right tyres for all four tyres are summarized in Appendix E in Table E.1, Table E.2 and Table E.3.

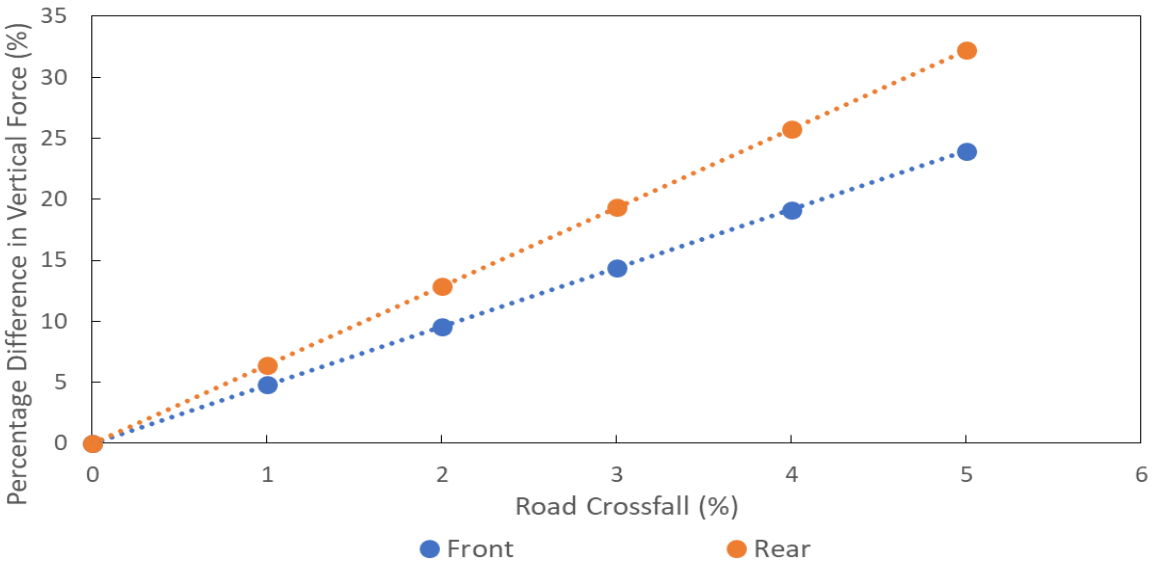

Figure 3.2: Percentage difference of the left and right tyres in the front and rear of the base model

3.1.2. The effect of crossfall on the DLC of the base model

Figure 3.3 provides a global view of the effect of the vehicle speed, road roughness and road crossfall on the DLC of the front left tyre. The results show that the DLC is highly dependent on all three of these parameters studied.

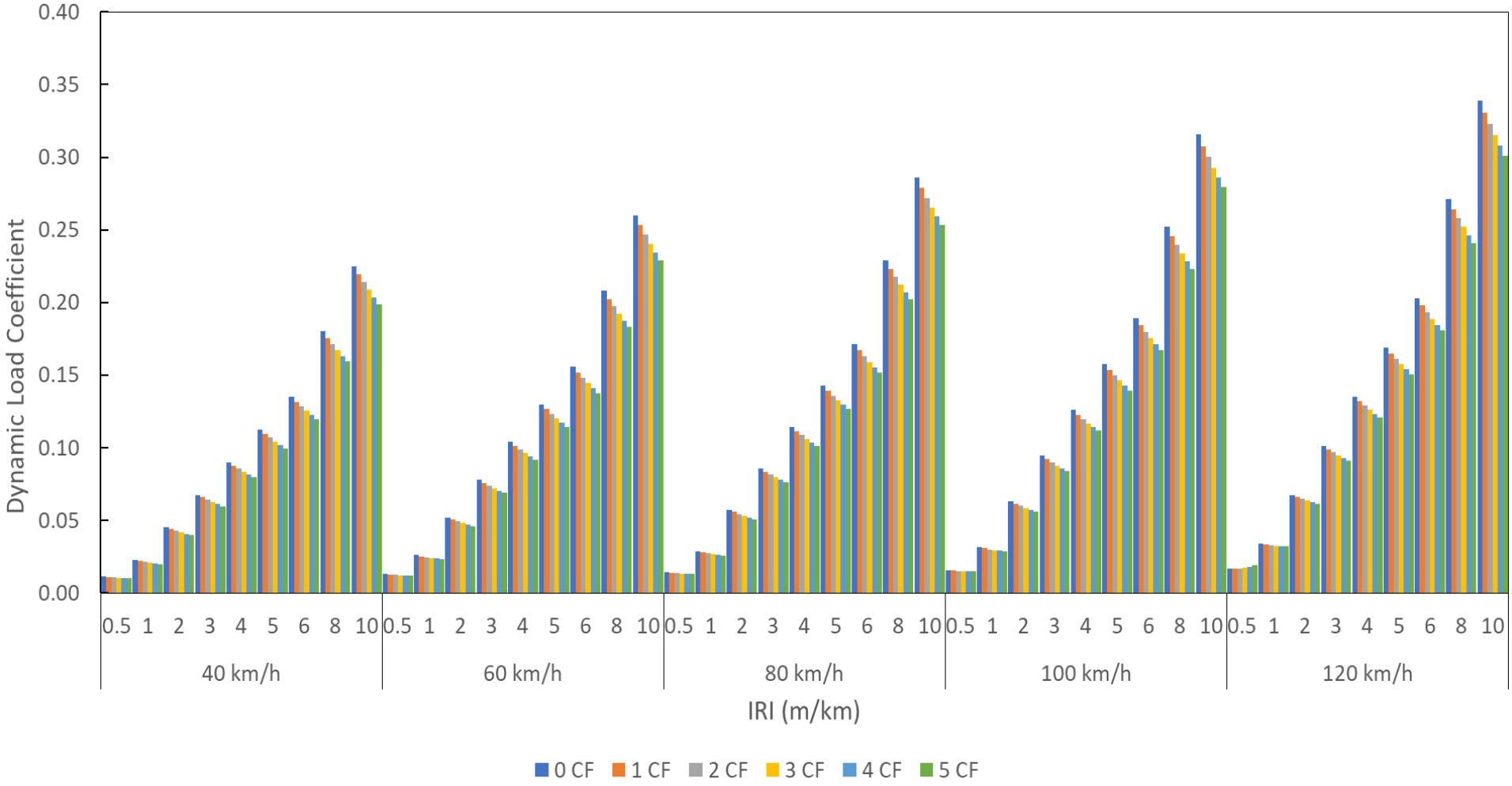

Figure 3.3: DLC of the front left tyre of the base model under all operating conditions

The results in Figure 3.3 highlight that the DLC decreases on the left front tyre as the road crossfall increases. Although not plotted, the DLC of the right front tyre however increases as the road crossfall increases. This result is in line with theory as higher loads decrease the DLC if all other conditions are kept constant [10].

Figure 3.4 shows that the DLC is once again a linear function of the road crossfall for all four of the tyres for a specific vehicle speeds and road roughness. The rear tyres have a lower DLC value compared to the front tyres. This is once again a result of the phenomena of higher loads causing lower DLC values [10].

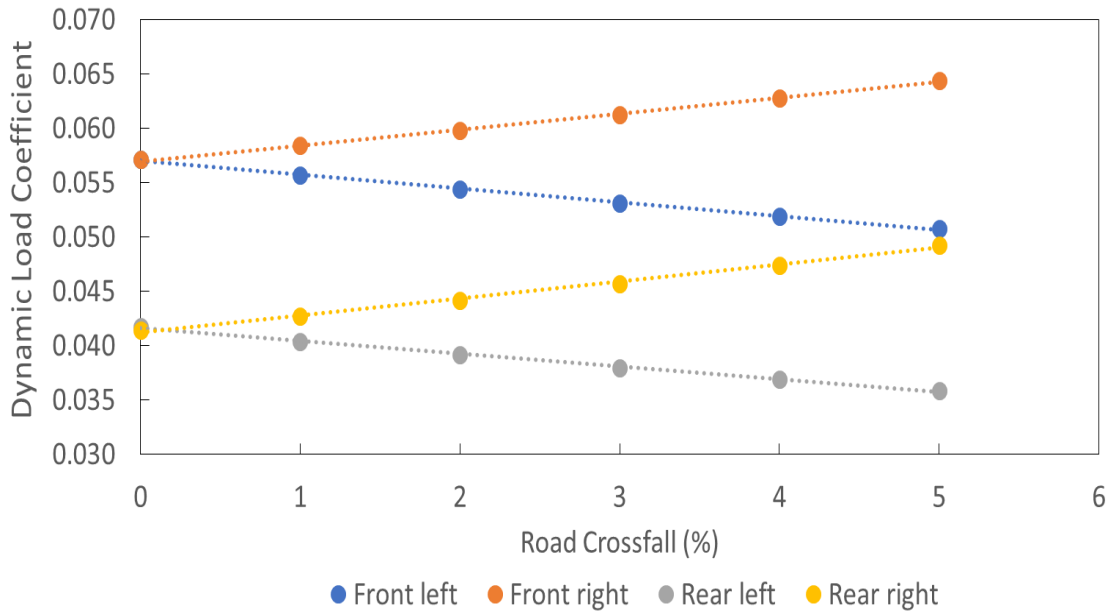

Figure 3.4: DLC of all four tyres of the base model at a vehicle speed of 80 km/h and an IRI 2 m/km

The DLC increases linearly for the left tyres with an increase in the road roughness for a specific road crossfall and vehicle speed as shown in Figure 3.5 as expected from literature [23]. The DLC increases linearly with the square root of the vehicle speed as shown in Figure 3.6, which is once again in line with literature [23]. A linear approximation is however reasonable, especially over a small change in the vehicle speed.

Figure 3.7 summarizes the percentage difference between the left and right DLC values over all the operating conditions to provide an overview of the parameter influences. Figure 3.7 shows that the difference in the DLC is almost completely independent of the road roughness values with only minute differences noted at different IRI values for the same crossfall and vehicle speed.

The relationship between the vehicle speeds and percentage difference in the DLC of the left and right side is however less clear. It appears as if the percentage difference remains more or less

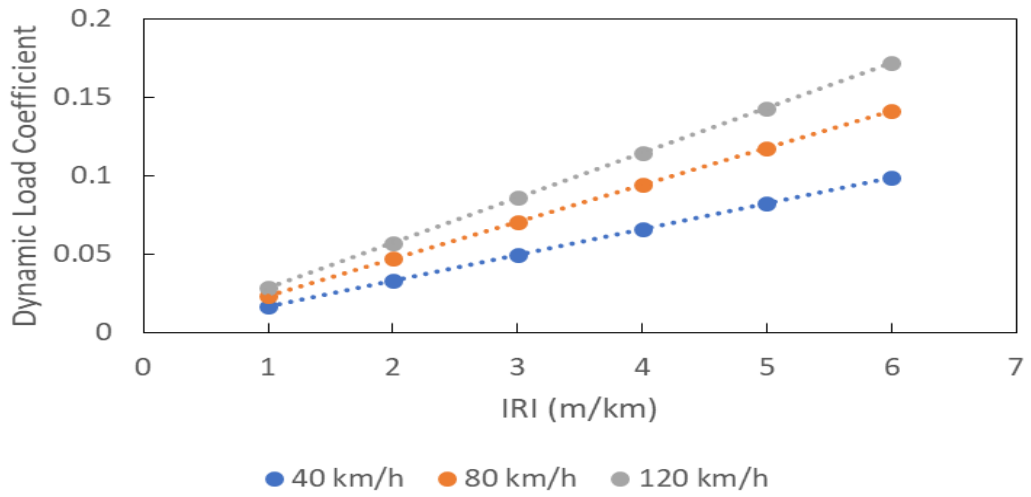

Figure 3.5: DLC of the front left tyre of the base model as a function of IRI and a crossfall of 0%.

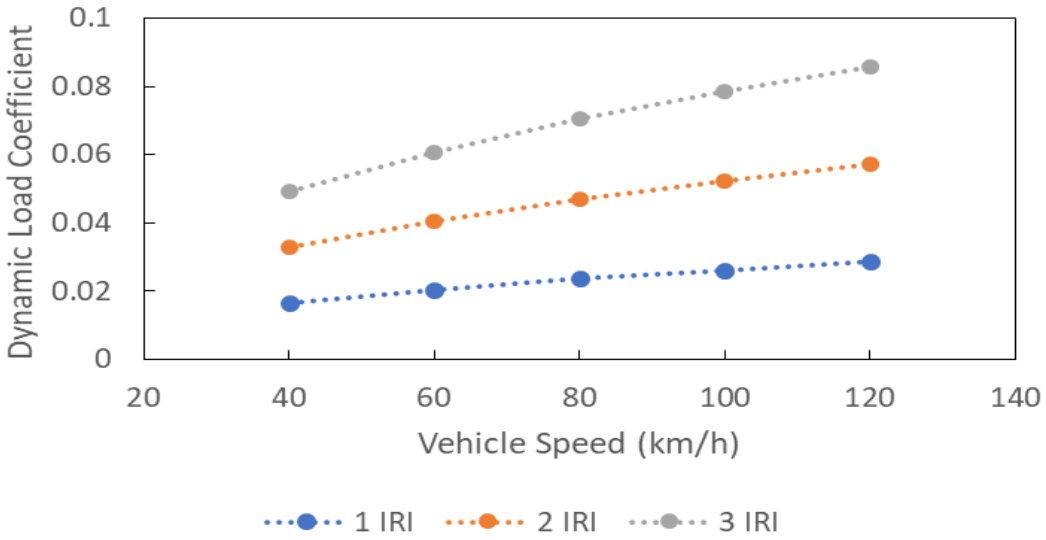

Figure 3.6: Dynamic load coefficient of the front left tyre of the base model as a function of vehicle speed and a crossfall of 0%.

constant for vehicles speeds from 40 km/h to 80 km/h. Subsequently it appears as if the percentage difference decreases as seen in Figure 3.7 and the again remains constant for the higher vehicle speeds. It appears as if this point of change is dependent on the vehicle damping values. During another run using a higher damping value, it was found that the DLC values remained approximately constant up to 100 km/h and only decreased for 120 km/h. This is most likely due to higher speeds resulting in more erratic and aggressive movement of the tyres for lower damping values which results in decrease in the percentage difference in the left and right values.

Considering the percentage difference in left and right DLC, it is observed that it also increases linearly with an increase in the road crossfall for both the front and rear axles. The rear axle however has a higher rate of change in the percentage difference between the left and right tyres. This is most likely due to the higher load transfer rate experienced by the rear axle as shown in Figure 3.2 of subsection 3.1.1

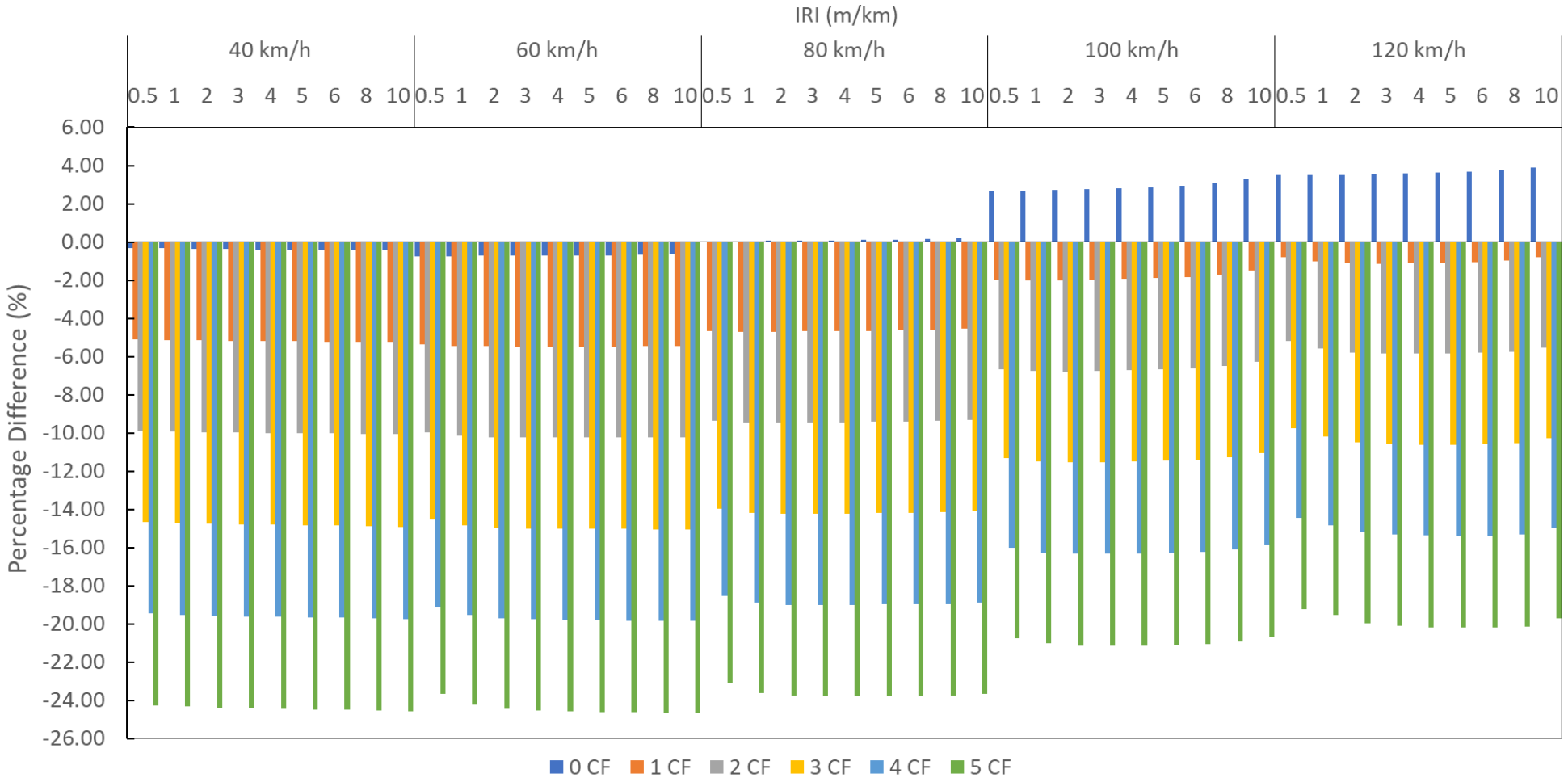

Figure 3.7: The percentage difference in the front left and right tyre DLC values of the base model over all the operating conditions

Furthermore, it appears as if one can accurately estimate the percentage difference in the DLC by using the difference in the average vertical tyre loads. As an example, at a crossfall value of 2% the percentage difference in right and left tyre average vertical force for the front and rear axle are 9.6 % and 12.9% respectively. The percentage difference for the DLC between the left and right tyres for the front and rear axle is 9.5% and 12.1% respectively.

The maximum difference in the right and left DLC values for the front and rear axles are 24.1% and 32.8% respectively. For a typical highway speed of 80 km/h and road roughness value of 2 m/km the difference between the left and right side is approximately 9.5% and 14.2% for the front axle at crossfall values of 2% and 3% respectively. In the case of the rear axle the difference is approximately 12.1% and 18.6%. The exact values of each simulation are summarized in Appendix E in Table E.4, Table E.5 and Table E.6.

A possible criticism of using DLC to describe the dynamic road damage when including road crossfall is that the DLC on the left side is lower than the right side due to crossfall. This contrasts with the fact that the tyre forces and road damage increase on the left side of the vehicle compared to the right side. The DLC values should therefore be considered in context.

3.1.3. The effect of crossfall on the first power aggregate forces of the base model

Aggregate forces are usually presented for three specific values namely the average value, the 95th percentile and the 99th percentile. This is also done in this dissertation, but the values are normalized by the static first power force (69 617 N obtained from static equilibrium).

As with the average vertical tyre forces in subsection 3.1.1, the average first power aggregate forces are independent of vehicle speed and road roughness and only change as a function of the road crossfall. The average first power aggregate forces change linearly once again with a change in the road crossfall as shown in Figure 3.8.

The percentage difference between the left and right-side average aggregate first power forces are shown in Figure 3.9 as a function of road crossfall. The difference is independent of the vehicle speed and road roughness and there are only minor variations under some operating conditions. The percentage change is once again a linear function of the road crossfall. The percentage difference appears to be equal to the weighted average of the front and rear percentage difference of the average loads as calculated in subsection 3.1.1. As an example, at a crossfall value of 2% the percentage difference in right and left tyre average vertical force for the front and rear axle are 9.6 % and 12.9% respectively as shown in subsection 3.1.1. The static front and rear axle load are 61.175 kN and 78.1 kN respectively. The weighted average value is 11.4%. The percentage difference in the average left and right first power aggregate force at a 2% crossfall is 11.4%. This

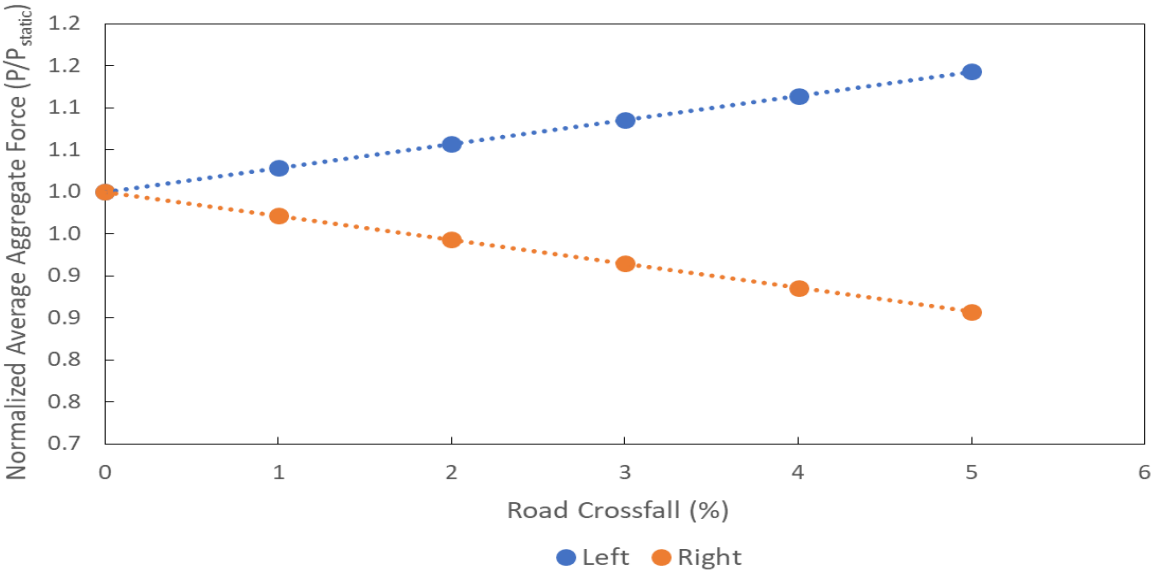

Figure 3.8: The normalized (by the static force) average first power aggregate forces of the left and right side of the base model over all the crossfall values

shows that the values are identical and that the average aggregate first power force can be directly calculated if the load transfer rates of axles are known. The detailed results for all the operating conditions are summarized in Appendix E in Table E.7 and Table E.8

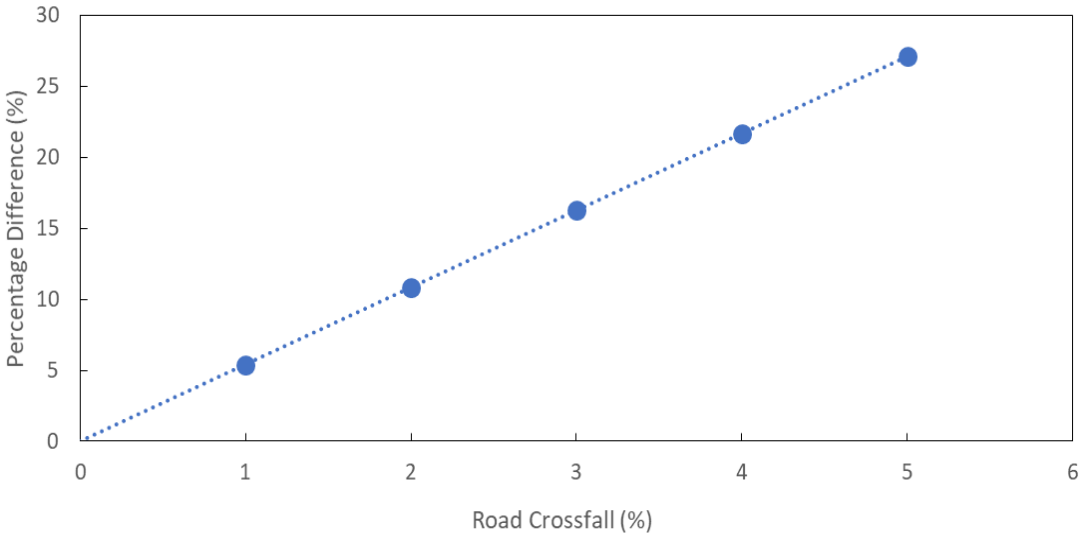

Figure 3.9: The average first power aggregate forces of the left and right side of the base model over all the crossfall values

Figure 3.10 contains the results of the normalized 95th percentile first power aggregate forces of the base model over all the operating conditions for the left side of the vehicle. This graph provides an overview of the relative influence of the different parameters. The graph of the normalized 99th percentile first power aggregate forces has the same trends as the DLC results. Specifically, the 95th percentile aggregate first power force is once again a linear function of the road crossfall as shown in Figure 3.11. The left side forces increase linearly, and the right-side forces decrease linearly with an increase in road crossfall.

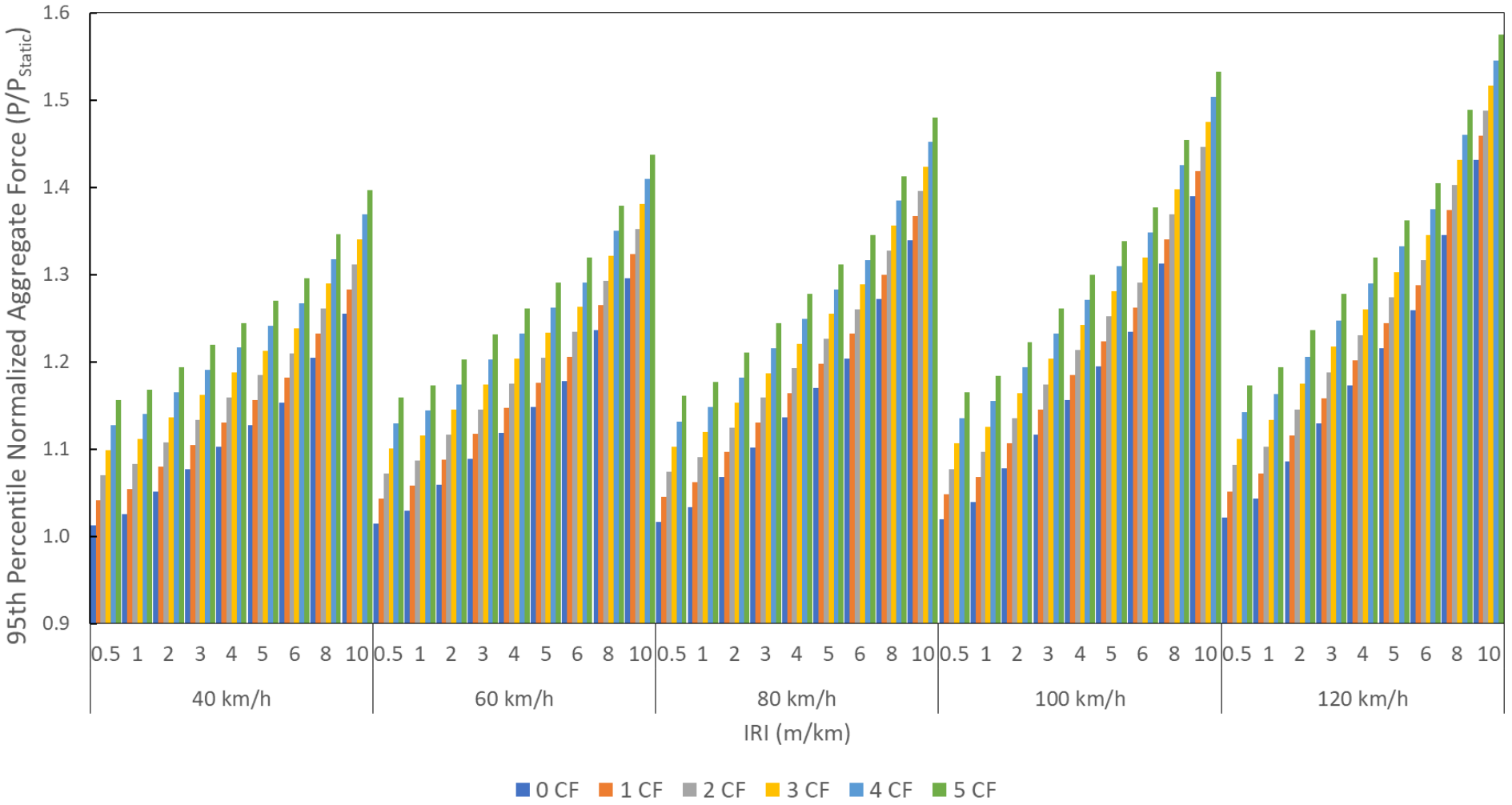

Figure 3.10: The normalized (by the static force) 95th percentile first power aggregate forces of the left side of the base model over all the operating conditions

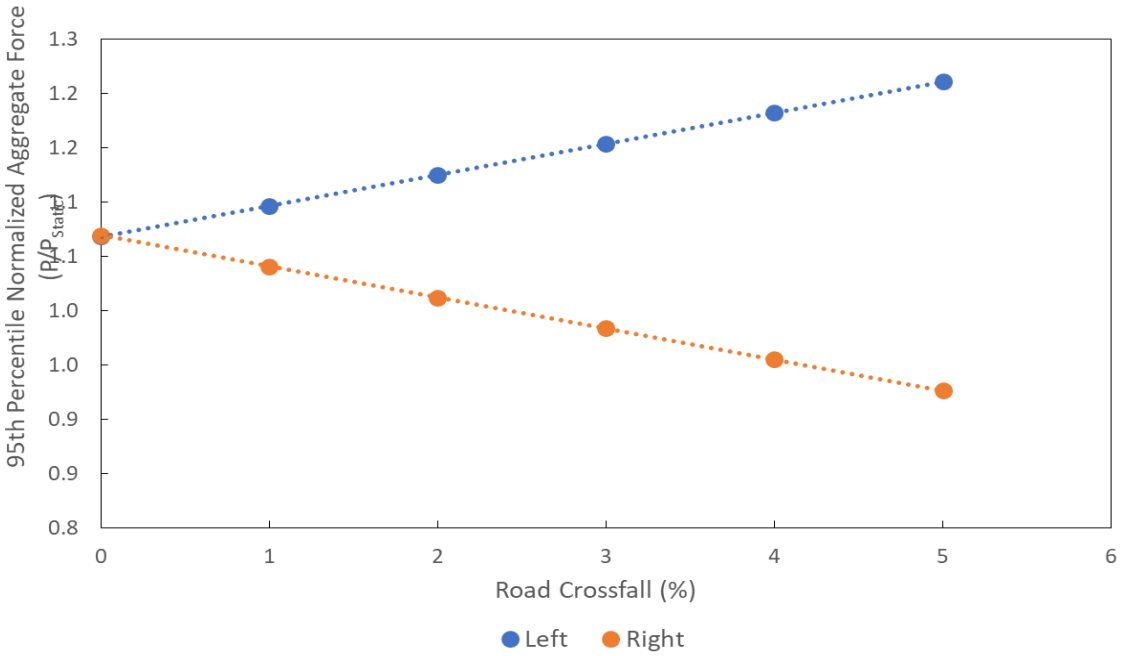

Figure 3.11: The normalized (by the static force) 95th percentile first power aggregate forces of the left and right side of the base model for all the crossfall values

The 95th percentile aggregate force also increases linearly with an increase in the road roughness at a specific road crossfall and vehicle speed as shown in Figure 3.12. The 95th percentile aggregate force increases with an increase in vehicle speed, but the slope becomes smaller at higher vehicles speeds as shown in Figure 3.13. This shows that the effect of vehicle speeds becomes slightly less pronounced with an increase in vehicle speed similar to the DLC results in section 3.1.2. A linear approximation would however be relatively accurate, especially over moderated changes in vehicle speeds.

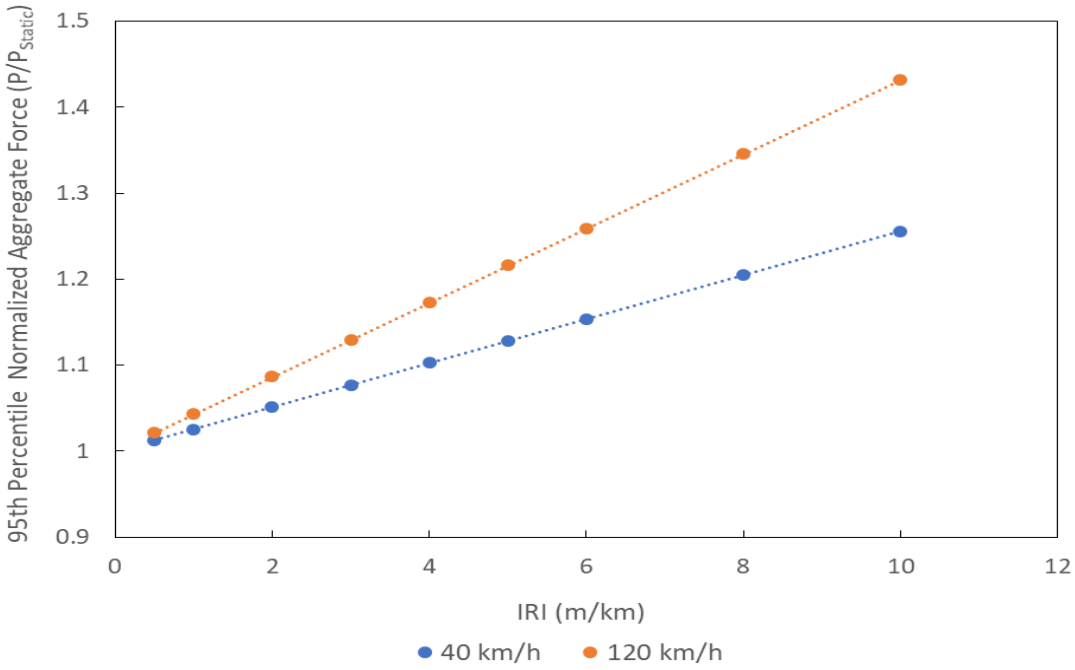

Figure 3.12: The normalized (by static values) 95th percentile first power aggregate forces of the left side as a function of road roughness

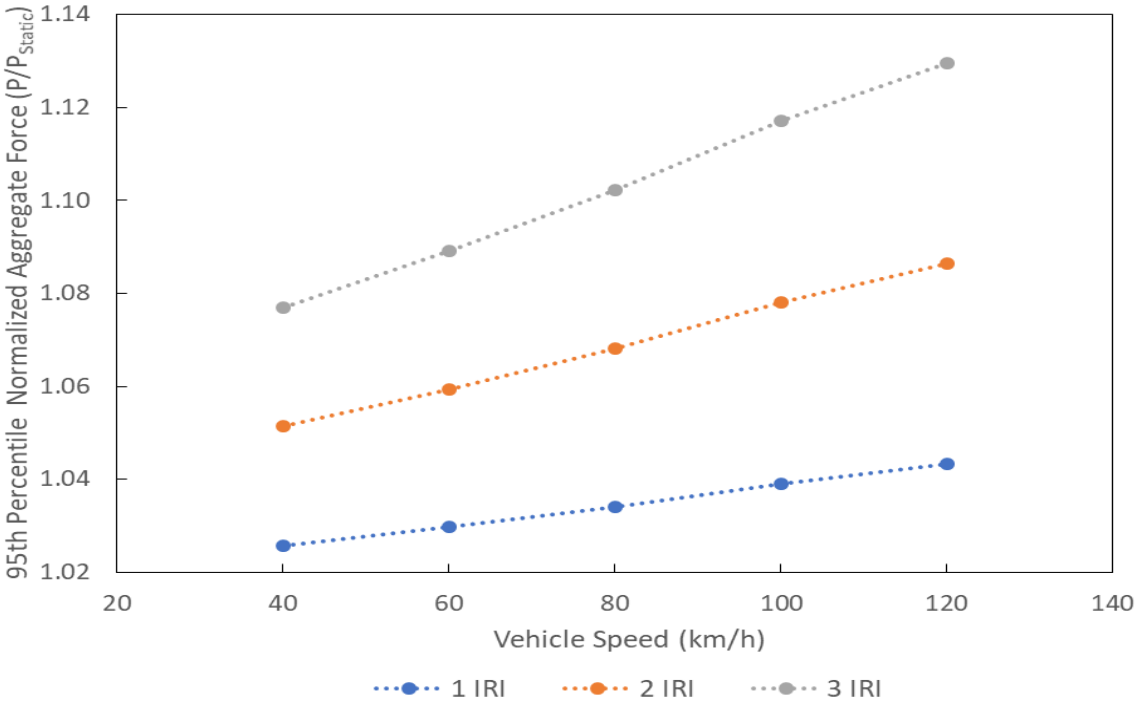

Figure 3.13: The normalized (by the static force) 95th percentile first power aggregate forces of the left side as a function of vehicle speed

The percentage difference between the left and right side 95th percentile aggregate forces are summarized in Figure 3.14 and Figure 3.15. The percentage difference between the left and right side decreases quadratically with an increase in road roughness but can be accurately estimated using a linear approximation. The vehicle speeds however have no influence on the percentage difference. Road crossfall once again linearly increases the percentage difference between the left and right side.

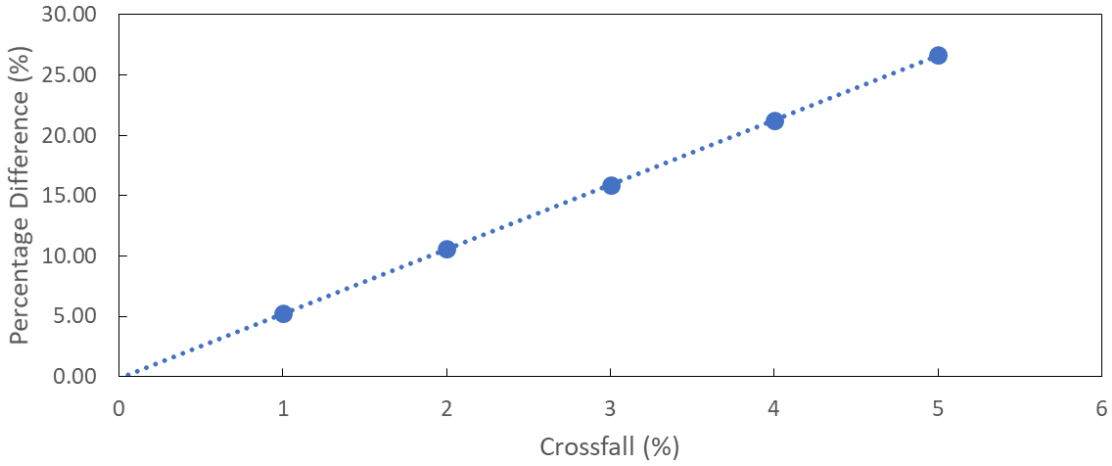

Figure 3.14: The percentage difference in left and right 95th percentile first power aggregate force as a function of crossfall at a vehicle speed of 80 km/h and road roughness of 2 m/km

The maximum difference between the left and right side 95th percentile aggregate force is 28.2%. At an operating speed of 80 km/h and road roughness value of 2 m/km the percentage difference

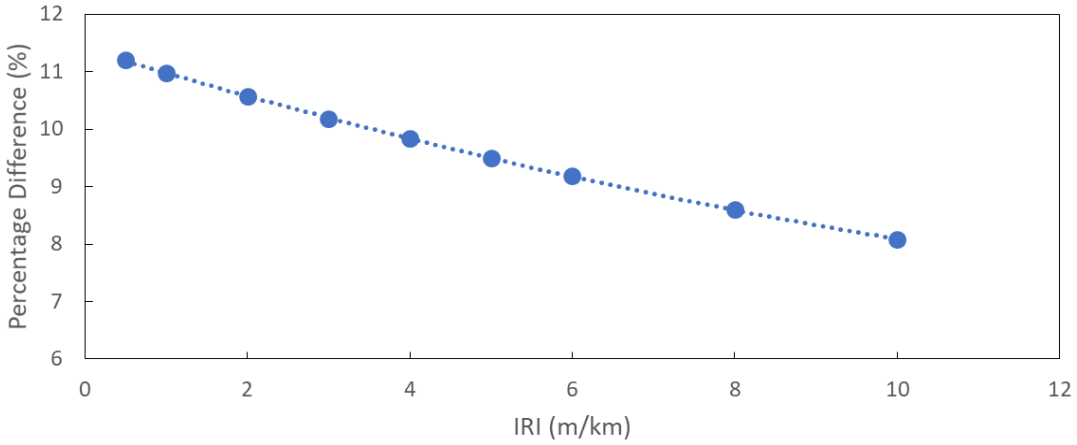

Figure 3.15: The percentage difference in left and right 95th percentile first power aggregate force as a function of road roughness at a vehicle speed of 80 km/h and crossfall of 2%

is 10.6% and 15.9% at a crossfall value of 2% and 3% respectively. Additional results for the 95th percentile first power aggregate forces can be obtained in Table E.9 and Table E.10.

The 99th percentile first power aggregate forces increase linearly once again with an increase in the road crossfall. The 99th percentile first power aggregate force increases with an increase in road roughness with the slope becoming more at higher road roughness values for a specific vehicle speed and crossfall as shown in Figure 3.16. This can be accurately estimated using a quadratic relationship. Figure 3.17 shows that the 99th percentile first power aggregate force increases linearly (with only minor fluctuations at specific values) with an increase in vehicle speed for a specific road roughness and crossfall value.

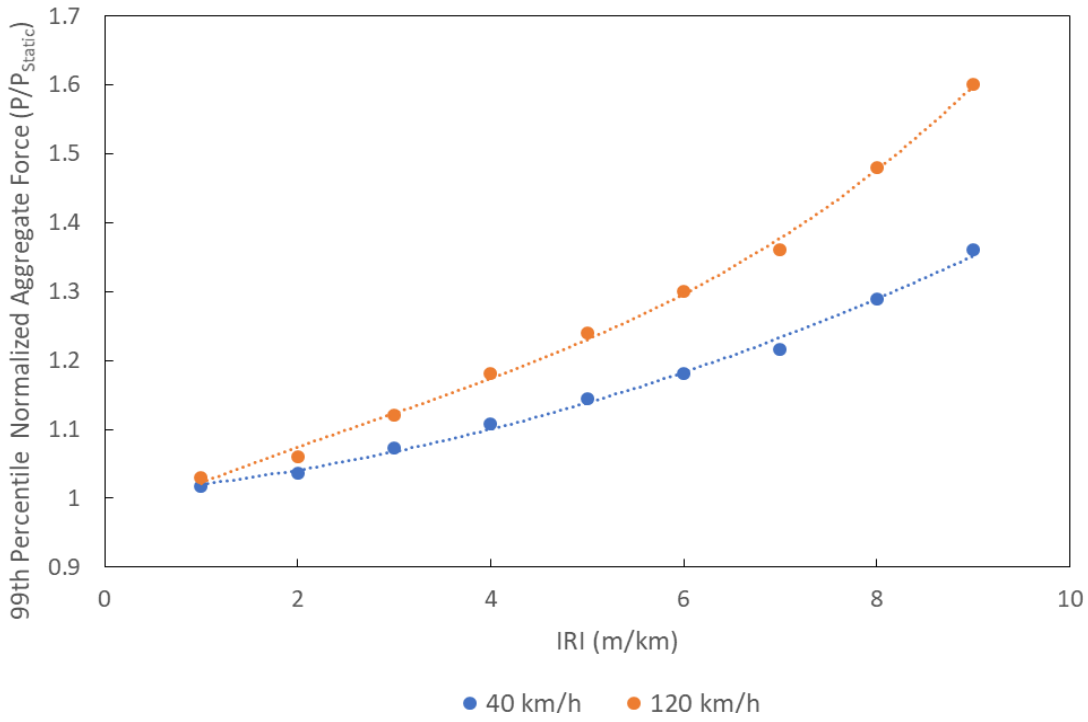

Figure 3.16: The normalized (by the static force) 99th percentile first power aggregate forces of the left side of the base model as a function of the road roughness

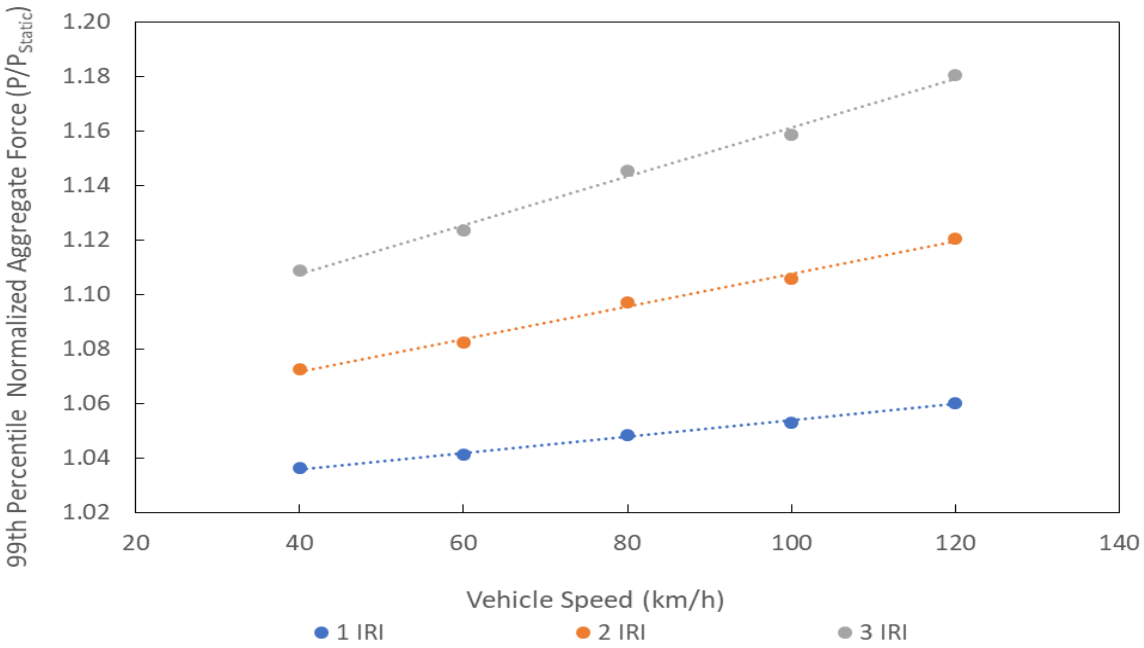

Figure 3.17: The normalized (by the static force) 99th percentile first power aggregate forces of the left side of the base model as a function of vehicle speed

The percentage difference of the 99th percentile first power aggregate forces follow the same trend as the 95th percentile first power forces. The maximum percentage difference recorded is 28.3%. For the typical highway speed of 80 km/h and road roughness value of 2 m/km the percentage difference is 10.4% and 15.6% at a crossfall value of 2% and 3% respectively. Additional results for the 99th percentile first power aggregate forces can be obtained in Table E.11 and Table E.12

3.1.4. The effect of crossfall on the fourth power aggregate forces of the base model

As with the first power aggregate forces, the fourth power aggregate forces are also often reported using the average, 95th percentile and 99th percentile forces. Specifically, the 95th percentile fourth power aggregate forces are often referred to as the road damage criteria [12]. The fourth power aggregate forces are often considered the most important criteria as this is related to the fatigue failure of road pavements which is the primary form of road failure especially for asphalt road pavements. The 95th percentile fourth power aggregate force is often normalized by the static aggregate fourth power force. This ratio is often referred to as the road damage coefficient [23]. The fourth power aggregate forces are normalized by 3.2×10^{18} N^4. The trends are very similar for the average, 95th percentile an 99th percentile fourth power aggregate forces. Focus is given to the 95th percentile fourth power aggregate force as this is often used as the main road damage criteria in similar studies. Figure 3.18 and Figure 3.19 present the results for the 95th percentile aggregate fourth power tyre forces for both sides of the base model over all the operating conditions. This provides an overview of the relative influence of the different parameters.

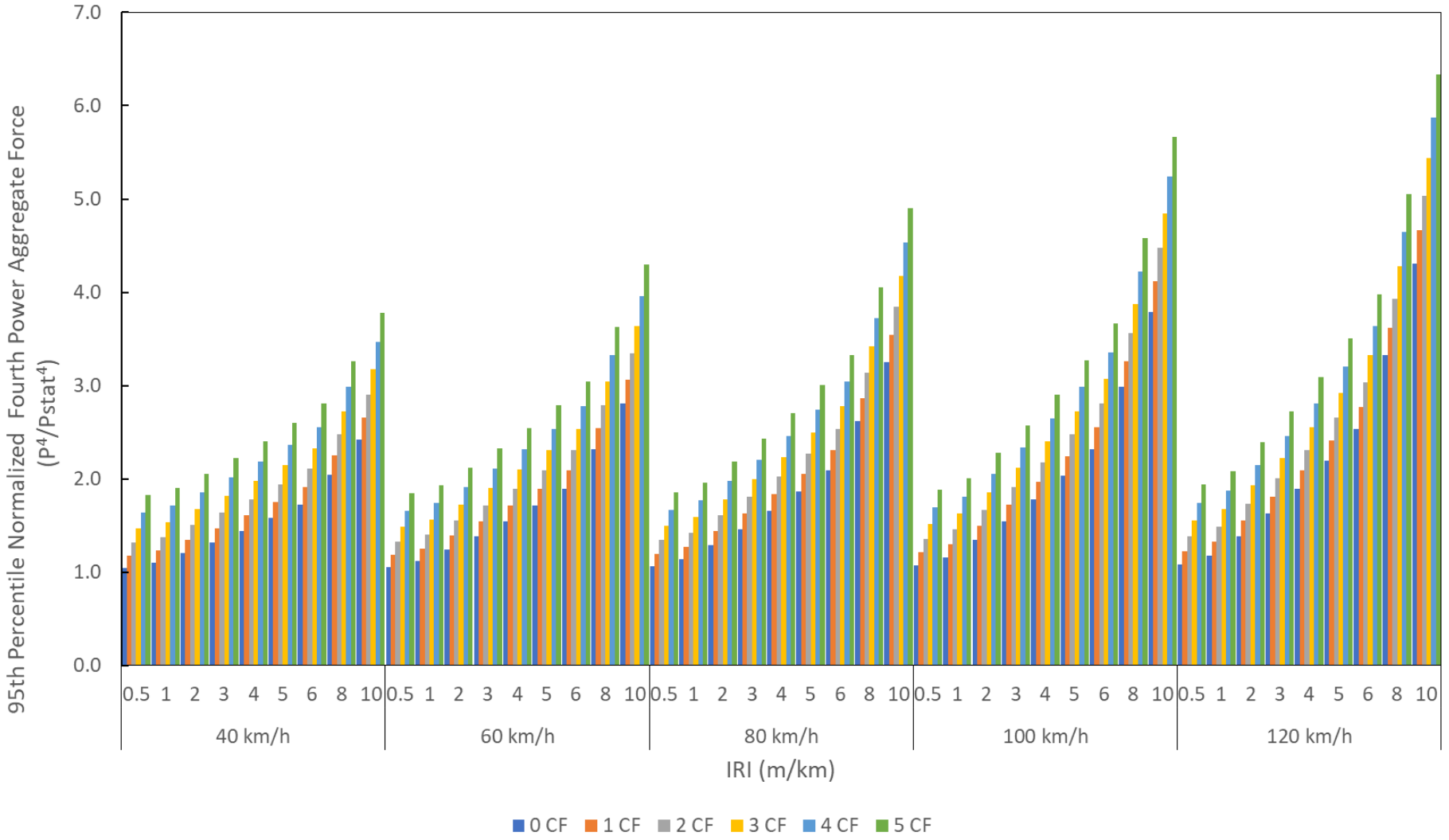

Figure 3.18: The normalized 95th percentile fourth power aggregate force of the left side of the base model over all of the operating conditions

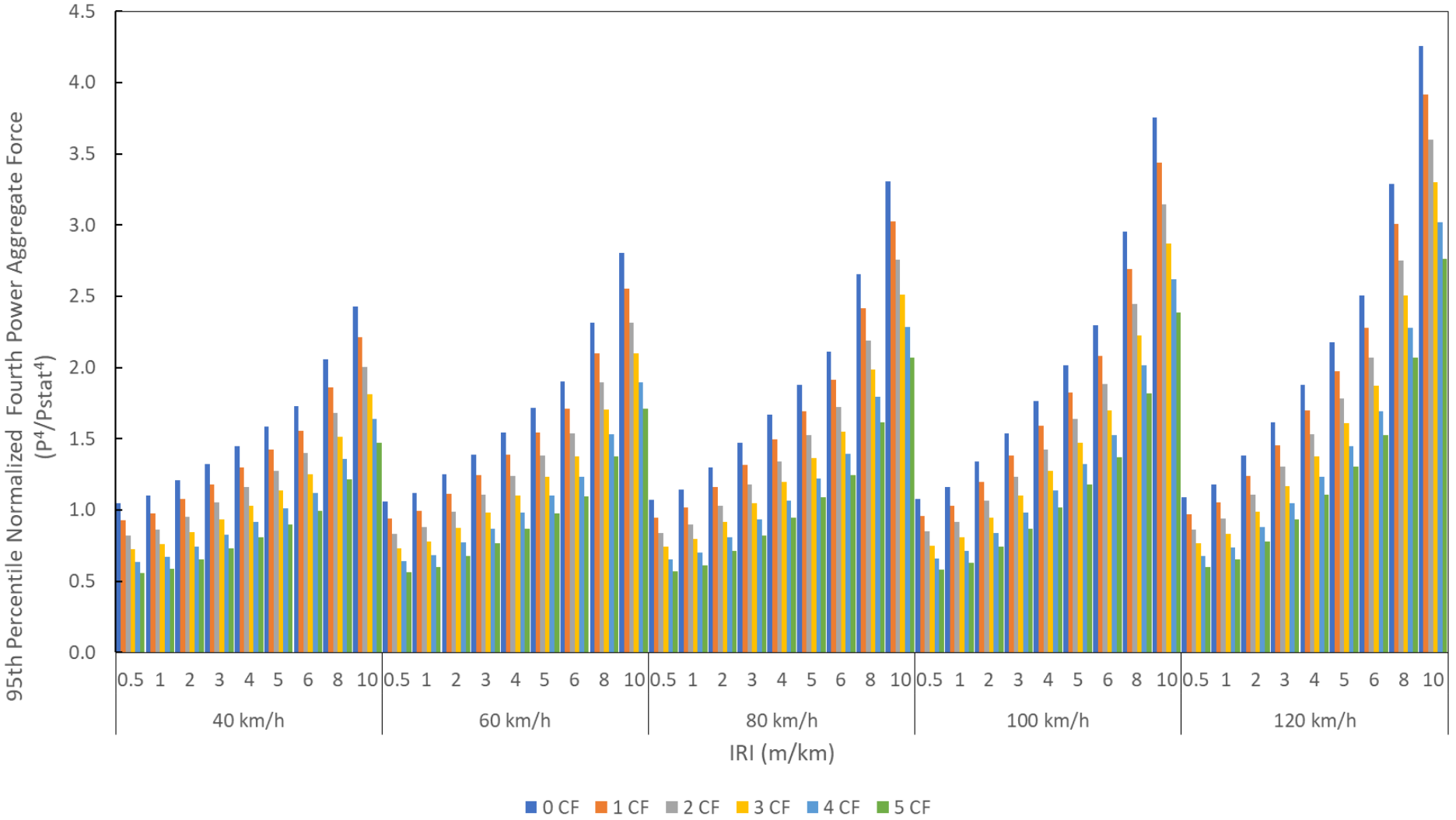

Figure 3.19: The normalized 95th percentile fourth power aggregate force of the right side of the base model over all of the operating conditions

The road crossfall still has a linear effect on the fourth power aggregate forces and increases on the left side and decreases on the right side as the crossfall increases. This is more clearly demonstrated in Figure 3.20.

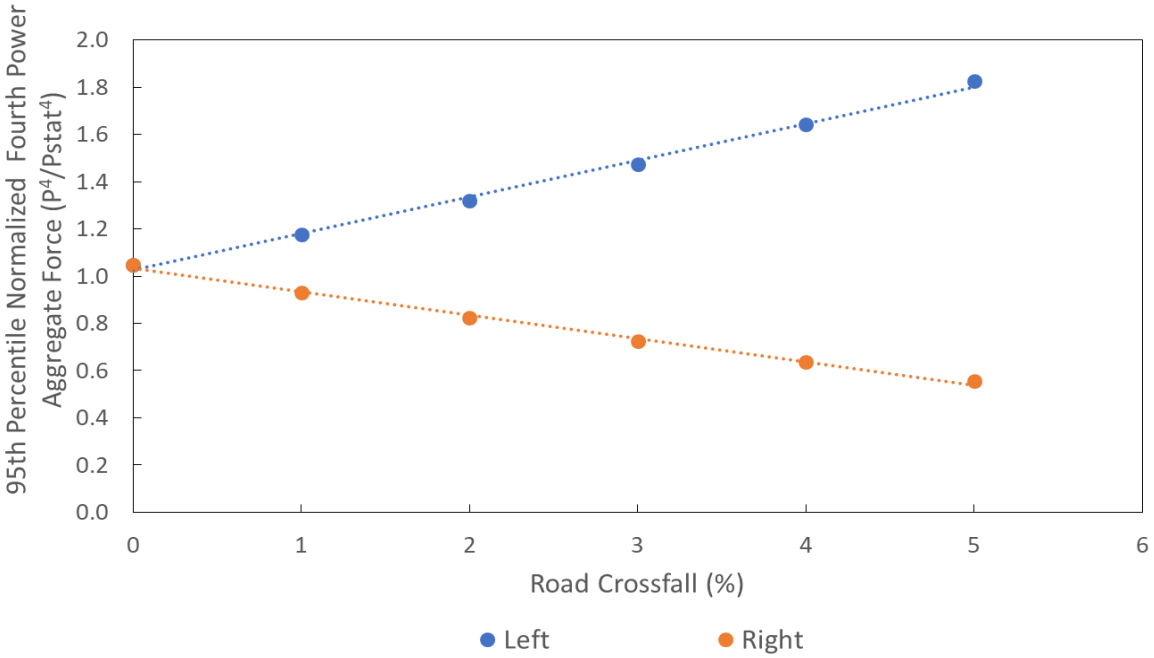

Figure 3.20: The normalized (by static values) 95th percentile fourth power aggregate force of the left and right side of the base model for different crossfall values ,a vehicle speed of 80km/h and road roughness of 2m/km

For a typical highway roughness value of 2 m/km and vehicle speed of 80 km/h, the left side normalized damage ranges from 1.293 at a road crossfall of zero to 2.189 at a road crossfall of 5%. This shows that a small change of 5% in the crossfall, increased the normalized damage by almost 70%. At a more typical crossfall value of 2% the normalized damage coefficient on the left side is 1.608. This is an increase of 24%. The dynamic damage is more than the static damage. Simply using the static fourth power forces severely underestimates the road damage produced.

Considering the right side normalized fourth power forces at a vehicle speed of 80 km/h and road roughness of 2 m/km, the values change from 1.297 at a crossfall of 0% to 0.711 at a road crossfall of 5%. This is a decrease of 46% which is much less than the increase of 70% on the left side of the vehicle. At a more typical crossfall value of 2% the normalized damage is 1.031 which shows a decrease of 21%. This is a value closer to the increase of 24% on the right side. Therefore, the rate of increase in damage is higher on the left side compared to the rate of decrease in damage on the right side. These differences are exacerbated at higher road roughness values and vehicle speeds. For example, using a road roughness of 4 m/km and a road crossfall of 3% which is typical on more urban roads, the normalized road damage is 2.238 on the left side and 1.199 on the right side. This shows that the road damage on the left is more than double the static value and, on the right, almost 20% greater than the static value.

The 95th percentile fourth power aggregate force increases with an increasing road roughness with the slope increasing with increasing roughness values as shown in Figure 3.21. It was found that a fourth power relationship (with an R^2 value of 0.999) exists between the road damage and the road roughness values. Therefore, road roughness has a considerable effect on the average aggregate fourth power force and even minor variations in the left and right road profile can have a substantial effect, especially at higher roughness values.

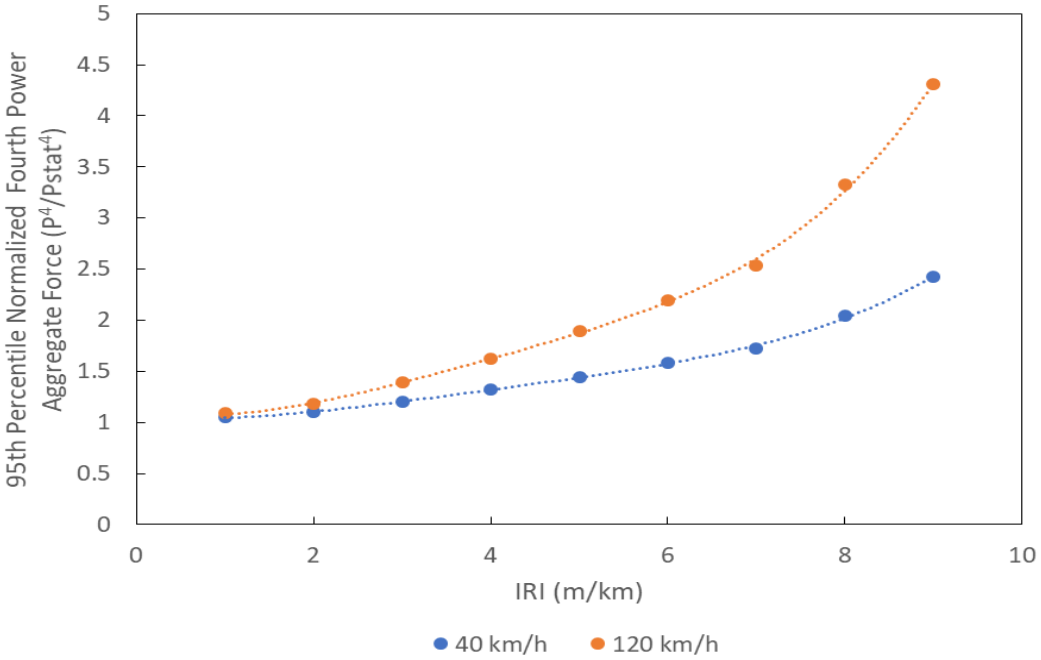

Figure 3.21: The normalized (by static values) 95th percentile fourth power aggregate force as a function of road roughness

The vehicle speed linearly increases the 95th percentile aggregate fourth power forces as shown in Figure 3.22. The rate of this change is dependent on the road roughness value and the crossfall with higher road roughness value and crossfall values having a higher rate of change for a specific vehicle speed.

The percentage difference in the left and right 95th percentile fourth power aggregate force is independent of vehicle speed. The percentage difference increases linearly as a function of the road crossfall as shown in Figure 3.23. The percentage difference decreases in a quadratic nature for a change in the road roughness, but a linear approximation will provide accurate results as shown in Figure 3.24. The maximum percentage difference in the left and right 95th percentile fourth power aggregate force is 106.7%. The percentage difference at a typical highway operating speed of 80 km/h and road roughness of 2 m/km is 43.7 % for a crossfall of 2% and 64.6% for a crossfall of 3%. This shows that under typical operating conditions in South Africa, crossfall will substantially affect the road damage on the left and right side. This could have a substantial effect on the expected operational life of the road. Even at a low crossfall value of 1%, the percentage difference was recorded as 21.9%.

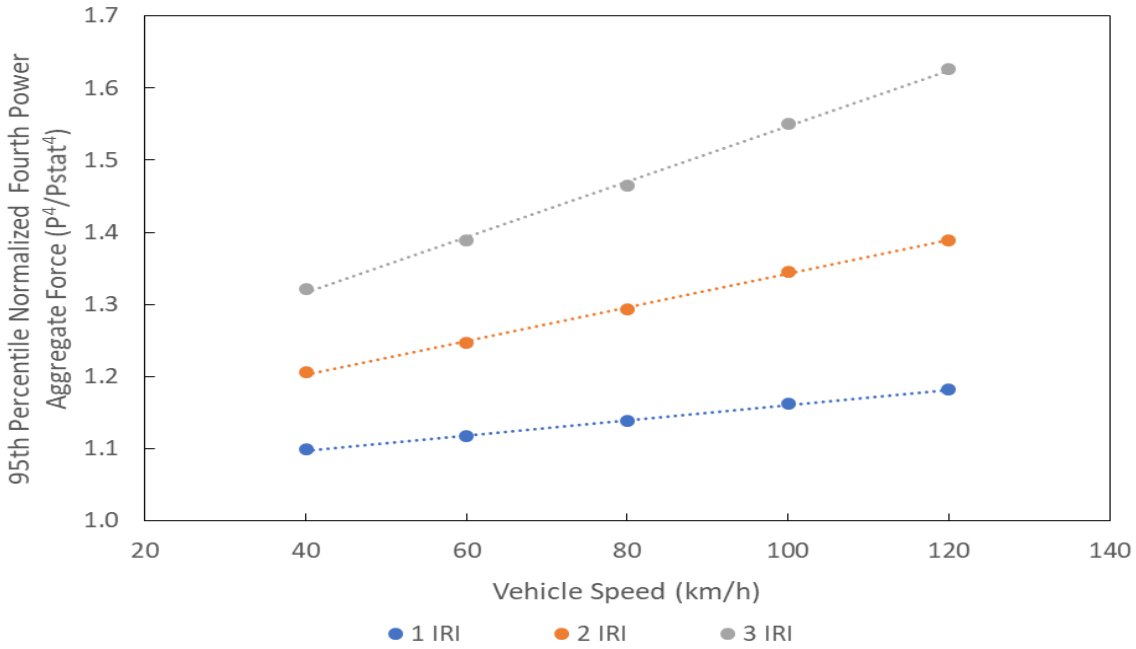

Figure 3.22: The normalized (by static values) 95th percentile fourth power aggregate force as a function of vehicle speed

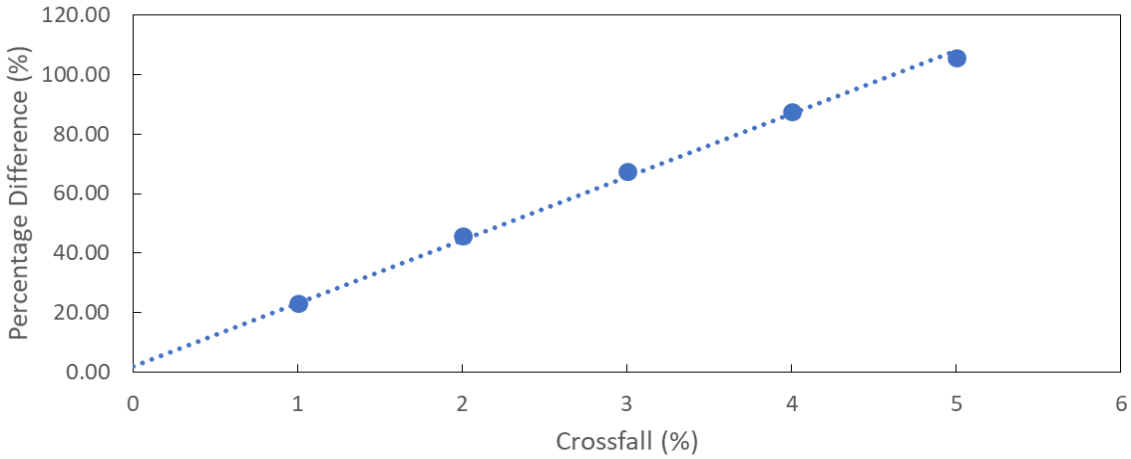

Figure 3.23: Percentage difference in the left and right 95th percentile fourth power aggregate forces for a vehicle speed of 80 km/h and road roughness of 2 m/km

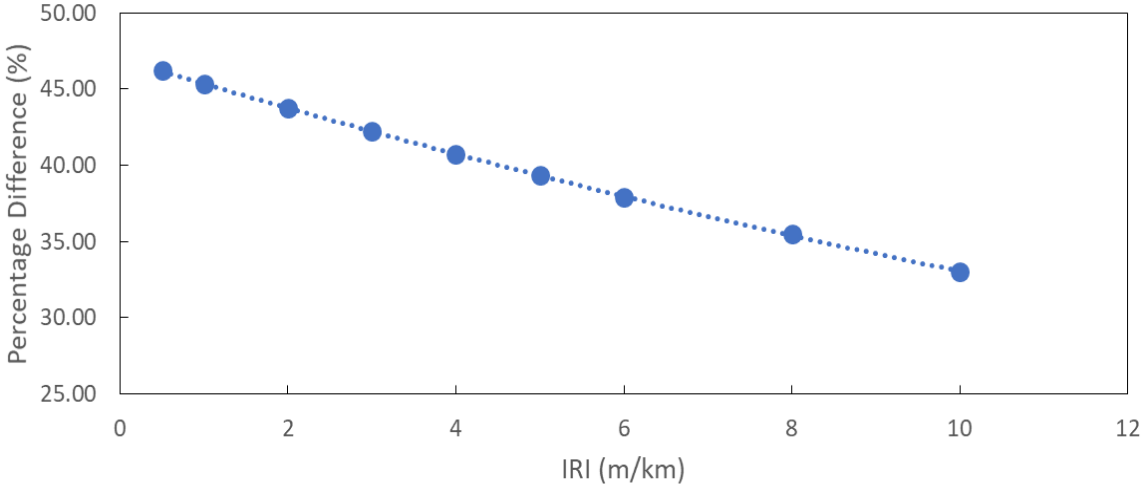

Figure 3.24: Percentage difference in the left and right 95th percentile fourth power aggregate forces for a vehicle speed of 80 km/h and road crossfall of 2%

To investigate if an approximation exists for obtaining the percentage difference in the fourth power aggregate force from the first power aggregate force, the ratio of the two values was taken as shown in Table E.19. This shows that one can reasonably estimate the percentage difference in the fourth power aggregate forces by multiplying the percentage difference of the first power aggregate forces by 4. The approximation is very accurate at crossfall values of 2-3%. The ratio decreases as the crossfall increases.

Additional results of the average, 95th percentile and 99th percentile fourth power aggregate forces are presented in Appendix E from Table E.13 to Table E.19.

3.2. The effect of different vehicle parameters on the fourth power damage when including crossfall

This section of the report contains a comparison of a selected number of heavy vehicle parameters on the fourth power aggregate force when including road crossfall. This includes both the percentage difference in the left and right road damage as well as the overall road damage produced. The comparison is limited to the normalized 95th percentile fourth power aggregate force which is often referred to as the damage coefficient and used as a road damage comparison criterion [42]. The comparison is further limited to a vehicle speed of 80 km/h and road roughness values between 0.5 m/km and 4 m/km are included. Normalized fourth power aggregate forces are presented and they are normalized by the static fourth power aggregate force which is equal to 3.2x10^{18} N^4.

3.2.1. The effect of including anti-roll bars

Figure 3.25 shows the percentage difference between the left and right 95th percentile fourth power forces using different anti-roll bar stiffnesses. The results show that the addition of anti-roll bars at the front and rear of the vehicle decrease the percentage difference between the left and right fourth power aggregate forces when including road crossfall. The influence is however highly non-linear as doubling the anti-roll bar stiffnesses decreased the percentage difference marginally. This makes sense as the vehicle suspension will eventually mimic a totally rigid suspension and stiffer suspension will no longer have any effect. For a typical crossfall value of 2% and road roughness of 2 m/km the percentage difference between left and right fourth power aggregate forces is 43.7% with no anti-roll bars, 34.3% for the lower stiffness anti-roll bars and 32.7% for the higher stiffness anti-roll bars.

It is also important to consider the overall fourth power aggregate force produced and not only focus on the percentage difference. Figure 3.26 shows the left side normalized 95th percentile fourth power aggregate forces with the different anti-roll bar values. The results show that the

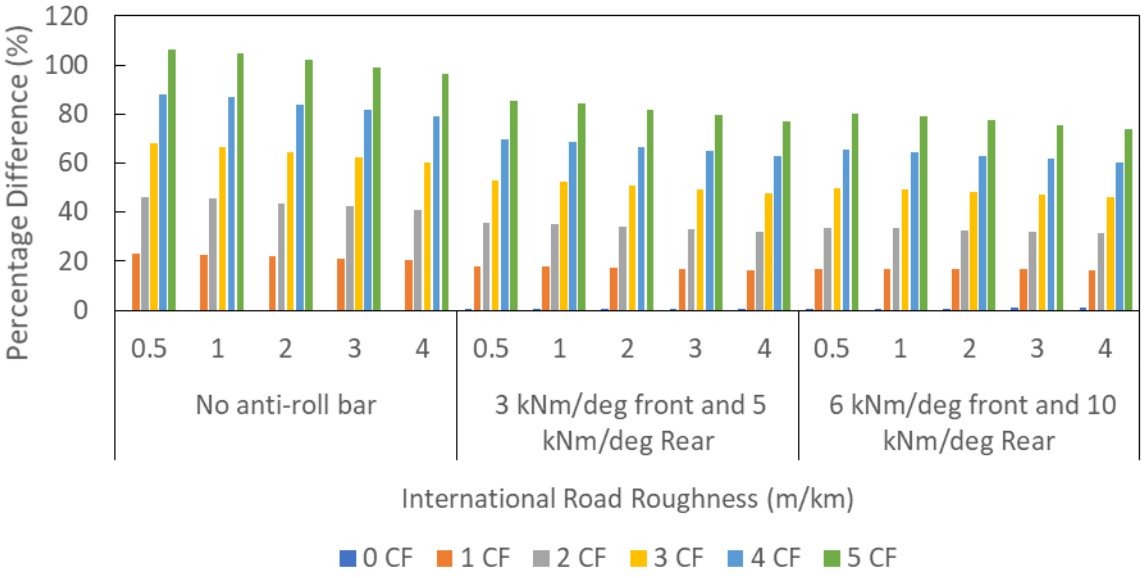

Figure 3.25: The percentage difference between the left and right 95th percentile fourth power aggregate forces using different anti-roll bar values at 80 km/h

addition of the anti-rollbar decreases the left side fourth power aggregate forces and therefore increases the road friendliness of the vehicle when including road crossfall. At a crossfall value of 2% and road roughness of 2 m/km the normalized value is 1.608 with no anti-roll bars, 1.530 with the lower stiffness anti-roll bars and 1.514 for the higher stiffness anti-roll bars. The same trend is observed on the right side.

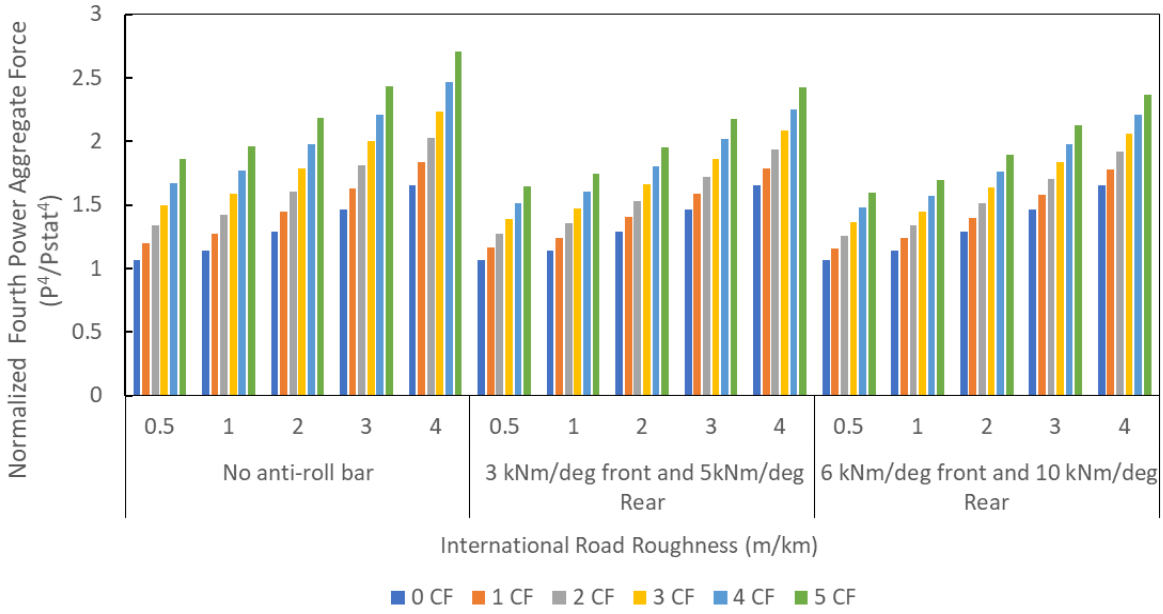

Figure 3.26: The left normalized 95th percentile fourth power aggregate forces using different anti-roll bar values at 80 km/h

Anti-roll bars therefore appear to offer value in decreasing the percentage difference in the left and right road damage as well as the overall road damage produced by the vehicle when including road crossfall. The gains however become negligible for higher stiffness values. Tables of fourth

power aggregate forces for different anti-roll bar values are presented in Appendix E in Table E.20 to Table E.22.

3.2.2. The effect of the sprung mass centre of gravity height

Figure 3.27 shows the percentage difference between the left and right 95th percentile fourth power forces for three different values of sprung mass centre of gravity heights. The results show that the percentage difference is highly dependent on the sprung mass centre of gravity height and increases with an increase in the sprung mass height. The percentage difference seems to increase linearly with an increase in the sprung mass CoG height. For a road crossfall of 2% and road roughness of 2 m/km the percentage difference between left and right is 26.4% for a CoG height of 1.5 m, 43.7% for a CoG height of 2.0 m and 73.6% for a CoG height of 2.5 m. This means that lower density products with high COG heights will have a larger percentage difference in the left and right road damage. Increasing the CoG height also increases the rate of change of the percentage difference at different crossfall values and therefore the effect becomes even more pronounced when including crossfall.

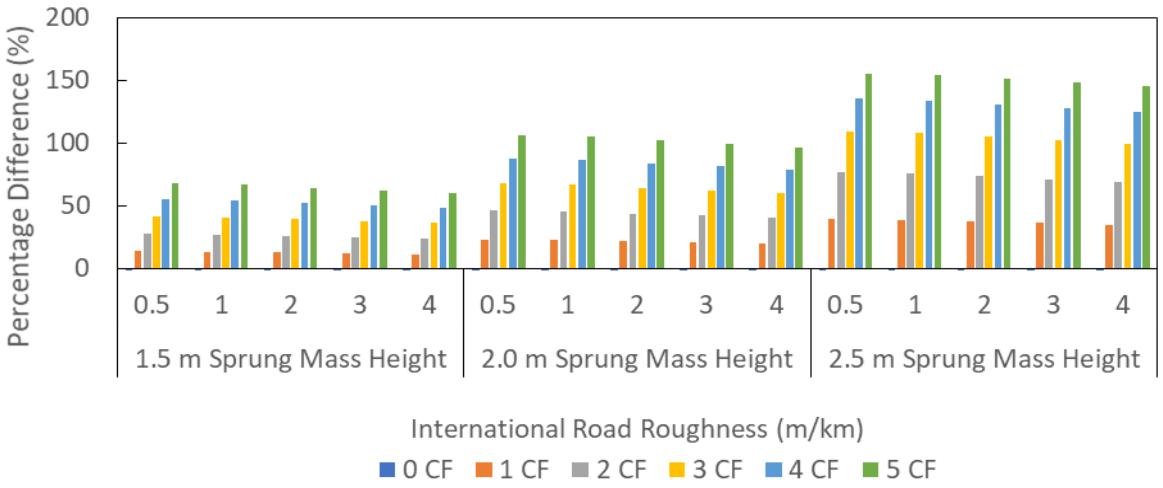

Figure 3.27: The percentage difference between the left and right 95th percentile fourth power aggregate forces using different sprung mass height values at 80 km/h

Considering the normalized left 95th percentile fourth power aggregate forces as shown in Figure 3.28, an increase in the CoG height will increase the normalized damage. At a crossfall value of 2% and road roughness of 2 m/km the normalized damage is 1.493 at CoG height of 1.5 m, 1.608 at a CoG height of 2 m and 1.873 at a CoG height of 2.5 m. Once again one can see that higher CoG heights increase the rate of change in the fourth power aggregate forces when increasing the road crossfall.

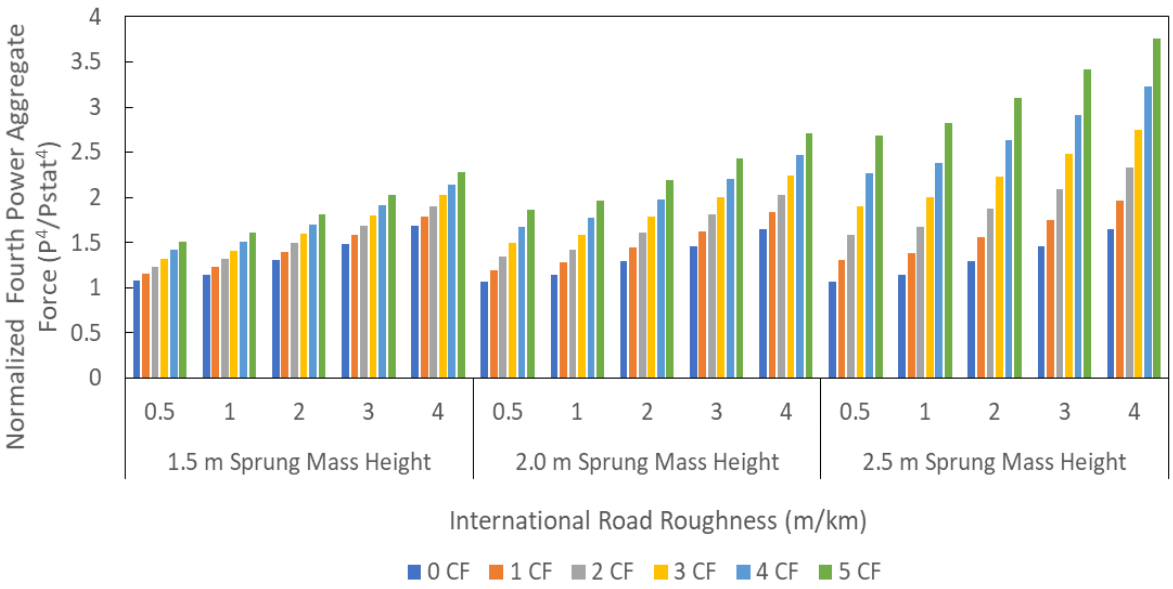

Figure 3.28: The left normalized 95th percentile fourth power aggregate forces using different sprung mass height values at 80 km/h

It is therefore imperative that the CoG height be kept as low as possible to reduce road damage whenever road crossfall is present. It is therefore possible that minor changes such as lower profile tyres and changes in truck and trailer CoG heights can have a substantial influence in the overall road damage caused on the roads. Additional results are available in Appendix E in Table E.23 to Table E.25 and show that the right side forces have the same trends.

3.2.3. The effect of the roll centre height

The effect of the roll centre height on the percentage difference between the left and right 95th percentile fourth power aggregate force is shown in Figure 3.29. The percentage difference increases as the roll centre height decreases. At a crossfall value of 2% and road roughness of 2 m/km the percentage difference is 49.1% at a roll centre height of 400 mm, 45.5% at a roll centre height of 500 mm and 42.2% at a roll centre height of 600 mm. This means that underslung types of suspension (assuming the same centre of gravity height) will have a larger percentage difference in the road damage between left and right compared to overslung suspensions which typically have high higher roll centre heights. Normally underslung suspensions are used to reduce the centre of gravity height and thus the overall effect is complex. Using other components such as control arms to increase the roll centre height is therefore also advisable as this will decrease the percentage difference in the left and right road damage.

Figure 3.30 shows the normalized left 95th percentile fourth power aggregate forces at the different roll centre heights. Increasing the roll centre height decreases the normalized road damage on the left side and therefore is beneficial to decreasing road damage when including road crossfall. At a crossfall of 2% and 2 m/km road roughness the normalized damage is 1.672 with a

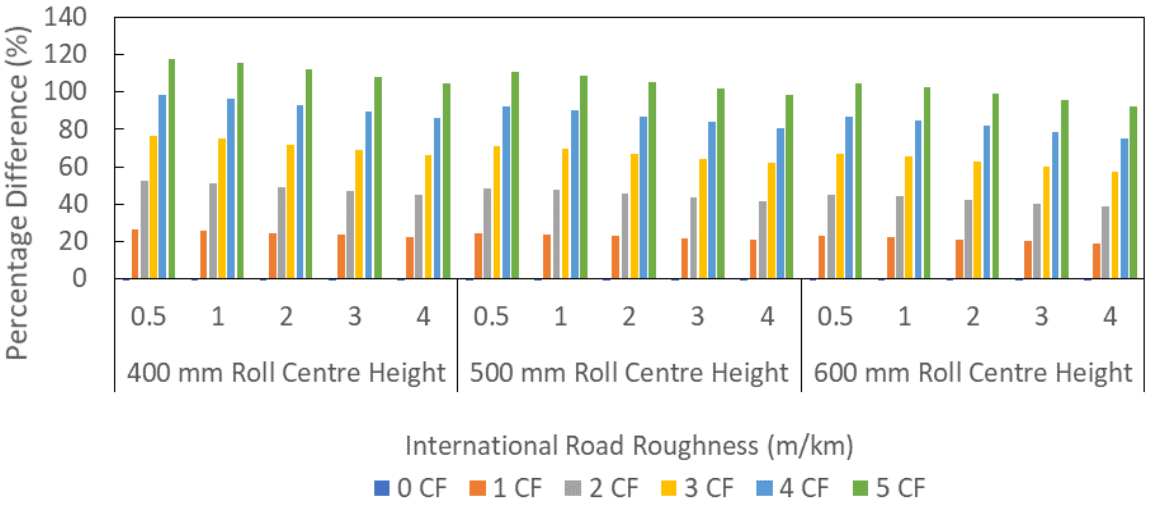

Figure 3.29: The percentage difference between the left and right 95th percentile fourth power aggregate forces using different roll centre height values at 80 km/h

roll centre height of 400 mm, 1.637 with a roll centre height of 500 mm and 1.608 with a roll centre height of 600 mm. The same trends are observed on the right side. Additional results are available in Appendix E in Table E.26 to Table E.28.

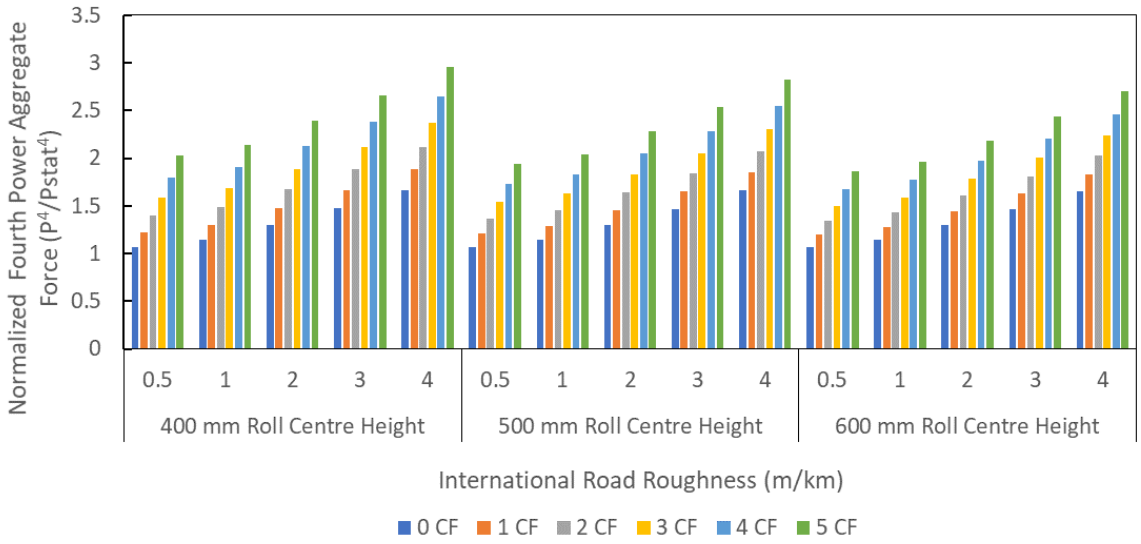

Figure 3.30: The left normalized 95th percentile fourth power aggregate forces using different roll centre height values at 80 km/h

3.2.4. The effect of the suspension stiffness

Figure 3.31 shows the percentage difference in the 95th percentile fourth power aggregate force when using different suspension stiffness values. The results show that increasing the suspension stiffness decreases the percentage difference in the left and right fourth power aggregate forces. For a crossfall value of 2% and road roughness of 2 m/km the difference is 43.7% at the original stiffness, 38.0% for the intermediate stiffness and 33.8% for the highest suspension stiffness. This

shows a decrease in the percentage difference will eventually plateau as the stiffness increases. This makes sense as the vehicle suspension will eventually mimic a totally rigid suspension and an increase in stiffness will no longer have any real effect on the percentage difference. The results indicate that air suspensions which are typically softer, will have higher percentage differences in the left and right road damage.

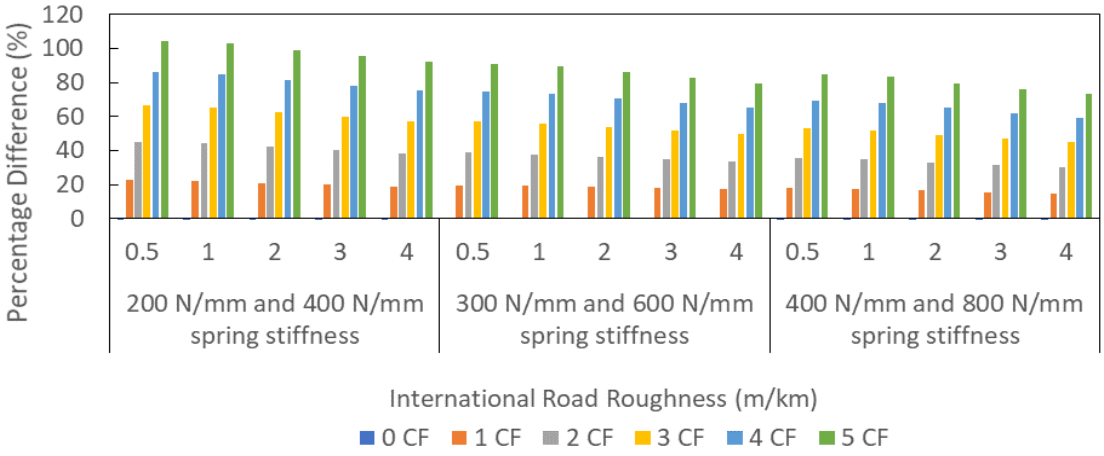

Figure 3.31: The percentage difference between the left and right 95th percentile fourth power aggregate forces using different suspension stiffness values at 80 km/h

Comparing Figure 3.31 and Figure 3.32 shows that although a stiffer suspension will decrease the percentage difference in the left and right fourth power aggregate forces, the overall damage will increase due to the higher stiffness. Specifically, the normalized road damage increases from 1.608 at the original stiffness, to 1.614 at the moderate stiffness and 1.658 at the higher stiffness at a crossfall value of 2% and road roughness 2 m/km. The same holds true on the right side of the vehicle. Therefore, increasing the vehicle suspension stiffness decreases the percentage difference

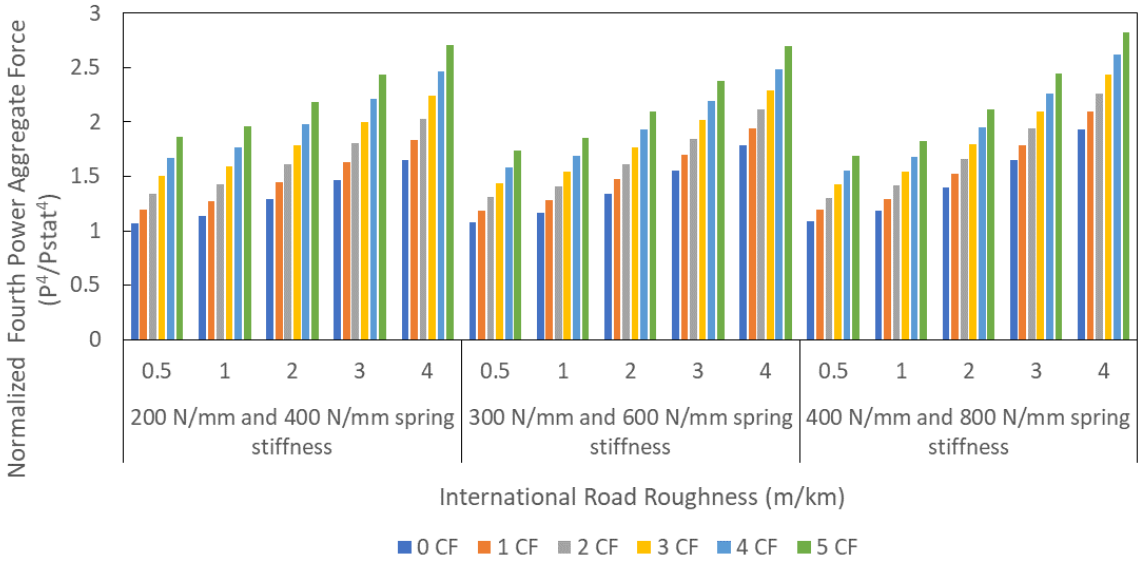

Figure 3.32: The left normalized 95th percentile fourth power aggregate forces using different suspension stiffness values at 80 km/h

in the left and right road damage, but at the detriment of increasing the overall road damage produced by the vehicle. Therefore, one would be able to decrease the percentage difference in the road damage, but still cause more damage on the left track causing the road to fail faster. Having steel suspension that has multi-stage springs could therefore be beneficial as the stiffness will then only increase for heavier loads and will be lower when unladen. Additional results are available in Appendix E in Table E.29 to Table E.31

3.2.5. The effect of the suspension damping

The influence of the suspension damping values on the percentage difference in the left and right 95th percentile fourth power aggregate forces is shown in Figure 3.33. It shows that the percentage difference in the 95th percentile fourth power aggregate forces is only slightly dependent on the suspension damping values but higher damping increases the percentage difference slightly. Specifically, the percentage difference is 43.7%, 44.8%, and 45.0% respectively at the three different damping values.

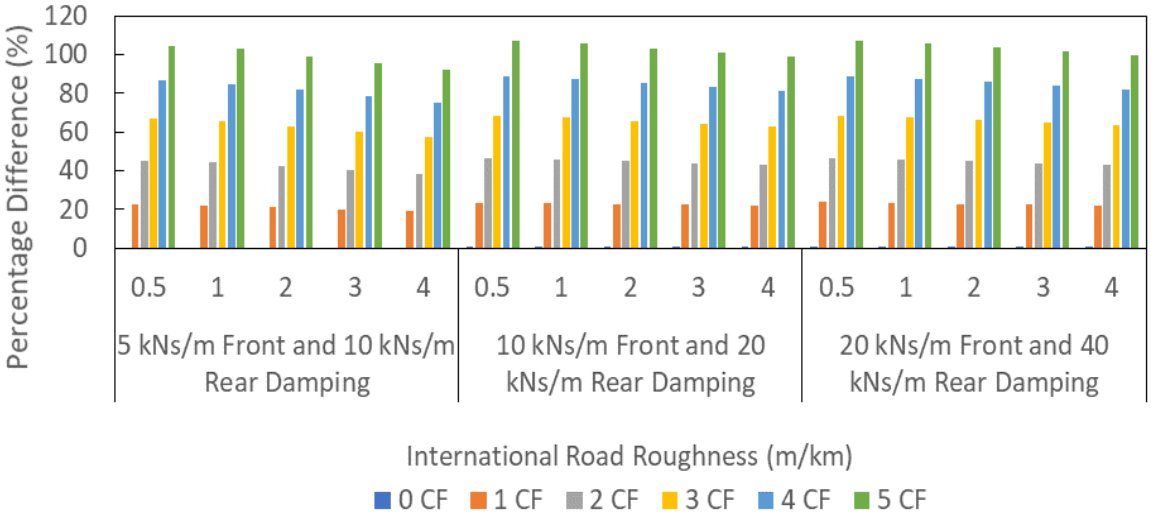

Figure 3.33: The percentage difference between the left and right 95th percentile fourth power aggregate forces using different suspension damping values at 80 km/h

Although the suspension damping values does not significantly influence the percentage difference in the road damage, it does influence the road damage caused on each side of the vehicle as shown in Figure 3.34. The left side normalized road damage decreases from 1.608 at the lowest damping values to 1.558 at the intermediate damping values and 1.547 at the highest damping values. Increasing the damping fourfold only decreased the normalized road damage by 4%. Therefore, the benefits of a higher damping value will eventually diminish, and an intermediate value will most likely provide the most economical solution for a heavy vehicle operator. Heavy vehicle damping is heavily studied as it is believed to be very beneficial for reducing dynamic road damage. It is worth noting that many of the other parameters that

influence the heavy vehicle rolling motion have a greater influence when including road crossfall. In order to fully quantify the effect of the dampers, the non-linear nature of the dampers should be considered in future work as the currently assumption of linear dampers is not realistic of typical damper behaviour. Additional results are available in Appendix E in Table E.32 to Table E.34.

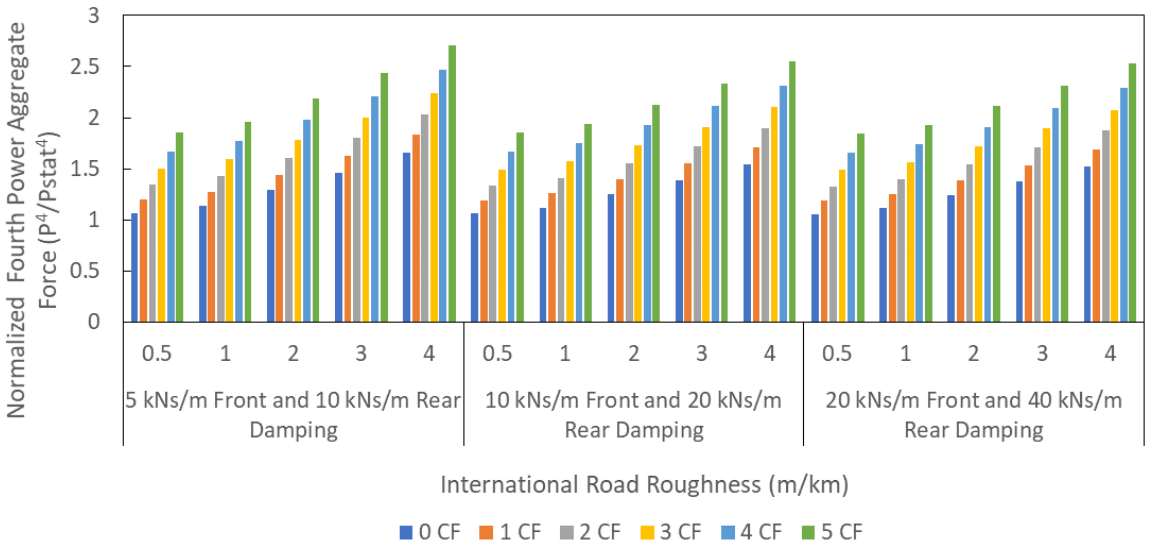

Figure 3.34: The left normalized 95th percentile fourth power aggregate forces using different suspension stiffness values at 80 km/h

3.2.6. The effect of the track width

Figure 3.35 shows the results for the percentage difference in left and right 95th percentile fourth power aggregate forces using different track width values typically seen on heavy vehicles. The results show that an increase in the track width will decrease the percentage difference between the left and right fourth power aggregate forces. This is due to the increased roll stability produced

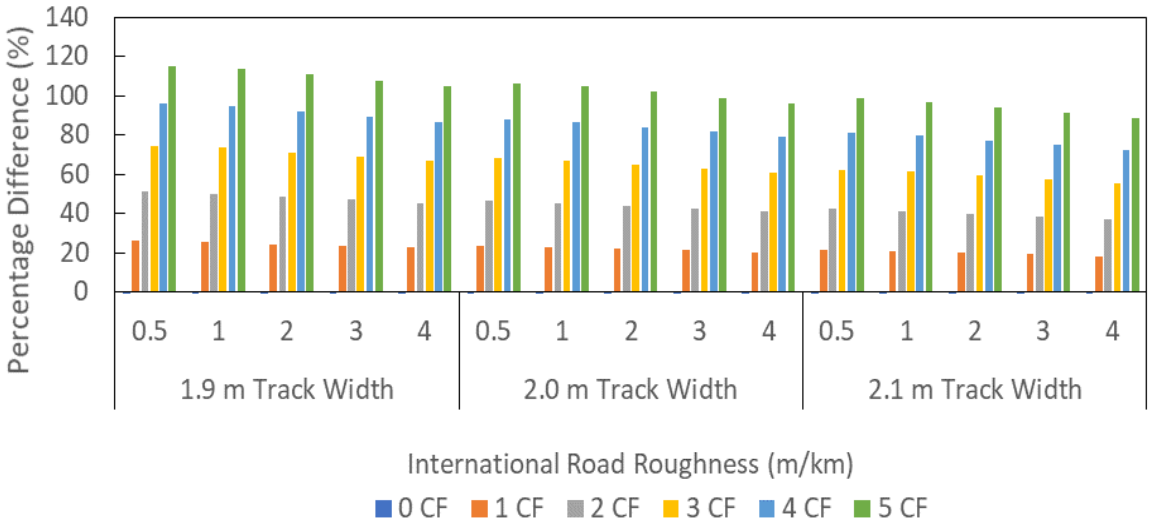

Figure 3.35: The percentage difference between the left and right 95th percentile fourth power aggregate forces using different track width values at 80 km/h

by the increased track width. At a crossfall of 2% and road roughness of 2 m/km the percentage difference is 48.4% using a track width of 1.9 m, 43.7% using a track width of 2 m and 39.8% using a track width of 2.1 m. The percentage difference will increase more rapidly as the track width becomes smaller as the vehicle will roll quicker in the presence of crossfall.

Figure 3.36 shows that an increase in track width will also decrease the left side 95th percentile fourth power aggregate force. At a road crossfall of 2% and road roughness of 2 m/km the normalized fourth power damage decreases from 1.641, to 1.608 and 1.576 for the three respective track widths. The same trends are observed on the right side of the vehicle. Increasing the track width therefore is a viable and worthwhile option to not only decrease the percentage difference in the road damage between the left and right side but also to decrease the overall road damage produced by a heavy vehicle. This result would suggest that dual tyre axles will tend to have a larger percentage difference in the left and right road damage due to the lower track widths compared to single axle tyres. Dual tyres however decrease road damage due to the increased contact area of the tyres and therefore are still considered to be more road friendly. Additional results are available in Appendix E in Table E.35 to Table E.37.

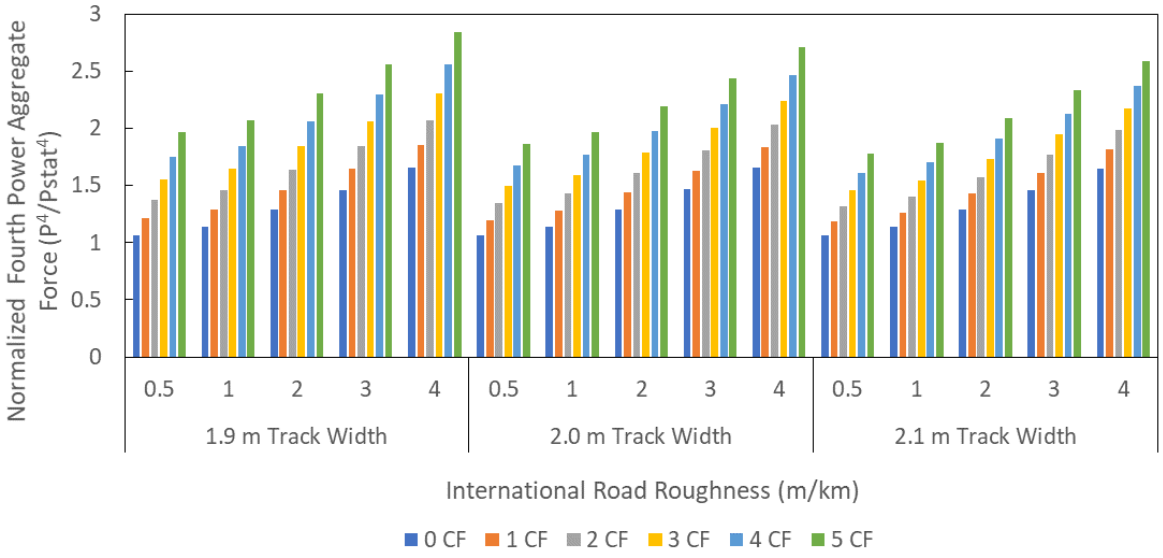

Figure 3.36: The left normalized 95th percentile fourth power aggregate forces using different track width values at 80 km/h

3.2.7. The effect of the suspension track width

Figure 3.37 illustrates the effect of different spring and damper track widths on percentage difference of the left and right 95th percentile fourth power aggregate forces. The results show that an increase in the spring track width decreases the percentage difference between the left and right side. The effect however appears to be highly non-linear and that the effect seems to become less pronounced as the spring track width increases. An attempt was originally made to include a spring track width of 0.8 m which is a common value used on heavy vehicles. The results

were however excluded as the vehicle tended to have large periods of tyre lift off on the right side at higher crossfall values. This shows that a decrease in the spring track width will have a detrimental effect on the vehicle stability and road damage produced by heavy vehicles. At a road crossfall of 2% and road roughness of 2 m/km the percentage difference decreases from 59.6%, to 43.7% to 38.5% using the three respective spring track width values.

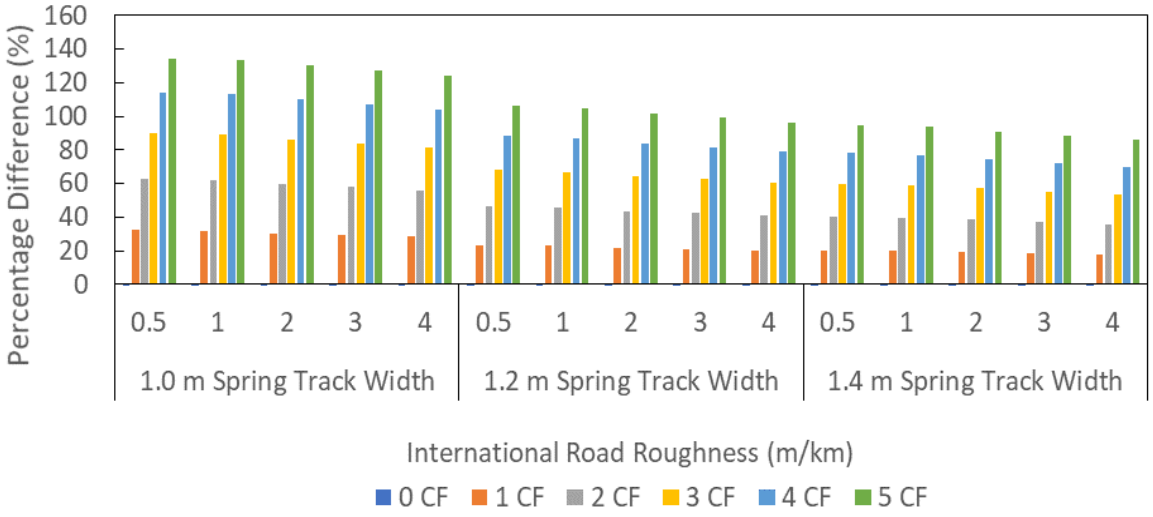

Figure 3.37: The percentage difference between the left and right 95th percentile fourth power aggregate forces using different spring track width values at 80 km/h

An increase in the spring track width also decreases the normalized fourth power aggregate force on the left side of the vehicle as shown in Figure 3.38. The normalized damage decreases from 1.764, to 1.608 and 1.551 using the three respective spring track widths. The same trends aer observed on the right side of the vehicle. Increasing the spring track width is therefore a viable and highly beneficial parameter when decreasing the overall road damage of a heavy vehicle when

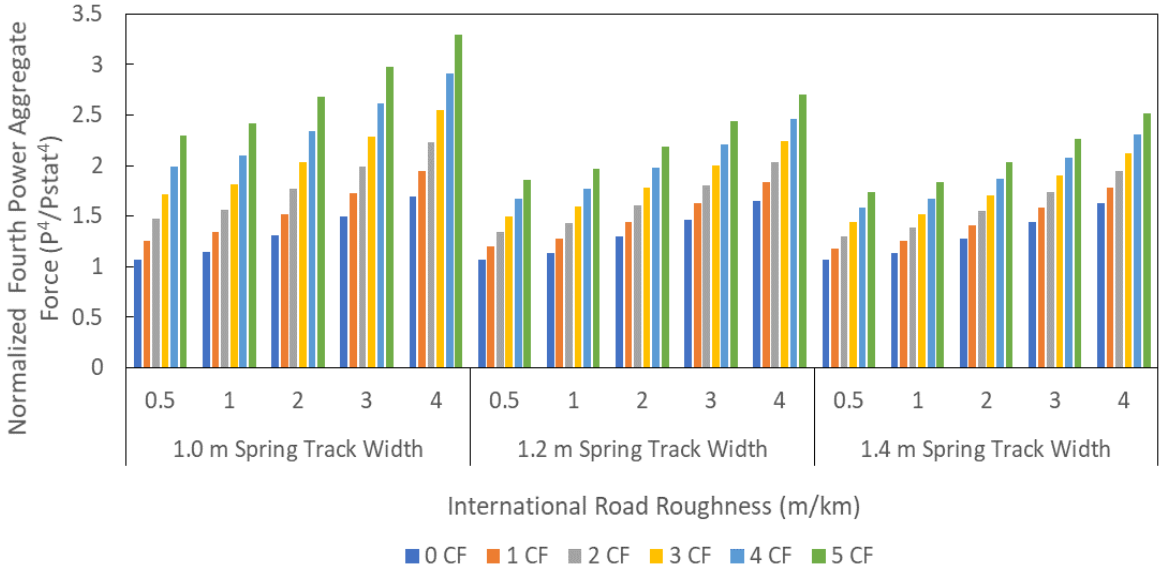

Figure 3.38: The left normalized 95th percentile fourth power aggregate forces using different spring track width values at 80 km/h

including road crossfall. The effect is also highly non-linear and slight decreases in the spring track width has a detrimental impact in the overall road damage and the percentage difference in left and right road damage. This result would suggest that dual tyre axles will tend to have a larger percentage difference in the left and right road damage due to the lower spring track widths used on dual tyre axles. Additional results are available in Appendix E in Table E.38 to Table E.40

3.2.8. The effect of an eccentric vehicle load

An eccentric load has a dramatic effect on the percentage difference of the left and right 95th percentile fourth power aggregate forces as shown in Figure 3.39. The results show that even if there is no crossfall and the load is only 50 mm eccentrically offset to the left, the percentage difference in the left and right aggregate forces are 58.9% for a road roughness of 2 m/km. For the typical highway crossfall of 2% and road roughness of 2 m/km the percentage difference in left and right fourth power aggregate forces is 43.7% with no offset, 98.8% with 50 mm offset and 166.2% with 150 mm offset. The results also show that as the eccentricity increases, the rate of change of the percentage difference in the fourth power aggregate force decreases for increasing crossfall values.

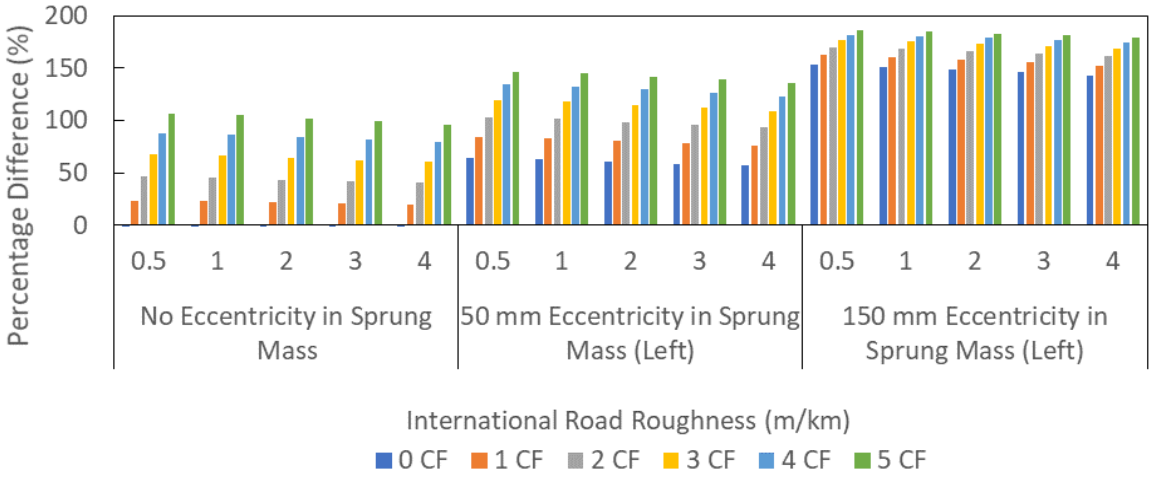

Figure 3.39: The percentage difference between the left and right 95th percentile fourth power aggregate forces using different eccentric sprung mass values at 80 km/h

Most vehicles are expected to have an eccentric sprung mass due to ancillary loads such as fuel tanks, drivers and safety equipment such as fire extinguishers. Many loads also tend to be off-centre or can shift while being transported. Well known examples of this include hay bales, meat carcasses and fuel tanks [50]. Limited information is given on typical values for eccentric loads, but one study has reported values as high as 300 mm in the case of loads on trailers [17]. Values of up to 150 mm therefore seem reasonable for the purpose of this study. Additional results are available in Appendix E in Table E.41 to Table E.43.

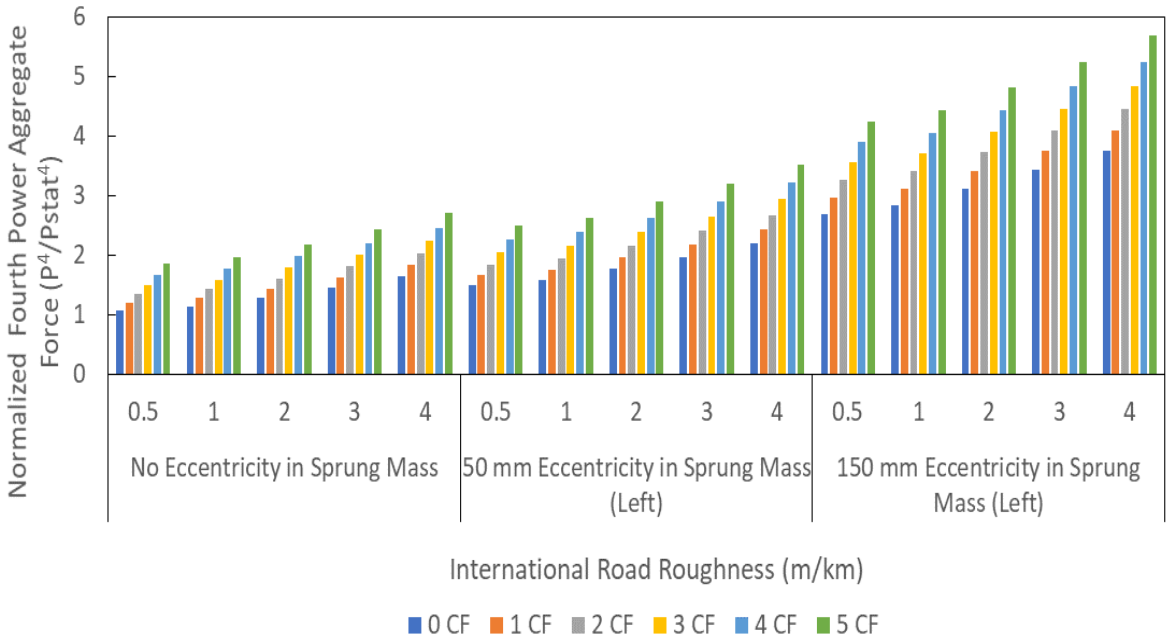

Figure 3.40: The left normalized 95th percentile fourth power aggregate forces using different eccentric sprung mass values at 80 km/h

An eccentric load to the left will also increase the overall road damage on the left side of the vehicle as shown in Figure 3.40. Contrary to the results in Figure 3.39, higher eccentric loads increase the rate of damage on the left side of the vehicle when including crossfall. The normalized road damage at a road crossfall of 2% and 2 m/km road roughness increases from 1.608 with a balanced load, to 2.167 using a 50 mm eccentric load and 3.7333 when using an eccentric load of 150 mm. A very small offset of 50 mm increases the normalized road damage by almost 33%. Ensuring that the loads are correctly balanced is essential in minimizing road damage and decreasing the percentage difference in the left and right road damage. If loads could be offset in the direction opposite to the crossfall, it can be an effective mechanism to reduce road damage. Perhaps this can be achieved by using more active types of suspension instead of the traditional passive suspensions. Placing ancillary equipment such as fuel tanks on the right side may also act to decrease the percentage difference in the left and right road damage. Additional results are available in Appendix E in Table E.41 to Table E.43.

3.2.9. The effect of sprung mass

The effect of the sprung mass on the percentage difference of the left and right 95th percentile fourth power aggregate forces is shown in Figure 3.41. As expected, a decrease in the sprung mass decreases the percentage difference in the left and right fourth power aggregate forces. At a crossfall of 2% and road roughness of 2 m/km the value increases from 33.2% using 7.5 tonnes, to 38.3% at 10 tonnes and finally to 43.7% using 12.5 tonne sprung mass. It therefore seems that there is a linear relationship between the percentage difference in the left and right road damage

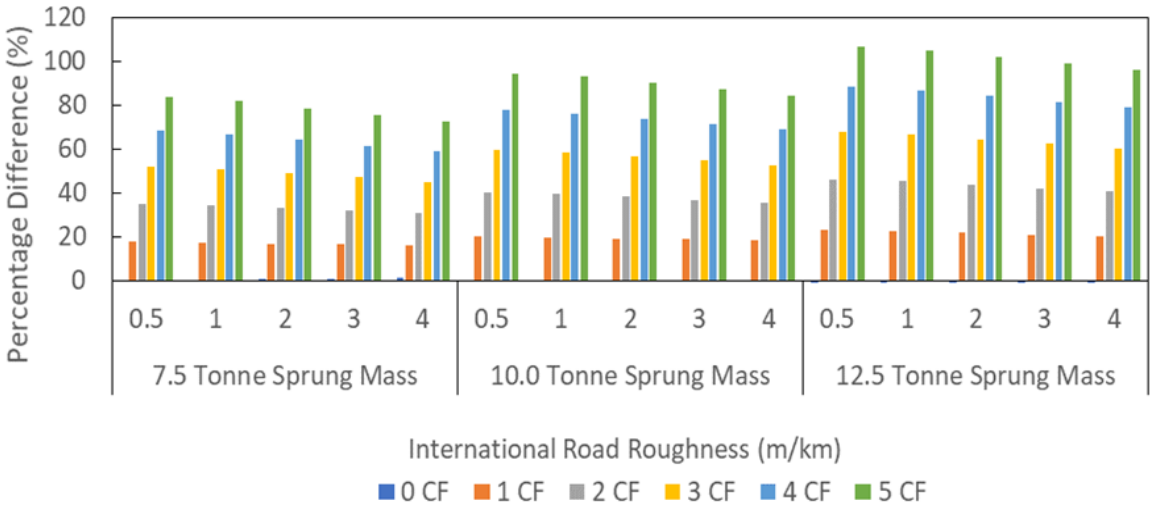

Figure 3.41: The percentage difference between the left and right 95th percentile fourth power aggregate forces using different sprung mass values at 80 km/h

and the sprung mass value. It is however worth noting that even with a decrease of the sprung mass by 40% from 12.5 tonnes to 7.5 tonnes, the percentage difference only decreases by 10.5%.

When looking at the normalized damage (still using the base model static forces) caused on the left side of the vehicle, it is clear that the sprung mass value has a notable effect as show in Figure 3.42. The normalized fourth power damage on the left side increases from 0.302 at a sprung mass of 7.5 tonnes, to 0.756 using 10 tonne sprung mass and finally 1.608 at a sprung mass of 12.5 tonnes at a road crossfall of 2% and road roughness of 2 m/km. The same trends are observed on the right side of the vehicle. In this case a decrease of 40% in the sprung mass decreased the normalized road damage by 80% and is therefore a very efficient way of decreasing the overall

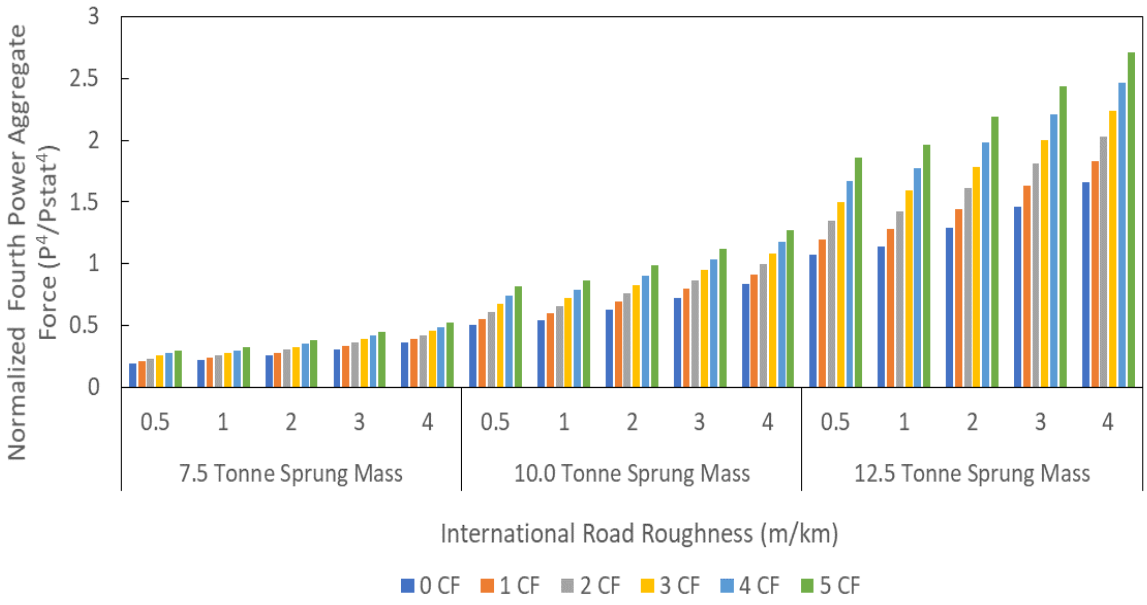

Figure 3.42: The left normalized 95th percentile fourth power aggregate forces using different sprung mass values at 80 km/h

road damage. The figures also show that the rate of change increases for higher sprung masses and therefore even small changes will have a marked impact on the overall road damage when including crossfall. Additional results are available in Appendix E in Table E.44 to Table E.46.

3.2.10. The effect of tyre stiffness

The final parameter that was studied during this dissertation is the effect of the tyre's stiffness on the percentage difference in the left and right 95th percentile fourth power aggregate forces. The effect of tyre stiffness is shown in Figure 3.43. The results show that the percentage difference decreases as the tyre stiffness increases. At a typical highway speed of 80 km/h, road roughness of 2 m/km and road crossfall of 2% the percentage difference changes from 45.4% to 43.7% at the intermediate stiffness and finally to 42.2% at the higher tyre stiffness. This shows that under-inflated tyres will have a higher percentage difference and that super single or dual tyres will have a lower percentage difference in the road damage. The decrease is however marginal for a substantial increase in the tyre stiffness.

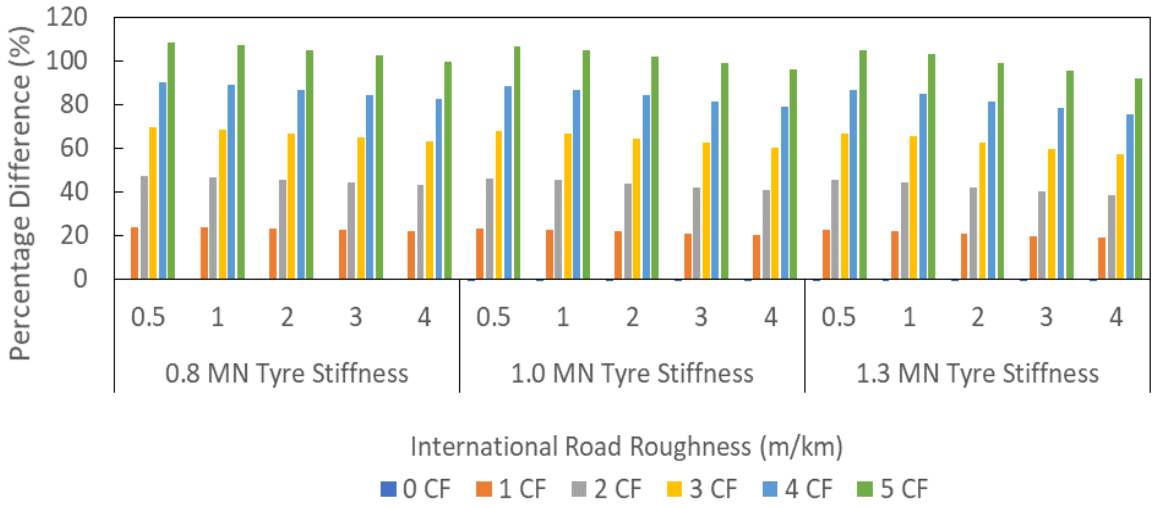

Figure 3.43: The percentage difference between the left and right 95th percentile fourth power aggregate forces using different tire stiffness values at 80 km/h

The effect of the tyre stiffness on the normalized fourth power 95th percentile aggregate force is shown in Figure 3.44. This shows that the normalized damage increases as the tyre stiffness increases. The normalized damage increase from 1.569, to 1.608 and finally 1.679 at the three respective tyre stiffnesses. The same trend is observed on the right side of the vehicle. Therefore, over inflating tyres will increase the overall road damage and will also decrease the contact area which would further increase road damage. A super single tyre will increase the fourth power aggregate force, but when normalizing the damage by the contact area, the super single will decrease the overall road damage as the super single tyre has a larger contact area compared to the standard tyre. Using dual tyres will also be beneficial as the contact area increases substantially

and increases the overall stiffness which will decrease the percentage difference in the left and right road damage. Operators often over inflate tyres as this increases their fuel efficiency and it is expected that it will be difficult to motivate them to decrease the inflation pressure in order to reduce road damage unless it can be shown to be beneficial to them. Additional results can be obtained in Appendix E in Table E.47 to Table E.49.

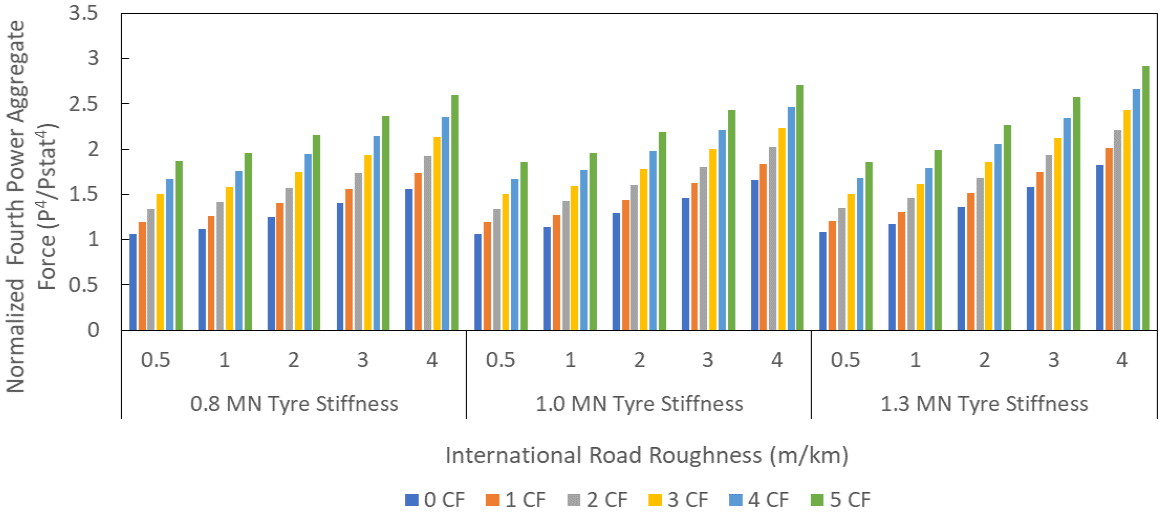

Figure 3.44: The left normalized 95th percentile fourth power aggregate forces using different tyre stiffness values at 80 km/h

3.3. General discussion on results

This section contains a summary and general discussion on the results obtained during this study and focusses on the 95th percentile fourth power aggregate forces. The subsections have been formulated to address the objectives in Section 1.3.

3.3.1. The influence of road crossfall on road damage

From all the results presented in Section 3, it is clear that the effect of rolling motion cannot be ignored when incorporating road crossfall. The results showed that the road crossfall linearly influenced all the road damage criteria considered. An increase in the road crossfall tended to increase the road damage on the left side and decrease the road damage on the right side. An exception to this rule is the DLC, where an increase in the crossfall decreases the DLC on the left and increases it on the right.

This linear relationship with the road damage and the road crossfall is convenient as one can obtain the road damage at any road crossfall if the rate of change is known as a function of cross-slope.

As mentioned previously, the 95th percentile fourth power aggregate force is the most used road damage criteria and is discussed in the rest of this subsection. At a typical highway speed of 80 km/h and road roughness value of 2m/km the percentage difference for the 95th percentile

aggregate fourth power force is 43.7% and 64.6% for the base model considered at crossfall values of 2% and 3% respectively. The value exceeds 100% for road crossfall values of 5% with values as high as 106% being recorded.

The 95th percentile fourth power aggregate force is often normalized by the static fourth power aggregate force. For a typical highway roughness value of 2 m/km and vehicle speed of 80 km/h, the left side normalized damage ranges from 1.293 at a road crossfall of zero to 2.189 at a road crossfall of 5%. This shows that a small change of 5% in the crossfall, increased the normalized damage by almost 70% on the left side. At a more typical crossfall value of 2% the normalized damage coefficient on the left side is 1.608. This is an increase of 24% over the 0% crossfall scenario. It is also worth noting how much the dynamic damage exceeds the static damage, and that simply using the static fourth power forces severely underestimate the road damage produced.

The results support previous findings that road crossfall produces more road damage on the outer track of the vehicle. It is clear therefore that road crossfall can no longer be ignored when studying the road damage effects of heavy vehicles.

3.3.2. The influence of vehicle speed and road roughness on the road damage when including road crossfall.

The results in section 3.1 showed that the vehicle speed has no influence on the average vertical tyre force or the average first power aggregate forces. As expected from literature, the DLC of the vehicles increases with a square root relationship with an increase in vehicle speed. The 95th percentile first power aggregate force also appears to increase linearly with the square root of the vehicle speed. All of the other road damage criteria, including the 95th percentile fourth power aggregate forces increase linearly with an increase in the vehicle speed.

The road roughness also has no effect on the average vertical tyre force or the average first power aggregate force. An increase in the road roughness however linearly increases the DLC of the tyres and the 95th percentile first power aggregate force. All of the other road damage criteria increase with an increase in the road roughness. The slope also increases with higher road roughness values. The effect is pronounced in the case of the fourth power aggregate forces as a small change in the road roughness has a marked effect on the road damage. It appears as if the first power aggregate forces have a quadratic relationship with the road roughness (R values over 0.99 were recorded), while the fourth power aggregate forces have a fourth power relationship (R values over 0.99 were once again recorded).

3.3.3. The influence of selected heavy vehicle parameters on the road damage when including road crossfall

The effect of several heavy vehicle parameters is studied in subsection 3.2. The section contains a large amount of detail and it is therefore challenging to understand and compare the impact of different vehicle parameters simultaneously. Table 3.1 is an attempt to provide a qualitative view of the impact of the different vehicle parameters studied for a typical highway operating condition with a vehicle speed of 80 km/h, road roughness of 2m/km and crossfall of 2%. Table 3.1 contains a column showing the impact on the percentage difference between the left and right fourth power aggregate forces and another column showing the effect of the vehicle parameter on the left side normalized fourth power aggregate force compared to the base model. This allows one to obtain a holistic view on the impact of a parameter on not only the percentage difference between the left and right fourth power aggregate forces, but also on the overall road damage (obtained by noting the increase in the left side normalized fourth power aggregate force).

Several qualitative classes have been created based on the percentage difference in the result of the specific vehicle parameter compared to the base model. The classes are:

- Negligible (0-2% change)
- Moderate (2-5% change)
- Significant (5-10% change)
- Major (10-15% change)
- Severe (more than 15% change)

The results are also colour coded with green indicating that the parameter has improved the result (namely to decrease the percentage difference between the left and right fourth power aggregate forces or to decrease the left side normalized fourth power aggregate force) or orange to show that the results have deteriorated compared to the base model (the percentage difference between the left and right fourth power aggregate forces have increased or the left side normalized fourth power aggregate force has increased).

As an example, if one wants to consider the effect of the suspension stiffness, one can look at row 7 or 8 in the Table 3.1. Considering row 8, it shows that a doubling in the suspension stiffness results in significant improvement in the percentage difference between the left and right fourth power aggregate forces compared to the base model, but that it moderately increases the left side normalized fourth power aggregate force compared to the base model. Therefore, the optimal parameters that improve the percentage difference between the left and right side fourth power aggregate forces and the left side aggregate force will both be green or at least one will be green

Table 3.1: Qualitative summary of the impact of various heavy vehicle parameters on the percentage difference between the left and right fourth power aggregate forces and the left normalized fourth power aggregate force compared to the base model

Model parameter changed	Relative change	Change in % difference between left and right fourth power aggregate force (compared to the base model)	Change in left side normalized fourth power aggregate force (compared to the base model)	Key
3 kNm/deg (front) and 5 kNm/deg (rear) anti-roll bars	Adding of soft anti-roll bars	Significant	Moderate	Negligible 0-2%
6 kNm/deg (front) and 10 kNm/deg (rear) anti-roll bars	Adding of stiff anti-roll bars	Major	Significant	Moderate 2-5%
1.5 m sprung mass height	25% decrease in sprung mass height	Severe	Significant	Significant 5-10%
2.5 m sprung mass height	25% increase in sprung mass height	Severe	Severe	Major 10-15%
400 mm roll centre height	33% decrease in roll centre height	Significant	Moderate	Severe 15% or more
500 mm roll centre height	17% mm decrease in roll centre height	Negligible	Negligible	Green = Improvement
300 N/mm stiffness (front) and 600 N/mm stiffness (rear)	50% increase in stifness values	Significant	Negligible	Orange = Deterioration
400 N/mm stiffness (front) and 800 N/mm stiffness (rear)	100% increase in stiffness values	Significant	Moderate	
10 kNs/m damping (front) and 20 kNs/m (rear)	100% increase in damping values	Negligible	Moderate	
20 kNs/m damping (front) and 40 kNs/m (rear)	200% increase in damping values	Negligible	Moderate	
1.9 m track width	5% decrease in track width	Moderate	Moderate	
2.1 m track width	5% increase in track width	Moderate	Negligible	
1 m spring track width	17% decrease in spring track width	Severe	Significant	
1.4 m spring track width	17% increase in spring track width	Significant	Moderate	
50 mm eccentric sprung mass	Adding 50 mm eccentricity to sprung mass	Severe	Severe	
150 mm eccentric sprung mass	Adding 150 mm eccentricity to sprung mass	Severe	Severe	
7.5 tonne sprung mass	40% decrease in sprung mass	Major	Severe	
10 tonne sprung mass	20% decrease in sprung mass	Significant	Severe	
0.8 MN tyre stiffness	20% decrease in tyre stifness	Negligible	Moderate	
1.3 MN tyre stiffness	30% inrease in tyre stiffness	Negligible	Moderate	

and the other white. This for example includes adding anti-roll bars to the vehicle as shown in row 1 and row 2.

Several key findings were also noted in subsection 3.2. One of the most notable findings is that an increase in the vehicle suspension stiffness and tyre stiffness will decrease the percentage difference in the left and right 95th percentile fourth power aggregate forces, but that it increases the total road damage produced by the heavy vehicle. This shows that steel suspension is still the less road friendly option when it comes to dynamic road damage.

Another notable finding is that the damping value of the suspension has almost no effect on the percentage difference in the 95th percentile fourth power aggregate forces. The higher damping value will however decrease the overall road damage produced by the heavy vehicle and is therefore still a useful parameter to decrease road damage.

All of the other parameters that tend to increase the roll stability of a heavy vehicle such as a higher track width or lower sprung mass, will decrease the percentage difference in the left and right 95th percentile aggregate forces. They also decrease the overall road damage produced by the heavy vehicle. Therefore, with the exception of the suspension and tyre stiffnesses, parameters that increase the roll stability of the heavy vehicle will decrease the percentage difference and overall damage when considering the 95th percentile fourth power aggregate forces.

A final notable finding is that an unbalanced load has a substantial effect on the road damage produced by a heavy vehicle. It is shown that even a small eccentric load of 50 mm can produce a difference of more than 40% between the left and right 95th percentile fourth power aggregate forces even with no crossfall.

These results show that under typical road crossfall values in South Africa of 2%-3%, consideration should be given to several heavy vehicle parameters when trying to optimize the road damage produced and not simply the suspension stiffness and damping values.

It is also worth noting that emphasis is usually only given to the vehicle stiffness, damping and sprung mass value when considering dynamic road damage. The results however show that many parameters have a greater influence on the road damage of heavy vehicles when including crossfall. Heavy vehicle damping and suspension can therefore no longer be considered in isolation.

3.3.4. Recommendations on how to minimize the adverse effects of road crossfall

From the results obtained in this dissertation, some notable recommendations can be made to reduce the road damage produced by heavy vehicles when including road crossfall.

The first is that a decrease in vehicle speed will decrease the road damage produced by heavy vehicles. It is therefore important that heavy vehicles are monitored to ensure compliance with the maximum speed limit. Over speeding will negatively influence road damage.

As the road roughness quadratically influences the road damage, it is important that roads are manufactured with as low an IRI value as possible. It is also important that regular maintenance be done, especially on the left side of the road as it will experience higher loads and more damage [22]. Road designers and agencies may need to update their design and inspection criteria in the light of these findings. For example, road designers may need to increase the strength of the road pavements due to these higher than expected loads being produced on the left side of the road. Performing proper maintenance is also important as the left side of the road will have more damage and higher IRI values compared to the right as found in other recent studies [22, 29]. If the left side is not properly maintained, the increase in the IRI will result in even more road damage and an accelerated failure of the roads at levels most likely higher than expected from traditional analysis.

Including a high enough road crossfall is important to ensure adequate drainage of the road surface that will prevent liquid build up that will damage the road and be a safety hazard for heavy vehicles. The results however show that the road crossfall should however be kept as low as possible. Road design guidelines may need to be revised to consider this trade-off in ensuring sufficient drainage while minimizing the road crossfall to reduce road damage on the left side of the road. Other options to ensure sufficient drainage of the road can also be explored including rather adding longitudinal elevation of the road profile instead of cross slope.

Heavy vehicle manufacturers and operators should also be made aware of the adverse effect of road crossfall on road wear. The results show that the wear on the heavy vehicles will be higher on the left side in South Africa (the outer side of the road) due to higher loads experienced and also the higher road roughness values. By increasing the heavy vehicle roll over stability, the road damage on the left side will decrease. The only two exceptions to this are the tyre stiffness and suspension stiffness that will increase the normalized damage on the left but decrease the percentage difference in the left and right road damage.

Operators should therefore be motivated to improve their vehicle roll stability as much as possible. This can include having a road tax that is calculated by knowing the road friendliness of the heavy

vehicle when including road crossfall. This could include having different scales on the severity of the load increase on the left/outer side of the vehicle and a correlated tax rate for the difference levels on the scale. Changes to vehicle speeds and vehicle weight limits can also be made on certain road sections given the understanding of the typical crossfall and road roughness values encountered on the specific route.

As mentioned, emphasis is usually only given to the vehicle stiffness, damping and sprung mass value when considering dynamic road damage. The results however show that many parameters have a greater influence on the road damage of heavy vehicles when including crossfall. Heavy vehicle damping and suspension can therefore no longer be considered in isolation. An overview of all the heavy vehicle parameters that influence heavy vehicle rolling motion is necessary.

More research on the effect of road crossfall is also required including adding more accurate vehicle parameter models and adding more vehicle units to investigate the effects of vehicle configurations.

4. Conclusion and Recommendations

This study in including the effects of rolling motion and road crossfall has produced notable and useful results. The first portion of this section highlights the major conclusions of this research and does so in the format of the original objectives. The latter portion is dedicated to recommendations on future work.

1. A 9-degree of freedom user-defined mathematical model was developed in order to include the rolling effects of a 4x2 heavy vehicle. The validation of the full car model was done using TruckSim 2019.1®. The software is a commercially available multibody simulation tool capable of assessing the performance of complex vehicle models performing complex manoeuvres. The user-defined model has the advantage of requiring significantly cheaper software to develop and has quicker run times compared to the commercially available software package. Although TruckSim 2019.1® is able to take into account a larger amount of vehicle parameters and arguably produce results with higher accuracy, the user-defined model allows one to consider only the critical parameters of interest and eliminate the other parameters that may potentially cloud and distort the results. This allows for a more fundamental understanding of the impact of the selected parameters to be developed.
2. The relative influence of various magnitudes of crossfall on dynamic road damage was successfully determined. It was noted that the 95th percentile fourth power aggregate force is the main damage criteria that needs to be considered.
    a. In the case of the first and fourth power aggregate forces as well as the average vertical forces, it was found that the road damage increases linearly on the left side and decreases linearly on the right side with an increase in the road crossfall.
    b. Using the DLC as the road damage criteria, the DLC decreases linearly on the left side and increases linearly on the right side with an increase in road crossfall.
    c. Using the base model under typical highway conditions of 80 km/h with a road roughness of 2 m/km and road crossfall of 2%, the percentage difference in the 95th percentile fourth power aggregate force is 43.7%. For this operating condition the left side fourth power aggregate force increases by 23.4% from its value on a flat surface while the right side decreases by 20%. This will have a definite effect on the overall road damage caused by heavy vehicles. A recent study of actual Australian road surface road roughness values has shown that the left side road roughness was almost always higher than the right side for all the roads sampled. This also supports a study in New Zealand that found the left side profile always had more rutting than the right-side road profile due to crossfall.

The effect of road crossfall is in all likelihood the reason for a recorded difference in the left and right road roughness values of real road profiles as shown in Figure 1.4 as was concluded in the New Zealand study as well [23, 35]. According to this Australian study differences of up to 38% were recorded in the road roughness on the left and right track. This increase in the road roughness on the left side compared to the right side will decrease the life of the road pavement and cause more damage on the vehicles that use the road pavement.

3. The relative importance of the major road parameters was also identified in this research.
    a. Vehicle speed and road roughness have no effect on the average vertical force as expected.
    b. The DLC and average first power aggregate forces of a tyre increase linearly with an increase in the road roughness and increases with an increase in the vehicle speed, but with the slope decreasing with increasing vehicle speeds.
    c. The damage from the 95th and 99th percentile first power aggregate forces, increases linearly with an increase in vehicle speed and increases with an increase in road roughness. The slope increases with higher road roughness values (a quadratic approximation is an almost perfect fit with an R value of 0.99 or higher in all cases).
    d. The damage from all the fourth power aggregate force criteria increases linearly with an increase in vehicle speed and increases with an increase in road roughness. The slope increases with higher road roughness values (a fourth power approximation is an almost perfect fit with an R value of 0.99 or higher in all cases).
4. The relative importance of the major vehicle parameters which influence dynamic road damage due to road crossfall were studied using the 95th percentile fourth power aggregate force criteria.
    a. It was found that all vehicle parameters that increases the roll stability of the vehicle, decreases the percentage difference between the left and right road damage.
    b. All the criteria that decreases the percentage difference in the left and right road damage also decreases the overall road damage, except for the tyre stiffness and suspension stiffness. These two stiffness values will decrease the percentage difference in the left and right road damage, but increase the overall damage produced by the heavy vehicle.
5. Recommendations were made on how to minimize the adverse effects of road crossfall.

a. The first is that a decrease in vehicle speed will decrease the road damage produced by heavy vehicles. It is therefore important that heavy vehicles are monitored to ensure compliance with the maximum speed limit.
b. As the road roughness has a fourth power influence on the 95th percentile fourth power road damage, it is important that roads are manufactured with as low an IRI value as possible. It is also important that regular maintenance be done, especially on the left side of the road as it will experience higher loads and more damage.
c. It is also important for road designers to be made aware of the effect of crossfall on road damage so that it can be considered in future road deign codes.
d. Road design guidelines may need to be revised to consider this trade-off in ensuring sufficient drainage while minimizing the road crossfall to reduce road damage on the left side of the road. Other options to ensure sufficient drainage of the road can also be explored including rather adding longitudinal elevation of the road profile instead of cross slope.
e. Heavy vehicle manufacturers and operators should also be made aware of the adverse effect of road crossfall on road wear as well as vehicle wear. The results show that the wear on the heavy vehicles will be higher on the left side due to higher loads experienced and the higher road roughness values. By increasing the heavy vehicle roll over stability, the road damage on the left side will decrease. The only two exceptions to this are the tyre stiffness and suspension stiffness that will increase the normalized damage on the left but decrease the percentage difference in the left and right road damage.

The results have clearly indicated that the effects of road crossfall should not be ignored when studying the road damage effects of heavy vehicles. There are also a number of heavy vehicle parameters that need to be considered when investigating the dynamic road damage of a heavy vehicle and not only the suspension stiffness and suspension damping of a vehicle.

Recommendations for future work include:

1. Increasing the detail of the suspension modelling by, for example, including a non-linear damper and spring. This will allow for a more accurate results to be obtained and to better understand the difference between steel and air suspensions. The effect of dual vs single tyres can also be studied as many heavy vehicles use dual tyres on the driving axles.
2. Although this is often a difficult task, it is necessary to compare simulation results with actual experimental data. Therefore, it is recommended that the results obtained from simulation be compared to field testing of a physical vehicle. This will allow one to quickly

determine if the models are sufficiently accurate to predict the real-life performance of the vehicles. It will also allow one to determine which vehicle parameters are the most critical and which can potentially be excluded if it is desired to reduce the model complexity.

3. Other recommendations include adding additional vehicle units such as different types of trailers to investigate their influence on the overall vehicle damage when including road crossfall. It is expected that trailers will have a notable effect on road damage due to their tendency to have higher payloads at much higher CoG heights.
4. Another possible improvement could be to use actual road surface data instead of generating artificial road profiles. This should also include the effect of varying road crossfall as this value will not be constant as is assumed in this study. Furthermore, the effect of road curvature and super elevation can be studied to determine if the centripetal forces generated by the vehicle will offset the increase in the forces produced by the high road crossfall values.
5. An attempt can also be made to determine if one can use a simple quarter-car model to estimate the road damage when including crossfall if the load on each tyre is known at the different road crossfall values.
6. The road damage criteria can also be improved by incorporating the effect of tyre contact area and modelling the time dependent behaviour of road surfaces, especially asphalt road pavements.
7. It would also be beneficial to study the additional wear on heavy vehicle components such as the tyres, suspension and dampers because of road crossfall. Showing the economic impact to operators would be an effective option in raising awareness of the effect of road crossfall and could spark a larger interest and uptake of solutions that minimizes road and vehicle damage.
8. Future research can also attempt to reconcile accelerated pavement testing or actual pavement testing data with the aggregate force damage criteria to determine the most suitable damage exponents. This is because the fourth power estimate is only a generalized rule and does not necessarily hold true for all pavement structures [19].
9. Another possible suggestion is to additional degrees of freedom to the user-defined models to study other important forms of road distress such as shoving

5. References

[1] J. H. Havenga, Z. P. Simpson, D. de Bod and M. Braun, “A logistics barometer for South Africa: Towards sustainable freight mobility,” Stellenbosch University, 2016.

[2] D. Ross and M. Townshend, “The road mainteance backlog in South Africa,” in *Southern Africa Transport Conference 2019*, Pretoria, 2019.

[3] S. Krygsman and J. Van Rensburg, “Funding for roads in South Africa: Understanding the principles of fair and efficient road user charges,” Stellenbosch, 2017.

[4] M. Hjort, M. Haraldsson and J. M. Jansen, “Road wear from heavy vehicles- an overview,” NVF committee Vehicles and Transports, Borlange, Sweden, 2008.

[5] M. Gäfvert and O. Lindgärde, “A 9-DOF tractor-semitrailer dynamic handling model for advanced chassis control studies,” *Vehicle System Dynamics,* vol. 41, no. 1, pp. 51-82, 2004.

[6] S. Sulaiman, P. M. Samin, H. Jamaluddin, R. A. Rahman and M. S. Burhaumudin, “Modeling and validation of 7-DOF ride model for heavy vehicle suspension,” in *International Conference on Automotive, Mechanical and Materials Engineering*, Penang (Malaysia), 2012.

[7] A. Faheem, F. Alam and V. Thomas, “The suspension dynamic analysis of a quarter car model and half car model,” in *3rd BSME-ASME International Conference on Thermal Engineering*, Dhaka, 2006.

[8] D. Cebon, “Road damaging effects of dynamic axle loads,” in *International Symposium on Heavy Vehicle Weights and Dimensions*, Canada, 1988.

[9] M. Constanize and D. Cebon, “An investigation of the effects of lorry suspension performance on road maintenace costs,” *The Proceedings of the Institution of Mechanical Engineers, Part C: Journal of Mechanical Engineering Science,* vol. 22, 2007.

[10] R. Buhari, M. M. Rohani and M. E. Abdullah, “Dynamic load coefficient of tyre forces from truck axles,” *Applied Mechanics and Materials,* Vols. 405-408, pp. 1900-1911, 2013.

[11] M. Hardy and D. Cebon, “Importance of speed and frequency in flexible pavement,” *Journal of Engineering Mechanics,* vol. 120, no. 3, pp. 463-482, 1994.

[12] D. Cebon, Handbook of vehicle-road interaction, Lisse, Netherlands: Swets & Zeitlinger, 1999.

[13] A. Ihs and G. Magnusson, “The significance of various road surface properties fo traffic and surroundings.,” Swedish National Road and Transport Research Intstitute, 2000.

[14] C. Bowen, “The importance of road drainage,” New England Sealcoating, 2017. [Online]. Available: https://www.newenglandsealcoating.com/the-importance-of-road-drainage/. [Accessed 28 September 2020].

[15] D. J. M. Sampson, “Active roll control of articulated heavy vehicles,” Cambridge University Engineering Department, Cambridge, 2000.

[16] P. S. Fancher, R. D. Ervin, C. B. Winkler and T. D. Gillespie, “A factbook of the mechanical properties of the components for single-unit and articulated heavy trucks,” UMTRI, 1986.

[17] R. Kamnik, F. Boettiger and K. Hunt, “Roll dynamics and lateral load transfer estimation in articulated heavy vehicles,” *Proceedings of the Institutatin of Mechanical Engineers, Part D: Journal of Automobile Engineering,* vol. 217, no. 11, pp. 985-997, 2003.

[18] The South African National Roads Agency LTD, “Chapter 10: Pavement design,” in *South African pavement engineering manual*, 2013.

[19] M. De Beer, I. Sallie, Y. Van Rensburg and M. Kemp, “Load equivalaency factors (LEFs) for abnormal vehicles (AVs) and mobile cranes in South Africa based on the mechanistic-emperical (M-E) design methodology,” *Southern African Transport Conference (SATC),* 2009.

[20] M. Constanzi and D. Cebon, “Generalized phenomenological model for the viscoelasticity of bitumen,” *Journal of Engineering Mechanics,* vol. 141, no. 5, 2015.

[21] M. Elischer and L. Bruzsa, “Dynamic wheel loads of heavy vehicles-preliminary analysis,” in *HVTT 12*, 2012.

[22] J. D. van der Walt, E. Scheepbouwer and S. L. Tighe, “Differtial rutting in Canterbury New Zealand, and its relation to road camber,” *international Journal of Pavement Engineering,* vol. 19, no. 9, pp. 798-804, 2018.

[23] S. Kakara and V. Chowdary, “Effect of pavement roughness and transverse slope on the magnitude of wheel loads,” *Arabian Journal for Science and Engineering,* vol. 45, pp. 4405-4418, 2020.

[24] H. Imine, Y. Delanne and N. K. M'Sirdi, “Road profile input estimation in vehicle dynamics simulation,” *Vehicle System Dynamics,* vol. 44, no. 4, pp. 285-303, 2006.

[25] International Orginisation of Standards, “ISO-8608: Mechanical vibration - road surface profiles - reporting measured values,” 1995.

[26] J. Oliva, J. M. Goicolea, M. A. Astiz and P. Antolin, “Fully three-dimensional vehicle dynamics over rough pavement,” *Proceedings of the Institution of Civil Engineers - Transport,* vol. 166, no. 3, pp. 144-157, 2013.

[27] O. Kropac and P. Mucka, “Be careful when using the international roughness index as an indicator of road uneveness,” *Journal of Sound and Vibration,* vol. 287, no. 4, pp. 989-1003, 2005.

[28] CSIR Building and Construction Technology, “Chapter 7- Roads: Geometric design and layout planning,” in *Guidelines for Human Settlement Planning and Design*, Department of Housing.

[29] M. J. Lamb and V. Rouillard, “Nonstationary coherence characteristics of dual track road,” *Mechanical Systems and Signal Processing,* vol. 140, 2019.

[30] COTO Road Network Management Systems Committee, “Guidelines for network level measurement of road roughness,” 2007.

[31] D. Ammon, “Problems in road surface modeling,” *Vehicle System Dyanmics,* vol. 20, pp. 28-41, 1992.

[32] J. O. Quecedo, “PRP generator User’s Manual,” Technical University of Madrid, Madrid, 2013.

[33] C. J. Dodds and J. D. Robson, “The description of road surface roughness,” *Journal of Sound Vibration,* vol. 31, pp. 175-183, 1973.

[34] K. M. Kamash and J. D. Robson, “Implications of isotropy in random surfaces,” *Journal of Sound Vibration,* vol. 54, pp. 131-145, 1977.

[35] J. Oliva, J. M. Goicolea, M. Antolin and M. A. Astiz, “Relevance of a completed road surface description in vehicle-bridge interaction dynamics,” *Engineering Structures,* vol. 56, pp. 466-476, 2013.

[36] M. W. Sayers, “Dynamic terrain inputs to predict structural integrity of ground vehicles,” The University of Michigan Transportation Research Institute, 1988.

[37] International Organization for Standardization, “ISO 8608: Mechanical vibration - Road surface profiles - Reporting of measured data,” ISO copyright office, Switzerland, 2016.

[38] M. W. Sayers, “Two quarter-car models for defining road roughness: IRI and HRI,” 1989.

[39] “Welch’s power spectral density estimate,” Mathworks, [Online]. Available: https://www.mathworks.com/help/signal/ref/pwelch.html. [Accessed 27 January 2020].

[40] “Cross power spectral density,” Mathworks, [Online]. Available: https://www.mathworks.com/help/signal/ref/cpsd.html. [Accessed 27 January 2020].

[41] P. Múčka, “Model of coherence function of road unevenness in parallel tracks for vehicle simulation,” *International Journal of Vehicle Desig,* 2015.

[42] D. J. Cole and D. Cebon, “Truck suspension design to minimize road damage,” *Journal of Automobile Engineering,* vol. 210, 1996.

[43] J. S. Loeb, “Lateral stiffness, cornering stiffness and relaxation length of the pneumatic tyre,” *SAE Proc,* 1990.

[44] Vehicle Dynamics Group, Division Vehicle and Autonomous Systems, “Vehicle Dynamics: Compendium,” Chalmers, 2017.

[45] V. Vantsevich and J. P. Gray, “Relaxation length review and time constant analysis for agile tire dynamics control,” in *IDETC/CIE 2015*, Massachusetts, 2015.

[46] Mechanical Simulation, “Tire Models,” Mechanical Simulation, 2019.

[47] V. R. Chaganti, A. S. Kumar, G. H. Bindu and K. V. Reddy, “Rollover stability analysis of commercial vehicle,” *International Journal of Application or Innovation Engineering and Management,* vol. 2, no. 9, 2013.

[48] D. Park, A. T. Papagiannakis and I. Kim, “Analysis of Dynamic Vehicle Loads using Vehicle Pavement Interaction Model,” *KSCE Journal of Civil Engineering,* 2014.

[49] V. Muluka, “Optimal suspension damping and axle vIbration absorber for reduction of dynamic tIre loads,” Concordia University, Quebec, 1998.

[50] University of Michigan Transportation Research Institute, “UMTRI Research Review: Rollover of heavy commercial vehicles,” 2000.

[51] G. Klančar, A. Zdešar, S. Blažič and I. Škrjanc, “Chapter 2 - Motion Modeling for Mobile Robots,” in *Wheeled Mobile Robotics: From Fundamentals Towards Autonomous Systems*, Elsevier, 2017, pp. 13-59.

[52] J. Cao, H. Lu, K. Guo and J. Zhang, “A driver modeling based on the preview-follower theory and the jerky dynamics,” *Advanced Control and Optimization with Applications to Complex Automotive Systems,* 2013.

[53] G. Loprencipe and P. Zoccali, “Use of generated artificial road profiles in road roughness evaluation,” *Journal of Modern Transportation,* vol. 25, no. 1, pp. 24-33, 2017.

[54] Dust-A-Side, “Road Management Services,” [Online]. Available: https://dustaside.com/services/road-management/. [Accessed 21 July 2020].

[55] National Roads Agency of South Africa, “Geometric Design Guide: Chapter 4 - Road Design Elements”.

[56] A. J. Steenkamp, R. Berman, L. Kemp and C. C. De Saxe, “The effect of road crossfall on road wear caused by heavy vehicles,” in *Southern African Transport Conference (SATC)*, 2019.

[57] J. Jia, Vehicle-structure interactions: Essentials of applied dynamic analysis., Berlin: Springer, 2014.

Appendix A: Road profiles used in the dissertation

This section contains all of the road profiles used during this study. The road profiles are provided in Figure A.1 to Figure A.9. The PSD results of the profiles are summarized in Figure A.10 to Figure A.18.

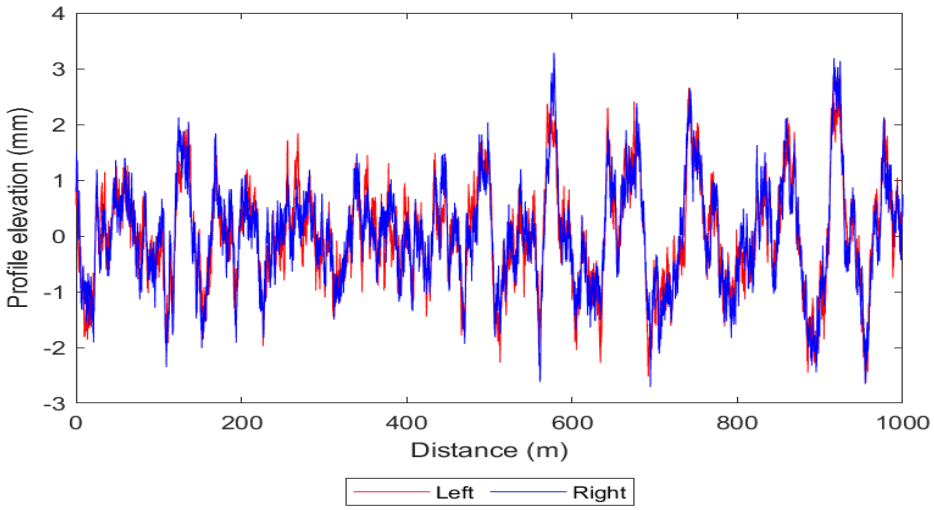

Figure A.1: Dual track road profile with design IRI of 0.5 m/km

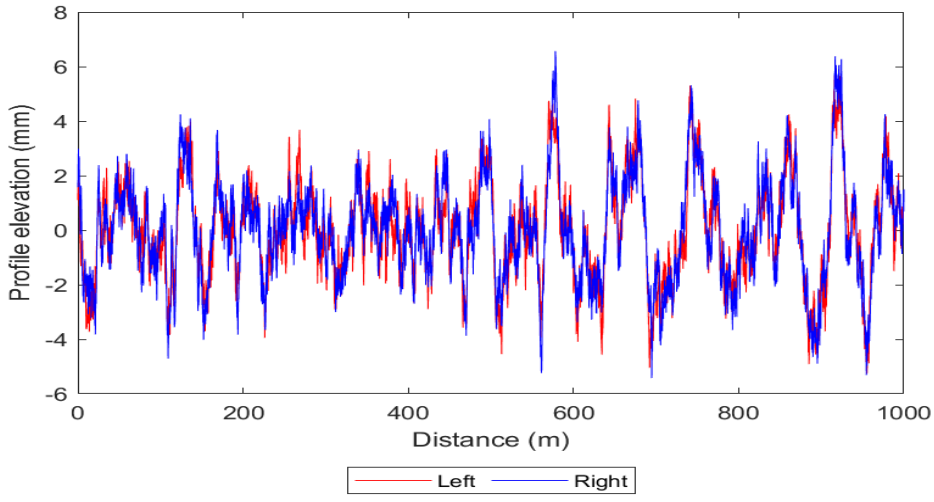

Figure A.2: Dual track road profile with design IRI of 1.0 m/km

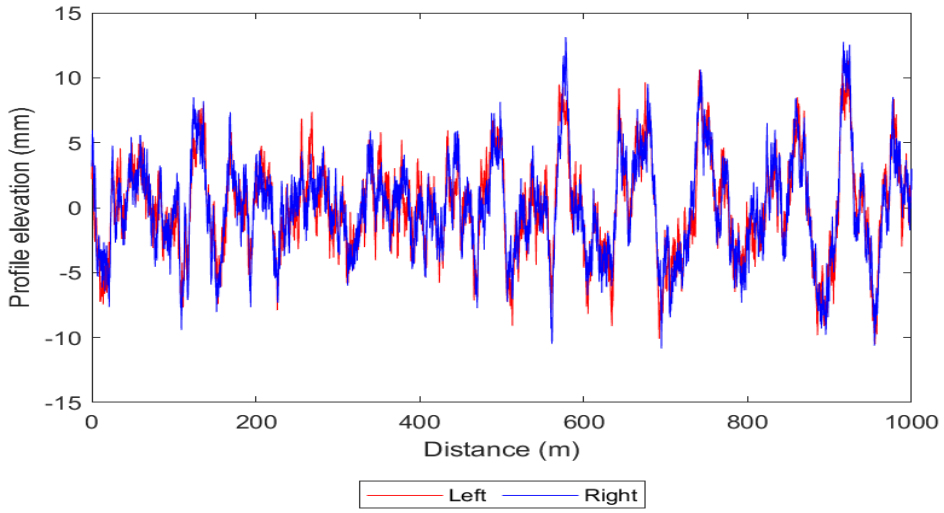

Figure A.3: Dual track road profile with design IRI of 2.0 m/km

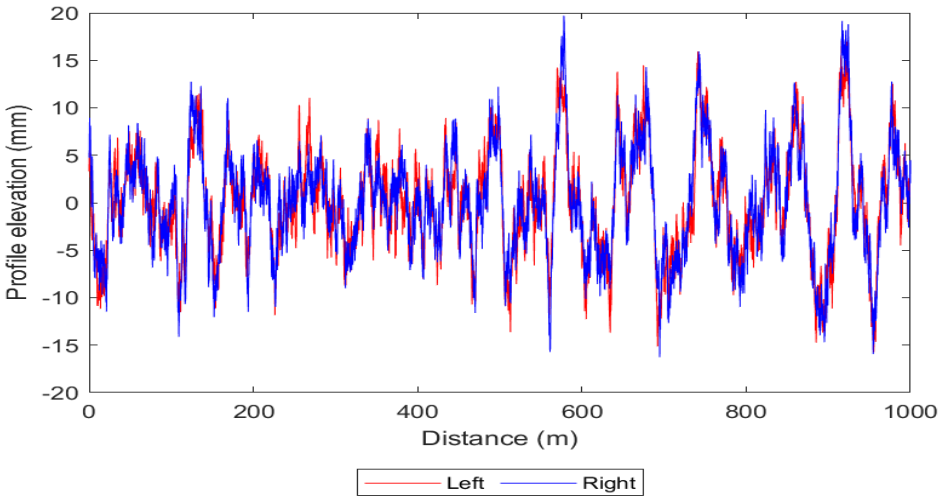

Figure A.4: Dual track road profile with design IRI of 3.0 m/km

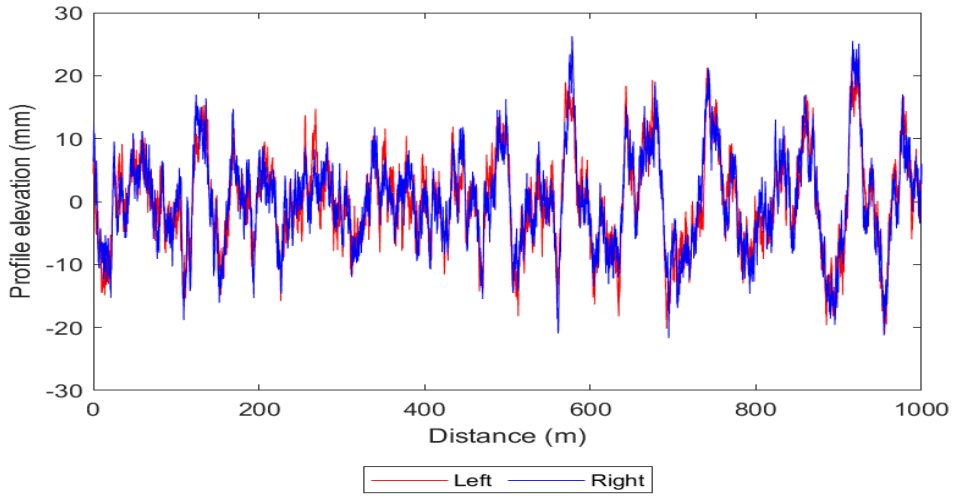

Figure A.5: Dual track road profile with design IRI of 4.0 m/km

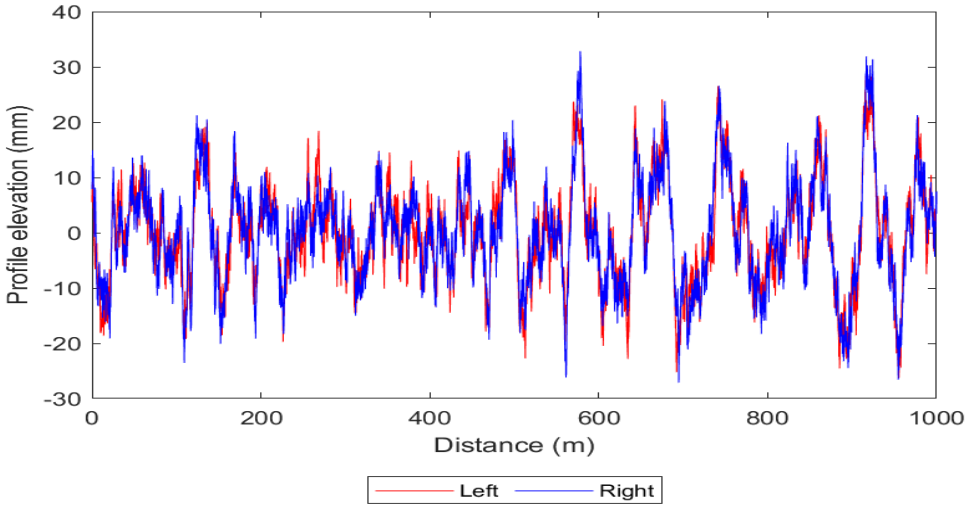

Figure A.6: Dual track road profile with design IRI of 5.0 m/km

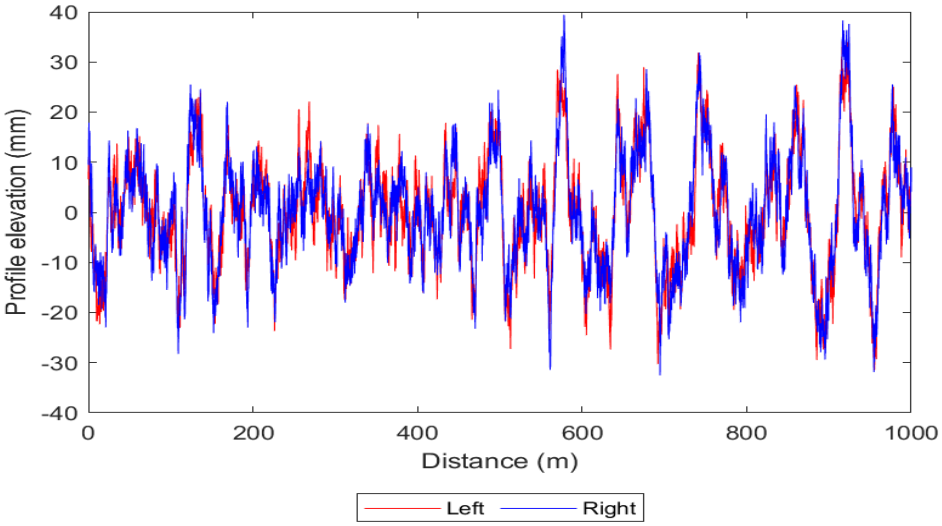

Figure A.7: Dual track road profile with design IRI of 6.0 m/km

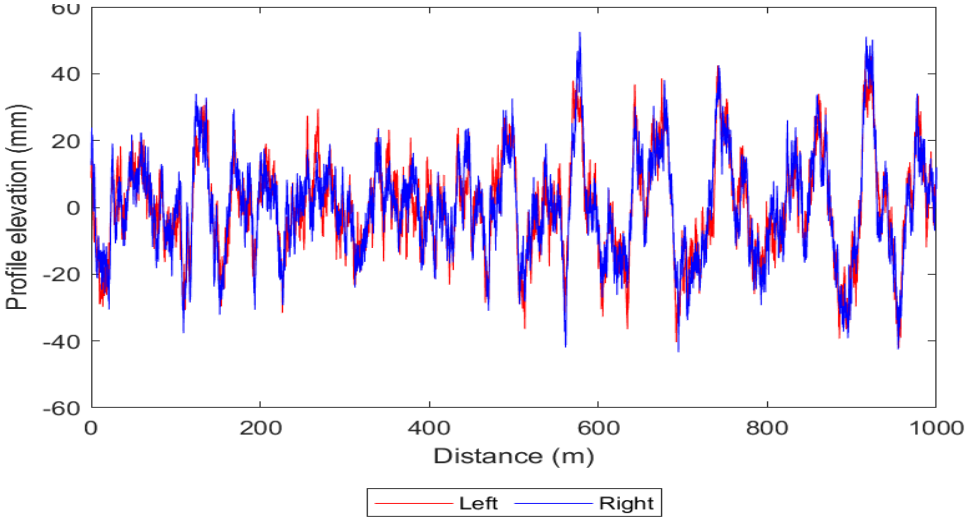

Figure A.8: Dual track road profile with design IRI of 8.0 m/km

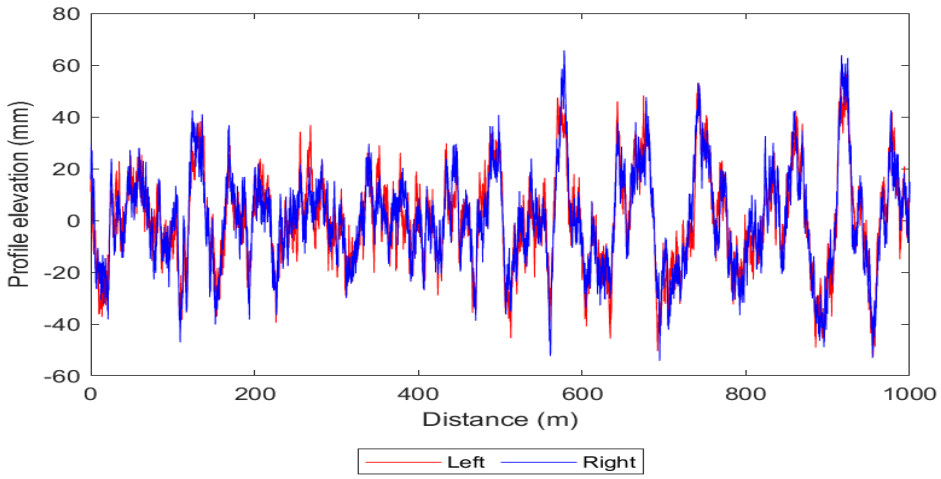

Figure A.9: Dual track road profile with design IRI of 10.0 m/km

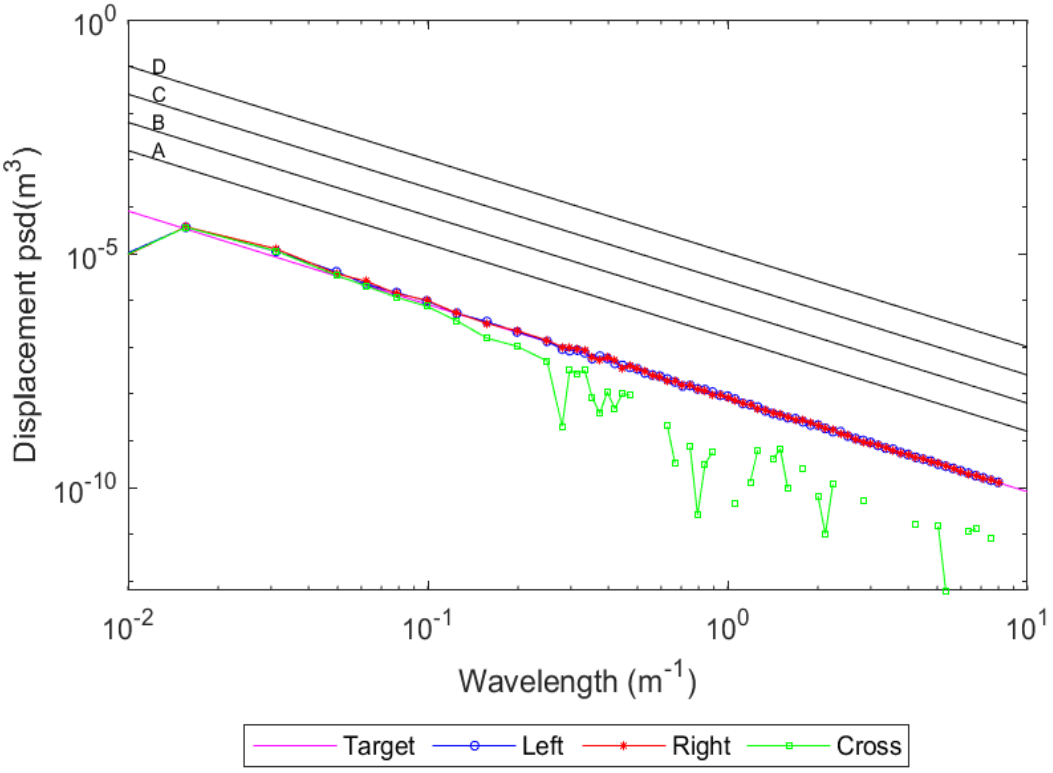

Figure A.10: PSD of Dual track road profile with design IRI of 0.5 m/km

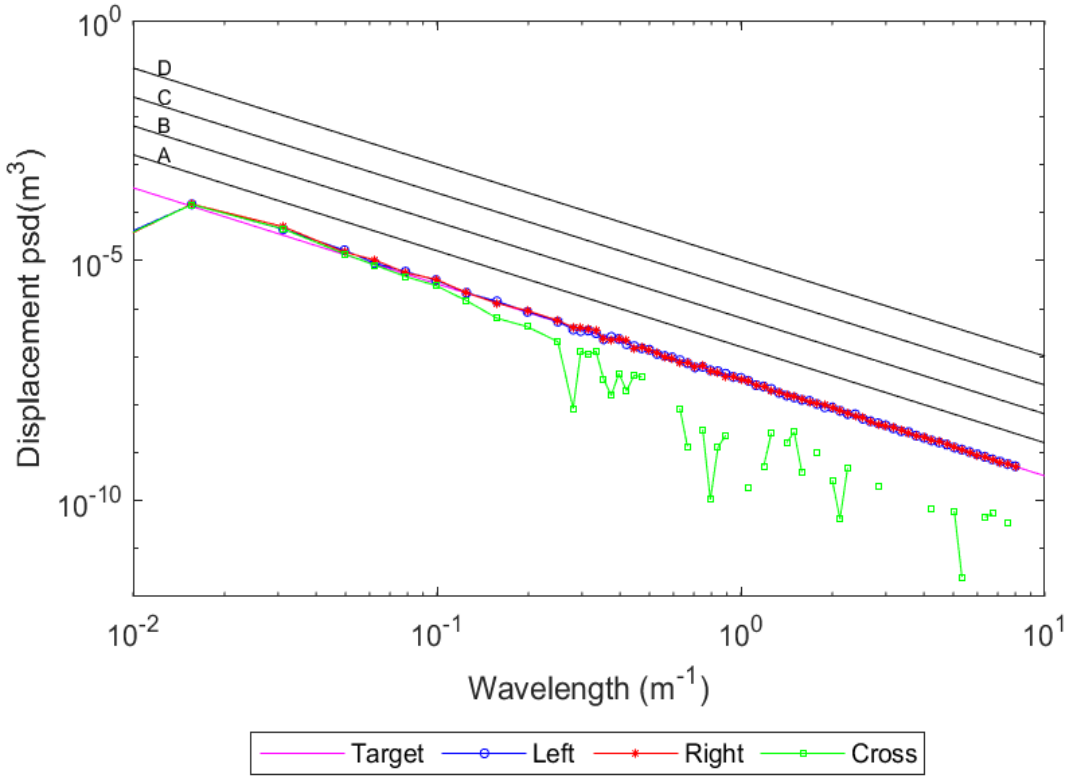

Figure A.11: PSD of Dual track road profile with design IRI of 1.0 m/km

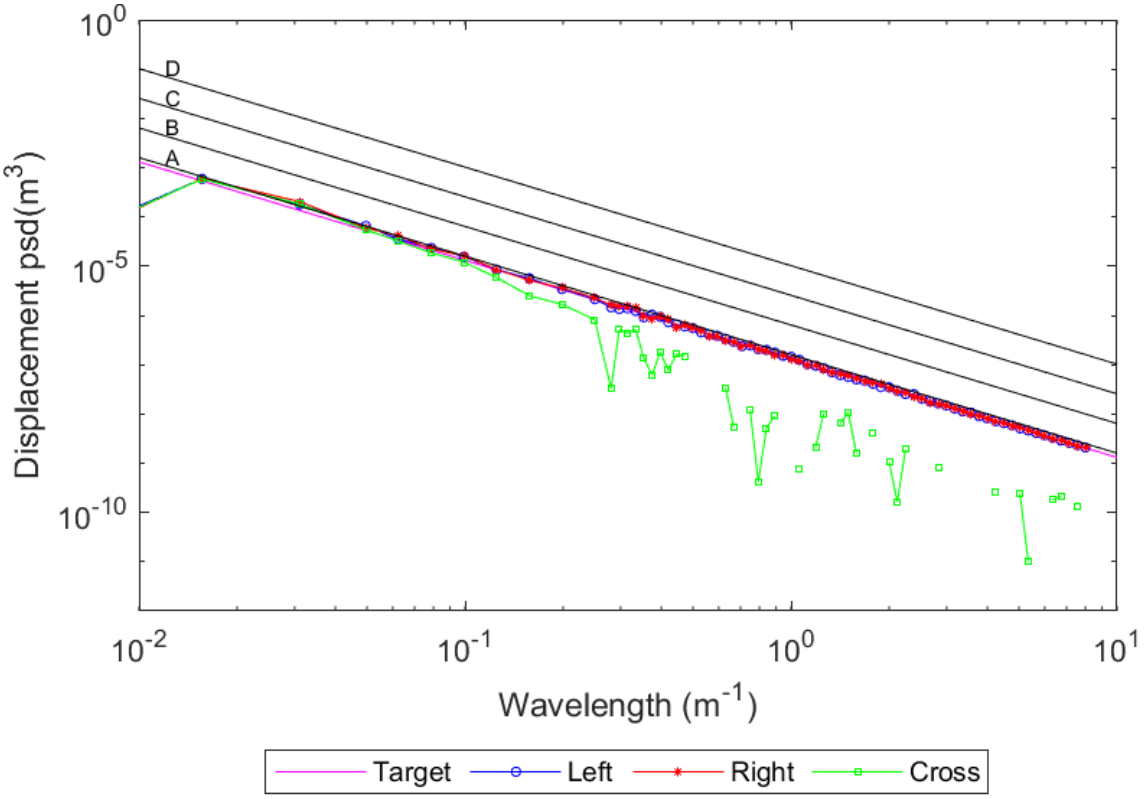

Figure A.12: PSD of Dual track road profile with design IRI of 2.0 m/km

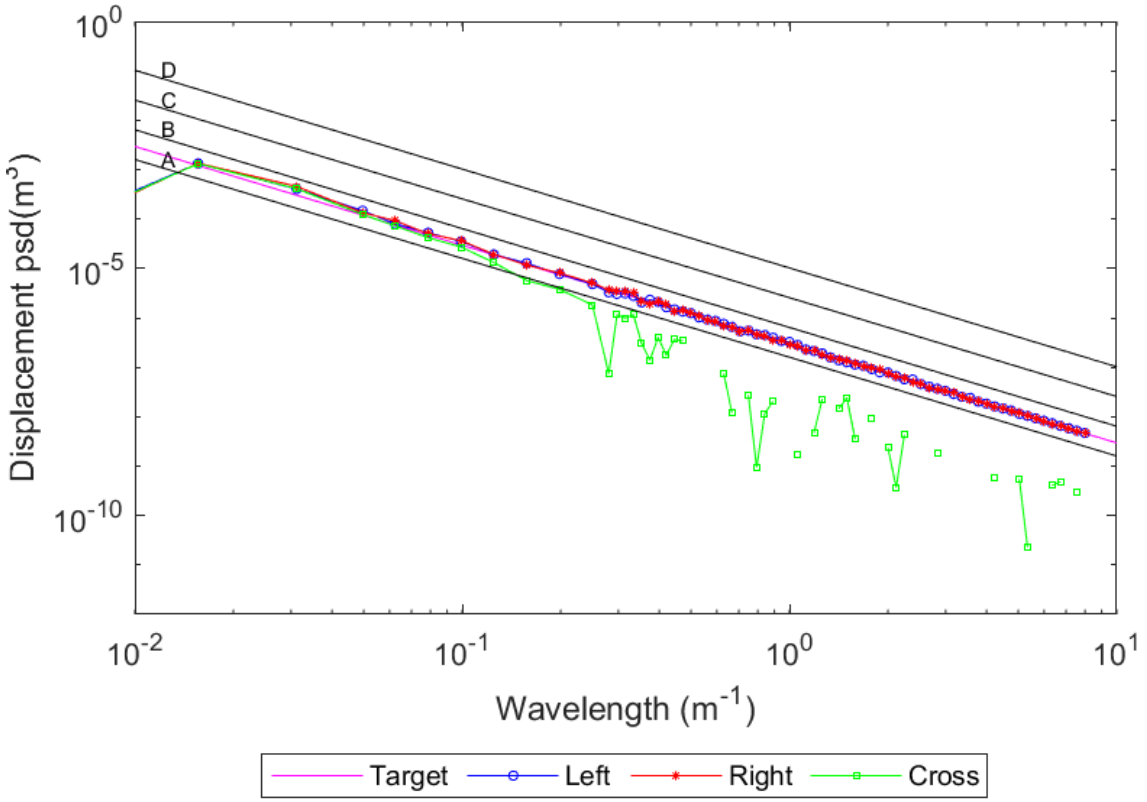

Figure A.13: PSD of Dual track road profile with design IRI of 3.0 m/km

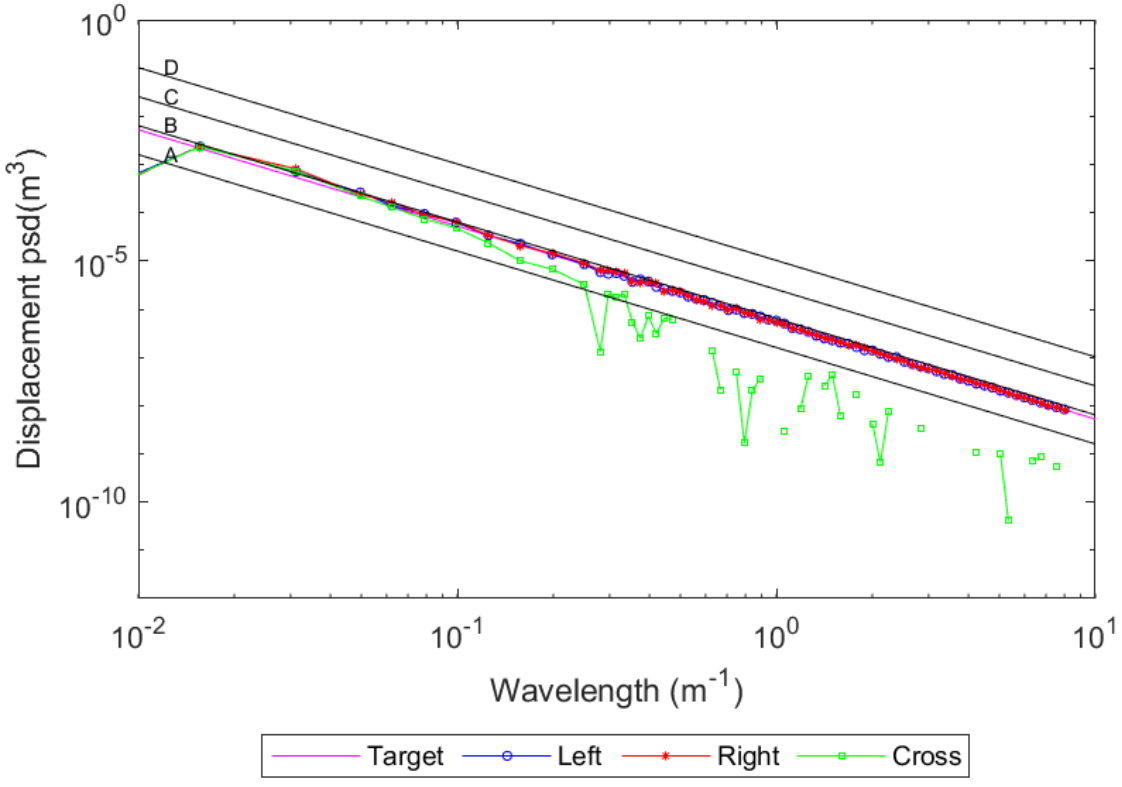

Figure A.14: PSD of Dual track road profile with design IRI of 4.0 m/km

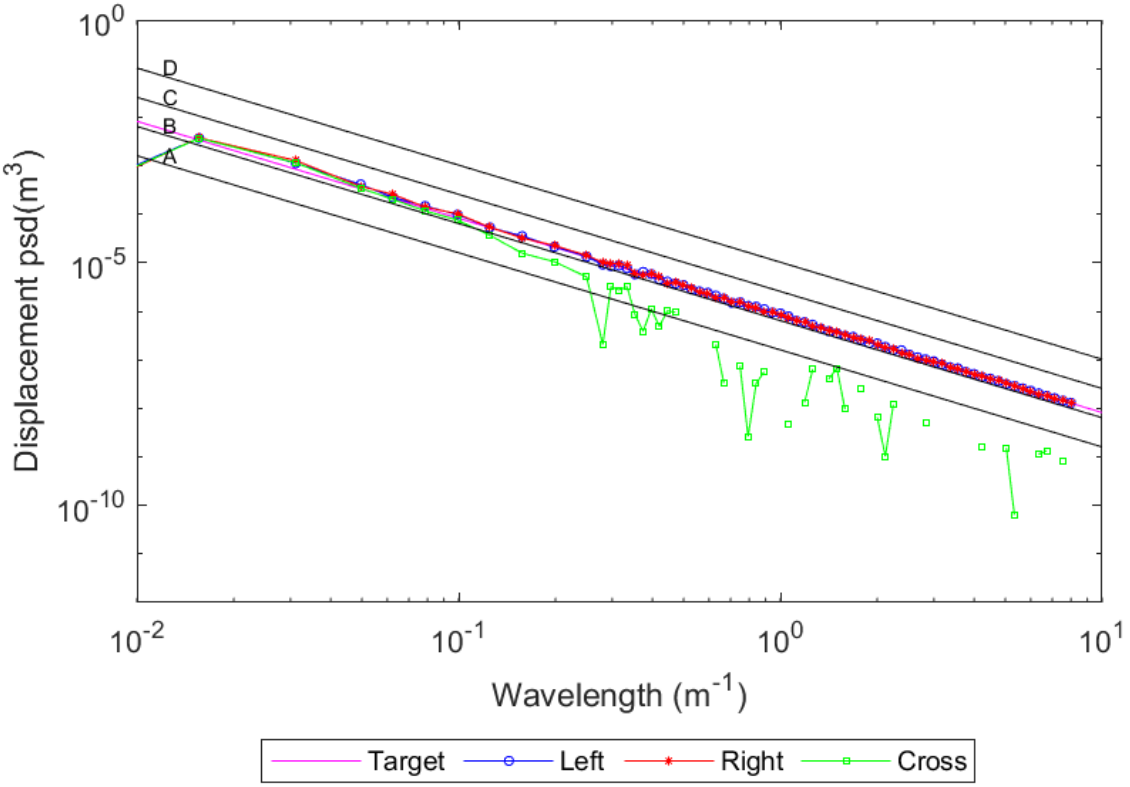

Figure A.15: PSD of Dual track road profile with design IRI of 5.0 m/km

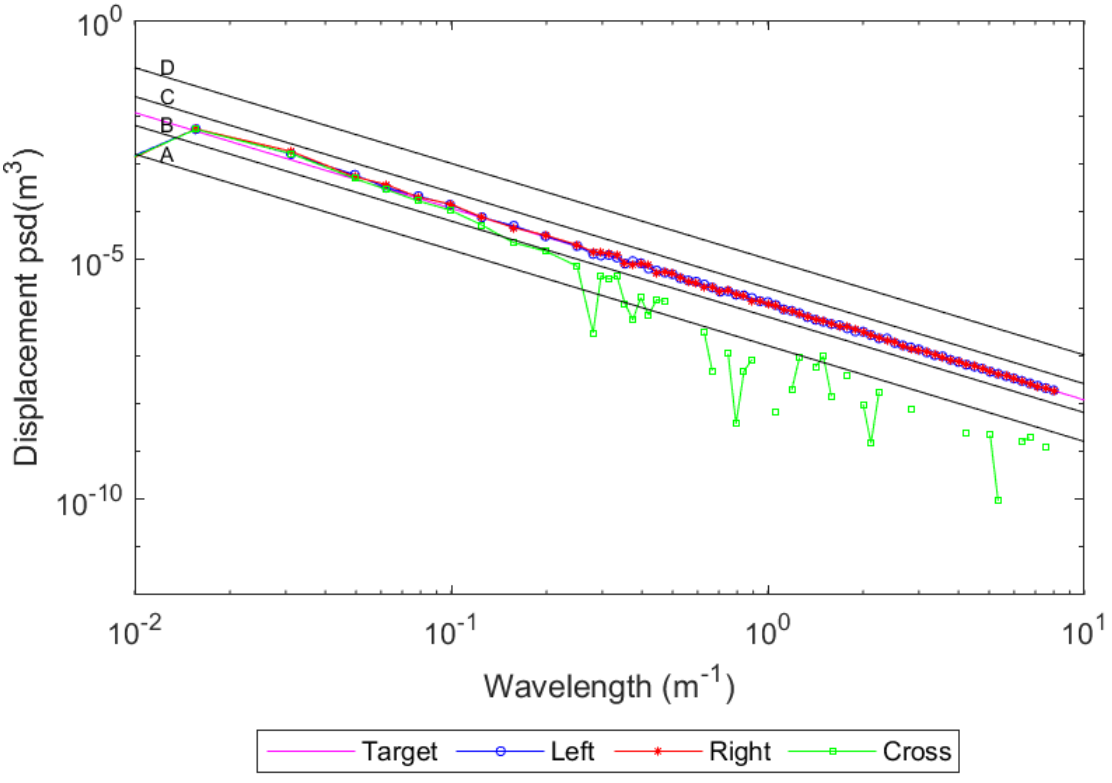

Figure A.16: PSD of Dual track road profile with design IRI of 6.0 m/km

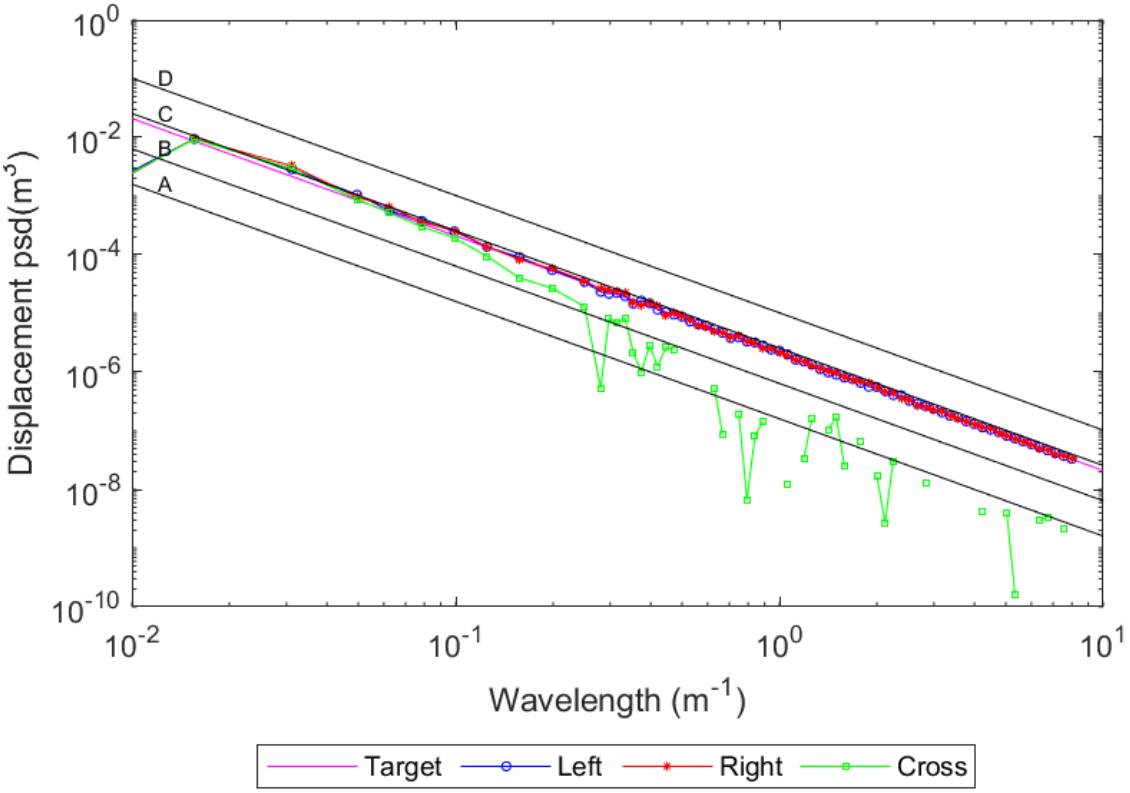

Figure A.17: PSD of Dual track road profile with design IRI of 8.0 m/km

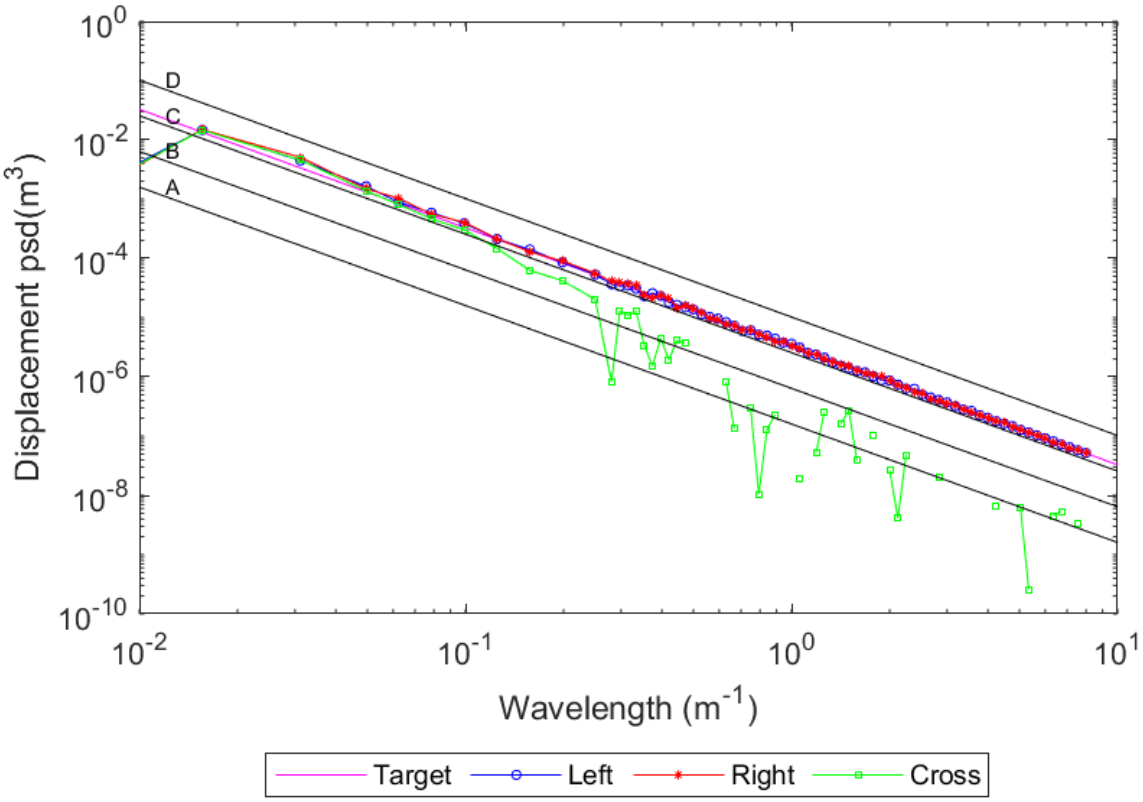

Figure A.18: PSD of Dual track road profile with design IRI of 10.0 m/km

Appendix B: TruckSim input data

This section contains some of the key input parameters specified in TruckSim2019.1® to validate the user defined model. Not all aspects are discussed as most of the parameters are simply specified in TruckSim2019.1® without the need for any modification.

Table B. provides the lateral tyre stiffness properties of both tyres. The relaxation length is also specified as 1 m as in the user defined model.

Table B.1: Lateral tyre stiffness properties used in TruckSim 2019.1®

Vertical load (N)→	7 358	14 715	29 430	44 145	58 860
Slip Angle (deg)	Lateral Force (N)				
0.05	6.4	12.8	25.7	38.5	51.4
1	1 104.3	2 208.7	4 417.4	6 626.1	8 834.8
2	2 208.7	4 417.4	8 834.8	13 252.2	17 669.6
4	4 417.4	8 834.8	17 669.6	26 504.4	35 339.1
6	6 626.1	13 252.2	26 504.4	39 756.5	53 008.7
8	8 834.8	17 669.6	35 339.1	53 008.7	70 678.3
10	11 043.5	22 087.0	44 173.9	66 260.9	88 347.9

Ackermann Geometry was selected for the steering system in TruckSim 2019.1® for a wheelbase of 3.5 m [51]. The steering angles as a function of gearbox output for both front tyres are shown in Table B.. A gearing ratio of 25 deg/deg is used for the steering wheel to gearbox output.

Table B.2: Tyre steer angles as a function of the gearbox output used in TruckSim 2019.1®

Gearbox output (Deg)	Steer output at ground left tyre (Deg)	Steer output at ground right tyre (Deg)
-10	-8.64	-9.45
-8	-6.97	-7.48
-6	-5.27	-5.56
-4	-3.54	-3.67
-2	-1.79	-1.82
0	0.00	0.00
2	1.82	1.79
4	3.67	3.54
6	5.56	5.27
8	7.48	6.97
10	9.45	8.64

The driver model parameters used are shown in Figure B.1 and are based on values typically used by the CSIR in performing heavy vehicle simulations. The preview times of driver models typically range from 0.5 s to 2 s [52]. This study used a value of 1 s as it was found that values higher than 1 s had a very similar response, whilst lower values tended to increase erratic steering wheel inputs.

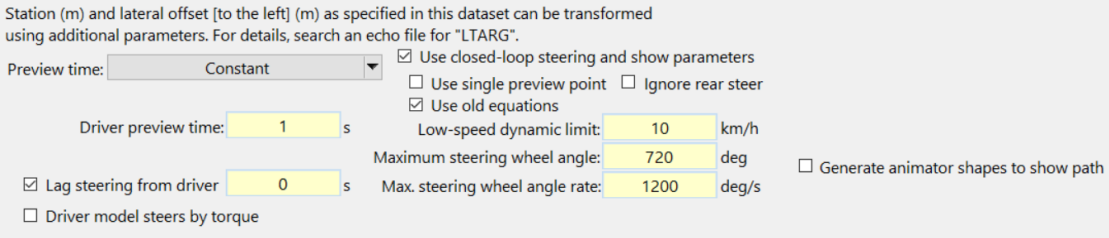

Figure B.1: Driver model parameters specified in TruckSim 2019.1®

The last aspect that needs clarification is specifying the unloaded free radius of the tyres such that the front and rear unsprung masses are both at 500 mm when loaded. In order to account for the tyre compression when loading the vehicle, the front and rear tyre free tyre radii needed to be set to 530.58 mm and 539.03 mm respectively.

Appendix C: Additional model information

This section contains the vehicle parameters used on the base model. All of the base model info is summarized in Table C.. The Simulink® implementation of the model is presented in Figure C. to Figure C.. The model is configured to group major heavy vehicle components into sub models.

Table C.1: Vehicle input parameters of the base user defined model

Parameter	Symbol	Unit	Value
Sprung mass	m_s	kg	12 500
Unsprung mass front	m_{uf}	kg	706
Unsprung mass rear	m_{ur}	kg	1 000
Track width front	$2 \cdot T_f$	m	2
Track width rear	$2 \cdot T_r$	m	2
Spring track width front	$2 \cdot S_f$	m	1.2
Spring track width rear	$2 \cdot S_r$	m	1.2
Tyre vertical spring stiffness front	k_{tf}	N/m	1 000 000
Tyre vertical spring stiffness rear	k_{tr}	N/m	1 000 000
Spring stiffness front	k_f	N/m	200 000
Spring stiffness rear	k_r	N/m	400 000
Distance front to CoG	a	m	1.95
Distance rear to CoG	b	m	1.55
Front RC height	h_{1f}	m	0.6
Rear RC height	h_{1r}	m	0.6
Front unsprung mass height	h_{2f}	m	0.5

Rear unsprung mass height	h_{2r}	m	0.5
Sprung mass height	h	m	2
Damper value front	c_f	Ns/m	5 000
Damper value rear	c_r	Ns/m	10 000
Roll inertia sprung mass	I_{sr}	kg·m^2	24 201
Pitch inertia	I_{sp}	kg·m^2	34 917
Unpsrung mass roll inertia front	I_{uf}	kg·m^2	572
Unpsrung mass roll inertia rear	I_{ur}	kg·m^2	810
Front tyre relaxation length	L_f	m	1.0
Rear tyre relaxation length	L_r	m	1.0

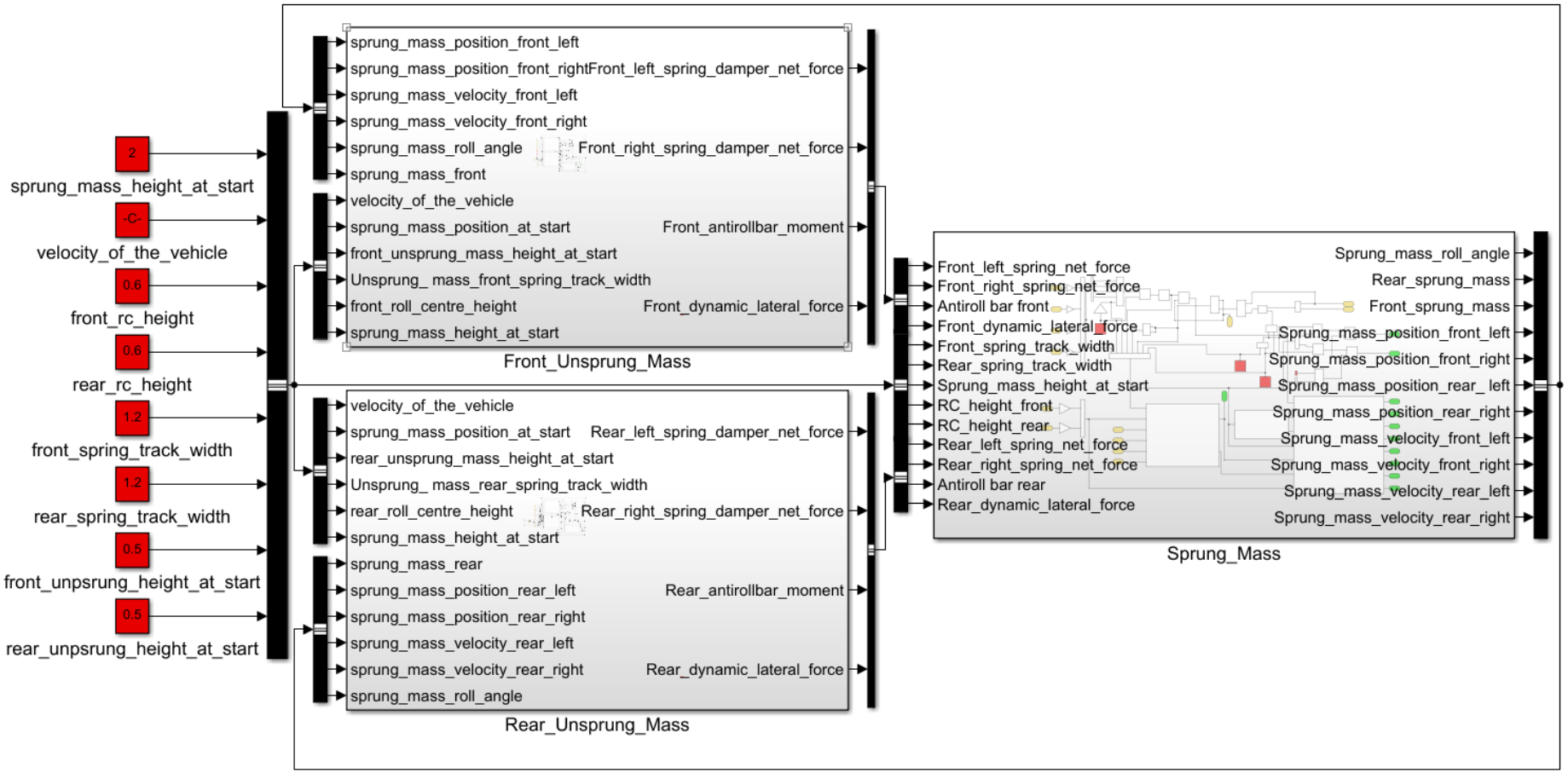

Figure C.1: Main window of Simunlink® heavy vehicle model

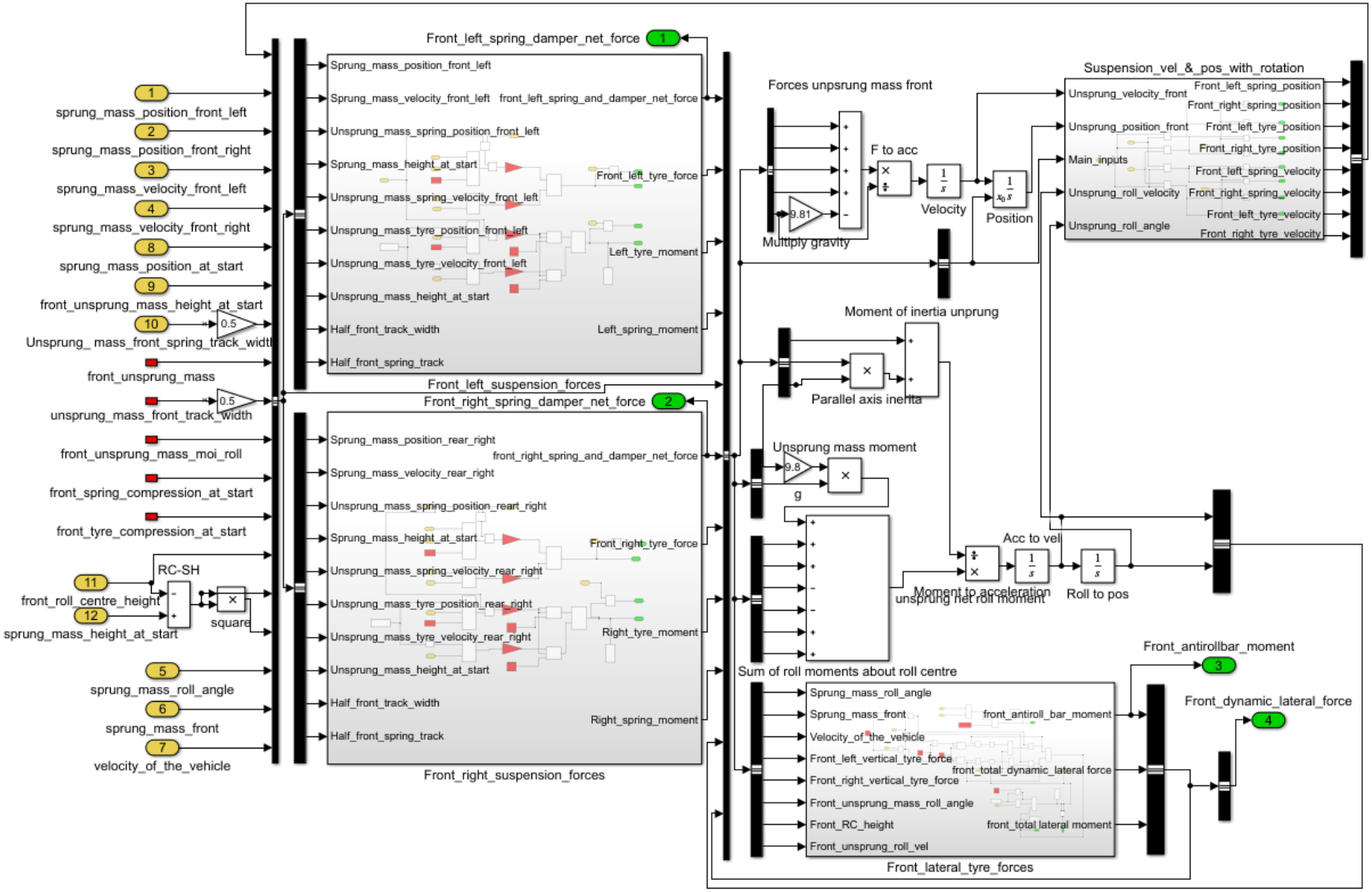

Figure C.2: Front unsprung mass sub model

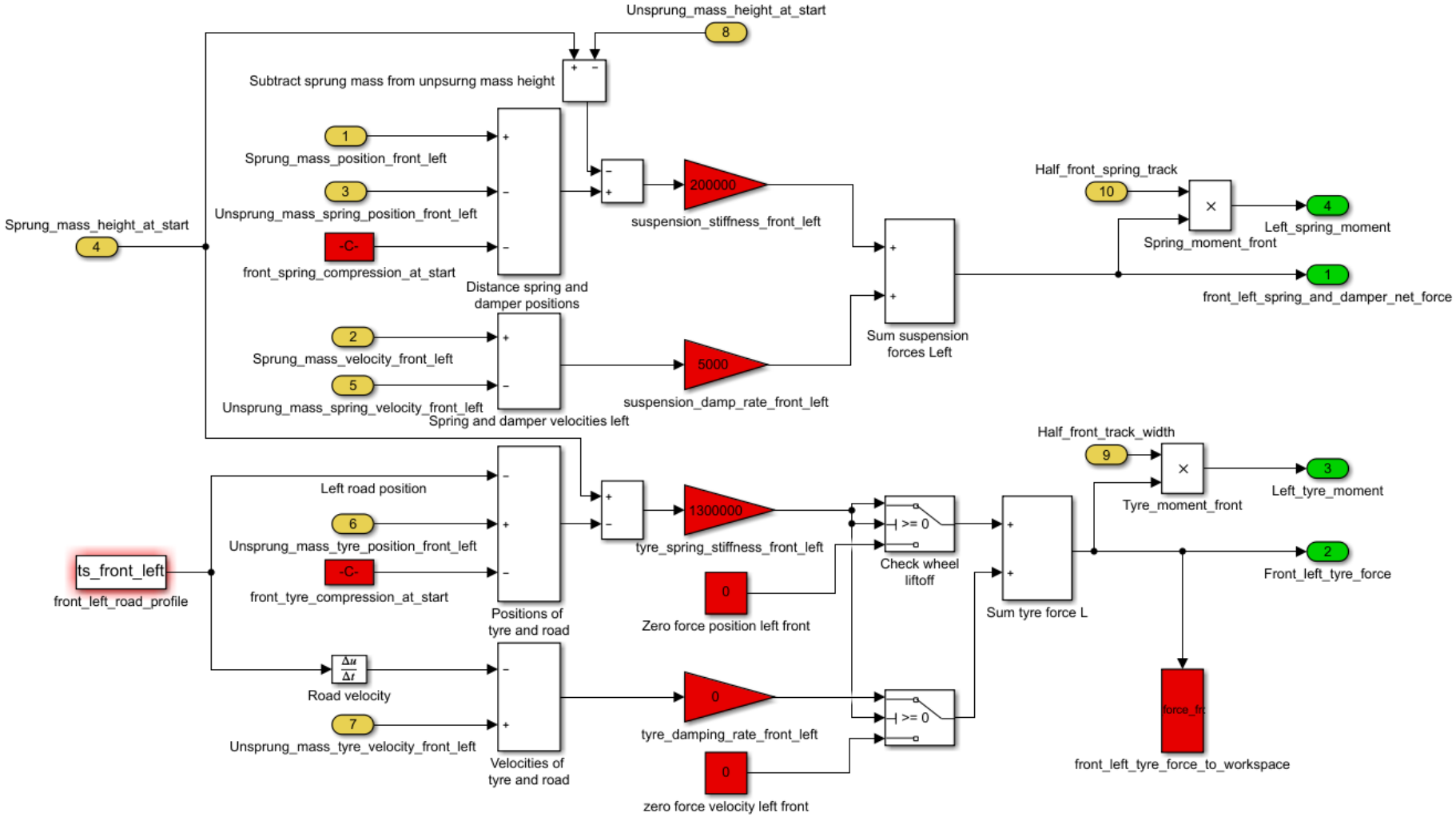

Figure C.3: Front left suspension sub model

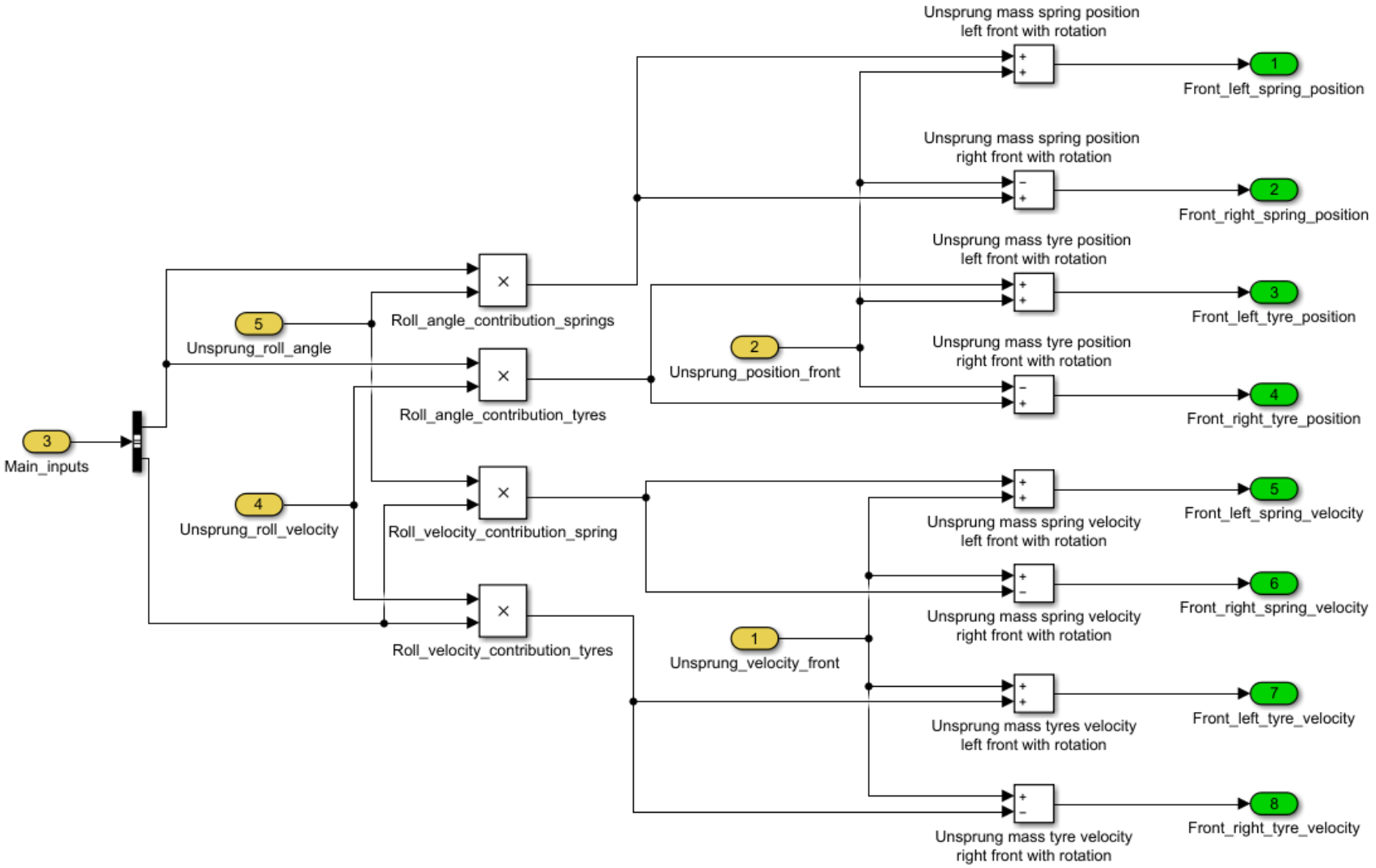

Figure C.4: Unsprung mass positions and velocities sub model

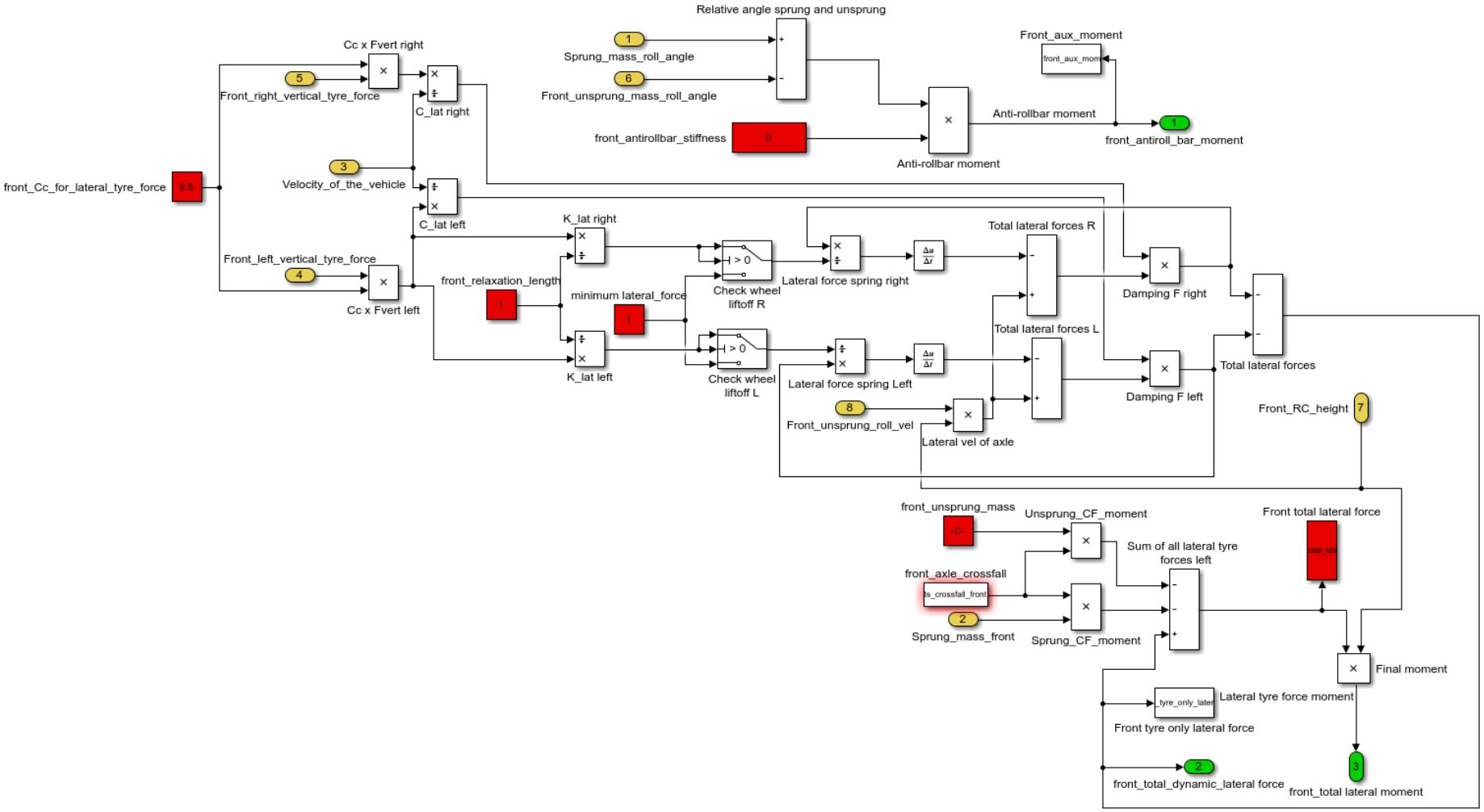

Figure C.5: Front axle tyre sub model

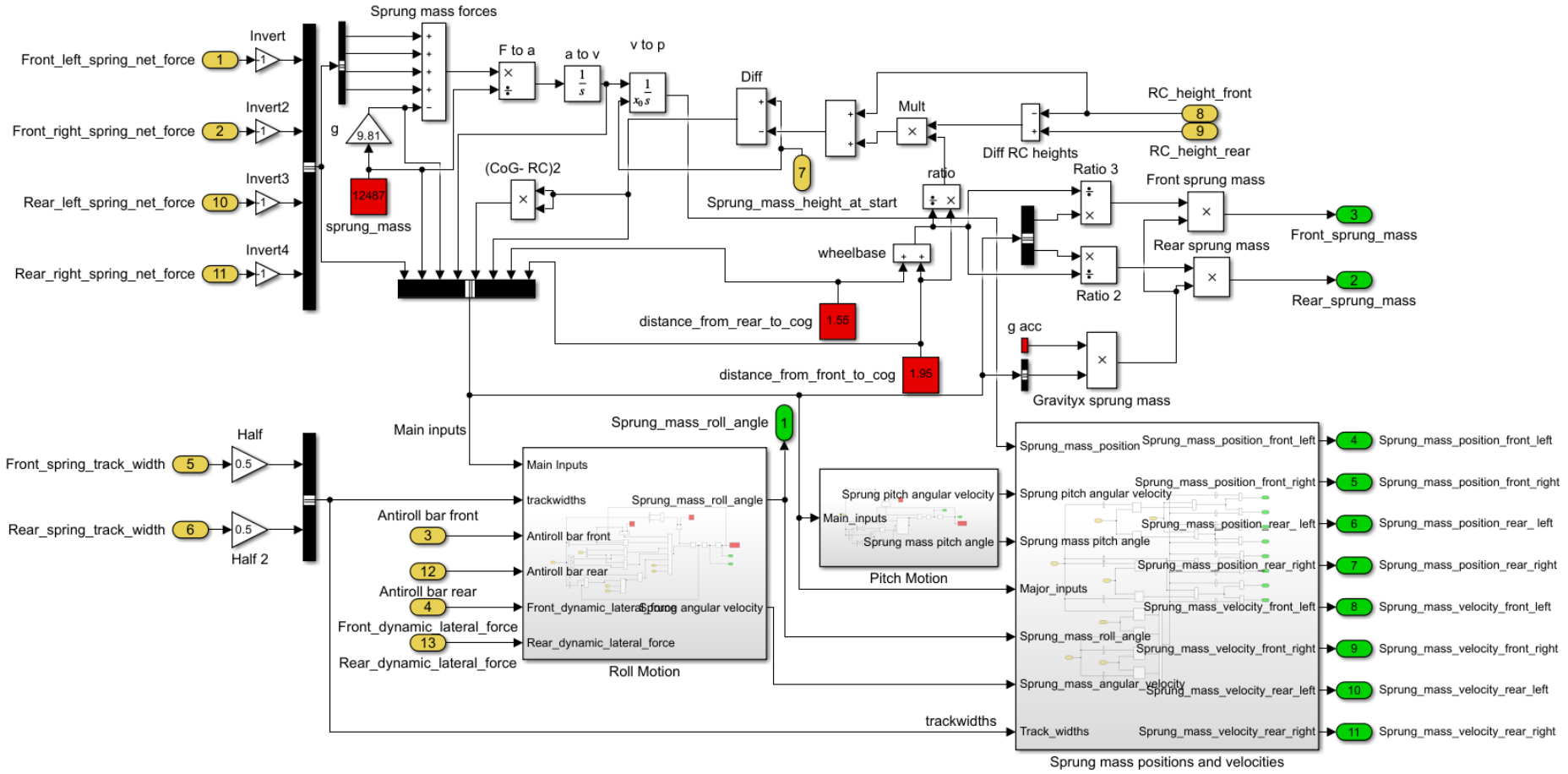

Figure C.6: Main sprung mass sub model

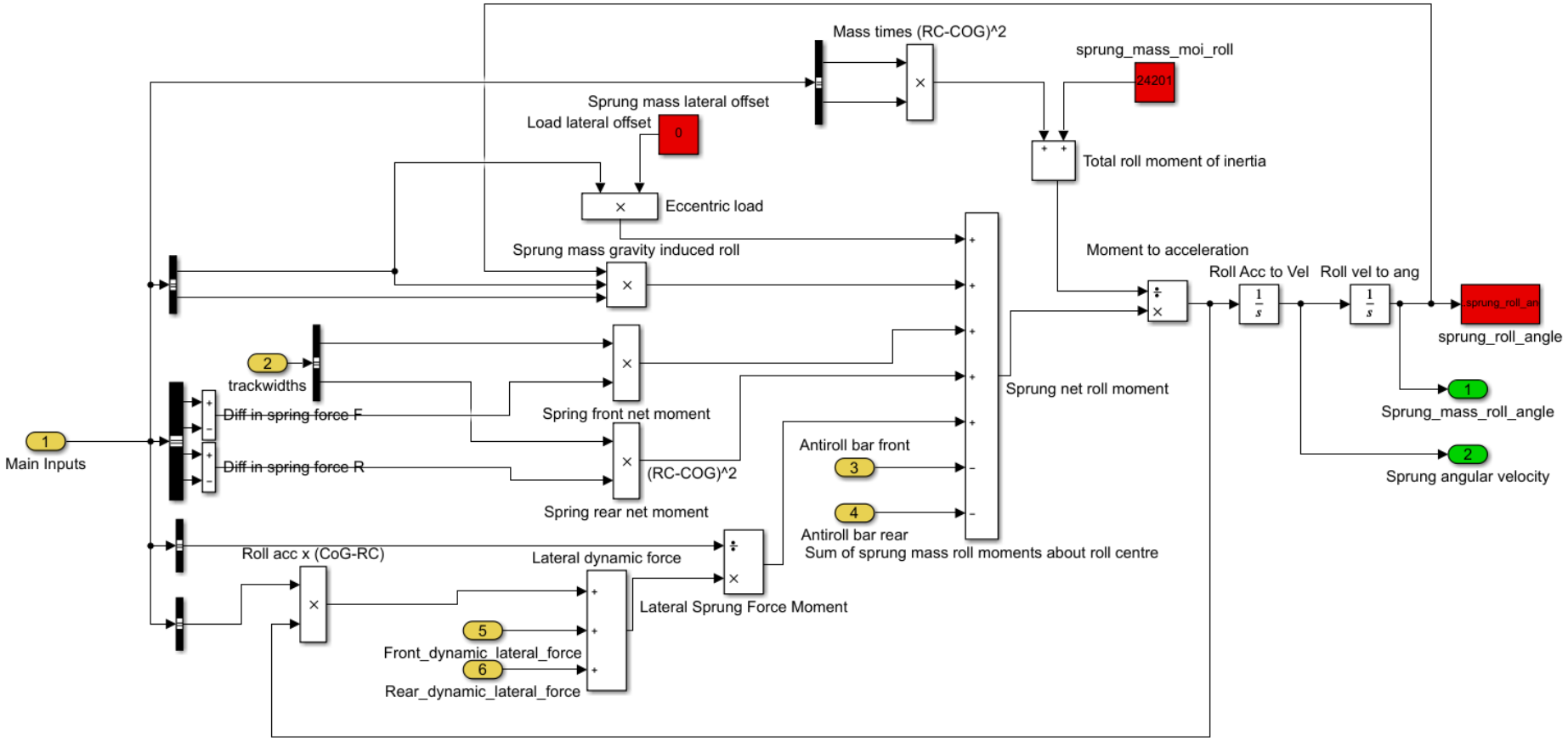

Figure C.7: Sprung mass roll motion sub model

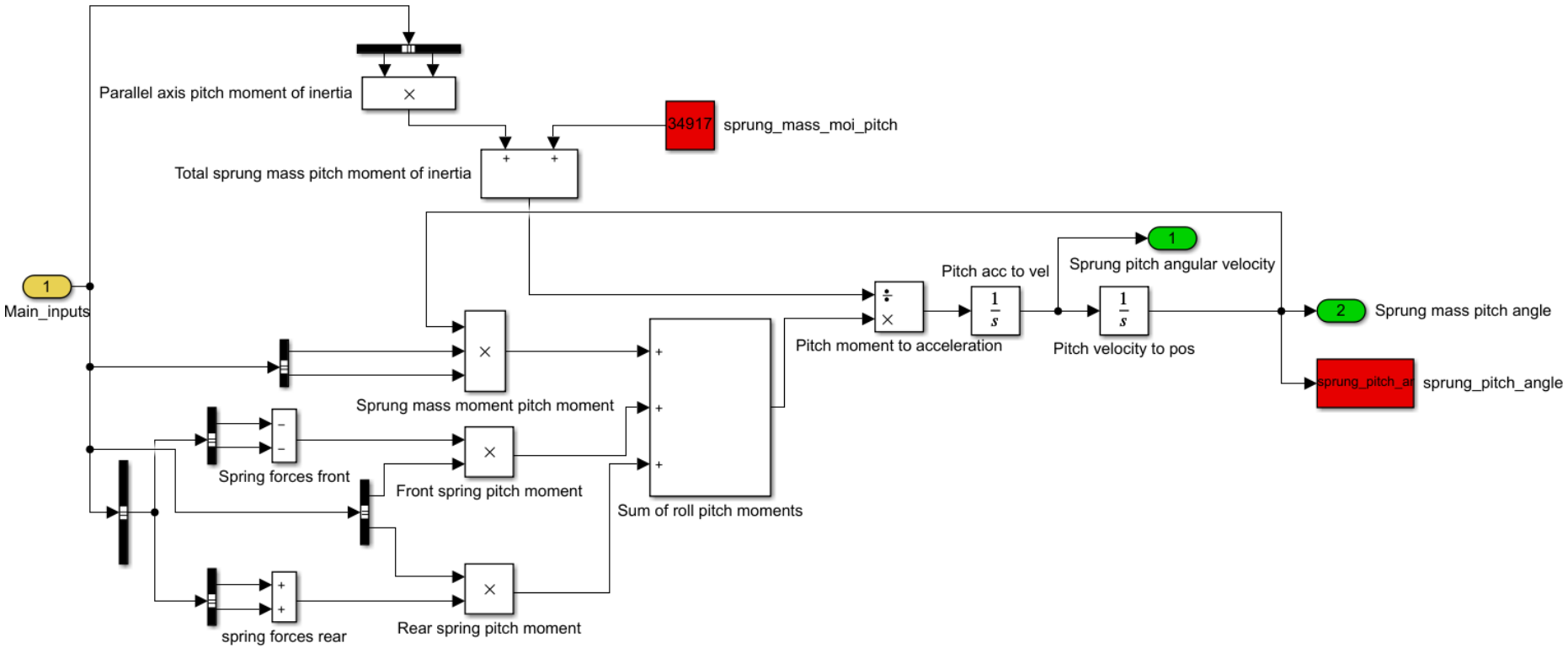

Figure C.8: Sprung mass pitch motion sub model

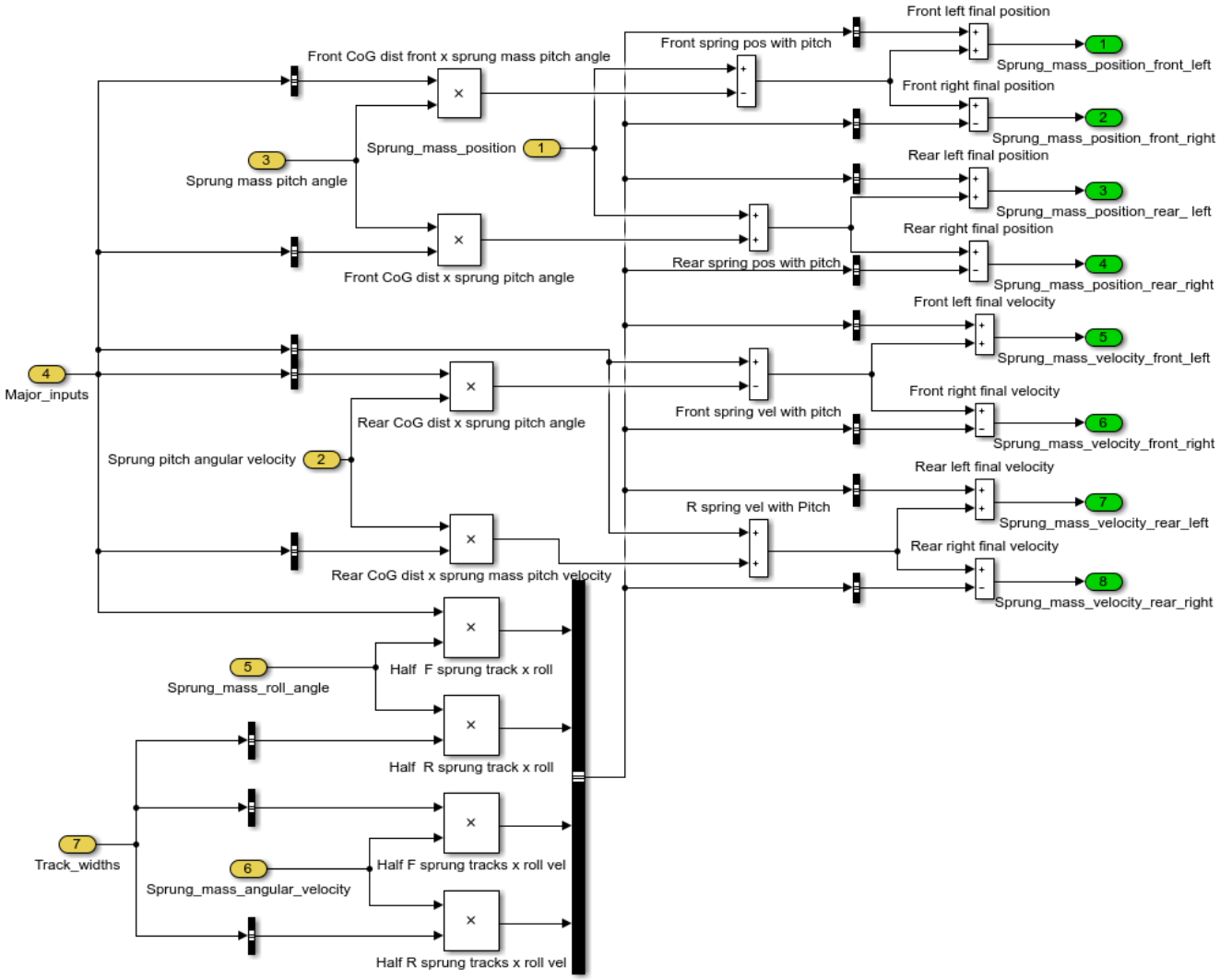

Figure C.9: Sprung mass final positions and velocities sub model

Appendix D: Additional validation results

Additional validation results comparing the performance of the Simulink model to TruckSim 2019.1 ® are summarized in Table D.1 to Table D.. The results show that the Simulink model achieves accurate results compared to TruckSim 2019.1® especially under typical highway operating conditions. Plots of the validation results are shown in Figure D. to Figure D..

Table D.1: Average absolute error of vertical tyre forces for validation simulations compared to TruckSim 2019.1® values at 0% crossfall and no anti-roll bar

	2 IRI & 80 km/h	10 IRI & 80 kmh	2 IRI & 40 km/h	10 IRI & 40 km/h	2 IRI & 120 km/h	10 IRI & 120 km/h
	(%)	(%)	(%)	(%)	(%)	(%)
Front left tyre	0.61	3.46	0.71	4.09	0.52	3.24
Front right tyre	0.59	3.43	0.71	4.08	0.52	3.13
Rear left tyre	0.57	3.17	0.61	3.44	0.49	3.11
Rear right tyre	0.56	3.19	0.61	3.42	0.50	3.13

Table D.2: Average absolute error of first power vertical tyre forces for validation simulations compared to TruckSim 2019.1® values at 0% crossfall and no anti-roll bar

	2 IRI & 80km/h	10 IRI & 80kmh	2 IRI & 40km/h	10 IRI & 40km/h	2 IRI & 120 km/h	10 IRI & 120 km/h
	(%)	(%)	(%)	(%)	(%)	(%)
Left side	0.49	2.78	0.60	3.48	0.38	2.47
Right side	0.47	2.77	0.60	3.47	0.38	2.46

Table D.3: Average absolute error of fourth power vertical tyre forces for validation simulations compared to TruckSim 2019.1® values at 0% crossfall and no anti-roll bar

	2 IRI & 80km/h	10 IRI & 80kmh	2 IRI & 40km/h	10 IRI & 40km/h	2 IRI & 120 km/h	10 IRI & 120 km/h
	(%)	(%)	(%)	(%)	(%)	(%)
Left side	2.00	11.59	2.39	13.87	1.61	10.69
Right side	1.95	11.59	2.39	13.81	1.62	10.70

Table D.4: Dynamic loading coefficient error for validation simulations compared to TruckSim 2019.1® values at 0% crossfall and no anti-roll bar

	2 IRI & 80km/h	10 IRI & 80kmh	2 IRI & 40km/h	10 IRI & 40km/h	2 IRI & 120 km/h	10 IRI & 120 km/h
	(%)	(%)	(%)	(%)	(%)	(%)
Front left tyre	1.42	2.49	2.76	2.93	0.63	1.81
Front right tyre	1.45	2.56	2.59	2.96	0.48	1.90
Rear left tyre	-7.77	-7.42	-1.34	-1.73	-7.59	-7.18
Rear right tyre	-7.79	-7.45	-1.84	-2.07	-7.80	-7.18

Table D.5: Average absolute error of vertical tyre forces for validation simulations compared to TruckSim 2019.1® values when including crossfall

	2 IRI & 80 km/h 2% CF	2 IRI & 80 km/h 5% CF	10 IRI & 80 km/h 5% CF	10 IRI & 80 km/h 5% CF with stabilizers	10 IRI & 40 km/h 5% CF with stabilizers
	(%)	(%)	(%)	(%)	(%)
Front left tyre	0.63	0.69	3.38	0.69	0.74
Front right tyre	0.64	0.78	3.92	0.73	0.84
Rear left tyre	0.57	0.63	2.94	0.61	0.65
Rear right tyre	0.65	0.86	3.81	0.78	0.81

Table D.6: Average absolute error of first power aggregate vertical tyre forces for validation simulations compared to TruckSim 2019.1® values when including crossfall

	2 IRI & 80 km/h 2% CF	2 IRI & 80 km/h 5% CF	10 IRI & 80 km/h 5% CF	10 IRI & 80 km/h 5% CF with stabilizers	10 IRI & 40 km/h 5% CF with stabilizers
	(%)	(%)	(%)	(%)	(%)
Left side	0.50	0.56	2.66	0.54	0.62
Right side	0.54	0.72	3.29	0.67	0.75

Table D.7: Average absolute error of the fourth power aggregate vertical tyre forces for validation simulations compared to TruckSim 2019.1® values when including crossfall

	2 IRI & 80 km/h 2% CF	2 IRI & 80 km/h 5% CF	10 IRI & 80 km/h 5% CF	10 IRI & 80 km/h 5% CF with stabilizers	10 IRI & 40 km/h 5% CF with stabilizers
	(%)	(%)	(%)	(%)	(%)
Left side	2.04	2.25	10.86	2.20	2.46
Right side	2.26	3.01	14.39	2.78	3.04

Table D.8: Average absolute error of the dynamic load coefficient for validation simulations compared to TruckSim 2019.1® values when including crossfall

	2 IRI & 80 km/h 2% CF	2 IRI & 80 km/h 5% CF	10 IRI & 80 km/h 5% CF	10 IRI & 80 km/h 5% CF with stabilizers	10 IRI & 40 km/h 5% CF with stabilizers
	(%)	(%)	(%)	(%)	(%)
Front left tyre	1.29	0.86	2.39	1.27	2.17
Front right tyre	1.03	0.08	1.63	0.97	1.45
Rear left tyre	-8.56	-10.53	-8.83	-9.74	-3.83
Rear right tyre	-7.86	-8.65	-6.72	-7.21	-1.84

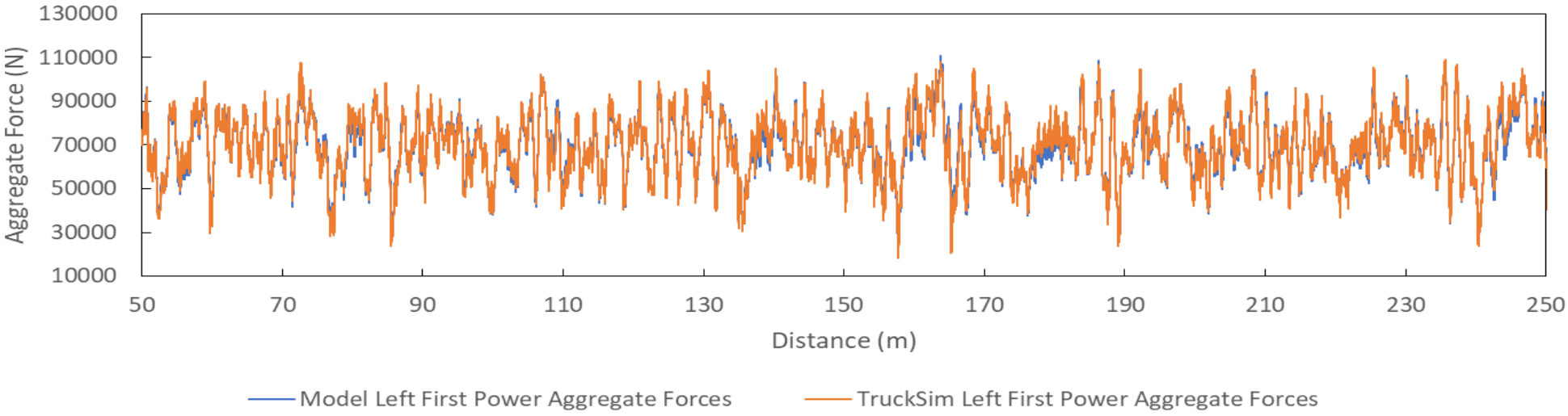

Figure D.1: Left side first power aggregate forces from TruckSim 2019.1® and the model over 200 m test section at 0% crossfall, 10 m/km IRI, 80 km/h and no anti-roll bar

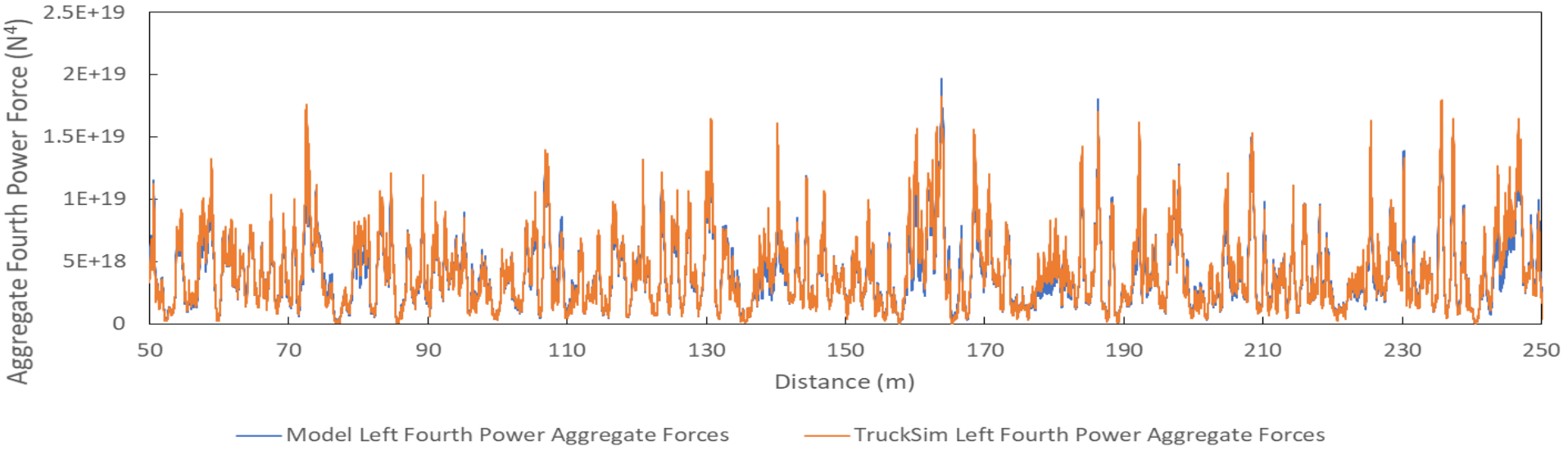

Figure D.2: Left side fourth power aggregate forces from TruckSim 2019.1® and the model over 200 m test section at 0% crossfall, 10 m/km IRI, 80 km/h and no anti-roll bar

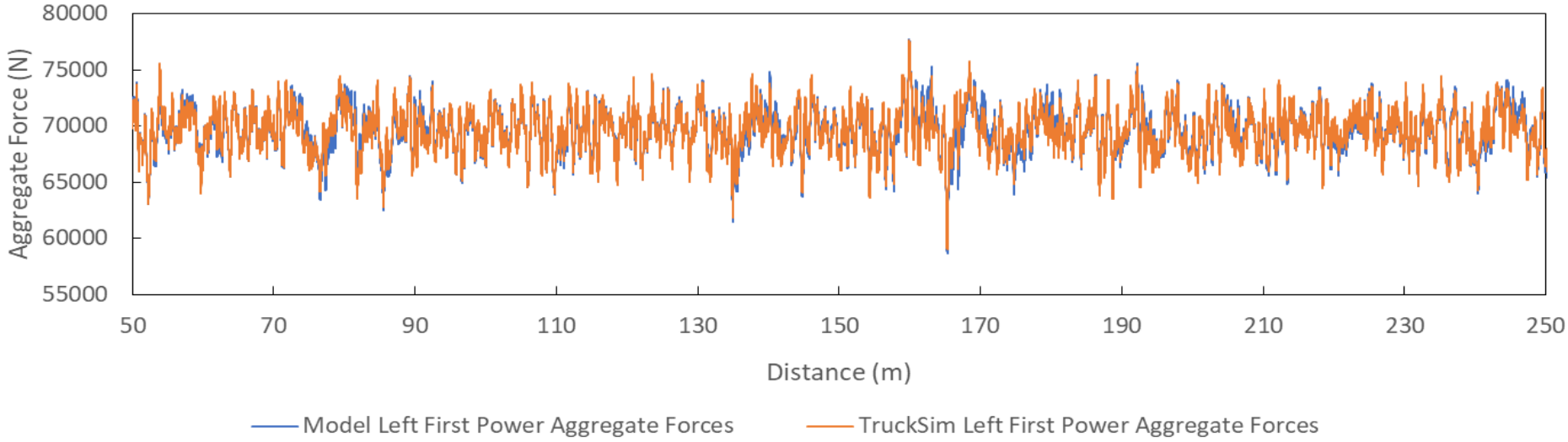

Figure D.3: Left side first power aggregate forces from TruckSim 2019.1® and the model over 200 m test section at 0% crossfall, 2 m/km IRI, 40 km/h and no anti-roll bar

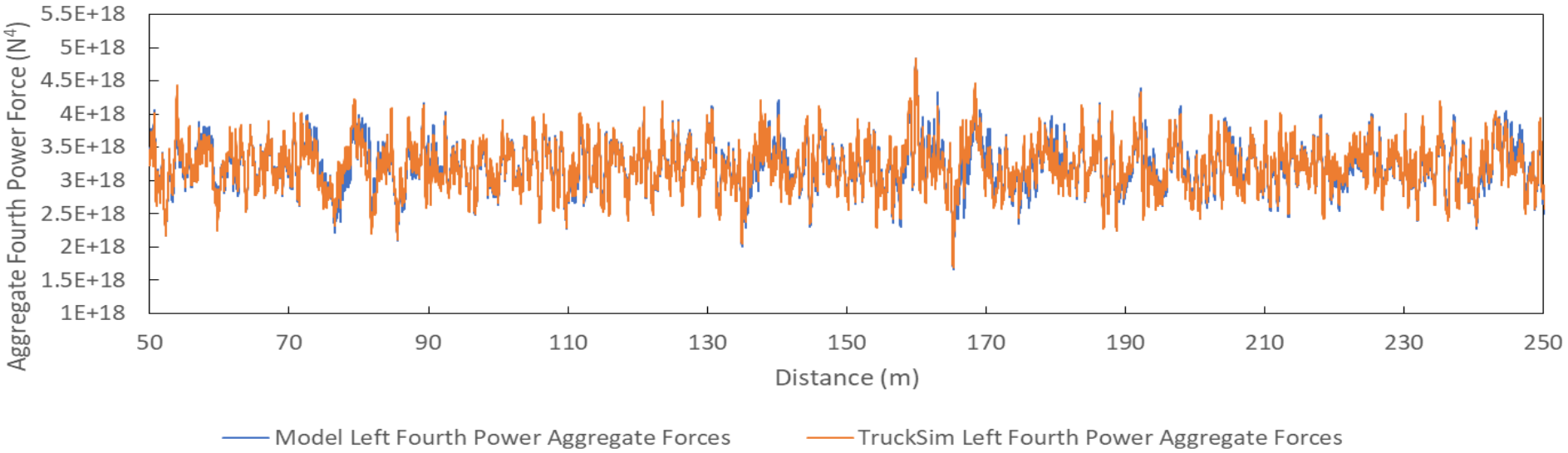

Figure D.4: Left side fourth power aggregate forces from TruckSim 2019.1® and the model over 200 m test section at 0% crossfall, 2 m/km IRI, 40 km/h and no anti-roll bar

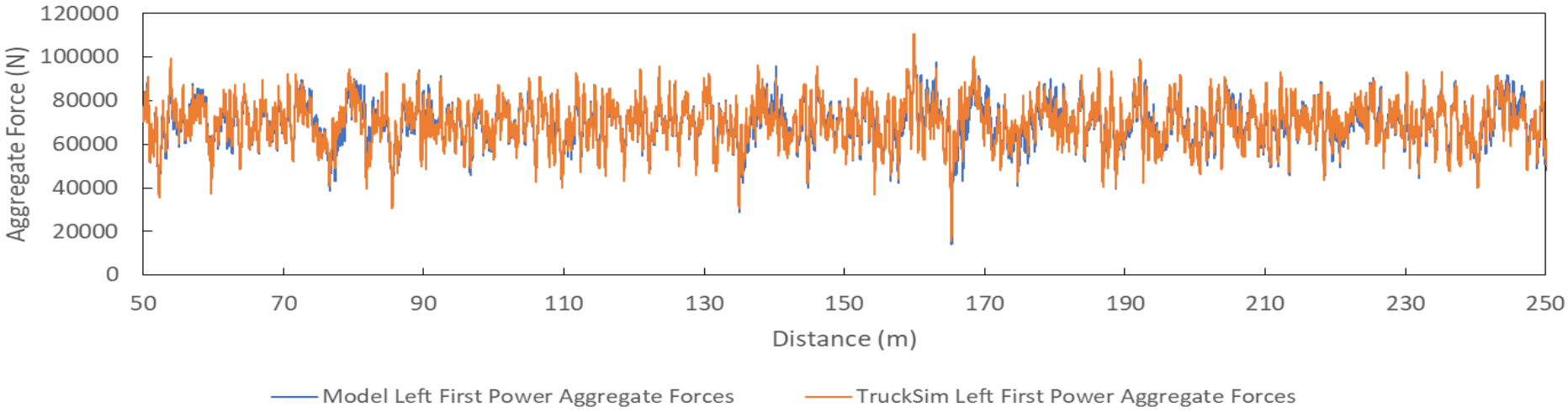

Figure D.5: Left side first power aggregate forces from TruckSim 2019.1® and the model over 200 m test section at 0% crossfall, 10 m/km IRI, 40 km/h and no anti-roll bar

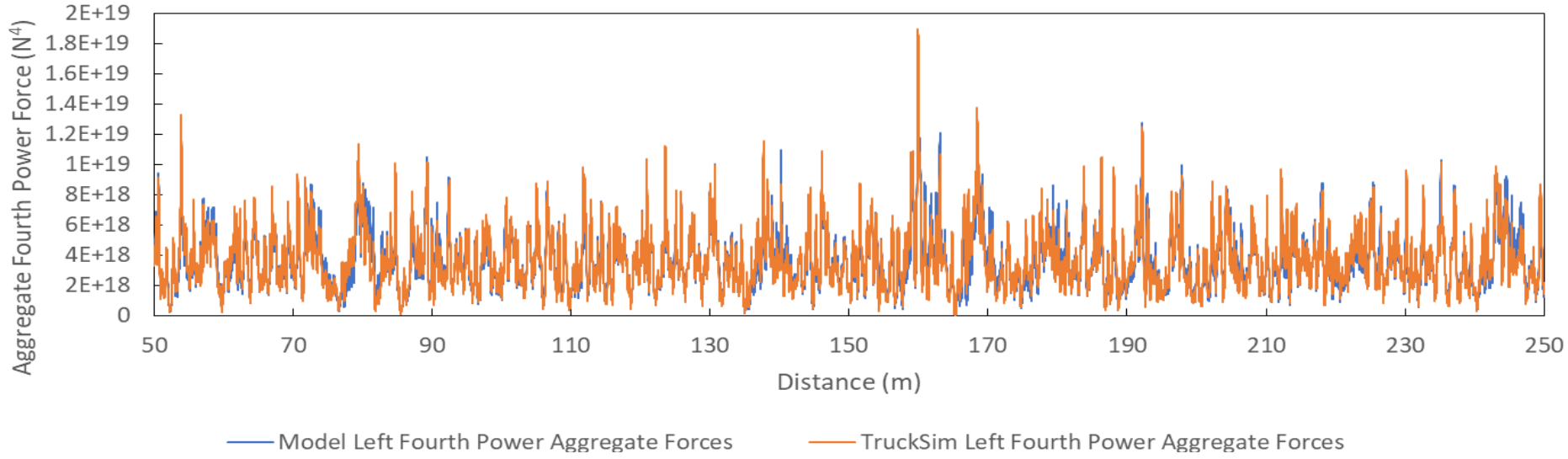

Figure D.6: Left side fourth power aggregate forces from TruckSim 2019.1® and the model over 200 m test section at 0% crossfall, 10 m/km IRI, 40 km/h and no anti-roll bar

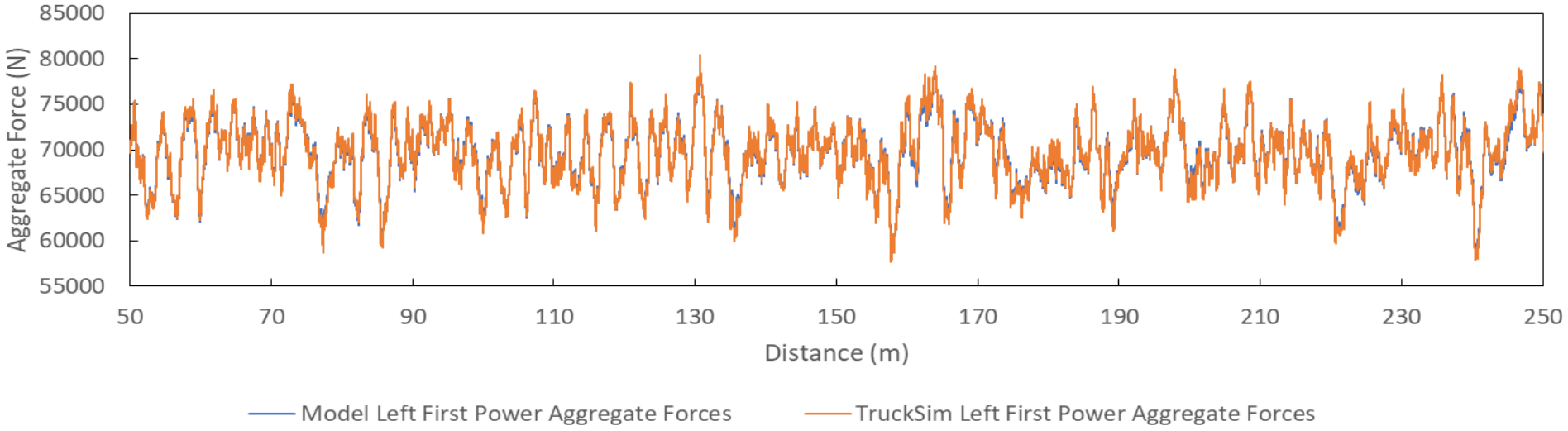

Figure D.7: Left side first power aggregate forces from TruckSim 2019.1® and the model over 200 m test section at 0% crossfall, 2 m/km IRI, 120 km/h and no anti-roll bar

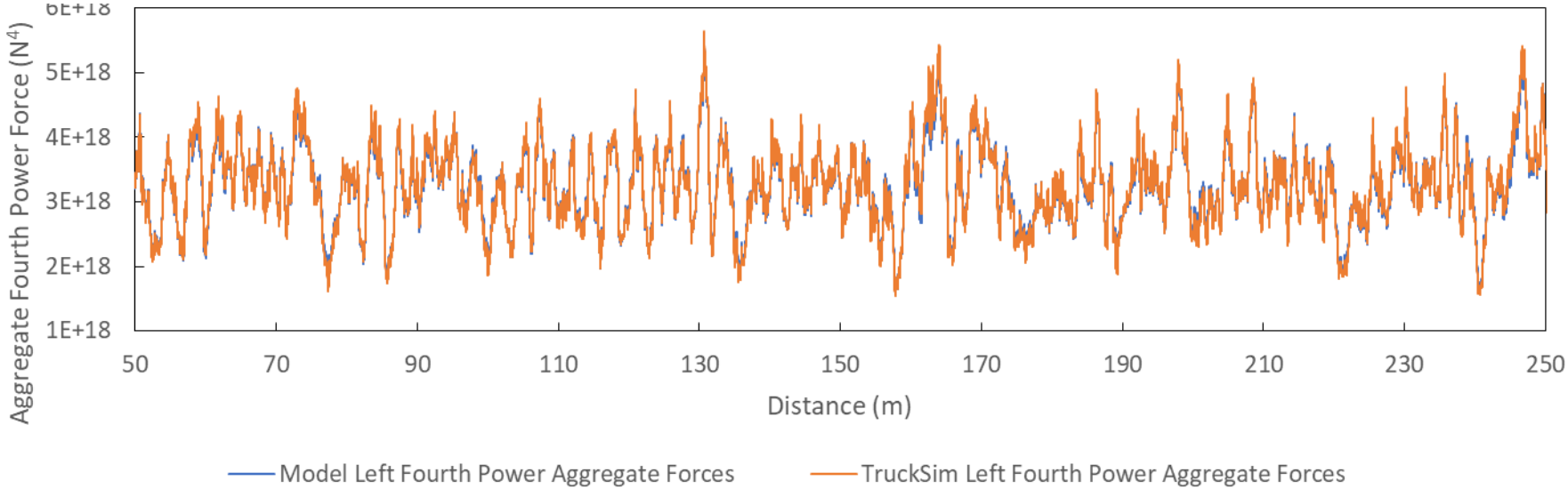

Figure D.8: Left side fourth power aggregate forces from TruckSim 2019.1® and the model over 200 m test section at 0% crossfall, 2 m/km IRI, 120 km/h and no anti-roll bar

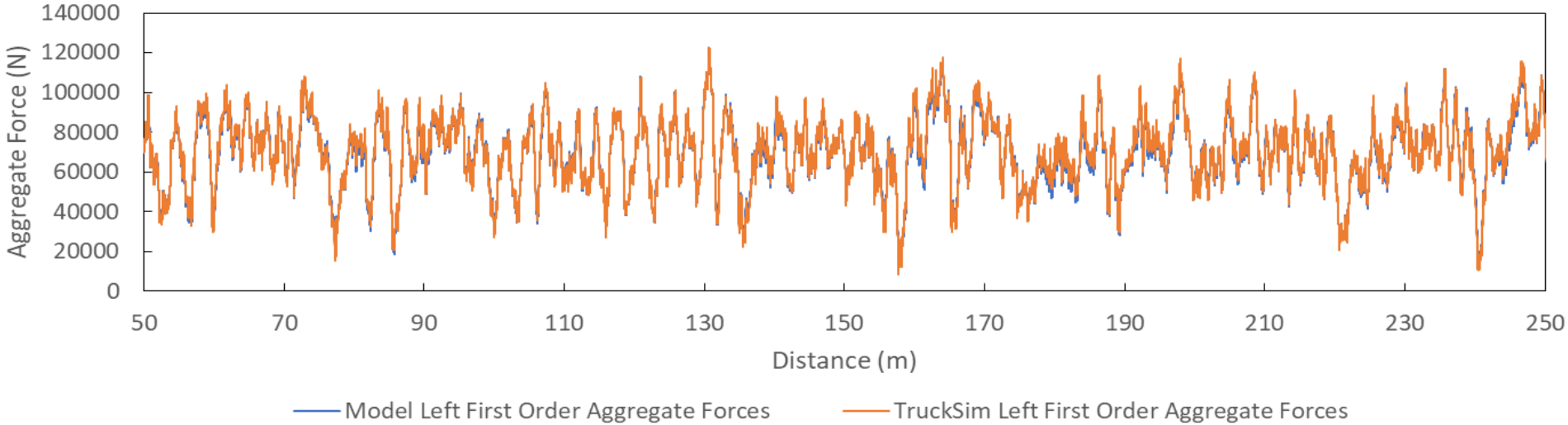

Figure D.9:Left side first power aggregate forces from TruckSim 2019.1® and the model over 200 m test section at 0% crossfall, 10 m/km IRI, 120 km/h and no anti-roll bar

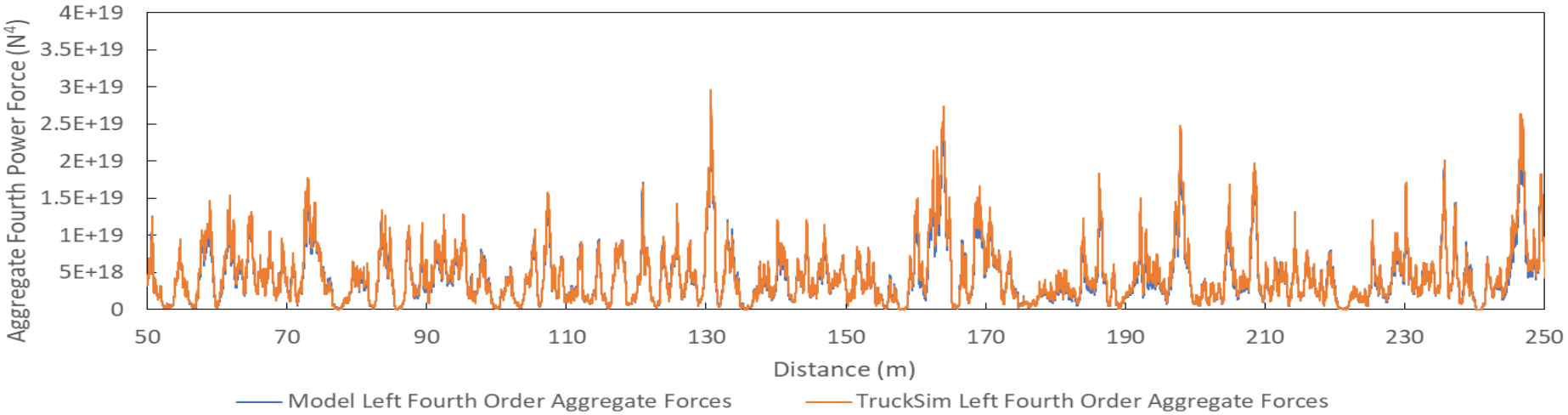

Figure D.10: Left side fourth power aggregate forces from TruckSim 2019.1® and the model over 200 m test section at 0% crossfall, 10 m/km IRI, 120 km/h and no anti-roll bar

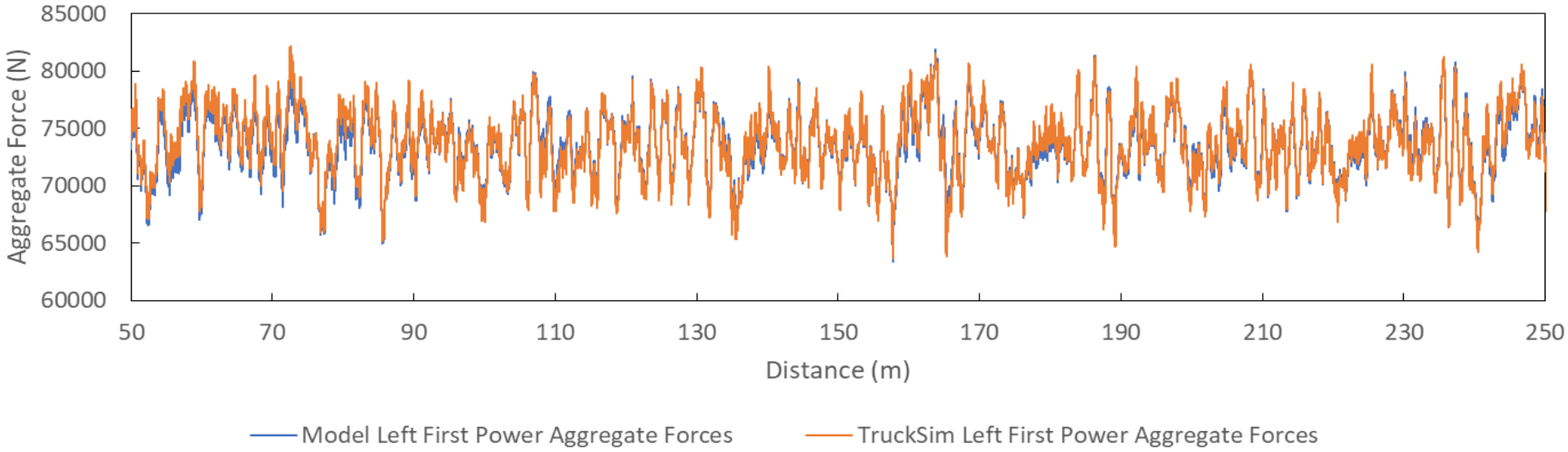

Figure D.11: Left side first power aggregate forces from TruckSim 2019.1® and the final model over 200 m test section at 2% crossfall, 2 m/km IRI, 80 km/h and no anti-roll bar

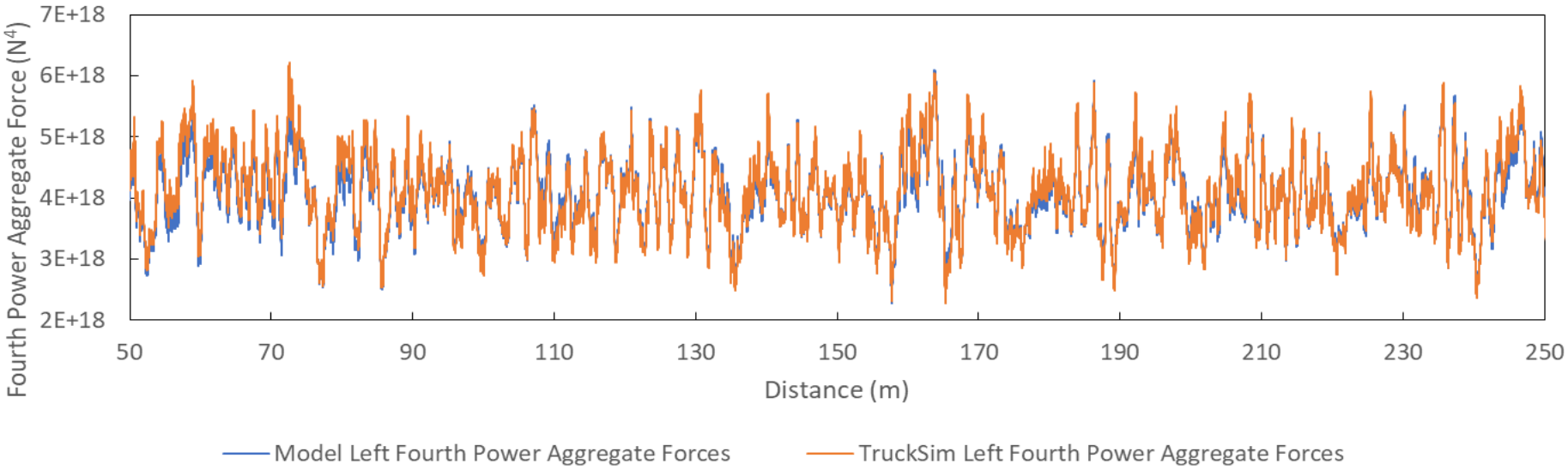

Figure D.12: Left side fourth power aggregate forces from TruckSim 2019.1® and the final model over 200 m test section at 2% crossfall, 2 m/km IRI, 80 km/h and no anti-roll bar

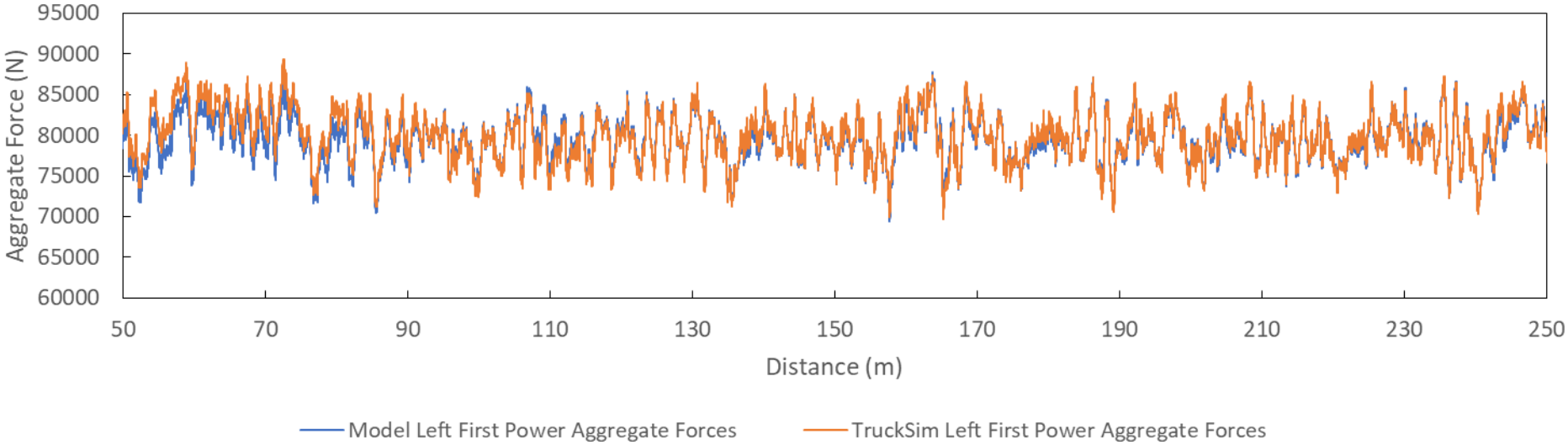

Figure D.13: Left side first power aggregate forces from TruckSim 2019.1® and the final model over 200 m test section at 5% crossfall, 2 m/km IRI, 80 km/h and no anti-roll bar

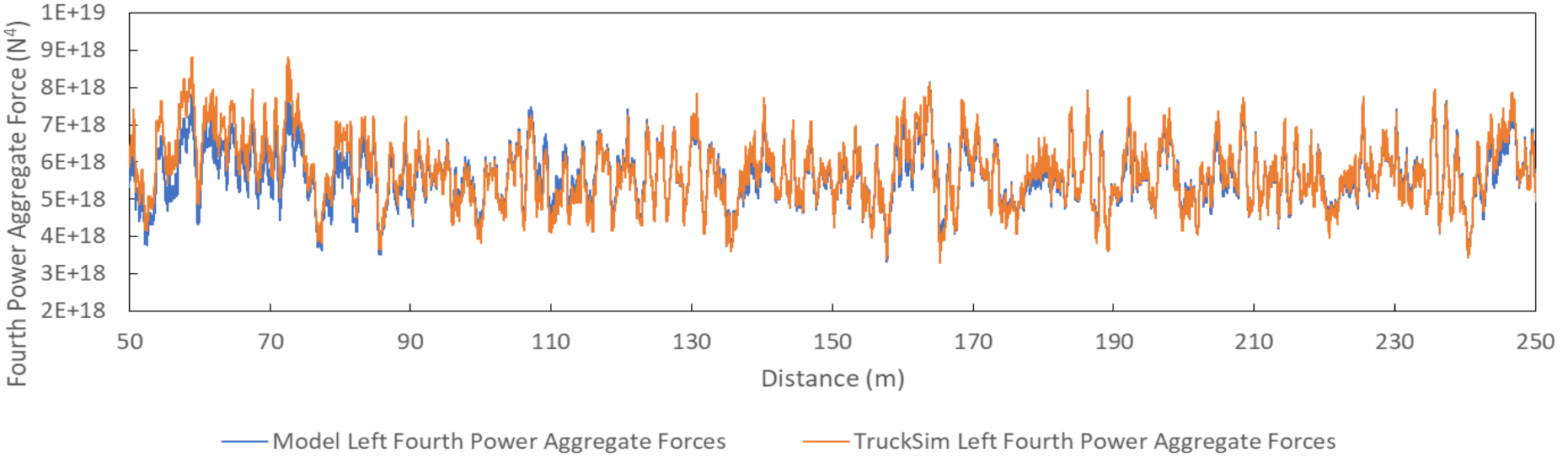

Figure D.14: Left side fourth power aggregate forces from TruckSim 2019.1® and the final model over 200 m test section at 5% crossfall, 2 m/km IRI, 80 km/h and no anti-roll bar

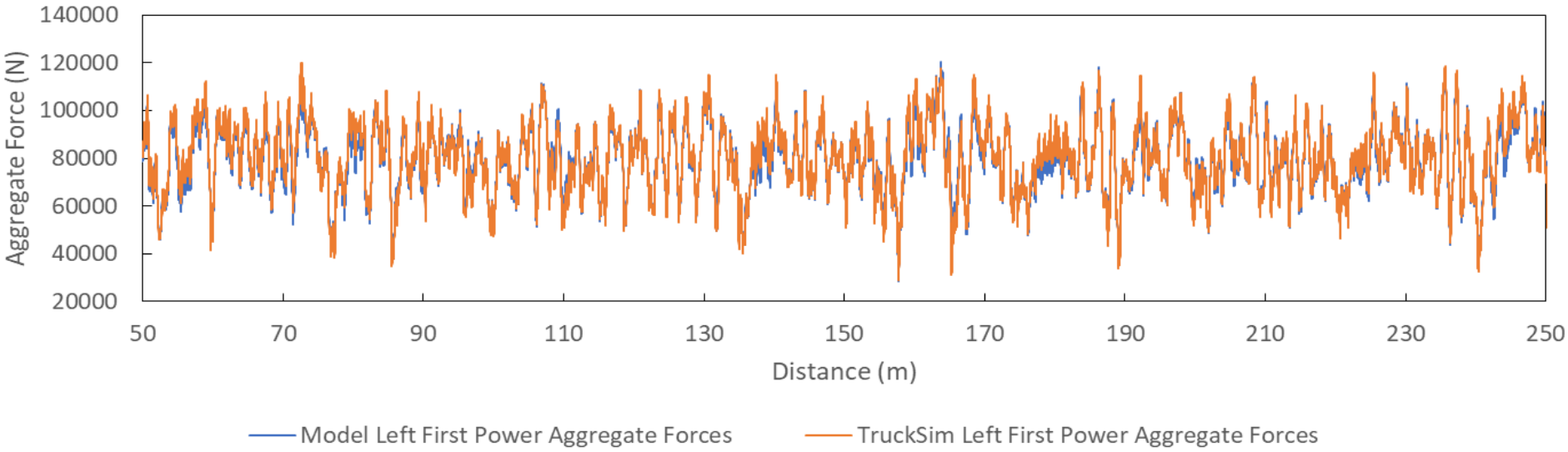

Figure D.15: Left side first power aggregate forces from TruckSim 2019.1® and the final model over 200 m test section at 5% crossfall, 2 m/km IRI, 80 km/h and with an anti-roll bar

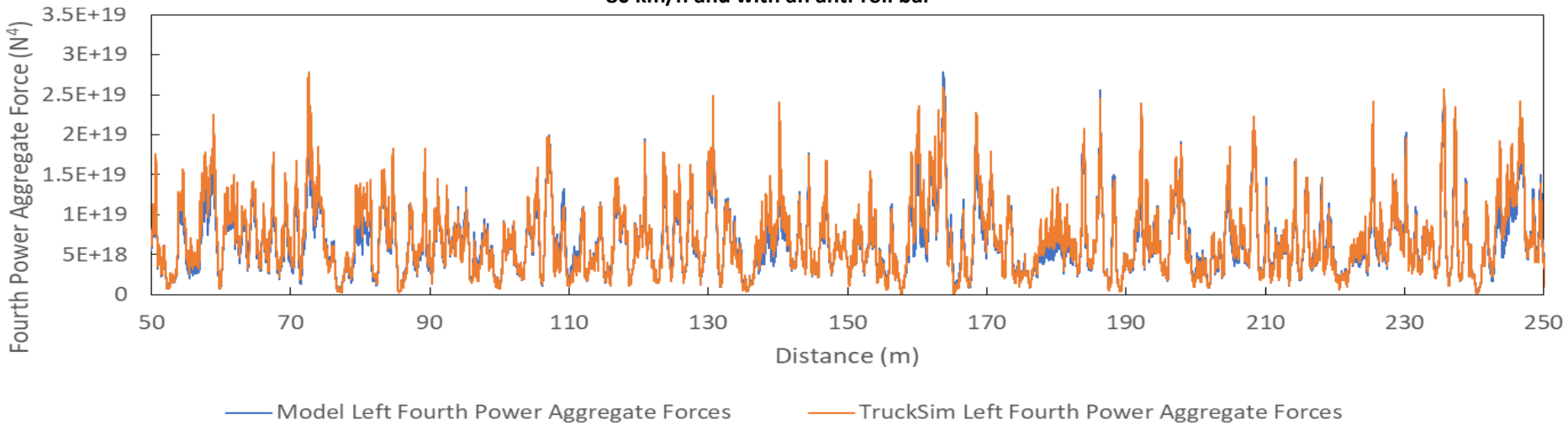

Figure D.16: Left side fourth power aggregate forces from TruckSim 2019.1® and the final model over 200 m test section at 5% crossfall, 2 m/km IRI, 80 km/h and with an anti-roll bar

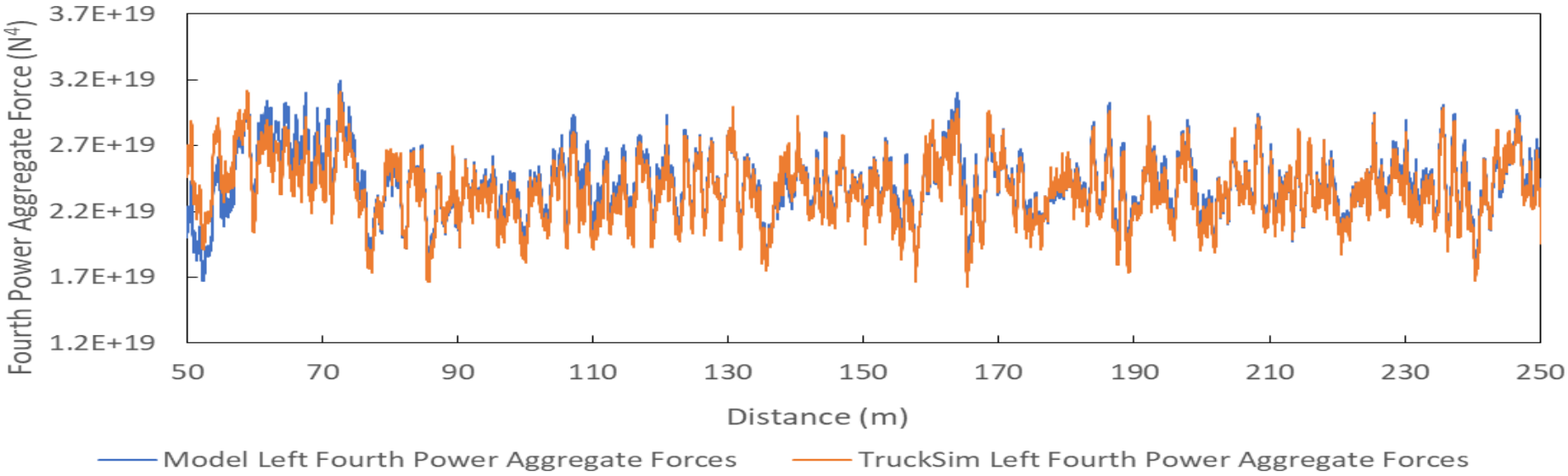

Figure D.17: Left side fourth power aggregate forces from TruckSim 2019.1® and the final model over 200 m test section at 5% crossfall, 2 m/km IRI, 80 km/h and with no anti-roll bar and an eccentric load of 300 mm to the left,

Appendix E: Additional results

This section contains additional results from Section 3. The results follow the same order as presented in Section 3 and contains the raw data and detailed comparisons of the different road damage criteria studied.

Table E.1: The average vertical tyre force of the front tyres of the base model under all operating conditions

		Front Left									Front Right								
	IRI (m/km) →	0.5	1	2	3	4	5	6	8	10	0.5	1	2	3	4	5	6	8	10
	Crossfall (%)	Vertical Tyre Force (N)																	
40 km/h	0	30 588	30 588	30 589	30 590	30 591	30 591	30 592	30 593	30 595	30 588	30 588	30 589	30 589	30 590	30 591	30 591	30 593	30 594
	1	31 319	31 319	31 320	31 321	31 322	31 323	31 324	31 327	31 330	29 857	29 857	29 858	29 858	29 859	29 859	29 860	29 860	29 860
	2	32 050	32 051	32 052	32 053	32 054	32 056	32 057	32 061	32 065	29 126	29 126	29 126	29 127	29 127	29 127	29 127	29 126	29 124
	3	32 783	32 783	32 784	32 786	32 787	32 789	32 791	32 796	32 802	28 393	28 394	28 394	28 394	28 394	28 394	28 393	28 391	28 388
	4	33 516	33 517	33 518	33 519	33 521	33 523	33 526	33 531	33 539	27 660	27 660	27 661	27 661	27 660	27 660	27 659	27 656	27 651
	5	34 250	34 251	34 252	34 254	34 256	34 258	34 261	34 268	34 277	26 926	26 926	26 927	26 926	26 926	26 925	26 923	26 919	26 913
60 km/h	0	30 587	30 587	30 587	30 587	30 587	30 587	30 588	30 589	30 587	30 586	30 585	30 584	30 583	30 581	30 580	30 576	30 572	30 589
	1	31 319	31 319	31 319	31 319	31 319	31 320	31 321	31 323	29 856	29 855	29 854	29 852	29 851	29 849	29 847	29 842	29 835	29 875
	2	32 051	32 051	32 051	32 051	32 052	32 053	32 055	32 059	29 123	29 123	29 121	29 120	29 118	29 116	29 113	29 106	29 098	29 160
	3	32 784	32 784	32 784	32 785	32 786	32 787	32 789	32 795	28 390	28 390	28 388	28 386	28 384	28 381	28 378	28 370	28 360	28 445
	4	33 518	33 518	33 518	33 519	33 521	33 522	33 525	33 532	27 657	27 656	27 654	27 652	27 650	27 646	27 643	27 633	27 622	27 729
	5	34 252	34 253	34 253	34 254	34 256	34 258	34 261	34 270	26 922	26 921	26 919	26 917	26 914	26 911	26 906	26 896	26 883	27 012
80 km/h	0	30 588	30 588	30 589	30 589	30 590	30 590	30 590	30 591	30 589	30 588	30 589	30 590	30 591	30 593	30 594	30 595	30 599	30 604
	1	31 319	31 319	31 320	31 320	31 321	31 322	31 323	31 324	31 324	29 857	29 857	29 859	29 860	29 861	29 862	29 863	29 865	29 869
	2	32 050	32 051	32 052	32 052	32 054	32 055	32 056	32 058	32 059	29 125	29 125	29 126	29 127	29 128	29 129	29 129	29 131	29 133
	3	32 783	32 783	32 784	32 785	32 787	32 788	32 790	32 793	32 795	28 392	28 392	28 393	28 394	28 395	28 395	28 395	28 395	28 397
	4	33 516	33 517	33 518	33 519	33 521	33 522	33 524	33 529	33 531	27 658	27 659	27 660	27 660	27 660	27 660	27 660	27 660	27 661
	5	34 250	34 251	34 252	34 254	34 255	34 257	34 260	34 265	34 268	26 924	26 924	26 925	26 925	26 925	26 925	26 925	26 923	26 924
100 km/h	0	30 588	30 589	30 591	30 592	30 593	30 594	30 594	30 592	30 583	30 588	30 589	30 592	30 595	30 598	30 602	30 606	30 616	30 633
	1	31 320	31 321	31 323	31 325	31 326	31 326	31 327	31 325	31 319	29 856	29 857	29 860	29 862	29 865	29 869	29 873	29 882	29 896
	2	32 053	32 054	32 056	32 058	32 059	32 060	32 060	32 060	32 054	29 123	29 124	29 127	29 129	29 132	29 135	29 139	29 148	29 162
	3	32 787	32 788	32 790	32 791	32 793	32 794	32 795	32 795	32 789	28 389	28 390	28 393	28 395	28 398	28 401	28 404	28 412	28 426
	4	33 521	33 522	33 524	33 526	33 527	33 529	33 530	33 530	33 525	27 655	27 656	27 658	27 660	27 663	27 666	27 669	27 677	27 690
	5	34 256	34 257	34 259	34 261	34 263	34 264	34 266	34 266	34 261	26 919	26 920	26 923	26 925	26 927	26 930	26 933	26 941	26 954
120 km/h	0	30 588	30 588	30 589	30 589	30 589	30 588	30 587	30 581	30 567	30 588	30 589	30 592	30 594	30 598	30 602	30 606	30 617	30 638
	1	31 322	31 323	31 323	31 324	31 323	31 323	31 321	31 316	31 302	29 853	29 854	29 857	29 859	29 863	29 866	29 871	29 882	29 902
	2	32 057	32 058	32 058	32 059	32 059	32 058	32 057	32 052	32 039	29 118	29 119	29 121	29 124	29 127	29 130	29 134	29 145	29 165
	3	32 793	32 793	32 794	32 795	32 795	32 794	32 793	32 788	32 775	28 381	28 382	28 385	28 387	28 390	28 394	28 398	28 408	28 427
	4	33 530	33 530	33 531	33 531	33 531	33 531	33 530	33 525	33 513	27 644	27 645	27 647	27 650	27 653	27 656	27 660	27 671	27 689
	5	34 267	34 268	34 268	34 269	34 269	34 269	34 267	34 262	34 249	26 906	26 907	26 909	26 912	26 914	26 918	26 922	26 933	26 952

Table E.2: The average vertical tyre force of the rear tyres of the base model under all operating conditions

		Rear Left									Rear Right								
	IRI (m/km) →	0.5	1	2	3	4	5	6	8	10	0.5	1	2	3	4	5	6	8	10
	Crossfall (%)	Vertical Tyre Force (N)																	
40 km/h	0	39 029	39 029	39 029	39 029	39 028	39 028	39 027	39 027	39 026	39 029	39 029	39 029	39 029	39 029	39 029	39 029	39 029	39 028
	1	40 284	40 284	40 284	40 284	40 284	40 284	40 284	40 285	40 287	37 774	37 774	37 774	37 773	37 773	37 772	37 772	37 770	37 768
	2	41 540	41 540	41 540	41 541	41 541	41 542	41 543	41 545	41 549	36 518	36 518	36 517	36 517	36 516	36 515	36 514	36 510	36 506
	3	42 798	42 798	42 798	42 799	42 799	42 801	42 802	42 806	42 813	35 261	35 261	35 260	35 259	35 258	35 256	35 254	35 249	35 242
	4	44 056	44 056	44 057	44 058	44 059	44 061	44 063	44 069	44 077	34 002	34 002	34 001	34 000	33 998	33 996	33 994	33 987	33 978
	5	45 316	45 316	45 317	45 318	45 319	45 322	45 325	45 332	45 343	32 743	32 743	32 741	32 740	32 738	32 735	32 732	32 724	32 712
60 km/h	0	39 030	39 030	39 032	39 033	39 035	39 036	39 038	39 042	39 048	39 029	39 029	39 028	39 027	39 026	39 025	39 024	39 021	39 017
	1	40 286	40 287	40 288	40 290	40 292	40 294	40 297	40 304	40 312	37 773	37 772	37 772	37 770	37 769	37 767	37 765	37 760	37 752
	2	41 543	41 544	41 546	41 548	41 551	41 554	41 557	41 566	41 577	36 515	36 515	36 514	36 512	36 510	36 508	36 505	36 497	36 487
	3	42 802	42 803	42 805	42 807	42 810	42 814	42 818	42 829	42 843	35 257	35 256	35 255	35 253	35 251	35 248	35 244	35 234	35 221
	4	44 062	44 063	44 065	44 068	44 071	44 076	44 081	44 094	44 110	33 997	33 996	33 995	33 993	33 990	33 986	33 981	33 970	33 954
	5	45 323	45 324	45 326	45 329	45 333	45 338	45 344	45 359	45 378	32 736	32 735	32 734	32 731	32 728	32 723	32 718	32 704	32 686
80 km/h	0	39 028	39 027	39 025	39 022	39 020	39 017	39 015	39 009	39 001	39 028	39 028	39 026	39 024	39 023	39 021	39 020	39 018	39 018
	1	40 284	40 283	40 280	40 278	40 276	40 274	40 273	40 269	40 263	37 773	37 772	37 770	37 768	37 766	37 764	37 762	37 758	37 756
	2	41 540	41 539	41 537	41 536	41 534	41 533	41 531	41 529	41 525	36 516	36 515	36 513	36 511	36 508	36 506	36 503	36 497	36 494
	3	42 798	42 797	42 796	42 794	42 793	42 792	42 791	42 790	42 788	35 257	35 256	35 254	35 252	35 249	35 246	35 243	35 236	35 230
	4	44 058	44 057	44 055	44 054	44 053	44 052	44 052	44 053	44 051	33 998	33 997	33 995	33 992	33 989	33 985	33 981	33 973	33 967
	5	45 318	45 317	45 315	45 314	45 314	45 314	45 314	45 316	45 315	32 737	32 736	32 734	32 731	32 727	32 723	32 719	32 710	32 702
100 km/h	0	39 031	39 032	39 034	39 036	39 037	39 038	39 037	39 035	39 025	39 031	39 033	39 037	39 041	39 046	39 052	39 058	39 073	39 095
	1	40 287	40 288	40 291	40 292	40 294	40 295	40 295	40 294	40 286	37 774	37 776	37 779	37 784	37 788	37 794	37 799	37 813	37 833
	2	41 544	41 546	41 548	41 550	41 552	41 553	41 554	41 554	41 546	36 516	36 517	36 521	36 525	36 530	36 534	36 540	36 553	36 572
	3	42 803	42 804	42 807	42 809	42 811	42 813	42 814	42 814	42 807	35 256	35 258	35 262	35 265	35 270	35 274	35 279	35 291	35 310
	4	44 063	44 064	44 067	44 069	44 071	44 073	44 075	44 075	44 070	33 996	33 997	34 001	34 005	34 009	34 013	34 018	34 029	34 047
	5	45 324	45 325	45 328	45 331	45 333	45 335	45 336	45 337	45 331	32 734	32 736	32 739	32 743	32 746	32 751	32 755	32 767	32 785
120 km/h	0	39 028	39 026	39 022	39 017	39 012	39 006	38 999	38 982	38 955	39 030	39 028	39 027	39 026	39 025	39 025	39 025	39 027	39 033
	1	40 288	40 286	40 282	40 278	40 272	40 267	40 260	40 244	40 217	37 789	37 767	37 766	37 764	37 764	37 763	37 764	37 765	37 770
	2	41 549	41 547	41 544	41 539	41 534	41 528	41 522	41 506	41 480	36 547	36 504	36 503	36 502	36 501	36 500	36 501	36 502	36 507
	3	42 812	42 810	42 806	42 802	42 797	42 791	42 785	42 769	42 743	35 303	35 241	35 240	35 238	35 237	35 237	35 237	35 237	35 243
	4	44 075	44 074	44 070	44 066	44 061	44 055	44 049	44 033	44 007	34 059	33 976	33 975	33 973	33 972	33 972	33 972	33 972	33 978
	5	45 340	45 339	45 335	45 331	45 326	45 320	45 314	45 297	45 271	32 813	32 710	32 709	32 707	32 706	32 705	32 705	32 706	32 712

Table E.3: The percentage difference in the average vertical tyre forces between the left and right side of the front and rear axles of the base model under all operating conditions

		Front									Rear								
	IRI (m/km) →	0.5	1	2	3	4	5	6	8	10	0.5	1	2	3	4	5	6	8	10
	Crossfall (%)	Percentage Difference Between Left and Right Forces (%)																	
40 km/h	0	0.00	0.00	0.00	0.00	0.00	0.00	0.00	0.00	0.00	0.00	0.00	0.00	0.00	0.00	0.00	0.00	-0.01	-0.01
	1	4.78	4.78	4.78	4.78	4.78	4.79	4.79	4.79	4.81	6.43	6.43	6.43	6.43	6.43	6.44	6.44	6.44	6.46
	2	9.56	9.56	9.56	9.57	9.57	9.57	9.58	9.59	9.61	12.87	12.87	12.87	12.87	12.88	12.88	12.89	12.90	12.92
	3	14.35	14.35	14.35	14.36	14.36	14.37	14.38	14.40	14.43	19.31	19.31	19.31	19.32	19.32	19.33	19.34	19.36	19.40
	4	19.14	19.14	19.15	19.15	19.16	19.17	19.18	19.21	19.25	25.76	25.76	25.76	25.77	25.78	25.79	25.80	25.83	25.88
	5	23.94	23.94	23.95	23.95	23.96	23.97	23.99	24.02	24.07	32.21	32.22	32.22	32.23	32.24	32.25	32.27	32.31	32.37
60 km/h	0	0.00	0.01	0.01	0.01	0.02	0.02	0.04	0.06	-0.01	0.00	0.00	0.01	0.01	0.02	0.03	0.04	0.06	0.08
	1	4.79	4.79	4.79	4.80	4.81	4.82	4.84	4.87	-0.06	6.44	6.44	6.45	6.46	6.46	6.47	6.49	6.52	6.56
	2	9.57	9.58	9.58	9.59	9.60	9.61	9.64	9.68	-0.13	12.88	12.89	12.89	12.90	12.91	12.93	12.94	12.99	13.04
	3	14.37	14.37	14.38	14.39	14.40	14.42	14.45	14.50	-0.19	19.33	19.34	19.34	19.35	19.37	19.39	19.41	19.46	19.53
	4	19.16	19.17	19.18	19.19	19.21	19.23	19.27	19.33	-0.26	25.79	25.79	25.80	25.81	25.83	25.85	25.88	25.94	26.02
	5	23.97	23.98	23.99	24.00	24.02	24.04	24.09	24.16	-0.34	32.25	32.25	32.26	32.28	32.30	32.32	32.35	32.42	32.52
80 km/h	0	0.00	0.00	0.00	-0.01	-0.01	-0.01	-0.02	-0.03	-0.05	0.00	0.00	0.00	-0.01	-0.01	-0.01	-0.01	-0.02	-0.04
	1	4.78	4.78	4.78	4.78	4.77	4.77	4.77	4.77	4.76	6.43	6.43	6.43	6.43	6.43	6.43	6.43	6.43	6.43
	2	9.56	9.56	9.56	9.56	9.56	9.56	9.57	9.57	9.56	12.88	12.87	12.88	12.88	12.88	12.88	12.89	12.90	12.90
	3	14.36	14.35	14.35	14.36	14.36	14.36	14.37	14.37	14.37	19.32	19.32	19.32	19.33	19.33	19.34	19.35	19.36	19.37
	4	19.15	19.15	19.15	19.15	19.16	19.16	19.17	19.18	19.19	25.78	25.78	25.78	25.78	25.79	25.80	25.81	25.84	25.85
	5	23.95	23.95	23.95	23.96	23.96	23.97	23.98	24.00	24.01	32.24	32.24	32.24	32.25	32.26	32.27	32.28	32.31	32.33
100 km/h	0	0.00	0.00	0.00	-0.01	-0.02	-0.03	-0.04	-0.08	-0.16	0.00	0.00	-0.01	-0.01	-0.02	-0.04	-0.05	-0.10	-0.18
	1	4.79	4.79	4.78	4.78	4.77	4.76	4.75	4.72	4.65	6.44	6.44	6.43	6.43	6.42	6.41	6.39	6.35	6.28
	2	9.58	9.58	9.58	9.57	9.57	9.56	9.55	9.52	9.45	12.88	12.88	12.88	12.87	12.86	12.85	12.84	12.81	12.74
	3	14.38	14.38	14.37	14.37	14.36	14.36	14.35	14.32	14.25	19.34	19.33	19.33	19.32	19.32	19.31	19.30	19.26	19.19
	4	19.18	19.18	19.18	19.17	19.17	19.16	19.15	19.13	19.07	25.79	25.79	25.79	25.78	25.78	25.77	25.76	25.72	25.66
	5	23.99	23.99	23.98	23.98	23.98	23.97	23.96	23.94	23.87	32.26	32.26	32.25	32.25	32.24	32.23	32.22	32.19	32.12
120 km/h	0	0.00	0.00	-0.01	-0.02	-0.03	-0.04	-0.06	-0.12	-0.23	-0.01	-0.01	-0.01	-0.02	-0.03	-0.05	-0.07	-0.11	-0.20
	1	4.80	4.80	4.79	4.79	4.77	4.76	4.74	4.69	4.58	6.40	6.45	6.45	6.44	6.43	6.42	6.40	6.36	6.27
	2	9.61	9.61	9.60	9.59	9.58	9.57	9.55	9.50	9.39	12.81	12.92	12.92	12.91	12.90	12.89	12.87	12.83	12.75
	3	14.42	14.42	14.42	14.41	14.40	14.38	14.37	14.31	14.21	19.22	19.40	19.39	19.38	19.38	19.36	19.35	19.31	19.24
	4	19.24	19.24	19.23	19.23	19.22	19.20	19.19	19.13	19.03	25.64	25.88	25.87	25.86	25.86	25.85	25.83	25.79	25.72
	5	24.07	24.06	24.06	24.05	24.04	24.03	24.01	23.95	23.85	32.06	32.36	32.36	32.35	32.34	32.33	32.32	32.28	32.21

Table E.4: The DLC of the front left and right tyres of the base model under all operating conditions

		Front Left									Front Right								
	IRI (m/km) →	0.5	1	2	3	4	5	6	8	10	0.5	1	2	3	4	5	6	8	10
	Crossfall (%)	Dynamic Load Coefficient																	
40 km/h	0	0.011	0.023	0.045	0.068	0.090	0.113	0.135	0.180	0.225	0.011	0.023	0.045	0.068	0.090	0.113	0.136	0.181	0.226
	1	0.011	0.022	0.044	0.066	0.088	0.110	0.132	0.175	0.219	0.012	0.023	0.046	0.069	0.092	0.116	0.139	0.185	0.231
	2	0.011	0.021	0.043	0.064	0.086	0.107	0.128	0.171	0.214	0.012	0.024	0.047	0.071	0.095	0.118	0.142	0.189	0.237
	3	0.011	0.021	0.042	0.063	0.084	0.104	0.125	0.167	0.209	0.012	0.024	0.048	0.073	0.097	0.121	0.145	0.194	0.242
	4	0.010	0.020	0.041	0.061	0.082	0.102	0.122	0.163	0.204	0.013	0.025	0.050	0.074	0.099	0.124	0.149	0.199	0.248
	5	0.010	0.020	0.040	0.060	0.080	0.100	0.119	0.159	0.199	0.013	0.026	0.051	0.076	0.102	0.127	0.153	0.204	0.255
60 km/h	0	0.013	0.026	0.052	0.078	0.104	0.130	0.156	0.208	0.260	0.013	0.026	0.052	0.078	0.105	0.131	0.157	0.209	0.262
	1	0.013	0.025	0.051	0.076	0.101	0.127	0.152	0.202	0.253	0.013	0.027	0.053	0.080	0.107	0.134	0.160	0.214	0.267
	2	0.012	0.025	0.049	0.074	0.099	0.123	0.148	0.197	0.247	0.014	0.027	0.055	0.082	0.109	0.137	0.164	0.219	0.273
	3	0.012	0.024	0.048	0.072	0.096	0.120	0.144	0.192	0.241	0.014	0.028	0.056	0.084	0.112	0.140	0.168	0.224	0.280
	4	0.012	0.024	0.047	0.070	0.094	0.117	0.141	0.188	0.235	0.015	0.029	0.057	0.086	0.114	0.143	0.172	0.229	0.286
	5	0.012	0.023	0.046	0.069	0.092	0.115	0.137	0.183	0.229	0.015	0.030	0.059	0.088	0.117	0.147	0.176	0.235	0.293
80 km/h	0	0.014	0.029	0.057	0.086	0.114	0.143	0.171	0.229	0.286	0.014	0.029	0.057	0.086	0.114	0.143	0.171	0.228	0.285
	1	0.014	0.028	0.056	0.084	0.111	0.139	0.167	0.223	0.279	0.015	0.029	0.058	0.088	0.117	0.146	0.175	0.233	0.292
	2	0.014	0.027	0.054	0.082	0.109	0.136	0.163	0.217	0.272	0.015	0.030	0.060	0.090	0.119	0.149	0.179	0.239	0.298
	3	0.013	0.027	0.053	0.080	0.106	0.133	0.159	0.212	0.265	0.015	0.031	0.061	0.092	0.122	0.153	0.183	0.245	0.306
	4	0.013	0.026	0.052	0.078	0.104	0.129	0.155	0.207	0.259	0.016	0.032	0.063	0.094	0.125	0.157	0.188	0.251	0.313
	5	0.013	0.026	0.051	0.076	0.101	0.127	0.152	0.202	0.253	0.016	0.032	0.064	0.096	0.129	0.161	0.193	0.257	0.321
100 km/h	0	0.016	0.031	0.063	0.094	0.126	0.157	0.189	0.252	0.316	0.015	0.031	0.061	0.092	0.122	0.153	0.184	0.245	0.306
	1	0.015	0.031	0.061	0.092	0.123	0.153	0.184	0.246	0.308	0.016	0.031	0.063	0.094	0.125	0.156	0.188	0.250	0.312
	2	0.015	0.030	0.060	0.090	0.120	0.150	0.180	0.240	0.300	0.016	0.032	0.064	0.096	0.128	0.160	0.192	0.256	0.320
	3	0.015	0.030	0.059	0.088	0.117	0.146	0.175	0.234	0.293	0.017	0.033	0.066	0.098	0.131	0.164	0.197	0.262	0.327
	4	0.015	0.029	0.057	0.086	0.114	0.143	0.171	0.228	0.286	0.018	0.034	0.068	0.101	0.134	0.168	0.201	0.268	0.335
	5	0.015	0.029	0.056	0.084	0.112	0.139	0.167	0.223	0.279	0.019	0.035	0.069	0.104	0.138	0.172	0.207	0.275	0.344
120 km/h	0	0.017	0.034	0.068	0.101	0.135	0.169	0.203	0.271	0.339	0.016	0.033	0.065	0.098	0.130	0.163	0.196	0.261	0.326
	1	0.017	0.033	0.066	0.099	0.132	0.165	0.198	0.264	0.331	0.017	0.033	0.067	0.100	0.133	0.167	0.200	0.267	0.334
	2	0.017	0.033	0.065	0.097	0.129	0.161	0.193	0.258	0.323	0.018	0.035	0.069	0.103	0.137	0.171	0.205	0.273	0.341
	3	0.017	0.032	0.063	0.095	0.126	0.157	0.189	0.252	0.315	0.019	0.036	0.070	0.105	0.140	0.175	0.210	0.280	0.349
	4	0.018	0.032	0.062	0.093	0.123	0.154	0.185	0.246	0.308	0.021	0.038	0.073	0.108	0.144	0.180	0.215	0.287	0.358
	5	0.019	0.032	0.061	0.091	0.121	0.151	0.181	0.241	0.301	0.023	0.039	0.075	0.111	0.148	0.185	0.221	0.295	0.367

Table E.5: The DLC of the rear left and right tyres of the base model under all operating conditions

		Rear Left									Rear Right								
	IRI (m/km) ⟶	0.5	1	2	3	4	5	6	8	10	0.5	1	2	3	4	5	6	8	10
	Crossfall (%)	Dynamic Load Coefficient																	
40 km/h	0	0.007	0.014	0.028	0.043	0.057	0.071	0.085	0.114	0.142	0.007	0.014	0.028	0.042	0.056	0.070	0.084	0.113	0.141
	1	0.007	0.014	0.027	0.041	0.055	0.069	0.082	0.110	0.137	0.007	0.014	0.029	0.043	0.058	0.073	0.087	0.116	0.145
	2	0.007	0.013	0.027	0.040	0.053	0.066	0.080	0.106	0.133	0.008	0.015	0.030	0.045	0.060	0.075	0.090	0.120	0.150
	3	0.007	0.013	0.026	0.039	0.052	0.064	0.077	0.103	0.129	0.008	0.015	0.031	0.046	0.062	0.077	0.093	0.124	0.155
	4	0.006	0.013	0.025	0.037	0.050	0.062	0.075	0.100	0.125	0.008	0.016	0.032	0.048	0.064	0.080	0.096	0.128	0.160
	5	0.006	0.012	0.024	0.036	0.048	0.061	0.073	0.097	0.121	0.008	0.017	0.033	0.050	0.066	0.083	0.100	0.133	0.166
60 km/h	0	0.009	0.017	0.035	0.052	0.070	0.087	0.105	0.140	0.174	0.009	0.018	0.035	0.052	0.070	0.087	0.105	0.140	0.175
	1	0.009	0.017	0.034	0.051	0.067	0.084	0.101	0.135	0.169	0.009	0.018	0.036	0.054	0.072	0.090	0.108	0.144	0.181
	2	0.008	0.016	0.033	0.049	0.065	0.082	0.098	0.131	0.163	0.010	0.019	0.037	0.056	0.075	0.093	0.112	0.149	0.186
	3	0.008	0.016	0.032	0.048	0.063	0.079	0.095	0.126	0.158	0.010	0.020	0.039	0.058	0.077	0.096	0.116	0.154	0.193
	4	0.009	0.016	0.031	0.046	0.061	0.077	0.092	0.123	0.153	0.011	0.020	0.040	0.060	0.080	0.100	0.120	0.160	0.200
	5	0.009	0.016	0.030	0.045	0.060	0.075	0.089	0.119	0.149	0.012	0.021	0.042	0.062	0.083	0.103	0.124	0.165	0.207
80 km/h	0	0.010	0.021	0.042	0.063	0.084	0.104	0.125	0.167	0.210	0.010	0.021	0.041	0.062	0.083	0.104	0.124	0.166	0.208
	1	0.010	0.020	0.040	0.061	0.081	0.101	0.121	0.162	0.203	0.011	0.021	0.043	0.064	0.086	0.107	0.128	0.171	0.214
	2	0.010	0.020	0.039	0.059	0.078	0.098	0.117	0.157	0.196	0.011	0.022	0.044	0.066	0.088	0.110	0.133	0.177	0.221
	3	0.010	0.019	0.038	0.057	0.076	0.095	0.114	0.152	0.190	0.012	0.023	0.046	0.069	0.091	0.114	0.137	0.183	0.229
	4	0.010	0.019	0.037	0.055	0.074	0.092	0.110	0.147	0.184	0.012	0.024	0.047	0.071	0.095	0.118	0.142	0.189	0.237
	5	0.010	0.018	0.036	0.054	0.071	0.089	0.107	0.143	0.179	0.013	0.025	0.049	0.074	0.098	0.123	0.147	0.197	0.246
100 km/h	0	0.012	0.024	0.048	0.072	0.096	0.120	0.144	0.192	0.240	0.012	0.024	0.047	0.071	0.094	0.118	0.142	0.189	0.236
	1	0.012	0.023	0.046	0.070	0.093	0.116	0.139	0.185	0.232	0.012	0.024	0.049	0.073	0.097	0.122	0.146	0.195	0.244
	2	0.012	0.023	0.045	0.067	0.090	0.112	0.135	0.180	0.225	0.013	0.026	0.051	0.076	0.101	0.126	0.151	0.201	0.252
	3	0.012	0.022	0.044	0.066	0.087	0.109	0.131	0.174	0.218	0.014	0.027	0.053	0.078	0.104	0.130	0.156	0.208	0.260
	4	0.012	0.022	0.043	0.064	0.085	0.106	0.127	0.169	0.211	0.016	0.028	0.055	0.081	0.108	0.135	0.162	0.216	0.270
	5	0.012	0.022	0.042	0.062	0.082	0.103	0.123	0.164	0.205	0.017	0.030	0.057	0.085	0.113	0.141	0.168	0.224	0.280
120 km/h	0	0.013	0.026	0.052	0.079	0.105	0.131	0.158	0.210	0.263	0.013	0.026	0.052	0.078	0.104	0.130	0.156	0.208	0.260
	1	0.013	0.026	0.051	0.076	0.102	0.127	0.153	0.204	0.255	0.014	0.027	0.054	0.081	0.107	0.134	0.161	0.215	0.268
	2	0.014	0.026	0.050	0.074	0.099	0.123	0.148	0.197	0.247	0.016	0.029	0.056	0.083	0.111	0.139	0.166	0.222	0.277
	3	0.015	0.026	0.049	0.072	0.096	0.120	0.144	0.191	0.239	0.018	0.031	0.059	0.087	0.115	0.144	0.172	0.230	0.287
	4	0.017	0.026	0.048	0.071	0.094	0.117	0.140	0.186	0.232	0.022	0.034	0.062	0.091	0.120	0.149	0.179	0.238	0.298
	5	0.018	0.027	0.048	0.069	0.091	0.114	0.136	0.181	0.226	0.026	0.037	0.065	0.095	0.125	0.156	0.186	0.248	0.309

Table E.6: The percentage difference in left and right DLC of the base model under all operating conditions

		Front									Rear								
	IRI (m/km) ⟶	0.5	1	2	3	4	5	6	8	10	0.5	1	2	3	4	5	6	8	10
	Crossfall (%)	Percentage Difference Between Left and Right (%)																	
40 km/h	0	-0.33	-0.34	-0.36	-0.38	-0.39	-0.40	-0.41	-0.42	-0.42	0.98	0.98	0.97	0.97	0.96	0.96	0.95	0.94	0.94
	1	-5.11	-5.14	-5.16	-5.18	-5.20	-5.21	-5.22	-5.24	-5.25	-5.37	-5.41	-5.43	-5.44	-5.45	-5.46	-5.47	-5.48	-5.50
	2	-9.89	-9.93	-9.97	-9.99	-10.01	-10.02	-10.03	-10.06	-10.08	-11.70	-11.80	-11.84	-11.86	-11.87	-11.88	-11.90	-11.92	-11.96
	3	-14.68	-14.73	-14.77	-14.80	-14.82	-14.84	-14.85	-14.88	-14.91	-18.02	-18.19	-18.26	-18.28	-18.30	-18.32	-18.34	-18.37	-18.42
	4	-19.46	-19.53	-19.58	-19.61	-19.63	-19.65	-19.67	-19.71	-19.75	-24.32	-24.59	-24.69	-24.72	-24.75	-24.77	-24.79	-24.84	-24.90
	5	-24.26	-24.34	-24.39	-24.42	-24.45	-24.47	-24.49	-24.54	-24.59	-30.61	-30.99	-31.13	-31.17	-31.20	-31.23	-31.25	-31.31	-31.38
60 km/h	0	-0.74	-0.74	-0.74	-0.73	-0.72	-0.72	-0.70	-0.68	-0.64	-0.31	-0.31	-0.31	-0.31	-0.31	-0.31	-0.31	-0.31	-0.31
	1	-5.37	-5.44	-5.47	-5.48	-5.48	-5.48	-5.48	-5.46	-5.44	-6.35	-6.57	-6.68	-6.72	-6.74	-6.75	-6.76	-6.78	-6.81
	2	-9.97	-10.14	-10.21	-10.23	-10.24	-10.25	-10.25	-10.26	-10.24	-12.36	-12.82	-13.04	-13.12	-13.16	-13.19	-13.21	-13.26	-13.30
	3	-14.55	-14.84	-14.96	-15.00	-15.01	-15.03	-15.04	-15.05	-15.05	-18.38	-19.06	-19.41	-19.52	-19.59	-19.63	-19.67	-19.73	-19.79
	4	-19.11	-19.54	-19.71	-19.76	-19.79	-19.81	-19.83	-19.86	-19.86	-24.44	-25.31	-25.77	-25.93	-26.02	-26.07	-26.12	-26.21	-26.29
	5	-23.66	-24.23	-24.46	-24.54	-24.57	-24.60	-24.62	-24.67	-24.67	-30.56	-31.56	-32.14	-32.34	-32.45	-32.52	-32.58	-32.68	-32.78
80 km/h	0	0.04	0.04	0.06	0.07	0.08	0.10	0.11	0.15	0.19	0.72	0.73	0.75	0.77	0.79	0.81	0.83	0.89	0.96
	1	-4.68	-4.70	-4.70	-4.69	-4.68	-4.66	-4.65	-4.61	-4.56	-5.56	-5.64	-5.68	-5.67	-5.66	-5.65	-5.64	-5.60	-5.54
	2	-9.34	-9.44	-9.46	-9.45	-9.44	-9.43	-9.41	-9.38	-9.32	-11.83	-12.02	-12.11	-12.12	-12.12	-12.12	-12.11	-12.08	-12.04
	3	-13.97	-14.18	-14.22	-14.22	-14.22	-14.20	-14.19	-14.17	-14.09	-18.12	-18.41	-18.54	-18.58	-18.59	-18.59	-18.59	-18.57	-18.54
	4	-18.55	-18.90	-18.99	-19.00	-19.00	-18.99	-18.98	-18.96	-18.87	-24.41	-24.79	-24.98	-25.03	-25.05	-25.07	-25.07	-25.07	-25.04
	5	-23.09	-23.63	-23.77	-23.79	-23.79	-23.79	-23.78	-23.76	-23.65	-30.71	-31.19	-31.42	-31.49	-31.53	-31.54	-31.56	-31.56	-31.55
100 km/h	0	2.67	2.68	2.72	2.76	2.80	2.86	2.92	3.07	3.27	1.36	1.37	1.38	1.40	1.42	1.44	1.46	1.52	1.60
	1	-1.99	-2.03	-2.03	-1.99	-1.95	-1.90	-1.84	-1.70	-1.50	-5.06	-5.04	-5.04	-5.03	-5.02	-5.00	-4.98	-4.93	-4.85
	2	-6.66	-6.76	-6.78	-6.76	-6.72	-6.68	-6.62	-6.49	-6.28	-11.70	-11.52	-11.49	-11.48	-11.47	-11.46	-11.44	-11.39	-11.32
	3	-11.34	-11.50	-11.56	-11.54	-11.51	-11.47	-11.42	-11.28	-11.07	-18.49	-18.06	-17.97	-17.95	-17.94	-17.92	-17.91	-17.87	-17.79
	4	-16.04	-16.26	-16.34	-16.34	-16.31	-16.27	-16.22	-16.10	-15.88	-25.37	-24.65	-24.46	-24.43	-24.42	-24.40	-24.39	-24.35	-24.28
	5	-20.75	-21.03	-21.14	-21.15	-21.13	-21.09	-21.04	-20.92	-20.68	-32.29	-31.28	-30.98	-30.93	-30.91	-30.89	-30.88	-30.84	-30.77
120 km/h	0	3.48	3.49	3.52	3.55	3.58	3.62	3.66	3.77	3.89	0.95	0.95	0.97	0.99	1.01	1.03	1.06	1.14	1.26
	1	-0.81	-1.03	-1.13	-1.14	-1.13	-1.10	-1.07	-0.98	-0.81	-5.11	-5.22	-5.33	-5.37	-5.37	-5.37	-5.35	-5.29	-5.19
	2	-5.21	-5.59	-5.80	-5.85	-5.86	-5.85	-5.82	-5.74	-5.53	-11.80	-11.58	-11.68	-11.75	-11.77	-11.78	-11.78	-11.74	-11.65
	3	-9.76	-10.20	-10.49	-10.58	-10.61	-10.61	-10.59	-10.52	-10.26	-18.82	-18.11	-18.09	-18.16	-18.19	-18.21	-18.22	-18.19	-18.10
	4	-14.45	-14.85	-15.21	-15.33	-15.38	-15.39	-15.39	-15.32	-14.99	-25.90	-24.77	-24.55	-24.59	-24.63	-24.66	-24.67	-24.65	-24.57
	5	-19.24	-19.55	-19.95	-20.11	-20.17	-20.19	-20.20	-20.14	-19.73	-32.92	-31.51	-31.06	-31.06	-31.10	-31.12	-31.13	-31.12	-31.03

Table E.7: The normalized (by the static values) average first power aggregate forces of the base model under all operating conditions

		Left									Right								
	IRI (m/km) →	0.5	1	2	3	4	5	6	8	10	0.5	1	2	3	4	5	6	8	10
	Crossfall (%)	Average Aggregate First Power Force (N)/Static Aggregate First Power Force (N)																	
40 km/h	0	1.000	1.000	1.000	1.000	1.000	1.000	1.000	1.000	1.000	1.000	1.000	1.000	1.000	1.000	1.000	1.000	1.000	1.000
	1	1.029	1.029	1.029	1.029	1.029	1.029	1.029	1.029	1.029	0.971	0.971	0.971	0.971	0.971	0.971	0.971	0.971	0.971
	2	1.057	1.057	1.057	1.057	1.057	1.057	1.057	1.057	1.057	0.943	0.943	0.943	0.943	0.943	0.943	0.943	0.943	0.943
	3	1.086	1.086	1.086	1.086	1.086	1.086	1.086	1.086	1.086	0.914	0.914	0.914	0.914	0.914	0.914	0.914	0.914	0.914
	4	1.114	1.114	1.114	1.114	1.114	1.114	1.115	1.115	1.115	0.886	0.886	0.886	0.886	0.886	0.886	0.886	0.885	0.885
	5	1.143	1.143	1.143	1.143	1.143	1.143	1.143	1.143	1.144	0.857	0.857	0.857	0.857	0.857	0.857	0.857	0.857	0.856
60 km/h	0	1.000	1.000	1.000	1.000	1.000	1.000	1.000	1.000	1.000	1.000	1.000	1.000	1.000	1.000	1.000	1.000	1.000	1.000
	1	1.029	1.029	1.029	1.029	1.029	1.029	1.029	1.029	1.029	0.971	0.971	0.971	0.971	0.971	0.971	0.971	0.971	0.971
	2	1.057	1.057	1.057	1.057	1.057	1.057	1.057	1.058	1.058	0.943	0.943	0.943	0.943	0.943	0.943	0.943	0.942	0.942
	3	1.086	1.086	1.086	1.086	1.086	1.086	1.086	1.086	1.087	0.914	0.914	0.914	0.914	0.914	0.914	0.914	0.914	0.913
	4	1.114	1.114	1.114	1.114	1.115	1.115	1.115	1.115	1.115	0.886	0.886	0.886	0.885	0.885	0.885	0.885	0.885	0.884
	5	1.143	1.143	1.143	1.143	1.143	1.143	1.143	1.144	1.144	0.857	0.857	0.857	0.857	0.857	0.857	0.856	0.856	0.856
80 km/h	0	1.000	1.000	1.000	1.000	1.000	1.000	1.000	1.000	1.000	1.000	1.000	1.000	1.000	1.000	1.000	1.000	1.000	1.000
	1	1.029	1.029	1.028	1.028	1.028	1.028	1.028	1.028	1.028	0.971	0.971	0.971	0.971	0.971	0.971	0.971	0.971	0.971
	2	1.057	1.057	1.057	1.057	1.057	1.057	1.057	1.057	1.057	0.943	0.943	0.943	0.943	0.943	0.943	0.943	0.943	0.943
	3	1.086	1.086	1.086	1.086	1.086	1.086	1.086	1.086	1.086	0.914	0.914	0.914	0.914	0.914	0.914	0.914	0.914	0.914
	4	1.114	1.114	1.114	1.114	1.114	1.114	1.114	1.114	1.114	0.886	0.886	0.886	0.886	0.886	0.885	0.885	0.885	0.885
	5	1.143	1.143	1.143	1.143	1.143	1.143	1.143	1.143	1.143	0.857	0.857	0.857	0.857	0.857	0.857	0.857	0.857	0.856
100 km/h	0	1.000	1.000	1.000	1.000	1.000	1.000	1.000	1.000	1.000	1.000	1.000	1.000	1.000	1.000	1.001	1.001	1.001	1.002
	1	1.029	1.029	1.029	1.029	1.029	1.029	1.029	1.029	1.029	0.971	0.971	0.972	0.972	0.972	0.972	0.972	0.972	0.973
	2	1.057	1.057	1.057	1.057	1.057	1.057	1.057	1.057	1.057	0.943	0.943	0.943	0.943	0.943	0.943	0.943	0.944	0.944
	3	1.086	1.086	1.086	1.086	1.086	1.086	1.086	1.086	1.086	0.914	0.914	0.914	0.914	0.915	0.915	0.915	0.915	0.916
	4	1.114	1.114	1.115	1.115	1.115	1.115	1.115	1.115	1.115	0.886	0.886	0.886	0.886	0.886	0.886	0.886	0.886	0.887
	5	1.143	1.143	1.143	1.143	1.143	1.143	1.143	1.143	1.143	0.857	0.857	0.857	0.857	0.857	0.857	0.857	0.858	0.858
120 km/h	0	1.000	1.000	1.000	1.000	1.000	1.000	1.000	0.999	0.999	1.000	1.000	1.000	1.000	1.000	1.000	1.000	1.000	1.001
	1	1.029	1.029	1.029	1.028	1.028	1.028	1.028	1.028	1.027	0.971	0.971	0.971	0.971	0.971	0.971	0.972	0.972	0.972
	2	1.057	1.057	1.057	1.057	1.057	1.057	1.057	1.057	1.056	0.943	0.943	0.943	0.943	0.943	0.943	0.943	0.943	0.944
	3	1.086	1.086	1.086	1.086	1.086	1.086	1.086	1.085	1.085	0.914	0.914	0.914	0.914	0.914	0.914	0.914	0.914	0.915
	4	1.115	1.115	1.115	1.115	1.115	1.114	1.114	1.114	1.114	0.885	0.885	0.885	0.885	0.885	0.885	0.885	0.886	0.886
	5	1.144	1.143	1.143	1.143	1.143	1.143	1.143	1.143	1.142	0.856	0.856	0.856	0.856	0.856	0.856	0.857	0.857	0.857

Table E.8: The percentage difference in left and right average first power aggregate forces of the base model under all operating conditions

	IRI (m/km) →	0.5	1	2	3	4	5	6	8	10
	Crossfall (%)	Percentage Difference Between Left and Right (%)								
40 km/h	0	0.00	0.00	0.00	0.00	0.00	0.00	0.00	0.00	0.00
	1	5.70	5.71	5.71	5.71	5.71	5.71	5.71	5.72	5.73
	2	11.41	11.42	11.42	11.42	11.42	11.43	11.43	11.45	11.47
	3	17.13	17.13	17.13	17.14	17.14	17.15	17.16	17.18	17.21
	4	22.85	22.85	22.86	22.86	22.87	22.88	22.89	22.92	22.96
	5	28.58	28.58	28.59	28.59	28.60	28.61	28.63	28.67	28.72
60 km/h	0	0.00	0.00	0.01	0.01	0.02	0.02	0.03	0.05	0.07
	1	5.71	5.71	5.72	5.73	5.73	5.74	5.75	5.78	5.82
	2	11.43	11.43	11.44	11.44	11.45	11.47	11.48	11.52	11.57
	3	17.15	17.15	17.16	17.17	17.18	17.20	17.22	17.27	17.33
	4	22.88	22.88	22.89	22.90	22.92	22.93	22.96	23.02	23.09
	5	28.61	28.61	28.62	28.64	28.65	28.68	28.70	28.77	28.86
80 km/h	0	0.00	0.00	0.00	-0.01	-0.01	-0.01	-0.01	-0.02	-0.04
	1	5.71	5.71	5.70	5.70	5.70	5.70	5.70	5.70	5.69
	2	11.42	11.42	11.42	11.42	11.42	11.43	11.43	11.43	11.43
	3	17.14	17.14	17.14	17.14	17.15	17.15	17.16	17.17	17.18
	4	22.87	22.87	22.87	22.87	22.88	22.88	22.89	22.91	22.92
	5	28.60	28.60	28.60	28.60	28.61	28.62	28.63	28.66	28.67
100 km/h	0	0.00	0.00	0.00	-0.01	-0.02	-0.03	-0.05	-0.09	-0.17
	1	5.71	5.71	5.71	5.70	5.69	5.68	5.67	5.63	5.56
	2	11.43	11.43	11.43	11.42	11.42	11.41	11.39	11.36	11.29
	3	17.16	17.16	17.15	17.15	17.14	17.13	17.12	17.09	17.02
	4	22.89	22.89	22.88	22.88	22.87	22.87	22.86	22.83	22.76
	5	28.62	28.62	28.62	28.61	28.61	28.60	28.59	28.56	28.50
120 km/h	0	0.00	0.00	-0.01	-0.02	-0.03	-0.05	-0.07	-0.12	-0.24
	1	5.73	5.73	5.72	5.71	5.70	5.69	5.67	5.61	5.50
	2	11.47	11.47	11.46	11.45	11.44	11.43	11.41	11.36	11.25
	3	17.21	17.21	17.21	17.20	17.19	17.18	17.16	17.11	17.00
	4	22.96	22.96	22.96	22.95	22.94	22.93	22.91	22.86	22.76
	5	28.72	28.72	28.71	28.71	28.70	28.68	28.67	28.61	28.51

Table E.9: The normalized (by the static values) 95th percentile first power aggregate forces of the base model under all operating conditions

		Left									Right								
	IRI (m/km) →	0.5	1	2	3	4	5	6	8	10	0.5	1	2	3	4	5	6	8	10
	Crossfall (%)	95th Percentile Aggregate First Power Force (N)/Static Aggregate First Power Force (N)																	
40 km/h	0	1.013	1.026	1.051	1.077	1.103	1.128	1.154	1.205	1.255	1.013	1.026	1.052	1.077	1.103	1.129	1.155	1.206	1.258
	1	1.041	1.054	1.080	1.105	1.131	1.156	1.182	1.233	1.284	0.984	0.997	1.023	1.049	1.075	1.100	1.126	1.178	1.229
	2	1.070	1.083	1.108	1.134	1.159	1.185	1.210	1.261	1.312	0.956	0.969	0.995	1.020	1.046	1.072	1.097	1.149	1.200
	3	1.099	1.111	1.137	1.162	1.188	1.213	1.239	1.290	1.340	0.927	0.940	0.966	0.992	1.017	1.043	1.069	1.120	1.172
	4	1.127	1.140	1.165	1.191	1.216	1.242	1.267	1.318	1.369	0.899	0.912	0.937	0.963	0.989	1.014	1.040	1.091	1.143
	5	1.156	1.169	1.194	1.220	1.245	1.270	1.296	1.346	1.397	0.870	0.883	0.909	0.934	0.960	0.986	1.011	1.062	1.113
60 km/h	0	1.015	1.030	1.059	1.089	1.119	1.148	1.178	1.237	1.296	1.015	1.030	1.059	1.089	1.119	1.148	1.178	1.237	1.297
	1	1.043	1.058	1.088	1.117	1.147	1.177	1.206	1.265	1.324	0.986	1.001	1.031	1.060	1.090	1.119	1.149	1.208	1.267
	2	1.072	1.087	1.116	1.146	1.175	1.205	1.235	1.293	1.352	0.958	0.972	1.002	1.031	1.061	1.090	1.120	1.179	1.237
	3	1.101	1.116	1.145	1.174	1.204	1.233	1.263	1.322	1.381	0.929	0.944	0.973	1.002	1.032	1.061	1.091	1.149	1.208
	4	1.130	1.145	1.174	1.203	1.233	1.262	1.291	1.351	1.409	0.901	0.915	0.944	0.974	1.003	1.032	1.061	1.120	1.179
	5	1.159	1.174	1.203	1.232	1.261	1.291	1.320	1.379	1.438	0.873	0.887	0.916	0.945	0.974	1.003	1.032	1.091	1.149
80 km/h	0	1.017	1.034	1.068	1.102	1.136	1.170	1.204	1.272	1.340	1.017	1.035	1.069	1.104	1.138	1.173	1.207	1.276	1.346
	1	1.046	1.063	1.097	1.130	1.164	1.198	1.232	1.300	1.368	0.989	1.006	1.041	1.075	1.110	1.144	1.179	1.248	1.317
	2	1.074	1.091	1.125	1.159	1.193	1.227	1.260	1.328	1.396	0.960	0.978	1.012	1.047	1.081	1.115	1.150	1.218	1.287
	3	1.103	1.120	1.154	1.187	1.221	1.255	1.289	1.356	1.424	0.932	0.949	0.983	1.018	1.052	1.087	1.121	1.189	1.258
	4	1.132	1.149	1.182	1.216	1.250	1.283	1.317	1.385	1.452	0.903	0.920	0.955	0.989	1.024	1.058	1.092	1.160	1.229
	5	1.161	1.177	1.211	1.244	1.278	1.312	1.345	1.413	1.480	0.875	0.892	0.926	0.960	0.995	1.029	1.063	1.131	1.200
100 km/h	0	1.020	1.039	1.078	1.117	1.156	1.195	1.234	1.312	1.390	1.019	1.038	1.077	1.115	1.153	1.191	1.230	1.306	1.383
	1	1.048	1.068	1.107	1.146	1.185	1.224	1.263	1.341	1.418	0.991	1.010	1.048	1.086	1.124	1.163	1.201	1.277	1.354
	2	1.078	1.097	1.136	1.175	1.213	1.252	1.291	1.369	1.447	0.963	0.981	1.019	1.057	1.096	1.134	1.172	1.248	1.325
	3	1.107	1.126	1.165	1.203	1.242	1.281	1.320	1.397	1.475	0.935	0.953	0.991	1.029	1.067	1.105	1.143	1.219	1.295
	4	1.136	1.155	1.194	1.232	1.271	1.310	1.348	1.426	1.504	0.907	0.925	0.963	1.000	1.038	1.076	1.114	1.190	1.266
	5	1.165	1.184	1.223	1.261	1.300	1.338	1.377	1.455	1.532	0.879	0.897	0.934	0.972	1.010	1.047	1.085	1.161	1.237
120 km/h	0	1.022	1.043	1.086	1.130	1.173	1.216	1.259	1.346	1.432	1.021	1.043	1.086	1.128	1.171	1.214	1.257	1.342	1.428
	1	1.052	1.073	1.116	1.159	1.202	1.245	1.288	1.374	1.460	0.994	1.015	1.057	1.100	1.142	1.185	1.228	1.313	1.399
	2	1.082	1.103	1.145	1.188	1.231	1.274	1.317	1.402	1.488	0.966	0.987	1.030	1.072	1.114	1.157	1.199	1.285	1.370
	3	1.112	1.133	1.175	1.217	1.260	1.303	1.346	1.431	1.517	0.939	0.960	1.002	1.044	1.087	1.129	1.171	1.256	1.341
	4	1.143	1.164	1.206	1.247	1.290	1.332	1.375	1.461	1.546	0.913	0.933	0.974	1.017	1.059	1.101	1.143	1.227	1.313
	5	1.173	1.194	1.237	1.278	1.320	1.362	1.404	1.489	1.575	0.886	0.905	0.947	0.989	1.031	1.073	1.115	1.200	1.285

Table E.10: The percentage difference in left and right 95th percentile first power aggregate forces of the base model under all operating conditions

	IRI (m/km) →	0.5	1	2	3	4	5	6	8	10
	Crossfall (%)	Percentage Difference Between Left and Right (%)								
40 km/h	0	-0.01	-0.01	-0.03	-0.05	-0.07	-0.09	-0.11	-0.16	-0.23
	1	5.63	5.55	5.39	5.25	5.10	4.96	4.82	4.56	4.32
	2	11.27	11.11	10.82	10.54	10.28	10.02	9.77	9.30	8.87
	3	16.92	16.69	16.26	15.86	15.47	15.08	14.72	14.07	13.43
	4	22.57	22.28	21.71	21.17	20.66	20.16	19.69	18.82	18.02
	5	28.22	27.87	27.17	26.50	25.86	25.25	24.67	23.59	22.62
60 km/h	0	0.00	0.01	0.01	0.01	0.01	0.00	0.00	-0.03	-0.06
	1	5.64	5.56	5.41	5.26	5.13	5.00	4.87	4.63	4.39
	2	11.28	11.12	10.81	10.53	10.26	10.00	9.75	9.29	8.88
	3	16.93	16.69	16.23	15.80	15.39	15.01	14.65	13.97	13.36
	4	22.54	22.26	21.64	21.07	20.54	20.03	19.55	18.65	17.85
	5	28.18	27.83	27.07	26.36	25.70	25.05	24.46	23.36	22.32
80 km/h	0	-0.03	-0.06	-0.11	-0.15	-0.20	-0.25	-0.28	-0.35	-0.47
	1	5.58	5.46	5.23	5.01	4.82	4.62	4.45	4.12	3.79
	2	11.20	10.98	10.57	10.18	9.83	9.50	9.18	8.61	8.08
	3	16.83	16.51	15.91	15.37	14.85	14.38	13.94	13.13	12.38
	4	22.46	22.05	21.26	20.55	19.88	19.27	18.69	17.64	16.65
	5	28.09	27.58	26.63	25.75	24.94	24.16	23.44	22.15	20.94
100 km/h	0	0.04	0.07	0.14	0.20	0.25	0.32	0.36	0.46	0.48
	1	5.65	5.59	5.46	5.33	5.22	5.12	5.01	4.84	4.63
	2	11.27	11.09	10.78	10.49	10.20	9.93	9.67	9.22	8.81
	3	16.85	16.62	16.09	15.63	15.18	14.75	14.36	13.64	12.97
	4	22.42	22.11	21.41	20.77	20.16	19.58	19.03	18.05	17.15
	5	27.99	27.59	26.74	25.89	25.13	24.39	23.73	22.46	21.33
120 km/h	0	0.02	0.04	0.08	0.12	0.15	0.16	0.20	0.26	0.24
	1	5.65	5.53	5.36	5.21	5.05	4.90	4.76	4.52	4.24
	2	11.27	11.07	10.61	10.25	9.92	9.63	9.33	8.78	8.23
	3	16.89	16.57	15.90	15.31	14.78	14.32	13.87	13.06	12.25
	4	22.39	22.04	21.23	20.39	19.66	19.02	18.41	17.35	16.27
	5	27.91	27.55	26.56	25.49	24.56	23.71	22.96	21.56	20.31

Table E.11: The normalized (by the static values) 99th percentile first power aggregate forces of the base model under all operating conditions

		Left									Right								
	IRI (m/km) →	0.5	1	2	3	4	5	6	8	10	0.5	1	2	3	4	5	6	8	10
	Crossfall (%)	99th Percentile Aggregate First Power Force (N)/Static Aggregate First Power Force (N)																	
40 km/h	0	1.018	1.036	1.072	1.109	1.145	1.181	1.217	1.289	1.360	1.018	1.036	1.073	1.109	1.146	1.182	1.218	1.291	1.363
	1	1.047	1.065	1.101	1.137	1.173	1.209	1.245	1.317	1.388	0.990	1.008	1.044	1.081	1.117	1.153	1.190	1.262	1.335
	2	1.075	1.093	1.129	1.165	1.201	1.237	1.273	1.345	1.417	0.961	0.979	1.016	1.052	1.088	1.124	1.161	1.233	1.306
	3	1.104	1.122	1.158	1.194	1.230	1.266	1.301	1.373	1.445	0.933	0.951	0.987	1.023	1.059	1.096	1.132	1.204	1.276
	4	1.133	1.150	1.186	1.222	1.258	1.294	1.330	1.402	1.474	0.904	0.922	0.958	0.995	1.031	1.067	1.103	1.175	1.247
	5	1.162	1.179	1.215	1.251	1.287	1.322	1.358	1.430	1.502	0.875	0.894	0.930	0.966	1.002	1.038	1.074	1.146	1.218
60 km/h	0	1.021	1.041	1.082	1.123	1.164	1.205	1.247	1.328	1.410	1.021	1.042	1.083	1.125	1.166	1.207	1.249	1.331	1.414
	1	1.049	1.070	1.111	1.152	1.193	1.233	1.274	1.356	1.438	0.992	1.013	1.054	1.096	1.137	1.178	1.219	1.302	1.384
	2	1.078	1.098	1.139	1.180	1.221	1.262	1.302	1.384	1.465	0.964	0.984	1.025	1.067	1.108	1.149	1.190	1.272	1.354
	3	1.108	1.127	1.168	1.208	1.249	1.290	1.330	1.412	1.493	0.935	0.956	0.997	1.038	1.079	1.120	1.161	1.243	1.324
	4	1.138	1.156	1.196	1.237	1.277	1.318	1.359	1.440	1.521	0.907	0.927	0.968	1.009	1.050	1.091	1.132	1.213	1.295
	5	1.168	1.186	1.225	1.266	1.306	1.347	1.387	1.468	1.549	0.879	0.899	0.939	0.980	1.021	1.062	1.102	1.184	1.265
80 km/h	0	1.024	1.048	1.097	1.145	1.194	1.242	1.290	1.387	1.483	1.024	1.049	1.097	1.146	1.194	1.243	1.291	1.387	1.484
	1	1.053	1.077	1.125	1.174	1.222	1.270	1.318	1.415	1.511	0.996	1.020	1.069	1.117	1.166	1.214	1.262	1.359	1.456
	2	1.082	1.106	1.154	1.202	1.250	1.298	1.347	1.443	1.539	0.967	0.992	1.040	1.088	1.137	1.185	1.233	1.329	1.426
	3	1.110	1.134	1.182	1.231	1.279	1.327	1.375	1.471	1.567	0.939	0.963	1.012	1.060	1.108	1.156	1.205	1.300	1.397
	4	1.140	1.163	1.211	1.259	1.307	1.355	1.403	1.499	1.595	0.911	0.935	0.983	1.031	1.079	1.128	1.176	1.271	1.368
	5	1.169	1.192	1.240	1.288	1.335	1.383	1.431	1.527	1.624	0.882	0.906	0.954	1.002	1.051	1.099	1.147	1.243	1.339
100 km/h	0	1.026	1.053	1.106	1.159	1.212	1.265	1.318	1.424	1.530	1.027	1.055	1.109	1.163	1.218	1.272	1.326	1.433	1.541
	1	1.055	1.082	1.134	1.187	1.240	1.293	1.346	1.452	1.558	0.999	1.026	1.080	1.135	1.189	1.243	1.297	1.404	1.512
	2	1.085	1.111	1.163	1.216	1.268	1.321	1.374	1.480	1.587	0.971	0.998	1.052	1.106	1.160	1.214	1.268	1.375	1.482
	3	1.116	1.141	1.192	1.244	1.297	1.349	1.402	1.509	1.615	0.943	0.969	1.023	1.078	1.132	1.185	1.239	1.346	1.453
	4	1.148	1.171	1.221	1.273	1.326	1.378	1.431	1.537	1.643	0.916	0.941	0.995	1.049	1.103	1.157	1.210	1.318	1.424
	5	1.179	1.201	1.251	1.303	1.355	1.407	1.459	1.565	1.671	0.889	0.913	0.966	1.020	1.074	1.128	1.181	1.288	1.395
120 km/h	0	1.030	1.060	1.120	1.180	1.241	1.301	1.361	1.481	1.601	1.030	1.060	1.119	1.179	1.239	1.298	1.358	1.476	1.595
	1	1.060	1.089	1.149	1.209	1.269	1.329	1.389	1.510	1.630	1.002	1.031	1.091	1.151	1.210	1.270	1.329	1.448	1.566
	2	1.094	1.120	1.179	1.238	1.298	1.358	1.418	1.538	1.658	0.976	1.003	1.063	1.122	1.181	1.241	1.300	1.419	1.538
	3	1.132	1.153	1.208	1.268	1.327	1.387	1.447	1.567	1.686	0.953	0.977	1.034	1.094	1.153	1.212	1.272	1.390	1.510
	4	1.171	1.188	1.240	1.297	1.357	1.416	1.476	1.595	1.715	0.931	0.951	1.006	1.065	1.125	1.184	1.243	1.361	1.480
	5	1.211	1.226	1.272	1.328	1.386	1.446	1.505	1.624	1.743	0.910	0.928	0.979	1.037	1.096	1.156	1.215	1.332	1.452

Table E.12: The percentage difference in left and right 99th percentile first power aggregate forces of the base model under all operating conditions

	IRI (m/km) →	0.5	1	2	3	4	5	6	8	10
	Crossfall (%)	Percentage Difference Between Left and Right (%)								
40 km/h	0	-0.01	-0.02	-0.04	-0.07	-0.09	-0.11	-0.14	-0.20	-0.23
	1	5.59	5.48	5.28	5.08	4.89	4.72	4.56	4.22	3.94
	2	11.19	10.99	10.59	10.22	9.88	9.56	9.26	8.67	8.15
	3	16.82	16.50	15.91	15.37	14.86	14.39	13.95	13.12	12.40
	4	22.47	22.02	21.25	20.54	19.88	19.26	18.67	17.58	16.63
	5	28.11	27.56	26.60	25.72	24.89	24.12	23.40	22.04	20.87
60 km/h	0	-0.02	-0.03	-0.07	-0.10	-0.13	-0.16	-0.16	-0.18	-0.25
	1	5.59	5.46	5.22	5.00	4.77	4.58	4.39	4.09	3.82
	2	11.21	10.96	10.51	10.10	9.70	9.34	9.00	8.41	7.90
	3	16.88	16.48	15.81	15.19	14.63	14.10	13.60	12.75	11.99
	4	22.54	22.00	21.11	20.31	19.56	18.88	18.24	17.08	16.08
	5	28.21	27.53	26.43	25.44	24.50	23.66	22.88	21.43	20.18
80 km/h	0	-0.01	-0.01	-0.03	-0.05	-0.05	-0.06	-0.07	-0.06	-0.06
	1	5.56	5.43	5.17	4.93	4.73	4.53	4.38	4.05	3.72
	2	11.14	10.87	10.37	9.93	9.51	9.15	8.79	8.19	7.59
	3	16.73	16.31	15.57	14.90	14.29	13.74	13.21	12.30	11.45
	4	22.34	21.79	20.80	19.91	19.08	18.33	17.64	16.44	15.36
	5	27.97	27.26	26.02	24.90	23.87	22.94	22.05	20.53	19.23
100 km/h	0	-0.08	-0.16	-0.30	-0.40	-0.50	-0.58	-0.62	-0.64	-0.70
	1	5.51	5.26	4.87	4.52	4.21	3.93	3.69	3.34	3.04
	2	11.15	10.74	10.02	9.43	8.91	8.46	8.03	7.35	6.79
	3	16.83	16.27	15.23	14.37	13.62	12.95	12.39	11.37	10.55
	4	22.45	21.74	20.47	19.35	18.37	17.47	16.73	15.36	14.29
	5	28.03	27.25	25.75	24.33	23.12	22.07	21.06	19.38	18.01
120 km/h	0	0.02	0.04	0.08	0.12	0.15	0.19	0.22	0.32	0.38
	1	5.66	5.46	5.21	4.96	4.76	4.55	4.41	4.19	3.97
	2	11.41	11.00	10.34	9.85	9.43	9.01	8.68	8.03	7.49
	3	17.14	16.52	15.53	14.73	14.07	13.45	12.88	11.95	11.06
	4	22.76	22.10	20.81	19.63	18.71	17.85	17.11	15.83	14.66
	5	28.31	27.70	26.07	24.62	23.32	22.32	21.32	19.73	18.25

Table E.13: The normalized (by the static values) average fourth power aggregate forces of the base model under all operating conditions

		Left									Right								
	IRI (m/km) →	0.5	1	2	3	4	5	6	8	10	0.5	1	2	3	4	5	6	8	10
	Crossfall (%)	Average Aggregate Fourth Power Force (N^4)/ Static Aggregate Fourth Power Force (N4)																	
40 km/h	0	1.000	1.002	1.007	1.015	1.027	1.043	1.062	1.111	1.174	1.000	1.002	1.007	1.015	1.027	1.043	1.062	1.110	1.173
	1	1.126	1.127	1.132	1.141	1.154	1.171	1.191	1.242	1.309	0.886	0.887	0.892	0.900	0.911	0.926	0.944	0.989	1.048
	2	1.262	1.264	1.270	1.279	1.293	1.310	1.331	1.385	1.456	0.782	0.783	0.788	0.795	0.806	0.819	0.836	0.879	0.934
	3	1.412	1.413	1.419	1.429	1.444	1.462	1.484	1.541	1.615	0.687	0.689	0.693	0.700	0.710	0.722	0.738	0.778	0.830
	4	1.574	1.576	1.582	1.593	1.608	1.627	1.650	1.710	1.788	0.602	0.603	0.607	0.613	0.622	0.634	0.649	0.686	0.735
	5	1.751	1.752	1.759	1.770	1.786	1.806	1.831	1.894	1.976	0.524	0.525	0.529	0.535	0.544	0.555	0.568	0.603	0.648
60 km/h	0	1.001	1.003	1.010	1.022	1.039	1.061	1.089	1.158	1.248	1.001	1.002	1.010	1.022	1.039	1.061	1.088	1.157	1.247
	1	1.126	1.128	1.136	1.149	1.167	1.190	1.219	1.292	1.387	0.886	0.888	0.895	0.906	0.922	0.943	0.968	1.033	1.117
	2	1.263	1.265	1.273	1.287	1.306	1.331	1.361	1.438	1.539	0.782	0.784	0.790	0.801	0.816	0.835	0.859	0.919	0.998
	3	1.412	1.415	1.423	1.438	1.458	1.484	1.516	1.597	1.703	0.687	0.689	0.695	0.705	0.719	0.737	0.759	0.816	0.889
	4	1.575	1.578	1.587	1.602	1.623	1.650	1.684	1.770	1.881	0.602	0.603	0.609	0.618	0.631	0.648	0.668	0.721	0.790
	5	1.752	1.755	1.764	1.780	1.802	1.831	1.866	1.956	2.073	0.524	0.526	0.531	0.539	0.552	0.567	0.586	0.636	0.700
80 km/h	0	1.001	1.003	1.013	1.029	1.051	1.081	1.116	1.209	1.329	1.001	1.003	1.013	1.029	1.051	1.081	1.117	1.209	1.331
	1	1.126	1.128	1.139	1.155	1.179	1.210	1.248	1.346	1.473	0.886	0.889	0.898	0.913	0.934	0.961	0.995	1.082	1.197
	2	1.263	1.266	1.276	1.294	1.319	1.352	1.392	1.494	1.628	0.782	0.784	0.793	0.807	0.827	0.852	0.884	0.966	1.073
	3	1.412	1.415	1.426	1.445	1.472	1.506	1.548	1.656	1.797	0.688	0.690	0.697	0.711	0.729	0.753	0.783	0.860	0.960
	4	1.575	1.578	1.590	1.609	1.637	1.673	1.718	1.831	1.979	0.602	0.604	0.611	0.623	0.641	0.663	0.691	0.763	0.857
	5	1.752	1.755	1.767	1.788	1.817	1.855	1.902	2.021	2.176	0.524	0.526	0.533	0.545	0.561	0.582	0.608	0.675	0.763
100 km/h	0	1.001	1.004	1.017	1.038	1.067	1.104	1.150	1.267	1.421	1.001	1.004	1.017	1.037	1.065	1.102	1.147	1.264	1.417
	1	1.127	1.130	1.143	1.165	1.196	1.235	1.284	1.408	1.569	0.887	0.890	0.901	0.920	0.947	0.982	1.024	1.133	1.278
	2	1.264	1.267	1.281	1.305	1.337	1.379	1.430	1.560	1.730	0.782	0.785	0.796	0.814	0.839	0.871	0.911	1.014	1.150
	3	1.413	1.417	1.432	1.456	1.491	1.534	1.588	1.726	1.904	0.688	0.690	0.700	0.717	0.741	0.771	0.808	0.905	1.032
	4	1.576	1.580	1.596	1.622	1.658	1.704	1.760	1.905	2.093	0.602	0.604	0.614	0.630	0.651	0.680	0.715	0.805	0.924
	5	1.753	1.758	1.774	1.801	1.839	1.887	1.947	2.099	2.295	0.525	0.527	0.536	0.550	0.571	0.597	0.630	0.714	0.826
120 km/h	0	1.001	1.005	1.019	1.043	1.077	1.121	1.175	1.316	1.499	1.001	1.005	1.019	1.042	1.075	1.118	1.171	1.307	1.488
	1	1.127	1.131	1.146	1.171	1.207	1.254	1.311	1.459	1.652	0.886	0.890	0.903	0.925	0.956	0.996	1.046	1.174	1.344
	2	1.265	1.269	1.285	1.312	1.350	1.399	1.459	1.614	1.818	0.782	0.785	0.797	0.818	0.847	0.885	0.932	1.052	1.212
	3	1.415	1.419	1.436	1.465	1.505	1.556	1.620	1.783	1.997	0.687	0.690	0.702	0.721	0.748	0.784	0.827	0.940	1.091
	4	1.579	1.584	1.601	1.631	1.673	1.728	1.794	1.966	2.190	0.601	0.604	0.615	0.633	0.659	0.692	0.733	0.839	0.980
	5	1.758	1.762	1.781	1.812	1.857	1.914	1.984	2.164	2.398	0.524	0.527	0.537	0.554	0.578	0.609	0.647	0.746	0.878

Table E.14: The percentage difference in left and right average fourth power aggregate forces of the base model under all operating conditions

	IRI (m/km) →	0.5	1	2	3	4	5	6	8	10
	Crossfall (%)	Percentage Difference Between Left and Right (%)								
40 km/h	0	0.00	0.00	0.01	0.01	0.02	0.02	0.03	0.04	0.07
	1	23.80	23.79	23.73	23.64	23.50	23.34	23.14	22.66	22.11
	2	46.99	46.96	46.85	46.67	46.41	46.08	45.70	44.76	43.67
	3	69.00	68.96	68.81	68.54	68.18	67.71	67.17	65.84	64.28
	4	89.38	89.33	89.13	88.81	88.36	87.79	87.12	85.49	83.55
	5	107.79	107.74	107.52	107.15	106.64	106.01	105.24	103.40	101.19
60 km/h	0	0.01	0.01	0.02	0.03	0.04	0.04	0.05	0.06	0.10
	1	23.83	23.81	23.74	23.61	23.42	23.19	22.92	22.29	21.57
	2	47.04	47.00	46.85	46.59	46.23	45.79	45.26	44.02	42.61
	3	69.07	69.02	68.80	68.43	67.92	67.29	66.54	64.78	62.76
	4	89.45	89.39	89.12	88.66	88.04	87.26	86.34	84.17	81.66
	5	107.87	107.80	107.49	106.98	106.28	105.40	104.37	101.90	99.04
80 km/h	0	0.00	-0.01	-0.01	-0.01	0.00	-0.01	-0.01	-0.03	-0.10
	1	23.81	23.78	23.66	23.48	23.23	22.92	22.56	21.70	20.69
	2	47.01	46.95	46.73	46.38	45.90	45.30	44.60	42.97	41.08
	3	69.03	68.95	68.64	68.14	67.46	66.62	65.64	63.32	60.67
	4	89.41	89.31	88.94	88.32	87.49	86.45	85.24	82.39	79.11
	5	107.83	107.72	107.30	106.61	105.67	104.50	103.12	99.88	96.14
100 km/h	0	0.00	0.01	0.03	0.07	0.12	0.17	0.22	0.30	0.24
	1	23.83	23.80	23.68	23.49	23.22	22.89	22.51	21.59	20.49
	2	47.04	46.98	46.73	46.32	45.76	45.08	44.29	42.45	40.33
	3	69.08	68.98	68.61	68.02	67.22	66.23	65.08	62.43	59.41
	4	89.46	89.34	88.89	88.15	87.15	85.92	84.49	81.18	77.45
	5	107.88	107.75	107.23	106.39	105.25	103.85	102.22	98.43	94.14
120 km/h	0	0.00	0.01	0.04	0.09	0.17	0.28	0.40	0.66	0.79
	1	23.90	23.87	23.73	23.52	23.23	22.89	22.51	21.64	20.57
	2	47.19	47.11	46.82	46.35	45.73	44.98	44.12	42.19	39.99
	3	69.27	69.16	68.74	68.05	67.14	66.03	64.76	61.89	58.69
	4	89.68	89.55	89.02	88.17	87.02	85.62	84.03	80.39	76.38
	5	108.11	107.96	107.36	106.39	105.08	103.48	101.64	97.44	92.79

Table E.15: The normalized (by the static values) 95th percentile fourth power aggregate forces of the base model under all operating conditions

		Left									Right								
	IRI (m/km) →	0.5	1	2	3	4	5	6	8	10	0.5	1	2	3	4	5	6	8	10
	Crossfall (%)	95th Percentile Aggregate Fourth Power Force (N^4)/ Static Aggregate Fourth Power Force (N^4)																	
40 km/h	0	1.048	1.099	1.206	1.321	1.446	1.581	1.726	2.049	2.422	1.049	1.099	1.206	1.322	1.448	1.584	1.730	2.055	2.431
	1	1.178	1.233	1.349	1.474	1.609	1.754	1.911	2.257	2.655	0.930	0.976	1.075	1.181	1.297	1.422	1.557	1.860	2.211
	2	1.320	1.379	1.505	1.640	1.785	1.942	2.110	2.481	2.907	0.822	0.864	0.954	1.052	1.158	1.273	1.398	1.678	2.005
	3	1.474	1.539	1.674	1.820	1.977	2.145	2.326	2.722	3.177	0.724	0.762	0.844	0.934	1.031	1.137	1.251	1.512	1.814
	4	1.642	1.712	1.858	2.015	2.184	2.364	2.557	2.983	3.468	0.635	0.670	0.744	0.826	0.915	1.012	1.118	1.357	1.638
	5	1.825	1.900	2.058	2.226	2.406	2.600	2.806	3.263	3.779	0.555	0.586	0.654	0.728	0.809	0.898	0.995	1.215	1.474
60 km/h	0	1.058	1.118	1.247	1.389	1.544	1.714	1.899	2.317	2.805	1.058	1.118	1.248	1.391	1.546	1.716	1.900	2.317	2.805
	1	1.188	1.253	1.394	1.547	1.714	1.897	2.095	2.545	3.065	0.939	0.994	1.112	1.243	1.386	1.541	1.712	2.099	2.552
	2	1.332	1.402	1.553	1.719	1.899	2.095	2.308	2.788	3.344	0.830	0.880	0.988	1.107	1.238	1.382	1.538	1.894	2.317
	3	1.490	1.565	1.727	1.906	2.099	2.310	2.537	3.048	3.642	0.732	0.777	0.875	0.983	1.102	1.234	1.378	1.707	2.097
	4	1.660	1.742	1.916	2.107	2.315	2.540	2.784	3.329	3.960	0.643	0.684	0.772	0.871	0.980	1.100	1.232	1.534	1.895
	5	1.847	1.935	2.121	2.325	2.548	2.789	3.048	3.631	4.297	0.562	0.599	0.679	0.768	0.867	0.977	1.098	1.377	1.710
80 km/h	0	1.067	1.139	1.293	1.465	1.655	1.864	2.094	2.623	3.251	1.068	1.141	1.297	1.472	1.666	1.879	2.113	2.653	3.308
	1	1.199	1.276	1.444	1.629	1.834	2.059	2.305	2.869	3.541	0.948	1.014	1.158	1.319	1.497	1.694	1.912	2.414	3.024
	2	1.343	1.427	1.608	1.808	2.028	2.270	2.533	3.136	3.849	0.839	0.899	1.031	1.177	1.342	1.524	1.725	2.190	2.758
	3	1.501	1.591	1.785	2.001	2.238	2.496	2.779	3.421	4.178	0.740	0.794	0.914	1.049	1.199	1.366	1.551	1.983	2.510
	4	1.673	1.769	1.978	2.210	2.464	2.741	3.042	3.726	4.530	0.650	0.699	0.808	0.931	1.068	1.222	1.392	1.793	2.284
	5	1.860	1.963	2.189	2.435	2.708	3.004	3.325	4.054	4.904	0.568	0.612	0.711	0.823	0.949	1.089	1.247	1.616	2.072
100 km/h	0	1.079	1.162	1.345	1.550	1.779	2.037	2.321	2.986	3.794	1.077	1.159	1.338	1.540	1.766	2.017	2.297	2.952	3.757
	1	1.212	1.304	1.502	1.724	1.971	2.248	2.554	3.263	4.123	0.957	1.032	1.196	1.381	1.590	1.822	2.081	2.691	3.437
	2	1.360	1.457	1.673	1.912	2.179	2.475	2.804	3.561	4.474	0.848	0.916	1.066	1.235	1.427	1.641	1.882	2.449	3.143
	3	1.521	1.627	1.858	2.117	2.403	2.721	3.071	3.878	4.844	0.749	0.810	0.946	1.102	1.277	1.474	1.697	2.224	2.873
	4	1.697	1.811	2.059	2.337	2.646	2.985	3.360	4.220	5.242	0.660	0.715	0.838	0.979	1.139	1.322	1.527	2.015	2.618
	5	1.888	2.011	2.277	2.574	2.906	3.270	3.669	4.585	5.666	0.580	0.628	0.740	0.868	1.014	1.181	1.370	1.821	2.384
120 km/h	0	1.088	1.182	1.389	1.626	1.894	2.194	2.532	3.331	4.309	1.087	1.180	1.384	1.617	1.880	2.176	2.508	3.290	4.259
	1	1.228	1.327	1.551	1.805	2.092	2.414	2.774	3.623	4.662	0.968	1.053	1.240	1.454	1.696	1.971	2.280	3.010	3.919
	2	1.384	1.493	1.730	2.003	2.312	2.654	3.037	3.935	5.036	0.862	0.938	1.109	1.305	1.529	1.783	2.069	2.748	3.599
	3	1.553	1.675	1.929	2.220	2.550	2.919	3.327	4.279	5.437	0.765	0.834	0.990	1.169	1.374	1.608	1.873	2.505	3.301
	4	1.739	1.872	2.151	2.457	2.809	3.203	3.639	4.647	5.875	0.678	0.739	0.880	1.046	1.234	1.447	1.692	2.279	3.023
	5	1.945	2.086	2.394	2.720	3.090	3.510	3.974	5.051	6.331	0.599	0.653	0.781	0.932	1.105	1.303	1.525	2.071	2.766

Table E.16: The percentage difference in left and right 95th percentile fourth power aggregate forces of the base model under all operating conditions

	IRI (m/km) →	0.5	1	2	3	4	5	6	8	10
	Crossfall (%)	Percentage Difference Between Left and Right (%)								
40 km/h	0	-0.01	-0.02	-0.05	-0.06	-0.10	-0.14	-0.20	-0.32	-0.36
	1	23.52	23.22	22.63	22.02	21.43	20.91	20.41	19.29	18.28
	2	46.46	45.89	44.77	43.68	42.61	41.61	40.59	38.62	36.72
	3	68.25	67.48	65.92	64.39	62.88	61.43	60.06	57.18	54.64
	4	88.45	87.52	85.61	83.70	81.90	80.10	78.33	74.91	71.67
	5	106.73	105.69	103.55	101.43	99.35	97.32	95.29	91.45	87.75
60 km/h	0	-0.03	-0.05	-0.09	-0.13	-0.14	-0.12	-0.06	0.00	-0.02
	1	23.48	23.14	22.47	21.81	21.18	20.71	20.14	19.23	18.28
	2	46.42	45.74	44.51	43.32	42.15	41.04	40.04	38.16	36.30
	3	68.17	67.27	65.51	63.88	62.26	60.71	59.21	56.39	53.85
	4	88.34	87.27	85.10	83.03	81.08	79.16	77.31	73.81	70.52
	5	106.61	105.43	103.02	100.66	98.44	96.26	94.07	90.04	86.15
80 km/h	0	-0.10	-0.18	-0.30	-0.48	-0.69	-0.82	-0.92	-1.15	-1.75
	1	23.33	22.85	21.94	21.05	20.26	19.47	18.65	17.25	15.74
	2	46.21	45.35	43.73	42.24	40.73	39.33	37.93	35.50	33.03
	3	67.94	66.79	64.55	62.47	60.45	58.51	56.69	53.21	49.87
	4	88.10	86.74	84.01	81.47	79.03	76.66	74.40	70.06	65.95
	5	106.37	104.87	101.87	98.97	96.22	93.58	90.90	86.01	81.21
100 km/h	0	0.13	0.25	0.48	0.64	0.76	0.95	1.05	1.16	0.98
	1	23.56	23.29	22.69	22.05	21.44	20.92	20.41	19.20	18.15
	2	46.37	45.67	44.34	43.00	41.72	40.53	39.34	37.02	34.95
	3	67.98	66.99	65.02	63.07	61.20	59.46	57.61	54.22	51.10
	4	87.95	86.81	84.27	81.90	79.60	77.27	75.00	70.71	66.78
	5	106.00	104.78	101.89	99.14	96.49	93.87	91.27	86.31	81.54
120 km/h	0	0.09	0.18	0.36	0.56	0.75	0.84	0.96	1.25	1.17
	1	23.62	23.06	22.25	21.54	20.89	20.17	19.57	18.49	17.32
	2	46.51	45.65	43.74	42.22	40.74	39.26	37.92	35.50	33.29
	3	68.00	67.08	64.31	62.02	59.96	57.90	55.94	52.29	48.90
	4	87.77	86.78	83.84	80.57	77.95	75.51	73.06	68.37	64.10
	5	105.79	104.64	101.63	97.97	94.62	91.73	89.07	83.70	78.39

Table E.17: The normalized (by the static values) 99th percentile fourth power aggregate forces of the base model under all operating conditions

		Left									Right								
	IRI (m/km) →	0.5	1	2	3	4	5	6	8	10	0.5	1	2	3	4	5	6	8	10
	Crossfall (%)	99th Percentile Aggregate Fourth Power Force (N^4)																	
40 km/h	0	1.069	1.141	1.298	1.472	1.663	1.874	2.107	2.643	3.284	1.069	1.141	1.297	1.470	1.663	1.877	2.110	2.646	3.286
	1	1.200	1.278	1.448	1.636	1.842	2.069	2.319	2.892	3.572	0.949	1.015	1.159	1.319	1.497	1.694	1.910	2.409	3.007
	2	1.343	1.428	1.612	1.814	2.036	2.280	2.548	3.160	3.882	0.839	0.900	1.031	1.179	1.342	1.524	1.725	2.189	2.746
	3	1.501	1.591	1.789	2.007	2.247	2.508	2.794	3.444	4.210	0.740	0.795	0.915	1.050	1.201	1.368	1.554	1.986	2.509
	4	1.673	1.769	1.981	2.216	2.473	2.752	3.058	3.752	4.563	0.649	0.699	0.809	0.933	1.071	1.226	1.398	1.800	2.287
	5	1.859	1.962	2.189	2.442	2.716	3.015	3.342	4.077	4.941	0.568	0.613	0.713	0.826	0.953	1.095	1.255	1.627	2.079
60 km/h	0	1.081	1.167	1.355	1.566	1.803	2.067	2.360	3.039	3.873	1.081	1.167	1.355	1.567	1.804	2.067	2.362	3.043	3.873
	1	1.214	1.307	1.510	1.738	1.993	2.277	2.590	3.320	4.198	0.960	1.038	1.211	1.405	1.624	1.869	2.140	2.776	3.551
	2	1.361	1.460	1.680	1.926	2.199	2.504	2.840	3.620	4.554	0.849	0.921	1.078	1.257	1.457	1.683	1.935	2.528	3.252
	3	1.524	1.628	1.865	2.128	2.421	2.748	3.107	3.937	4.928	0.750	0.814	0.957	1.121	1.305	1.513	1.744	2.296	2.971
	4	1.709	1.812	2.064	2.347	2.662	3.009	3.394	4.276	5.323	0.661	0.717	0.847	0.996	1.165	1.356	1.570	2.080	2.707
	5	1.913	2.014	2.280	2.584	2.919	3.291	3.698	4.638	5.749	0.581	0.629	0.746	0.883	1.036	1.212	1.409	1.880	2.462
80 km/h	0	1.096	1.199	1.429	1.691	1.991	2.328	2.708	3.612	4.740	1.095	1.198	1.425	1.684	1.982	2.320	2.702	3.612	4.732
	1	1.230	1.342	1.590	1.873	2.195	2.558	2.963	3.927	5.121	0.973	1.067	1.276	1.517	1.792	2.106	2.462	3.307	4.363
	2	1.377	1.498	1.766	2.071	2.417	2.805	3.239	4.265	5.528	0.862	0.948	1.139	1.360	1.616	1.908	2.237	3.026	4.022
	3	1.538	1.668	1.956	2.285	2.655	3.072	3.534	4.625	5.959	0.761	0.839	1.014	1.218	1.455	1.722	2.027	2.764	3.695
	4	1.716	1.852	2.163	2.516	2.913	3.357	3.850	5.006	6.415	0.669	0.740	0.899	1.087	1.303	1.549	1.833	2.517	3.389
	5	1.910	2.053	2.387	2.765	3.188	3.662	4.186	5.416	6.901	0.586	0.649	0.796	0.966	1.163	1.391	1.653	2.291	3.105
100 km/h	0	1.108	1.224	1.486	1.791	2.143	2.544	3.000	4.097	5.468	1.111	1.232	1.504	1.820	2.184	2.602	3.077	4.222	5.664
	1	1.246	1.372	1.655	1.983	2.364	2.793	3.281	4.446	5.894	0.988	1.098	1.348	1.639	1.978	2.366	2.809	3.879	5.238
	2	1.399	1.536	1.841	2.192	2.600	3.061	3.581	4.819	6.356	0.876	0.976	1.205	1.473	1.785	2.147	2.560	3.559	4.835
	3	1.574	1.715	2.043	2.421	2.856	3.349	3.904	5.220	6.850	0.776	0.865	1.074	1.320	1.610	1.943	2.325	3.257	4.458
	4	1.767	1.909	2.264	2.668	3.130	3.658	4.245	5.642	7.374	0.685	0.764	0.954	1.181	1.445	1.753	2.108	2.979	4.100
	5	1.978	2.126	2.504	2.936	3.431	3.990	4.617	6.092	7.917	0.605	0.673	0.845	1.051	1.295	1.579	1.909	2.718	3.767
120 km/h	0	1.124	1.261	1.571	1.936	2.366	2.863	3.438	4.848	6.654	1.124	1.259	1.566	1.929	2.354	2.845	3.408	4.791	6.571
	1	1.267	1.411	1.746	2.140	2.599	3.133	3.745	5.248	7.162	1.001	1.123	1.406	1.742	2.134	2.590	3.117	4.412	6.078
	2	1.442	1.584	1.941	2.364	2.857	3.427	4.080	5.669	7.686	0.898	1.002	1.260	1.568	1.931	2.356	2.847	4.063	5.633
	3	1.664	1.782	2.153	2.611	3.135	3.743	4.436	6.126	8.249	0.811	0.899	1.126	1.408	1.744	2.139	2.594	3.732	5.214
	4	1.920	2.017	2.395	2.877	3.439	4.087	4.821	6.600	8.847	0.738	0.805	1.006	1.263	1.571	1.935	2.363	3.423	4.810
	5	2.216	2.301	2.661	3.163	3.770	4.454	5.239	7.116	9.480	0.673	0.721	0.899	1.130	1.413	1.748	2.145	3.140	4.444

Table E.18: The percentage difference in left and right 99th percentile fourth power aggregate forces of the base model under all operating conditions

	IRI (m/km) →	0.5	1	2	3	4	5	6	8	10
	Crossfall (%)	Percentage Difference Between Left and Right (%)								
40 km/h	0	-0.01	0.01	0.04	0.10	0.03	-0.17	-0.15	-0.09	-0.06
	1	23.37	22.97	22.20	21.45	20.65	19.93	19.31	18.25	17.17
	2	46.20	45.39	43.95	42.47	41.08	39.75	38.54	36.30	34.26
	3	67.96	66.78	64.66	62.60	60.65	58.81	57.04	53.72	50.63
	4	88.15	86.67	84.01	81.52	79.09	76.74	74.50	70.31	66.47
	5	106.44	104.80	101.72	98.91	96.10	93.40	90.79	85.91	81.53
60 km/h	0	-0.02	-0.04	-0.05	-0.07	-0.06	-0.04	-0.11	-0.11	0.01
	1	23.38	22.90	22.01	21.17	20.40	19.72	19.03	17.83	16.71
	2	46.25	45.32	43.65	42.07	40.61	39.22	37.91	35.51	33.38
	3	68.12	66.68	64.30	62.04	59.94	57.98	56.22	52.66	49.55
	4	88.44	86.62	83.61	80.86	78.25	75.74	73.51	69.11	65.16
	5	106.84	104.79	101.35	98.18	95.17	92.33	89.62	84.65	80.06
80 km/h	0	0.08	0.15	0.27	0.39	0.43	0.34	0.21	0.02	0.17
	1	23.33	22.85	21.94	21.03	20.21	19.39	18.46	17.12	15.98
	2	46.01	45.01	43.14	41.42	39.72	38.04	36.59	33.98	31.55
	3	67.67	66.17	63.47	60.89	58.43	56.35	54.22	50.35	46.91
	4	87.81	85.87	82.54	79.32	76.37	73.68	71.01	66.18	61.72
	5	106.04	103.89	99.99	96.43	93.08	89.90	86.79	81.10	75.88
100 km/h	0	-0.29	-0.59	-1.20	-1.57	-1.93	-2.26	-2.54	-3.00	-3.52
	1	23.11	22.19	20.45	18.98	17.78	16.58	15.51	13.63	11.78
	2	46.04	44.56	41.77	39.27	37.15	35.09	33.28	30.07	27.19
	3	67.96	65.94	62.18	58.84	55.81	53.13	50.71	46.30	42.32
	4	88.22	85.71	81.43	77.31	73.64	70.40	67.27	61.77	57.06
	5	106.34	103.78	99.08	94.52	90.38	86.62	83.00	76.59	71.03
120 km/h	0	0.06	0.13	0.29	0.35	0.47	0.62	0.88	1.18	1.26
	1	23.43	22.72	21.58	20.50	19.62	19.00	18.30	17.31	16.37
	2	46.42	44.98	42.57	40.49	38.66	37.03	35.58	33.01	30.83
	3	68.95	65.90	62.66	59.87	57.02	54.57	52.41	48.58	45.09
	4	88.94	85.84	81.70	77.93	74.58	71.46	68.44	63.41	59.12
	5	106.87	104.54	99.01	94.68	90.93	87.27	83.80	77.55	72.35

Table E.19: Ratio of the percentage difference in left and right average fourth power aggregate forces to the percentage difference in the left and right average percentile first power aggregate forces

	IRI (m/km) →	0.5	1	2	3	4	5	6	8	10
	Crossfall (%)	Ratio of percetnage difference in fourth power and first power aggregate forces								
40 km/h	0	4.20	4.98	7.39	12.72	33.23	-108.29	-26.72	-18.51	-49.88
	1	4.17	4.17	4.16	4.14	4.12	4.09	4.05	3.96	3.86
	2	4.12	4.11	4.10	4.09	4.06	4.03	4.00	3.91	3.81
	3	4.03	4.03	4.02	4.00	3.98	3.95	3.91	3.83	3.73
	4	3.91	3.91	3.90	3.88	3.86	3.84	3.81	3.73	3.64
	5	3.77	3.77	3.76	3.75	3.73	3.70	3.68	3.61	3.52
60 km/h	0	3.96	3.62	3.01	2.50	2.10	1.79	1.56	1.32	1.32
	1	4.17	4.17	4.15	4.12	4.09	4.04	3.98	3.85	3.71
	2	4.12	4.11	4.10	4.07	4.04	3.99	3.94	3.82	3.68
	3	4.03	4.02	4.01	3.99	3.95	3.91	3.86	3.75	3.62
	4	3.91	3.91	3.89	3.87	3.84	3.80	3.76	3.66	3.54
	5	3.77	3.77	3.76	3.74	3.71	3.68	3.64	3.54	3.43
80 km/h	0	3.28	2.69	1.69	0.97	0.56	0.45	0.61	1.39	2.37
	1	4.17	4.17	4.15	4.12	4.07	4.02	3.95	3.80	3.63
	2	4.12	4.11	4.09	4.06	4.02	3.97	3.90	3.76	3.59
	3	4.03	4.02	4.00	3.98	3.93	3.88	3.83	3.69	3.53
	4	3.91	3.91	3.89	3.86	3.82	3.78	3.72	3.60	3.45
	5	3.77	3.77	3.75	3.73	3.69	3.65	3.60	3.49	3.35
100 km/h	0	-7.28	-7.25	-6.91	-6.46	-5.92	-5.33	-4.69	-3.35	-1.41
	1	4.17	4.17	4.15	4.12	4.08	4.03	3.97	3.83	3.68
	2	4.12	4.11	4.09	4.06	4.01	3.95	3.89	3.74	3.57
	3	4.03	4.02	4.00	3.97	3.92	3.87	3.80	3.65	3.49
	4	3.91	3.90	3.88	3.85	3.81	3.76	3.70	3.56	3.40
	5	3.77	3.76	3.75	3.72	3.68	3.63	3.58	3.45	3.30
120 km/h	0	0.53	-1.55	-3.80	-4.95	-5.55	-5.83	-5.86	-5.32	-3.33
	1	4.17	4.17	4.15	4.11	4.07	4.02	3.97	3.85	3.74
	2	4.11	4.11	4.08	4.05	4.00	3.94	3.87	3.71	3.55
	3	4.02	4.02	3.99	3.96	3.91	3.84	3.77	3.62	3.45
	4	3.91	3.90	3.88	3.84	3.79	3.73	3.67	3.52	3.36
	5	3.76	3.76	3.74	3.71	3.66	3.61	3.55	3.41	3.26

Table E.20: Left normalized (by base model static values) 95th percentile fourth power aggregate forces for different anti-roll bar stiffness values

	No Anti-Roll Bar					3 kNm/deg Front and 5kNm/deg Rear					6 kNm/deg Front and 10 kNm/deg Rear				
IRI (m/km) →	**0.5**	**1**	**2**	**3**	**4**	**0.5**	**1**	**2**	**3**	**4**	**0.5**	**1**	**2**	**3**	**4**
Crossfall (%)	**Normalized 95th Percentile Fourth Power Aggregate Forces**														
0	1.067	1.139	1.293	1.465	1.655	1.068	1.139	1.293	1.464	1.654	1.068	1.139	1.293	1.465	1.653
1	1.199	1.276	1.444	1.629	1.834	1.168	1.243	1.407	1.589	1.789	1.161	1.237	1.400	1.582	1.781
2	1.343	1.427	1.608	1.808	2.028	1.276	1.356	1.530	1.722	1.934	1.260	1.341	1.514	1.706	1.917
3	1.501	1.591	1.785	2.001	2.238	1.392	1.476	1.661	1.864	2.088	1.366	1.451	1.635	1.837	2.060
4	1.673	1.769	1.978	2.210	2.464	1.516	1.605	1.800	2.016	2.252	1.479	1.569	1.763	1.977	2.211
5	1.860	1.963	2.189	2.435	2.708	1.649	1.743	1.949	2.177	2.426	1.599	1.694	1.898	2.124	2.370

Table E.21: Right normalized (by base model static values) 95th percentile fourth power aggregate forces for different anti-roll bar stiffness values

	No Anti-Roll Bar					3 kNm/deg Front and 5kNm/deg Rear					6 kNm/deg Front and 10 kNm/deg Rear				
IRI (m/km) →	**0.5**	**1**	**2**	**3**	**4**	**0.5**	**1**	**2**	**3**	**4**	**0.5**	**1**	**2**	**3**	**4**
Crossfall (%)	**Normalized 95th Percentile Fourth Power Aggregate Forces**														
0	1.068	1.141	1.297	1.472	1.666	1.067	1.138	1.291	1.462	1.650	1.066	1.135	1.284	1.450	1.633
1	0.948	1.014	1.158	1.319	1.497	0.974	1.040	1.183	1.343	1.520	0.979	1.043	1.184	1.339	1.512
2	0.839	0.899	1.031	1.177	1.342	0.887	0.949	1.082	1.231	1.398	0.897	0.957	1.089	1.236	1.398
3	0.740	0.794	0.914	1.049	1.199	0.807	0.864	0.988	1.127	1.283	0.821	0.878	1.000	1.138	1.290
4	0.650	0.699	0.808	0.931	1.068	0.732	0.785	0.900	1.030	1.176	0.749	0.802	0.917	1.046	1.190
5	0.568	0.612	0.711	0.823	0.949	0.662	0.711	0.818	0.939	1.075	0.683	0.732	0.839	0.960	1.095

Table E.22: Percentage difference in left and right 95th percentile fourth power aggregate forces for different anti-roll bar stiffness values

	No Anti-Roll Bar					3 kNm/deg Front and 5kNm/deg Rear					6 kNm/deg Front and 10 kNm/deg Rear				
IRI (m/km) →	**0.5**	**1**	**2**	**3**	**4**	**0.5**	**1**	**2**	**3**	**4**	**0.5**	**1**	**2**	**3**	**4**
Crossfall (%)	**Percentage Difference in Left and Right 95th Percentile Fourth Power Aggregate Forces**														
0	-0.1	-0.2	-0.3	-0.5	-0.7	0.0	0.1	0.1	0.2	0.2	0.2	0.4	0.7	1.0	1.3
1	23.3	22.8	21.9	21.0	20.3	18.1	17.8	17.3	16.8	16.3	17.0	17.0	16.8	16.6	16.4
2	46.2	45.3	43.7	42.2	40.7	35.9	35.3	34.3	33.2	32.2	33.7	33.3	32.7	32.0	31.3
3	67.9	66.8	64.6	62.5	60.5	53.2	52.4	50.8	49.3	47.8	49.9	49.3	48.2	47.0	45.9
4	88.1	86.7	84.0	81.5	79.0	69.8	68.7	66.6	64.7	62.8	65.5	64.6	63.1	61.6	60.0
5	106.4	104.9	101.9	99.0	96.2	85.4	84.1	81.7	79.4	77.2	80.3	79.3	77.4	75.5	73.6

Table E.23: Left normalized (by base model static values) 95th percentile fourth power aggregate forces for different sprung mass heights

	1.5 m Sprung Mass Height					2.0 m Sprung Mass Height					2.5 m Sprung Mass Height				
IRI (m/km) →	**0.5**	**1**	**2**	**3**	**4**	**0.5**	**1**	**2**	**3**	**4**	**0.5**	**1**	**2**	**3**	**4**
Crossfall (%)	**Normalized 95th Percentile Fourth Power Aggregate Forces**														
0	1.074	1.148	1.309	1.488	1.685	1.067	1.139	1.293	1.465	1.655	1.070	1.141	1.293	1.462	1.649
1	1.152	1.230	1.398	1.585	1.792	1.199	1.276	1.444	1.629	1.834	1.306	1.387	1.562	1.756	1.969
2	1.234	1.316	1.493	1.688	1.904	1.343	1.427	1.608	1.808	2.028	1.582	1.674	1.873	2.093	2.335
3	1.322	1.407	1.593	1.797	2.021	1.501	1.591	1.785	2.001	2.238	1.902	2.005	2.231	2.478	2.749
4	1.415	1.504	1.698	1.912	2.146	1.673	1.769	1.978	2.210	2.464	2.268	2.386	2.639	2.918	3.222
5	1.513	1.605	1.808	2.032	2.277	1.860	1.963	2.189	2.435	2.708	2.685	2.820	3.102	3.416	3.756

Table E.24: Right normalized (by base model static values) 95th percentile fourth power aggregate forces for different sprung mass heights

	1.5 m Sprung Mass Height					2.0 m Sprung Mass Height					2.5 m Sprung Mass Height				
IRI (m/km) →	**0.5**	**1**	**2**	**3**	**4**	**0.5**	**1**	**2**	**3**	**4**	**0.5**	**1**	**2**	**3**	**4**
Crossfall (%)	**Normalized 95th Percentile Fourth Power Aggregate Forces**														
0	1.075	1.150	1.312	1.494	1.695	1.068	1.141	1.297	1.472	1.666	1.071	1.143	1.298	1.469	1.661
1	1.001	1.072	1.227	1.399	1.590	0.948	1.014	1.158	1.319	1.497	0.871	0.932	1.065	1.213	1.377
2	0.931	0.998	1.145	1.308	1.490	0.839	0.899	1.031	1.177	1.342	0.700	0.752	0.865	0.992	1.134
3	0.866	0.929	1.067	1.222	1.396	0.740	0.794	0.914	1.049	1.199	0.557	0.600	0.696	0.804	0.926
4	0.804	0.863	0.994	1.141	1.305	0.650	0.699	0.808	0.931	1.068	0.438	0.473	0.554	0.645	0.749
5	0.746	0.801	0.925	1.064	1.220	0.568	0.612	0.711	0.823	0.949	0.339	0.369	0.435	0.512	0.599

Table E.25: Percentage difference in left and right 95th percentile fourth power aggregate forces for different sprung mass heights

	1.5 m Sprung Mass Height					2.0 m Sprung Mass Height					2.5 m Sprung Mass Height				
IRI (m/km) →	**0.5**	**1**	**2**	**3**	**4**	**0.5**	**1**	**2**	**3**	**4**	**0.5**	**1**	**2**	**3**	**4**
Crossfall (%)	**Percentage Difference in Left and Right 95th Percentile Fourth Power Aggregate Forces**														
0	-0.1	-0.1	-0.2	-0.4	-0.6	-0.1	-0.2	-0.3	-0.5	-0.7	-0.1	-0.2	-0.4	-0.5	-0.7
1	14.0	13.7	13.1	12.5	11.9	23.3	22.8	21.9	21.0	20.3	40.0	39.3	37.9	36.6	35.4
2	28.0	27.5	26.4	25.4	24.4	46.2	45.3	43.7	42.2	40.7	77.3	76.0	73.6	71.4	69.2
3	41.7	40.9	39.5	38.1	36.6	67.9	66.8	64.6	62.5	60.5	109.4	107.8	104.9	102.0	99.2
4	55.0	54.1	52.3	50.5	48.8	88.1	86.7	84.0	81.5	79.0	135.3	133.8	130.6	127.6	124.6
5	67.9	66.8	64.7	62.6	60.5	106.4	104.9	101.9	99.0	96.2	155.2	153.8	150.8	147.9	145.0

Table E.26: Left normalized (by base model static values) 95th percentile fourth power aggregate forces for different roll centre heights

	400 mm Roll Centre Height					500 mm Roll Centre Height					600 mm Roll Centre Height				
IRI (m/km) →	**0.5**	**1**	**2**	**3**	**4**	**0.5**	**1**	**2**	**3**	**4**	**0.5**	**1**	**2**	**3**	**4**
Crossfall (%)	**Normalized 95th Percentile Fourth Power Aggregate Forces**														
0	1.068	1.141	1.298	1.473	1.668	1.068	1.140	1.296	1.470	1.661	1.067	1.139	1.293	1.465	1.655
1	1.223	1.303	1.476	1.668	1.881	1.210	1.289	1.459	1.648	1.856	1.199	1.276	1.444	1.629	1.834
2	1.396	1.483	1.673	1.883	2.114	1.367	1.453	1.638	1.843	2.068	1.343	1.427	1.608	1.808	2.028
3	1.587	1.683	1.889	2.118	2.371	1.540	1.633	1.834	2.055	2.300	1.501	1.591	1.785	2.001	2.238
4	1.798	1.902	2.128	2.377	2.650	1.729	1.830	2.047	2.287	2.550	1.673	1.769	1.978	2.210	2.464
5	2.030	2.143	2.389	2.659	2.956	1.937	2.044	2.279	2.538	2.821	1.860	1.963	2.189	2.435	2.708

Table E.27: Right normalized (by base model static values) 95th percentile fourth power aggregate forces for different roll centre heights

	400 mm Roll Centre Height					500 mm Roll Centre Height					600 mm Roll Centre Height				
IRI (m/km) →	**0.5**	**1**	**2**	**3**	**4**	**0.5**	**1**	**2**	**3**	**4**	**0.5**	**1**	**2**	**3**	**4**
Crossfall (%)	**Normalized 95th Percentile Fourth Power Aggregate Forces**														
0	1.070	1.144	1.304	1.482	1.681	1.069	1.142	1.300	1.476	1.671	1.068	1.141	1.297	1.472	1.666
1	0.930	0.997	1.142	1.304	1.485	0.940	1.006	1.150	1.311	1.490	0.948	1.014	1.158	1.319	1.497
2	0.805	0.865	0.996	1.142	1.307	0.823	0.883	1.014	1.161	1.325	0.839	0.899	1.031	1.177	1.342
3	0.694	0.747	0.864	0.996	1.145	0.718	0.772	0.891	1.024	1.174	0.740	0.794	0.914	1.049	1.199
4	0.595	0.642	0.747	0.866	1.000	0.624	0.672	0.779	0.900	1.036	0.650	0.699	0.808	0.931	1.068
5	0.507	0.548	0.642	0.748	0.870	0.539	0.582	0.679	0.788	0.912	0.568	0.612	0.711	0.823	0.949

Table E.28: Percentage difference in left and right 95th percentile fourth power aggregate forces for different roll centre heights

	400 mm Roll Centre Height					500 mm Roll Centre Height					600 mm Roll Centre Height				
IRI (m/km) →	**0.5**	**1**	**2**	**3**	**4**	**0.5**	**1**	**2**	**3**	**4**	**0.5**	**1**	**2**	**3**	**4**
Crossfall (%)	**Percentage Difference in Left and Right 95th Percentile Fourth Power Aggregate Forces**														
0	-0.038	-0.101	-0.259	-0.521	-0.718	-0.037	-0.088	-0.173	-0.398	-0.643	-0.096	-0.216	-0.513	-0.710	-0.871
1	26.563	25.937	24.754	23.572	22.363	24.571	24.027	22.924	21.830	20.707	22.829	22.225	21.098	20.018	19.002
2	52.353	51.215	49.055	46.914	44.848	48.558	47.506	45.519	43.561	41.671	45.292	44.208	42.202	40.334	38.524
3	76.479	74.952	71.957	69.068	66.233	71.239	69.738	67.006	64.349	61.784	66.634	65.260	62.497	59.914	57.434
4	98.347	96.590	93.001	89.541	86.120	92.114	90.357	86.952	83.756	80.653	86.506	84.862	81.551	78.396	75.382
5	117.587	115.738	111.830	108.001	104.177	110.809	108.906	105.118	101.555	97.987	104.562	102.750	99.101	95.556	92.120

Table E.29: Left normalized (by base model static values) 95th percentile fourth power aggregate forces for different spring stiffness values

	200 N/mm Front and 400 N/mm Rear Stiffness					300 N/mm Front and 600 N/mm Rear Stiffness					400 N/mm Front and 800 N/mm Rear Stiffness				
IRI (m/km) →	**0.5**	**1**	**2**	**3**	**4**	**0.5**	**1**	**2**	**3**	**4**	**0.5**	**1**	**2**	**3**	**4**
Crossfall (%)	**Normalized 95th Percentile Fourth Power Aggregate Forces**														
0	1.067	1.139	1.293	1.465	1.655	1.078	1.161	1.344	1.551	1.784	1.089	1.185	1.401	1.650	1.936
1	1.199	1.276	1.444	1.629	1.834	1.190	1.278	1.474	1.695	1.943	1.193	1.295	1.525	1.789	2.093
2	1.343	1.427	1.608	1.808	2.028	1.311	1.406	1.614	1.849	2.113	1.305	1.414	1.658	1.938	2.259
3	1.501	1.591	1.785	2.001	2.238	1.442	1.543	1.765	2.015	2.295	1.425	1.540	1.799	2.097	2.437
4	1.673	1.769	1.978	2.210	2.464	1.582	1.691	1.927	2.192	2.488	1.554	1.677	1.951	2.265	2.623
5	1.860	1.963	2.189	2.435	2.708	1.733	1.850	2.100	2.383	2.696	1.692	1.822	2.113	2.445	2.822

Table E.30: Right normalized (by base model static values) 95th percentile fourth power aggregate forces for different spring stiffness values

	200 N/mm Front and 400 N/mm Rear Stiffness					300 N/mm Front and 600 N/mm Rear Stiffness					400 N/mm Front and 800 N/mm Rear Stiffness				
IRI (m/km) →	**0.5**	**1**	**2**	**3**	**4**	**0.5**	**1**	**2**	**3**	**4**	**0.5**	**1**	**2**	**3**	**4**
Crossfall (%)	**Normalized 95th Percentile Fourth Power Aggregate Forces**														
0	1.068	1.141	1.297	1.472	1.666	1.075	1.154	1.330	1.528	1.752	1.090	1.187	1.405	1.658	1.948
1	0.948	1.014	1.158	1.319	1.497	0.973	1.047	1.209	1.395	1.603	0.994	1.085	1.288	1.525	1.799
2	0.839	0.899	1.031	1.177	1.342	0.879	0.947	1.098	1.270	1.465	0.905	0.989	1.179	1.401	1.658
3	0.740	0.794	0.914	1.049	1.199	0.792	0.855	0.994	1.154	1.336	0.822	0.900	1.077	1.285	1.527
4	0.650	0.699	0.808	0.931	1.068	0.712	0.769	0.898	1.046	1.215	0.745	0.817	0.982	1.176	1.403
5	0.568	0.612	0.711	0.823	0.949	0.639	0.691	0.810	0.947	1.103	0.674	0.740	0.894	1.075	1.288

Table E.31: Percentage difference in left and right 95th percentile fourth power aggregate forces for different spring stiffness values

	200 N/mm Front and 400 N/mm Rear Stiffness					300 N/mm Front and 600 N/mm Rear Stiffness					400 N/mm Front and 800 N/mm Rear Stiffness				
IRI (m/km) →	**0.5**	**1**	**2**	**3**	**4**	**0.5**	**1**	**2**	**3**	**4**	**0.5**	**1**	**2**	**3**	**4**
Crossfall (%)	**Percentage Difference in Left and Right 95th Percentile Fourth Power Aggregate Forces**														
0	-0.1	-0.2	-0.3	-0.5	-0.7	0.3	0.6	1.0	1.5	1.8	-0.1	-0.2	-0.3	-0.5	-0.6
1	23.3	22.8	21.9	21.0	20.3	20.0	19.9	19.7	19.4	19.2	18.2	17.7	16.8	15.9	15.1
2	46.2	45.3	43.7	42.2	40.7	39.5	39.0	38.0	37.1	36.2	36.2	35.3	33.8	32.2	30.7
3	67.9	66.8	64.6	62.5	60.5	58.2	57.4	55.8	54.3	52.8	53.7	52.5	50.2	48.0	45.9
4	88.1	86.7	84.0	81.5	79.0	75.9	74.9	72.8	70.8	68.8	70.4	69.0	66.0	63.3	60.6
5	106.4	104.9	101.9	99.0	96.2	92.2	91.3	88.7	86.3	83.9	86.1	84.5	81.1	77.8	74.7

Table E.32: Left normalized (by base model static values) 95th percentile fourth power aggregate forces for different damping values

	5 kNs/m Front and 10 kNs/m Rear Damping					10 kNs/m Front and 20 kNs/m Rear Damping					20 kNs/m Front and 40 kNs/m Rear Damping				
IRI (m/km) →	0.5	1	2	3	4	0.5	1	2	3	4	0.5	1	2	3	4
Crossfall (%)	Normalised 95th Percentile Fourth Power Aggregate Forces														
0	1.067	1.139	1.293	1.465	1.655	1.061	1.122	1.251	1.391	1.543	1.056	1.115	1.241	1.376	1.523
1	1.199	1.276	1.444	1.629	1.834	1.193	1.258	1.398	1.550	1.714	1.187	1.251	1.387	1.534	1.693
2	1.343	1.427	1.608	1.808	2.028	1.337	1.407	1.558	1.722	1.900	1.330	1.400	1.547	1.706	1.877
3	1.501	1.591	1.785	2.001	2.238	1.494	1.570	1.733	1.909	2.101	1.487	1.562	1.720	1.893	2.078
4	1.673	1.769	1.978	2.210	2.464	1.665	1.747	1.923	2.113	2.317	1.657	1.738	1.910	2.094	2.294
5	1.860	1.963	2.189	2.435	2.708	1.851	1.939	2.128	2.332	2.552	1.842	1.930	2.114	2.313	2.526

Table E.33: Right normalized (by base model static values) 95th percentile fourth power aggregate forces for different damping values

	5 kNs/m Front and 10 kNs/m Rear Damping					10 kNs/m Front and 20 kNs/m Rear Damping					20 kNs/m Front and 40 kNs/m Rear Damping				
IRI (m/km) →	0.5	1	2	3	4	0.5	1	2	3	4	0.5	1	2	3	4
Crossfall (%)	Normalised 95th Percentile Fourth Power Aggregate Forces														
0	1.068	1.141	1.297	1.472	1.666	1.069	1.141	1.298	1.471	1.664	1.066	1.136	1.286	1.452	1.633
1	0.948	1.014	1.158	1.319	1.497	0.951	1.017	1.161	1.321	1.498	0.948	1.012	1.150	1.302	1.469
2	0.839	0.899	1.031	1.177	1.342	0.843	0.903	1.035	1.183	1.346	0.840	0.899	1.025	1.165	1.318
3	0.740	0.794	0.914	1.049	1.199	0.745	0.800	0.920	1.055	1.205	0.742	0.795	0.911	1.039	1.180
4	0.650	0.699	0.808	0.931	1.068	0.655	0.705	0.815	0.939	1.077	0.653	0.701	0.806	0.923	1.053
5	0.568	0.612	0.711	0.823	0.949	0.575	0.620	0.720	0.833	0.959	0.572	0.616	0.711	0.818	0.937

Table E.34: Percentage difference in left and right 95th percentile fourth power aggregate forces for different damping values

	5 kNs/m Front and 10 kNs/m Rear Damping					10 kNs/m Front and 20 kNs/m Rear Damping					20 kNs/m Front and 40 kNs/m Rear Damping				
IRI (m/km) →	0.5	1	2	3	4	0.5	1	2	3	4	0.5	1	2	3	4
Crossfall (%)	Percentage Difference in Left and Right 95th Percentile Fourth Power Aggregate Forces														
0	-0.1	-0.2	-0.3	-0.5	-0.7	0.1	0.1	0.3	0.4	0.5	0.1	0.2	0.3	0.5	0.6
1	23.3	22.8	21.9	21.0	20.3	23.6	23.3	22.8	22.3	21.8	23.6	23.4	22.9	22.5	22.0
2	46.2	45.3	43.7	42.2	40.7	46.5	45.9	44.8	43.7	42.7	46.6	46.0	45.0	44.0	43.0
3	67.9	66.8	64.6	62.5	60.5	68.3	67.5	65.8	64.2	62.7	68.4	67.6	66.0	64.5	63.1
4	88.1	86.7	84.0	81.5	79.0	88.5	87.4	85.4	83.4	81.5	88.6	87.6	85.6	83.8	82.0
5	106.4	104.9	101.9	99.0	96.2	106.8	105.6	103.3	101.0	98.8	106.9	105.8	103.5	101.4	99.3

Table E.35: Left normalized (by base model static values) 95th percentile fourth power aggregate forces for different track widths

	1.9 m Track Width					2.0 m Track Width					2.1 m Track Width				
IRI (m/km) →	**0.5**	**1**	**2**	**3**	**4**	**0.5**	**1**	**2**	**3**	**4**	**0.5**	**1**	**2**	**3**	**4**
Crossfall (%)	**Normalized 95th Percentile Fourth Power Aggregate Forces**														
0	1.067	1.138	1.292	1.463	1.652	1.067	1.139	1.293	1.465	1.655	1.067	1.138	1.292	1.462	1.650
1	1.213	1.291	1.459	1.645	1.850	1.199	1.276	1.444	1.629	1.834	1.186	1.263	1.428	1.611	1.814
2	1.375	1.459	1.642	1.844	2.067	1.343	1.427	1.608	1.808	2.028	1.316	1.398	1.576	1.772	1.988
3	1.553	1.645	1.843	2.062	2.302	1.501	1.591	1.785	2.001	2.238	1.457	1.545	1.735	1.944	2.175
4	1.749	1.848	2.063	2.299	2.558	1.673	1.769	1.978	2.210	2.464	1.610	1.703	1.907	2.130	2.376
5	1.963	2.070	2.303	2.558	2.837	1.860	1.963	2.189	2.435	2.708	1.774	1.874	2.092	2.330	2.591

Table E.36: Right normalized (by base model static values) 95th percentile fourth power aggregate forces for different track widths

	1.9 m Track Width					2.0 m Track Width					2.1 m Track Width				
IRI (m/km) →	**0.5**	**1**	**2**	**3**	**4**	**0.5**	**1**	**2**	**3**	**4**	**0.5**	**1**	**2**	**3**	**4**
Crossfall (%)	**Normalized 95th Percentile Fourth Power Aggregate Forces**														
0	1.068	1.139	1.294	1.466	1.657	1.068	1.141	1.297	1.472	1.666	1.068	1.141	1.297	1.471	1.664
1	0.936	1.001	1.141	1.298	1.472	0.948	1.014	1.158	1.319	1.497	0.959	1.025	1.170	1.331	1.509
2	0.817	0.875	1.002	1.145	1.304	0.839	0.899	1.031	1.177	1.342	0.858	0.919	1.052	1.201	1.367
3	0.710	0.762	0.877	1.006	1.150	0.740	0.794	0.914	1.049	1.199	0.765	0.821	0.944	1.081	1.234
4	0.614	0.661	0.764	0.880	1.012	0.650	0.699	0.808	0.931	1.068	0.681	0.732	0.845	0.971	1.112
5	0.529	0.570	0.662	0.767	0.886	0.568	0.612	0.711	0.823	0.949	0.604	0.650	0.753	0.870	1.000

Table E.37: Percentage difference in left and right 95th percentile fourth power aggregate forces for different track widths

	1.9 m Track Width					2.0 m Track Width					2.1 m Track Width				
IRI (m/km) →	**0.5**	**1**	**2**	**3**	**4**	**0.5**	**1**	**2**	**3**	**4**	**0.5**	**1**	**2**	**3**	**4**
Crossfall (%)	**Percentage Difference in Left and Right 95th Percentile Fourth Power Aggregate Forces**														
0	-0.1	-0.1	-0.2	-0.2	-0.3	-0.1	-0.2	-0.3	-0.5	-0.7	-0.1	-0.2	-0.4	-0.6	-0.8
1	25.8	25.3	24.4	23.6	22.8	23.3	22.8	21.9	21.0	20.3	21.2	20.8	19.9	19.1	18.3
2	50.9	50.0	48.4	46.8	45.3	46.2	45.3	43.7	42.2	40.7	42.2	41.3	39.8	38.4	37.0
3	74.5	73.4	71.0	68.9	66.7	67.9	66.8	64.6	62.5	60.5	62.2	61.2	59.0	57.1	55.2
4	96.0	94.6	91.9	89.2	86.6	88.1	86.7	84.0	81.5	79.0	81.1	79.8	77.2	74.7	72.4
5	115.2	113.6	110.7	107.7	104.8	106.4	104.9	101.9	99.0	96.2	98.5	97.0	94.1	91.3	88.6

Table E.38: Left normalized (by base model static values) 95th percentile fourth power aggregate forces for different spring track widths

	1.0 m Spring Track Width					1.2 m Spring Track Width					1.4 m Spring Track Width				
IRI (m/km) →	0.5	1	2	3	4	0.5	1	2	3	4	0.5	1	2	3	4
Crossfall (%)	Normalized 95th Percentile Fourth Power Aggregate Forces														
0	1.071	1.146	1.309	1.491	1.693	1.067	1.139	1.293	1.465	1.655	1.065	1.133	1.281	1.443	1.623
1	1.258	1.341	1.522	1.723	1.947	1.199	1.276	1.444	1.629	1.834	1.179	1.252	1.411	1.585	1.776
2	1.474	1.564	1.764	1.987	2.232	1.343	1.427	1.608	1.808	2.028	1.303	1.381	1.551	1.737	1.940
3	1.717	1.818	2.035	2.282	2.553	1.501	1.591	1.785	2.001	2.238	1.437	1.521	1.702	1.901	2.118
4	1.991	2.102	2.340	2.609	2.908	1.673	1.769	1.978	2.210	2.464	1.583	1.670	1.865	2.077	2.308
5	2.299	2.419	2.681	2.972	3.298	1.860	1.963	2.189	2.435	2.708	1.737	1.833	2.038	2.265	2.512

Table E.39: Right normalized (by base model static values) 95th percentile fourth power aggregate forces for different spring track widths

	1.0 m Spring Track Width					1.2 m Spring Track Width					1.4 m Spring Track Width				
IRI (m/km) →	0.5	1	2	3	4	0.5	1	2	3	4	0.5	1	2	3	4
Crossfall (%)	Normalized 95th Percentile Fourth Power Aggregate Forces														
0	1.071	1.146	1.311	1.494	1.697	1.068	1.141	1.297	1.472	1.666	1.066	1.135	1.284	1.450	1.633
1	0.910	0.976	1.121	1.283	1.464	0.948	1.014	1.158	1.319	1.497	0.961	1.024	1.163	1.317	1.488
2	0.770	0.826	0.954	1.097	1.258	0.839	0.899	1.031	1.177	1.342	0.864	0.923	1.051	1.194	1.353
3	0.649	0.696	0.807	0.933	1.076	0.740	0.794	0.914	1.049	1.199	0.776	0.829	0.947	1.079	1.226
4	0.543	0.584	0.678	0.790	0.915	0.650	0.699	0.808	0.931	1.068	0.695	0.743	0.852	0.974	1.110
5	0.450	0.486	0.567	0.663	0.774	0.568	0.612	0.711	0.823	0.949	0.620	0.664	0.764	0.877	1.002

Table E.40: Percentage difference in left and right 95th percentile fourth power aggregate forces for different spring track widths

	1.0 m Spring Track Width					1.2 m Spring Track Width					1.4 m Spring Track Width				
IRI (m/km) →	0.5	1	2	3	4	0.5	1	2	3	4	0.5	1	2	3	4
Crossfall (%)	Percentage Difference in Left and Right 95th Percentile Fourth Power Aggregate Forces														
0	0.0	-0.1	-0.2	-0.2	-0.2	-0.1	-0.2	-0.3	-0.5	-0.7	-0.1	-0.1	-0.3	-0.5	-0.6
1	32.1	31.5	30.4	29.3	28.3	23.3	22.8	21.9	21.0	20.3	20.4	20.0	19.2	18.5	17.7
2	62.7	61.7	59.6	57.8	55.9	46.2	45.3	43.7	42.2	40.7	40.5	39.8	38.4	37.1	35.7
3	90.3	89.2	86.5	83.9	81.4	67.9	66.8	64.6	62.5	60.5	59.8	58.8	57.0	55.1	53.3
4	114.3	113.0	110.1	107.1	104.2	88.1	86.7	84.0	81.5	79.0	78.0	76.9	74.6	72.3	70.1
5	134.5	133.1	130.2	127.0	123.9	106.4	104.9	101.9	99.0	96.2	94.7	93.7	91.0	88.4	85.9

Table E.41: Left normalized (by base model static values) 95th percentile fourth power aggregate forces for different sprung mass eccentricities

	No Eccentricity in Sprung Mass					50 mm Eccentricity in Sprung Mass (Left)					150 mm Eccentricity in Sprung Mass (Left)				
IRI (m/km) →	**0.5**	**1**	**2**	**3**	**4**	**0.5**	**1**	**2**	**3**	**4**	**0.5**	**1**	**2**	**3**	**4**
Crossfall (%)	**Normalized 95th Percentile Fourth Power Aggregate Forces**														
0	1.067	1.139	1.293	1.465	1.655	1.489	1.576	1.765	1.976	2.210	2.699	2.830	3.118	3.429	3.759
1	1.199	1.276	1.444	1.629	1.834	1.660	1.755	1.958	2.185	2.435	2.966	3.107	3.415	3.747	4.096
2	1.343	1.427	1.608	1.808	2.028	1.846	1.948	2.166	2.410	2.676	3.255	3.404	3.733	4.087	4.457
3	1.501	1.591	1.785	2.001	2.238	2.046	2.157	2.391	2.653	2.938	3.565	3.723	4.073	4.451	4.842
4	1.673	1.769	1.978	2.210	2.464	2.263	2.383	2.634	2.913	3.220	3.896	4.062	4.436	4.837	5.256
5	1.860	1.963	2.189	2.435	2.708	2.498	2.627	2.895	3.194	3.521	4.250	4.427	4.824	5.249	5.697

Table E.42: Right normalized (by base model static values) 95th percentile fourth power aggregate forces for different sprung mass eccentricities

	No Eccentricity in Sprung Mass					50 mm Eccentricity in Sprung Mass (Left)					150 mm Eccentricity in Sprung Mass (Left)				
IRI (m/km) →	**0.5**	**1**	**2**	**3**	**4**	**0.5**	**1**	**2**	**3**	**4**	**0.5**	**1**	**2**	**3**	**4**
Crossfall (%)	**Normalized 95th Percentile Fourth Power Aggregate Forces**														
0	1.068	1.141	1.297	1.472	1.666	0.766	0.820	0.941	1.079	1.232	0.361	0.391	0.461	0.539	0.629
1	0.948	1.014	1.158	1.319	1.497	0.674	0.723	0.833	0.958	1.099	0.310	0.337	0.399	0.469	0.551
2	0.839	0.899	1.031	1.177	1.342	0.590	0.635	0.734	0.848	0.977	0.265	0.289	0.344	0.407	0.481
3	0.740	0.794	0.914	1.049	1.199	0.515	0.555	0.645	0.748	0.866	0.225	0.246	0.296	0.352	0.418
4	0.650	0.699	0.808	0.931	1.068	0.447	0.484	0.564	0.658	0.765	0.190	0.208	0.252	0.303	0.362
5	0.568	0.612	0.711	0.823	0.949	0.386	0.419	0.492	0.576	0.673	0.159	0.175	0.214	0.260	0.312

Table E.43: Percentage difference in left and right 95th percentile fourth power aggregate forces for different sprung mass eccentricities

	No Eccentricity in Sprung Mass					50 mm Eccentricity in Sprung Mass (Left)					150 mm Eccentricity in Sprung Mass (Left)				
IRI (m/km) →	**0.5**	**1**	**2**	**3**	**4**	**0.5**	**1**	**2**	**3**	**4**	**0.5**	**1**	**2**	**3**	**4**
Crossfall (%)	**Percentage Difference in Left and Right 95th Percentile Fourth Power Aggregate Forces**														
0	-0.096	-0.181	-0.299	-0.480	-0.690	64.159	63.083	60.887	58.773	56.848	152.798	151.445	148.519	145.688	142.693
1	23.331	22.846	21.940	21.047	20.258	84.562	83.255	80.641	78.050	75.631	162.131	160.889	158.134	155.488	152.595
2	46.205	45.347	43.729	42.240	40.732	103.091	101.623	98.758	95.855	93.037	169.888	168.742	166.219	163.745	161.059
3	67.940	66.791	64.550	62.472	60.452	119.590	118.083	115.024	111.988	108.976	176.244	175.220	172.926	170.653	168.219
4	88.098	86.745	84.013	81.468	79.031	134.046	132.522	129.415	126.326	123.246	181.396	180.499	178.477	176.393	174.199
5	106.374	104.866	101.874	98.972	96.224	146.485	144.973	141.942	138.871	135.836	185.537	184.764	182.998	181.141	179.201

Table E.44: Left normalized (by base model static values) 95th percentile fourth power aggregate forces for different sprung mass values

	7.5 Tonne Sprung Mass					10.0 Tonne Sprung Mass					12.5 Tonne Sprung Mass				
IRI (m/km) →	0.5	1	2	3	4	0.5	1	2	3	4	0.5	1	2	3	4
Crossfall (%)	Normalized 95th Percentile Fourth Power Aggregate Forces														
0	0.196	0.215	0.258	0.308	0.366	0.501	0.540	0.627	0.725	0.835	1.067	1.139	1.293	1.465	1.655
1	0.213	0.234	0.279	0.332	0.394	0.554	0.596	0.689	0.793	0.911	1.199	1.276	1.444	1.629	1.834
2	0.233	0.254	0.302	0.358	0.423	0.611	0.656	0.756	0.867	0.992	1.343	1.427	1.608	1.808	2.028
3	0.253	0.276	0.327	0.386	0.454	0.674	0.721	0.827	0.946	1.079	1.501	1.591	1.785	2.001	2.238
4	0.276	0.299	0.353	0.415	0.486	0.741	0.792	0.905	1.031	1.172	1.673	1.769	1.978	2.210	2.464
5	0.300	0.324	0.381	0.446	0.521	0.814	0.868	0.987	1.121	1.271	1.860	1.963	2.189	2.435	2.708

Table E.45: Right normalized (by base model static values) 95th percentile fourth power aggregate forces for different sprung mass values

	7.5 Tonne Sprung Mass					10.0 Tonne Sprung Mass					12.5 Tonne Sprung Mass				
IRI (m/km) →	0.5	1	2	3	4	0.5	1	2	3	4	0.5	1	2	3	4
Crossfall (%)	Normalized 95th Percentile Fourth Power Aggregate Forces														
0	0.195	0.214	0.256	0.304	0.361	0.500	0.539	0.625	0.721	0.829	1.068	1.141	1.297	1.472	1.666
1	0.179	0.196	0.235	0.281	0.335	0.451	0.487	0.567	0.656	0.758	0.948	1.014	1.158	1.319	1.497
2	0.163	0.179	0.216	0.259	0.310	0.406	0.439	0.513	0.596	0.690	0.839	0.899	1.031	1.177	1.342
3	0.149	0.164	0.198	0.239	0.286	0.365	0.395	0.463	0.540	0.628	0.740	0.794	0.914	1.049	1.199
4	0.135	0.149	0.182	0.220	0.264	0.327	0.355	0.417	0.488	0.570	0.650	0.699	0.808	0.931	1.068
5	0.123	0.136	0.166	0.201	0.244	0.292	0.317	0.374	0.440	0.516	0.568	0.612	0.711	0.823	0.949

Table E.46: Percentage difference in left and right 95th percentile fourth power aggregate forces for different sprung mass values

	7.5 Tonne Sprung Mass					10.0 Tonne Sprung Mass					12.5 Tonne Sprung Mass				
IRI (m/km) →	0.5	1	2	3	4	0.5	1	2	3	4	0.5	1	2	3	4
Crossfall (%)	Percentage Difference in Left and Right 95th Percentile Fourth Power Aggregate Forces														
0	0.210	0.432	0.831	1.152	1.347	0.101	0.206	0.341	0.473	0.688	-0.096	-0.181	-0.299	-0.480	-0.690
1	17.719	17.484	17.114	16.650	16.163	20.361	20.053	19.453	18.894	18.368	23.331	22.846	21.940	21.047	20.258
2	35.124	34.361	33.152	32.011	30.769	40.242	39.596	38.303	37.054	35.854	46.205	45.347	43.729	42.240	40.732
3	52.020	50.937	48.859	47.036	45.189	59.405	58.426	56.518	54.674	52.844	67.940	66.791	64.550	62.472	60.452
4	68.187	66.834	64.082	61.553	59.138	77.524	76.230	73.853	71.421	69.097	88.098	86.745	84.013	81.468	79.031
5	83.469	81.876	78.590	75.542	72.597	94.392	92.855	90.062	87.187	84.419	106.374	104.866	101.874	98.972	96.224

Table E.47: Left normalized (by base model static values) 95th percentile fourth power aggregate forces for different tyre stiffness values

	0.8 MN Tyre Stiffness					1.0 MN Tyre Stiffness					1.3 MN Tyre Stiffness				
IRI (m/km) →	0.5	1	2	3	4	0.5	1	2	3	4	0.5	1	2	3	4
Crossfall (%)	Normalized 95th Percentile Fourth Power Aggregate Forces														
0	1.059	1.121	1.255	1.401	1.561	1.067	1.139	1.293	1.465	1.655	1.082	1.169	1.361	1.579	1.827
1	1.193	1.260	1.405	1.564	1.737	1.199	1.276	1.444	1.629	1.834	1.212	1.306	1.514	1.748	2.013
2	1.340	1.412	1.569	1.741	1.928	1.343	1.427	1.608	1.808	2.028	1.355	1.456	1.679	1.931	2.214
3	1.500	1.579	1.748	1.934	2.134	1.501	1.591	1.785	2.001	2.238	1.510	1.620	1.859	2.129	2.432
4	1.675	1.761	1.943	2.142	2.358	1.673	1.769	1.978	2.210	2.464	1.679	1.797	2.054	2.343	2.666
5	1.866	1.957	2.154	2.368	2.599	1.860	1.963	2.189	2.435	2.708	1.863	1.989	2.265	2.573	2.918

Table E.48: Right normalized (by base model static values) 95th percentile fourth power aggregate forces for different tyre stiffness values

	0.8 MN Tyre Stiffness					1.0 MN Tyre Stiffness					1.3 MN Tyre Stiffness				
IRI (m/km) →	0.5	1	2	3	4	0.5	1	2	3	4	0.5	1	2	3	4
Crossfall (%)	Normalized 95th Percentile Fourth Power Aggregate Forces														
0	1.059	1.120	1.253	1.398	1.558	1.068	1.141	1.297	1.472	1.666	1.083	1.171	1.368	1.590	1.842
1	0.937	0.994	1.115	1.248	1.395	0.948	1.014	1.158	1.319	1.497	0.963	1.045	1.225	1.430	1.664
2	0.827	0.878	0.989	1.111	1.245	0.839	0.899	1.031	1.177	1.342	0.854	0.929	1.094	1.283	1.499
3	0.727	0.773	0.874	0.985	1.108	0.740	0.794	0.914	1.049	1.199	0.755	0.823	0.974	1.147	1.347
4	0.637	0.678	0.769	0.871	0.983	0.650	0.699	0.808	0.931	1.068	0.665	0.726	0.864	1.023	1.207
5	0.555	0.593	0.675	0.766	0.869	0.568	0.612	0.711	0.823	0.949	0.584	0.639	0.764	0.909	1.077

Table E.49: Percentage difference in left and right 95th percentile fourth power aggregate forces for different tyre stiffness values

	0.8 MN Tyre Stiffness					1.0 MN Tyre Stiffness					1.3 MN Tyre Stiffness				
IRI (m/km) →	0.5	1	2	3	4	0.5	1	2	3	4	0.5	1	2	3	4
Crossfall (%)	Percentage Difference in Left and Right 95th Percentile Fourth Power Aggregate Forces														
0	0.048	0.086	0.129	0.162	0.201	-0.096	-0.181	-0.299	-0.480	-0.690	-0.096	-0.216	-0.513	-0.710	-0.871
1	23.966	23.648	23.034	22.447	21.841	23.331	22.846	21.940	21.047	20.258	22.829	22.225	21.098	20.018	19.002
2	47.282	46.637	45.403	44.192	43.011	46.205	45.347	43.729	42.240	40.732	45.292	44.208	42.202	40.334	38.524
3	69.391	68.501	66.703	65.001	63.274	67.940	66.791	64.550	62.472	60.452	66.634	65.260	62.497	59.914	57.434
4	89.840	88.732	86.533	84.402	82.299	88.098	86.745	84.013	81.468	79.031	86.506	84.862	81.551	78.396	75.382
5	108.309	107.040	104.615	102.179	99.792	106.374	104.866	101.874	98.972	96.224	104.562	102.750	99.101	95.556	92.120